ANALYSIS OF THE CONFORM PROCESS: A SPECIFIC FORM OF ALUMINIUM EXTRUSION

XAVIER VELAY

A thesis submitted in partial fulfilment of the requirements of Bournemouth University for the degree of Doctor of Philosophy

December 2004

Bournemouth University

ANALYSIS OF THE CONFORM PROCESS: A SPECIFIC FORM OF ALUMINIUM EXTRUSION

Xavier Velay

Abstract

Since the Conform process was patented 30 years ago, there have only been approximately 200 machines sold worldwide. Given that Conform competes economically with conventional extrusion and is also reported to be a more energy efficient process, it is surprising that the use of Conform is not more widespread in today's increasingly environmentally conscious and high-production focussed world. One explanation for this is likely to be due to the fact that there is still limited knowledge of the thermo-mechanical behaviour of the workpiece during extrusion. Furthermore, for the aluminium industry, there are still issues remaining regarding the production of flash and the quality of the extrudate in terms of mechanical properties.

This study provides the reader with the findings of the research and experimental work undertaken by the author, his co-workers and fellow specialists, in the field of aluminium extrusion including Conform. The experimental work includes both laboratory experiments performed with a direct extrusion press and an experimental machine set up to replicate the Conform process. The experimental work is also simulated using finite element modelling techniques. The results from these analyses are then validated by comparing industrial and experimental data. The finite element analyses are enhanced by using parallel processing technology and user sub-routines.

The author proposes new models to allow for the study of the different sub-processes in Conform. These include the coining of the feedstock, formation of the upset zone, extrusion of the flash, the filling-up of the expansion chamber / feeder plate and the extrusion of the extrudate. The author also investigates methods which predict microstructure and surface cracks in the extrudate. The author suggests innovative techniques to improve the efficiency of finite element analysis in metal forming. Finally the author recommends procedures for the study of structural integrity and the optimisation of the tooling used in Conform.

List of Contents

List of Symbols

A area of contact (eq 2.32, 2.33, G.1, G.2)
material constant 'structure factor' (eq 2.37, 2.38)
material consistency (eq 3.6)
material constant (eq 5.12)

A' constant

A_{AOC} cross sectional area of unfilled groove

A_C cross sectional area of the container bore

A_E cross sectional area of the extrudate

A_F cross sectional area of the feedstock

A_{Fl} cross sectional area of the flash

A_i area of initial grip

A_{ig} total contact area groove-material in the grip length

A_{ig}^{base} contact area groove base-material in the grip length

A_{ig}^{side} contact area one groove side-material in the grip length

A_{is} contact area shoe-material in the grip length

A_m fitting parameter for the friction factor

A_P cross sectional area of the extrudate with a puller action

A_{ug} total contact area groove-material in the upset zone

A_{us} contact area shoe-material in the upset zone

a constant (eq 2.6)
constant contribution to the redundant work (eq 2.18, A.8)
constant (eq 5.9)

B linear operator
material constant (eq 5.12)

B_m fitting parameter for the friction factor

b constant (eq 2.6)
constant linked to the semi-dead metal zone angle (eq 2.18)
constant contribution to die friction (eq A.8)
Burgers vector (eq 5.5)

b'	constant
b_{Al}	aluminium effusivity
b_i	material *i* effusivity
b_{Tool}	tool effusivity
$C_{p(air)}$	specific heat of air
$C_{p(Al)}$	specific heat of aluminium
$C_{p(i)}$	specific heat of material *i*
C	geometric parameter
C'	temperature-dependent material constant
c	constant (eq 2.6)
	constant dependent of the friction coefficients (eq 2.18)
	constant (eq 5.9)
CL	Cockcroft and Latham criterion
D_C	diameter of the container bore
D_E	equivalent diameter of the extrudate
d	Constant (eq 2.6)
	thickness of the material (eq 3.32)
	half of the groove width (eq G.1, G.2)
d_0	initial grain size
F	force required for the Conform extrusion to occur (eq 2.21)
	resultant force on the ram (eq 4.1)
F_a	reaction force of the abutment on the feedstock
F_d	Frictional force generated at the die surface(s)
F_f	total frictional force acting toward the abutment
F_{fi}	frictional forward force generated in the initial grip length
F_{fu}	frictional forward force generated in the upset zone
F_s	opposing frictional force feedstock-shoe interface,
F_{si}	frictional force shoe-material interface in initial grip length
F_{su}	frictional force shoe-material interface in the upset zone
F_X	reaction force acting on the ram

F_Y reaction force acting on the ram

G universal gas constant (eq 2.39)

shear modulus (eq 5.6)

h global transfer coefficient for conduction and convection

ram stroke (eq 4.3)

height of a sector (eq G.3, G.4)

h_c convection heat transfer coefficient (film coefficient)

i constant

J_1 first invariant of the stress tensor

J_2 second invariant of the stress tensor

J_3 third invariant of the stress tensor

j constant

K material consistency

K_0 constant for the material consistency

K_1 model parameter

K_2 model parameter

k thermal conductivity (eq 2.32)

Avrami exponent (eq 5.7)

k_{air} thermal conductivity of air

k_i thermal conductivity of material i

L billet length

L' die bearing length (for a solid die)

L_B billet length

L_D die land length

L_M contact length at the dead metal zone

L_V line length per unit volume

l_i length of initial grip

l_u length of upset zone

M_{GB} grain boundary mobility

m friction factor (eq 2.8)

	stress rate sensitivity index (eq 3.1)
	material constant (eq 5.12)
m_0	constant of the stress rate sensitivity index
m_1	constant of the stress rate sensitivity index
$m_1 \sim m_5$	regression coefficients
$m_7 \sim m_9$	regression coefficients
$\overline{m}$	Tresca friction coefficient
m'	friction factor at the container-billet interface
m''	friction factor at the die bearing-material interface
m'''	friction factor at the dead metal zone-material interface
M_m	compatible shape functions
N_n	shape functions
N_V	density of nucleation sites
n	number of holes in the die (eq 2.1)
	inverse of the temperature compensated strain rate sensitivity (eq 2.9, 2.37, 2.38)
	coefficient of sensitivity to strain hardening (eq 3.4, 3.5)
P	power requirement for the wheel
P_D	total stored energy
P_i	material properties invariant
P_V	number of grain corners per unit volume
p	extrusion pressure in Conform (eq 2.19, 2.20)
	sensitivity to the sliding velocity (eq 3.24)
$[p]$	pressure field
$p_1 \sim p_4$	probabilities of finding subgrains with a size larger than a critical value
p_B	Pressure to 'breakout'
p_D	pressure for the plastic deformation of the billet
p_F	pressure for the friction interfaces
P_m	nodal pressure
P_θ	probability of finding sub-boundaries with a misorientation angle

	larger than a critical value within the grain
p_r	radial pressure
p_{RW}	pressure to compensate redundant work
Q	Quality parameter for tetrahedral finite element
$\dot{Q}_d$	heat generation rate due to deformation per unit of volume
Q_{rex}	activation energy for recrystallization
$\dot{q}_{cond}$	rate of heat transfer due to conduction
$\dot{q}_{conv}$	rate of heat transfer due to convection
R	extrusion ratio (eq 2.1)
	correlation coefficient (Fig 3.3, 3.4)
R_c	extrusion ratio for Conform
R_{m}	modified extrusion ratio
R_{mc}	modified extrusion ratio for Conform
r	radius of the original feedstock
r_c	radius of the coining roll
r_g	radius of the wheel at the groove base.
S_i	state variables
S_V	grain boundary surface area per unit volume
T	temperature
	torque of the wheel (eq 2.24)
T_0	tooling temperature
T_a	annealing temperature
T_{amb}	ambient temperature
T_{fA}	final temperature of air in the groove
T_{iA}	initial temperature of air in the groove
T_{iW}	initial temperature of the wheel
T_m	lowest melting point
t	time (eq G.1, G.2)
	holding time (eq 5.7)
$t_{0.5}$	time for 50% recrystallization

V_{air} volume of air in the groove

V_E exit speed of the extrudate

V_{Fl} velocity of the flash

V_M speed of the flowing material

V_n nodal velocity vectors

V_R ram speed

$[v]$ velocity field

v_{rel} sliding velocity

w groove width

x initial contact with the groove wall

X weighted solute content

X_V recrystallized volume fraction

$[x]$ displacement field

Z temperature compensated strain rate parameter

Z_d averaged temperature compensated strain rate

α material constant 'reciprocal flow stress' (eq 2.10, 3.37, 2.38)

friction coefficient (eq 3.24)

angle of contact with the coining roll (eq G.3, G.4)

α_{Al} thermal diffusivity of aluminium

β temperature constant

ΔH activation energy for hot deformation

ΔT_{bf} temperature increase due to friction at container-billet

ΔT_{cond} temperature gradient due to conduction

ΔT_{conv} temperature gradient due to convection

ΔT_d temperature increase due to plastic deformation

ΔT_{df} temperature increase due to friction at die land-material

ΔT_{dmf} temperature increase due to friction at the dead metal zone

ΔV relative velocity between workpiece and tooling

δ spacing between dislocation walls

δ_{ss} subgrain size at steady state

$\bar{\varepsilon}$	mean equivalent strain
$[\dot{\varepsilon}]$	strain rate tensor
$\dot{\bar{\varepsilon}}$	mean equivalent strain rate, effective strain rate
ε_0	constant for strain hardening regulation
$\bar{\varepsilon}_f$	equivalent strain to fracture
$\bar{\varepsilon}_f^p$	critical effective plastic strain
$\dot{\varepsilon}_{ij}$	strain rate tensor
ε_r	material emissivity
ε_δ	characteristic strain
θ	misorientation
θ_C	critical angle for grain characterisation
λ	peripheral ratio parameter
	heat generation efficiency (eq 2.24)
$\lambda_1 \sim \lambda_4$	geometric parameters
μ	constant friction coefficient
μ_i	coefficient of friction groove-feedstock in the grip length
μ_u	coefficient of friction groove-feedstock in the upset zone
ξ	local co-ordinate vector
ρ_{air}	air density
ρ_{Al}	aluminium density
ρ_g	'geometrically necessary' dislocation density
ρ_b	boundary dislocation density
ρ_i	material *i* density
	internal dislocation density (eq 5.3)
ρ_r	'random' dislocation density
ρ_{tot}	total dislocation density
$\bar{\sigma}$	flow stress, equivalent stress, effective stress
σ_0	equivalent von Mises yield stress
σ_{cys}	compressive yield stress of the feedstock

σ_{H-S} Hansel-Spittel flow stress

σ_I maximum principal tensile stress

$\overline{\sigma}_i$ mean compressive yield strength in grip length

σ_{ij} Cauchy stress tensor

σ_N normal stress

σ_{N-H} Norton-Hoff flow stress

$\sigma_{N-H}^{\exp}$ Norton-Hoff exponential flow stress law

σ_{N-H}^{power} Norton-Hoff power flow stress

σ_r Stefan-Boltzmann constant

$\overline{\sigma}_u$ mean compressive yield strength in upset zone

σ_{Z-H} Zener-Hollomon flow stress

τ_F friction stress

τ_{ys} yield strength of the feedstock in shear

τ_0 Tresca equivalent yield stress

φ plastic strain

Φ_c conduction and convection flux

Φ_{cst} constant flux

Φ_{fr} friction dissipation flux

Φ_r radiation flux

ϕ_i angle of the initial grip length

ϕ_u angle of the upset zones

ω cone semi-angle of the dead metal zone in direct extrusion (eq 2.6, 2.29)

angular velocity (eq 2.24)

List of Figures

List of Tables

List of Abbreviations

AISI	American Iron and Steel Institute
ALE	Arbitrary Lagrangian Eulerian
CAD	Computer-Aided Design
CAM	Computer-Aided Manufacture
CCD	Circumscribed Circle Diameter
CNC	Computerised Numerical Control
CPU	Central Processing Unit
CVD	Chemical Vapour Deposition
DMZ	Dead Metal Zone
EBSD	Electron BackScatter Diffraction
ECAE	Equal Channel Angular Extrusion
EDM	Electrical Discharge Machining
fcc	face centred cubic
FE	Finite Element
FEA	Finite Element Analysis
FEM	Finite Element Modelling
JMAK	Johnson-Melh-Avrami-Kolmogorov
OIM	Orientation Imaging Microscopy
PCG	Peripheral Coarse Grain
PCs	Personal Computers
PSZ	Partially Stabilised Zirconia
PVD	Physical Vapour Deposition
SFE	Stacking Fault Energy
SPMD	Single Program Multiple Data
TEM	Transmission Electron Microscope
UKAEA	United Kingdom Atomic Energy Authority
WEDM	Wire Electrical Discharge Machining

Acknowledgements

Having worked within the field of research and academia for a number of years at Bournemouth University, there are many people who have contributed directly and indirectly to the work of this thesis, and whom I would like to thank:

Professor Terry Sheppard for his unwavering supervision, encouragement and support. Terry is a true expert in the field of aluminium extrusion and through numerous formal (and informal) discussions I have benefited greatly from his wealth of experience.

Dr Kamran Tabeshfar, Professor Peter Hogarth and Mr Andy Wilson from the Design Group within the School of Design, Engineering & Computing, for their support and trust right from the beginning of my academic and research career at the University.

Dr Isaac Flitta, Dr Xinjian Duan and Mr Zhi Peng of the Virtual Manufacturing research group at Bournemouth University, for their close collaboration and help throughout various stages of the thesis.

Colleagues from Bournemouth University including the IT support, librarians, administrative team and fellow academics.

Dr Mike Clode from King's College London and Norman Carr, for their invaluable experimental results.

Martin Smith and Brian Maddock from Holton Machinery, for their expertise on the design and commercialisation of Conform machines and for their financial support.

The support staff at Transvalor (France) for their high quality technical support with the use of the Forge 2 and Forge 3 software.

Ms Deborah Newton-Perks for her invaluable support, patience and encouragement and for never being afraid to tell me when my sentences didn't make sense.

Finally, I would like to thank friends and family for their patience and reassure them that I am now available for all of those things that I have been putting off until after the thesis has been written. In particular I would like to pay tribute to my parents for their continuous support through my long student life!

This valuable metal possesses the whiteness of silver, the indestructibility of gold, the tenacity of iron, the fusibility of copper, the lightness of glass It is easily wrought, is very widely distributed, forming the base of most of the rocks, is three times lighter than iron, and seems to have been created for the express purpose of furnishing us with the material for our projectile.

(Excerpt from "From the Earth to the Moon", chapter 7, Jules Verne 1865)

1 Introduction

In this chapter the reader is introduced to aluminium alloys and the different techniques required to extrude them. A continuous extrusion process, Conform, is presented. The use of numerical analyses to simulate extrusion is introduced. Finally a brief overview of the remainder of the thesis is provided.

1.1 Aluminium alloys and aluminium extrusion

Aluminium Production

Aluminium makes up approximately eight percent of the earth's crust and is the third most abundant element. The form 'aluminium' does not occur naturally as a metal but originates as an oxide 'alumina'. Alumina is obtained by refining deposits of bauxite ore. In 1807, the English chemist Sir Humphrey Davy suggested the name 'alumium' for a still undiscovered metal and later agreed to change it to 'aluminum'. Following on from Davy's experiments, in 1825 the Danish physicist H.C. Oersted produced the first nodules of aluminium. In 1854, a small but significant step towards producing aluminium on an industrial scale was made by the Frenchman Henri Sainte-Claire Deville. By 1866, a French metallurgist Paul Héroult and an American Charles Hall, who had worked separately but simultaneously, invented the smelting process. Both patents showed how to dissolve aluminium oxide in molten cryolite so that aluminium could be subsequently extracted by electrolysis. The process was further advanced in 1888 by Karl Bayer's invention which allowed aluminium oxide to be produced from bauxite. This meant that aluminium had become a commercially affordable metal. However, the production of primary aluminium did not take off until the 1940s as this was dependent on, and restricted by, the availability of electricity. There are two main production methods for aluminium which are currently used (a) primary aluminium from bauxite ore and (b)

recycled aluminium from process scrap and used products. This latter method is almost twenty times more energy efficient than producing new aluminium from ore. By the year 2004 the annual world-wide production of aluminium has been estimated to have reached approximately 25 million tonnes. Almost ten million tonnes of this aluminium per year have been used by the extrusion industry. A quarter of these industries are situated within Western Europe (Rüttimann 2004).

Aluminium alloys

Various aluminium alloys can be produced by combining common elements. The main elements include copper, magnesium, manganese, silicone and zinc. Probably the best known advantage of aluminium alloys is their lightweight property. Aluminium also has other important characteristics such as its high strength-to-weight ratio, resilience, corrosion resistance, heat and electrical conductivity, reflectivity, and cryogenic strength. Furthermore it is non-magnetic and non-sparking (Despoy *et Al* 1988). Casting and wrought alloys are the two principal classifications for aluminium alloys, based on their suitability for specific manufacturing processes. These are further subdivided into the categories of heat or non-heat treatable alloys, which are then further classified into seven main series depending on their chemical composition. These series are divided as follows:

- 1XXX (*≤99% Al*), excellent corrosion together with high thermal and electrical conductivity,
- 2XXX (*Al-Cu & Al-Cu-Mg*), high strength,
- 3XXX (*Al-Mn*), moderate strength,
- 4XXX (*Al-Si*), lower melting point,
- 5XXX (*Al-Mg*), good corrosion resistance and high strength,
- 6XXX (*Al-Mg-Si*), good formability, machinability and weldability,
- and 7XXX (*Al-Zn-Mg & Al-Zn-Mg-Cu*).

Aluminium extrusions

The extrusion of aluminium is mainly used for the building industry (e.g. windows and door frames, exterior cladding etc) and the mass transport industry (e.g. airframes, road and rail chassis, hull structures etc). Within the transport industry, there is a fast growing automotive market for thin-section aluminium profiles. Currently the production of such profiles is an expensive process and therefore there is a niche in the industry for a more economical and efficient extrusion method.

The most common extrusion process is the direct extrusion process, also known as forward or conventional extrusion. This consists of a heated billet of aluminium which is placed within a container and then pushed forward by a ram. The subsequent pressure created inside the container extrudes the aluminium through a shaped die. Throughout this thesis this process will be referred to as conventional extrusion and the shaped aluminium as extrudate. Other extrusion processes, not covered in this study, include the following:

- indirect extrusion (also called inverse, reversed, backward, or inverted extrusion),
- hydrostatic extrusion,
- side extrusion,
- impact extrusion,
- equal channel angular extrusion (ECAE) (Saito *et Al* 1999),
- friction assisted extrusions,
- friction extrusion – batch technique (Thomas 2000),
- friction co-extrusion (Thomas 2000),
- friction hydro-pillar (Thomas 2000).

A significant disadvantage in all of the above methods is that production must always be temporarily halted so that the workpiece can be renewed once extrusion has taken place. To try and remedy this problem researchers have developed a small number of continuous extrusion processes. These include Conshearing (Saito *et Al* 1999), Context, Linex (Shcherba *et Al* 2000), Extrolling (Shcherba *et Al* 2000) and Conform. To date, Conform is the only method utilised substantially and effectively by industry.

1.2 The Conform process

Conform is the result of many years research to find a truly continuous method of extrusion. The process was invented by Derek Green (Green 1972) and developed by the Advanced Metal Forming Group at the United Kingdom Atomic Energy Authority (UKAEA) Springfield Laboratories in the 1970s. The UKAEA further developed Green's concept to create the first Conform machine (Etherington 1977a and 1977b). Since the 1970s approximately 200 Conform machines have been sold

worldwide, and almost half of these have been designed and manufactured by Holton Machinery. Aluminium and copper are the most commonly used materials in the Conform process. For the purposes of this thesis only the use of aluminium will be studied. There are two main modes in Conform: Radial and Tangential. The principle of the Radial Conform process is shown schematically in Figure 1.1.

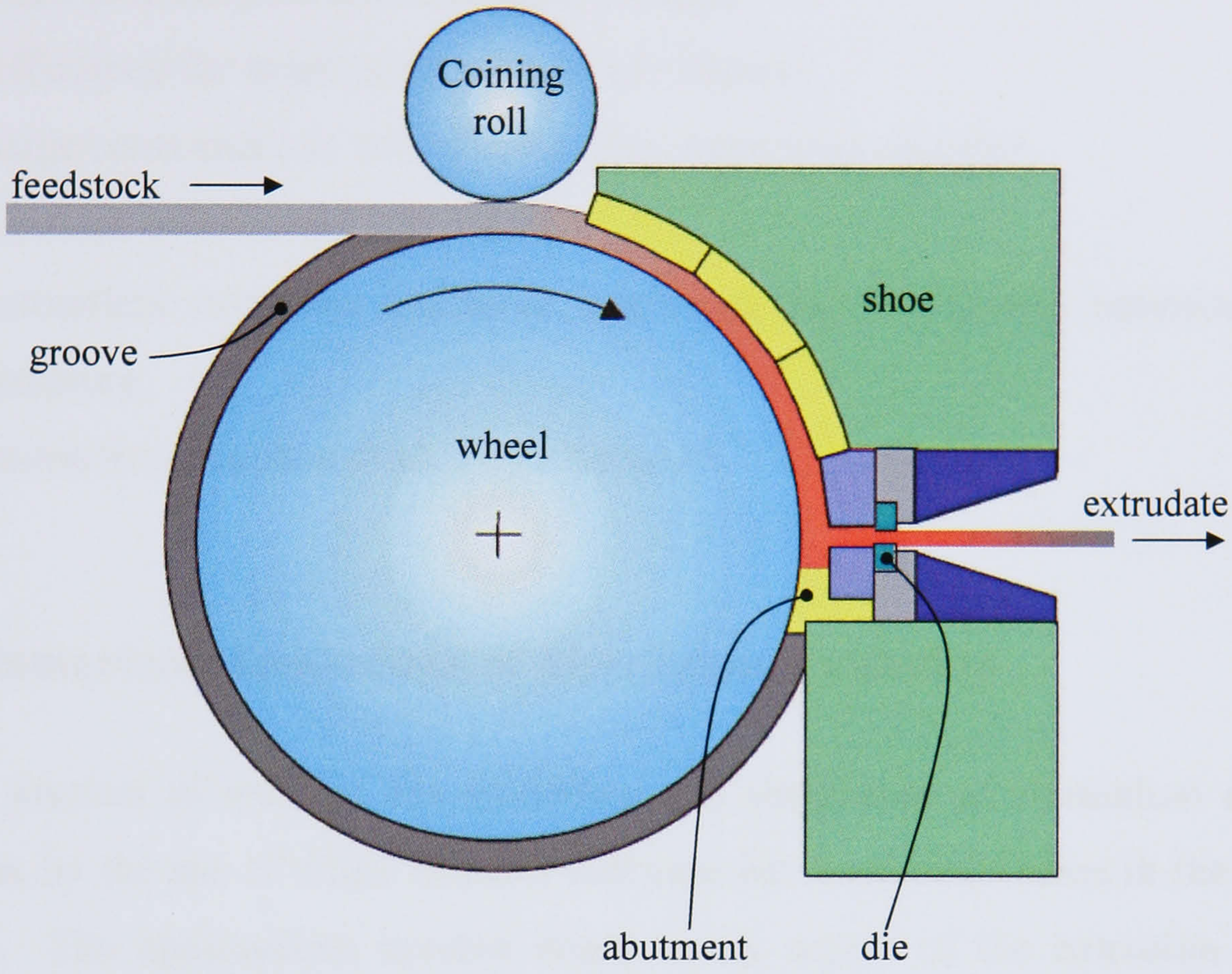

Figure 1.1 Schematic of Radial Conform (courtesy of Holton Machinery)

The feedstock is fed into the groove of the rotating extrusion wheel by the coining roll. The tools are pre-heated to a relatively high temperature. The feedstock is then driven by friction between the wheel groove and the shoe until it hits the abutment. Due to the high pressure generated by this and also the high temperature within the abutment area the feedstock deforms plastically and consequently extrudes through the die. The Tangential Conform mode is similar to the Radial mode but allows for the introduction of a secondary feedstock as a core of the extrudate. Thus this mode is used for aluminium sheathing and cladding. In this thesis only the Radial Conform mode will be studied in more detail and will be referred to as the Conform process.

The feedstock generally consists of a cast product which is rolled into a rounded shape. However some Conform machines are fed with either an extremely fine powder, coarse granules or a continuously cast bar of aluminium (Langerweger and Maddock 1988, Slater and Coon 1988).

The Conform process offers several advantages:

- low operational and capital cost,
- good production rate (around 200kg/hr),
- low scrap loss (<1%),
- lower repeated starting shock loads on die (ideal for thin walled extrusions such as multi-port tubes (Dawson 1996)),
- efficiency for small scale extrusion (<10mm),
- large cross sections with the use of an expansion chamber,
- absence of billet to billet joints,
- consistent extrusion and close tolerances due to constant temperature and pressure,
- extrusions uncontaminated by lubricants.

1.3 Numerical simulations of aluminium extrusion

A large amount of work in the modelling and simulation of aluminium extrusion processes by the use of finite element software has been undertaken in the last few decades. The applications involve nearly every aspect of the extrusion process: predicting load, temperature, material flow, surface formation, surface cracks, recrystallisation and die wear. Substantial progress has been made in the past decade with the use of finite element software and its supporting hardware. The technology currently available can be used for most production purposes at an industrial level. However it is very important that the numerical model is verified and validated with experimental data. Figure 1.2 shows a flow diagram of the different stages of a simulation. The validation and verification processes are also indicated.

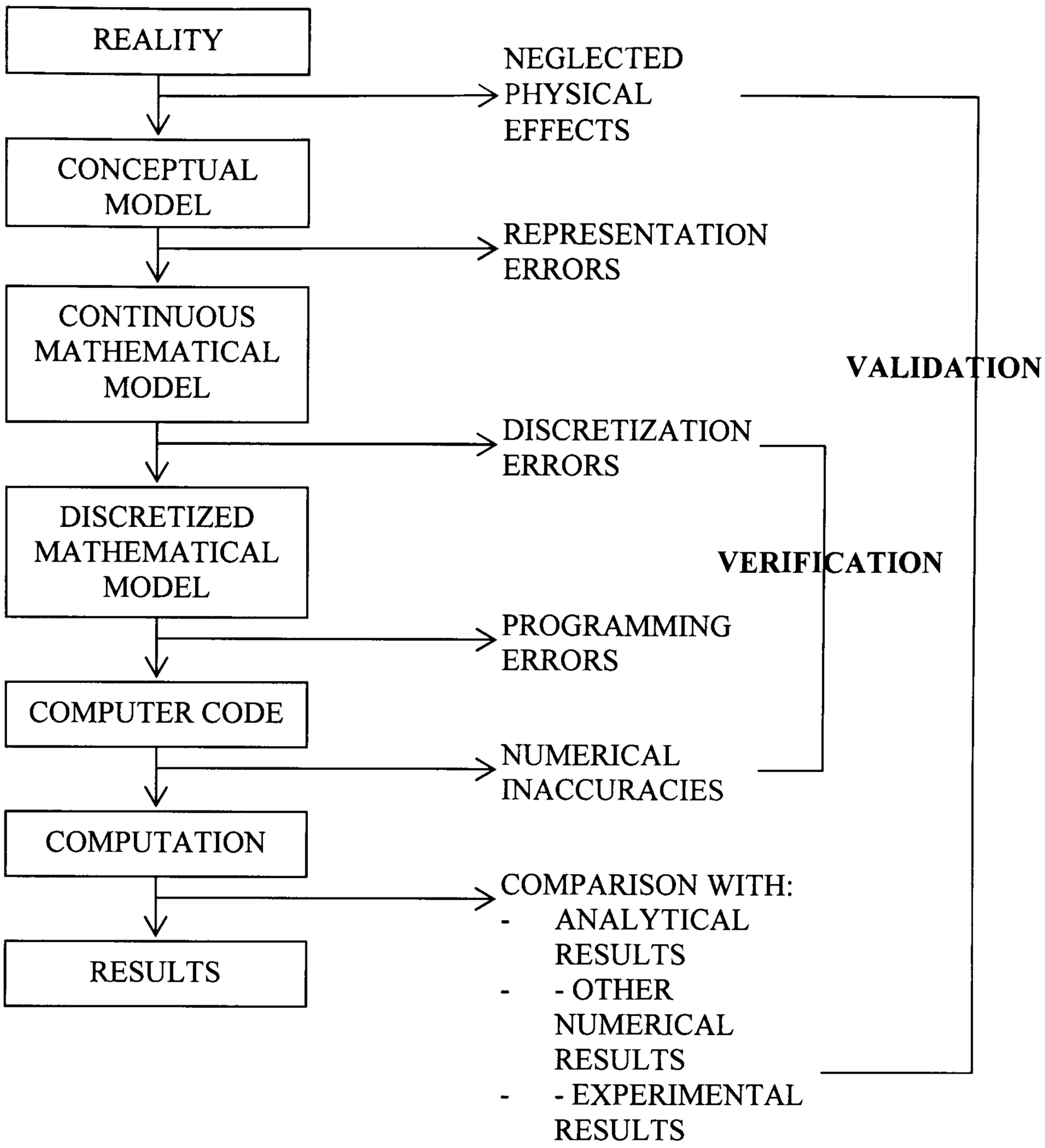

Figure 1.2 Verification and validation of a numerical model

1.4 Overview of the thesis

The main objective of this thesis is to provide a better understanding of the thermo-mechanical behaviour of an aluminium workpiece during Conform extrusion. The dissemination of the findings will hopefully widen the use of Conform technology in the aluminium extrusion industry. The main conclusions from this work put forward innovative and modern methodologies for enhancing the quality of extrudate in terms of mechanical properties and for optimising the tooling used in Conform machines. The experimental and laboratory work undertaken for this thesis take into account both direct and Conform extrusion processes. The thermo-mechanical behaviour of various aluminium alloys is studied at different temperatures and strain rates. The interaction between the workpiece and the tools is also investigated.

The Literature Review, critically reviews the current research available for both conventional and Conform extrusion. There is extensive research available for conventional extrusion, however Conform is still a relatively unknown process. Both forming processes share similar characteristics, therefore this chapter is broken into various sections which cover the mechanics of extrusion, the constitutive laws of aluminium alloys, the quality of the extrudate, the tooling required for extrusion (including a more detailed look at feeder plates and expansion chambers) and the modelling of aluminium extrusion.

Chapter three details the various results and discussions on the different aspects of the simulation of aluminium extrusion with metal forming software. This includes different finite element formulations and constitutive equations. The chapter also covers the issue of discretisation and friction models as well as heat transfer and the prediction of substructure and properties.

The following chapter details the thermo-mechanical simulations of Conform. In this section the metal forming code is validated against experimental work and the use of scaling is investigated. The influence of the coining roll on the feedstock is also studied. Finally, the results from two simulations of Conform extrusion (with and without flash) are discussed.

Chapter five is comprised of two main studies: the expansion chamber in Conform and the feeder plate in normal extrusion. The expansion chamber is investigated both in plane strain and three-dimension. The use of feeder plates is investigated by comparing forward extrusion with and without the plate. Results such as temperature, velocity profile, microstructure and pressure distribution are discussed. A section of this chapter describes the simulation of microstructure in aluminium extrusion and its integration into a metal forming software.

Chapter six covers the tooling used in Conform. In the first part of this chapter the structural integrity of the wheel is studied using boundary conditions from an estimated linear static load. The second part of this chapter makes use of the Taguchi method to look in more detail at the influence of die profile on the initiation of surface cracks and subgrain size.

The final chapter provides the reader with a summary of the main findings of this thesis and points towards the future work recommended by the author for the study and use of Conform and finite element modelling software.

2 Literature Review

2.1 Mechanics of hot extrusion of aluminium alloys

The conventional extrusion process of aluminium alloys is complex and has been extensively studied. A relatively small amount of literature has been published regarding hot extrusion using the Conform process. However both forming processes share similar characteristics, such as high temperature, high strain rate and interaction of the aluminium alloy with the tooling. Therefore, the literature regarding conventional extrusion can be utilised to explain some of the phenomena occurring in Conform.

2.1.1 Plastic deformation and material flow

2.1.1.1 Direct Extrusion

The flow of aluminium in conventional extrusions has been described at length over the last four decades. Researchers have used several methodologies to study the material flow, from the use of modelling clay (Valberg 1988), gridded billet (Valberg and Malvik 1996; Thackray *et al* 2000), mixture of material billet with discs and/or pegs (Finkelnburg and Scharf 1992, Grasmo *et al* 1992), photomacrograph (Castle 1976, p.202-207; Clode 1992a) and finite element modelling (FEM) (Mooi *et al* 1996; Kusiak *et al* 1996, Chanda *et al* 2001, Sano *et al* 2004; Velay *et al* 2004).

In unlubricated direct extrusion the material is first upset (compressed) in order to fill the clearance between the container and the billet. Then a rapid flow of the central core of the billet towards the die is observed. The peripheral parts of the billet remain stationary because of the sticking friction along the container wall. In combination with friction on the die face this leads to the development of dead metal zones (DMZ). The surfaces of the extrudate are generated from the interior of the billet. The stationary billet surface layers combined with the rapidly flowing central

material produces a flow imbalance in the centre near the pressure pad. Metal from the peripheral zone is pulled to the centre. The potential back-end defect created by this inverse flow can be avoided with an appropriate discard of the end-billet. This was described by Parson *et al* (1992) and simulated by Hou *et al* (2000).

2.1.1.2 Conform extrusion

Different approaches, such as photomacrograph (Sinha and Chia 1988), coloured clays (Carr *et al.* 1996), analytical models (Maddock 2000) and numerical models (Velay and Sheppard 2000a and Manninen *et al* 2002), have been used in order to investigate the deformation and flow of materials during the Conform extrusion. These techniques, although very valuable for the understanding of the complex plastic flow, have limitations. As with indirect extrusion, the Conform process involves severe thermomechanical deformation of the aluminium. The flow of the material during the continuous extrusion is distinctly inhomogeneous and three different stages of deformation can be identified (see Figure 2.1).

The first deformation occurs just after the coining roll, where the round section of the feedstock is pushed into the square (or U shape) section of the groove. This small deformation produces an interference fit at the groove walls and generates the primary grip length (see Figure A.2a in Appendix A). There is a net tangential force applied to the abutment as a result of the wheel torque acting on the initial grip length. This reaction force triggers the second stage of deformation.

The tangential force must be sufficient to overcome the yield strength of the aluminium rod in order to upset the feedstock, fill the chamber (delimited by the groove and the shoe), and produce the upset zone (see Figure A.2b in Appendix A). In the second stage, the flow component is perpendicular to the shoe and is greater in the region of the entrance of the die than in the centre of the groove.

Finally, once steady state extrusion is achieved, dead metal zones are created at the die face closest to the abutment and at the upper apex of the die entry (half-teardrop shape). This suggests that the material at the lower entrance is strained to a greater extent than that in the upper entrance. Therefore the flow at the entrance of the die is imbalanced and the extrudate could curve upwards. There is no effective sealing between the wheel, the abutment and the shoe. Thus, the wheel-abutment and wheel-shoe clearances produce a thin strip of material called flash. Holton Machinery Ltd has improved the tooling so that for aluminium conductor profiles the flash over a

properly set machine will be nil (Bridgewater and Maddock 1992) or actively controlled (Khawaja *et al* 2000).

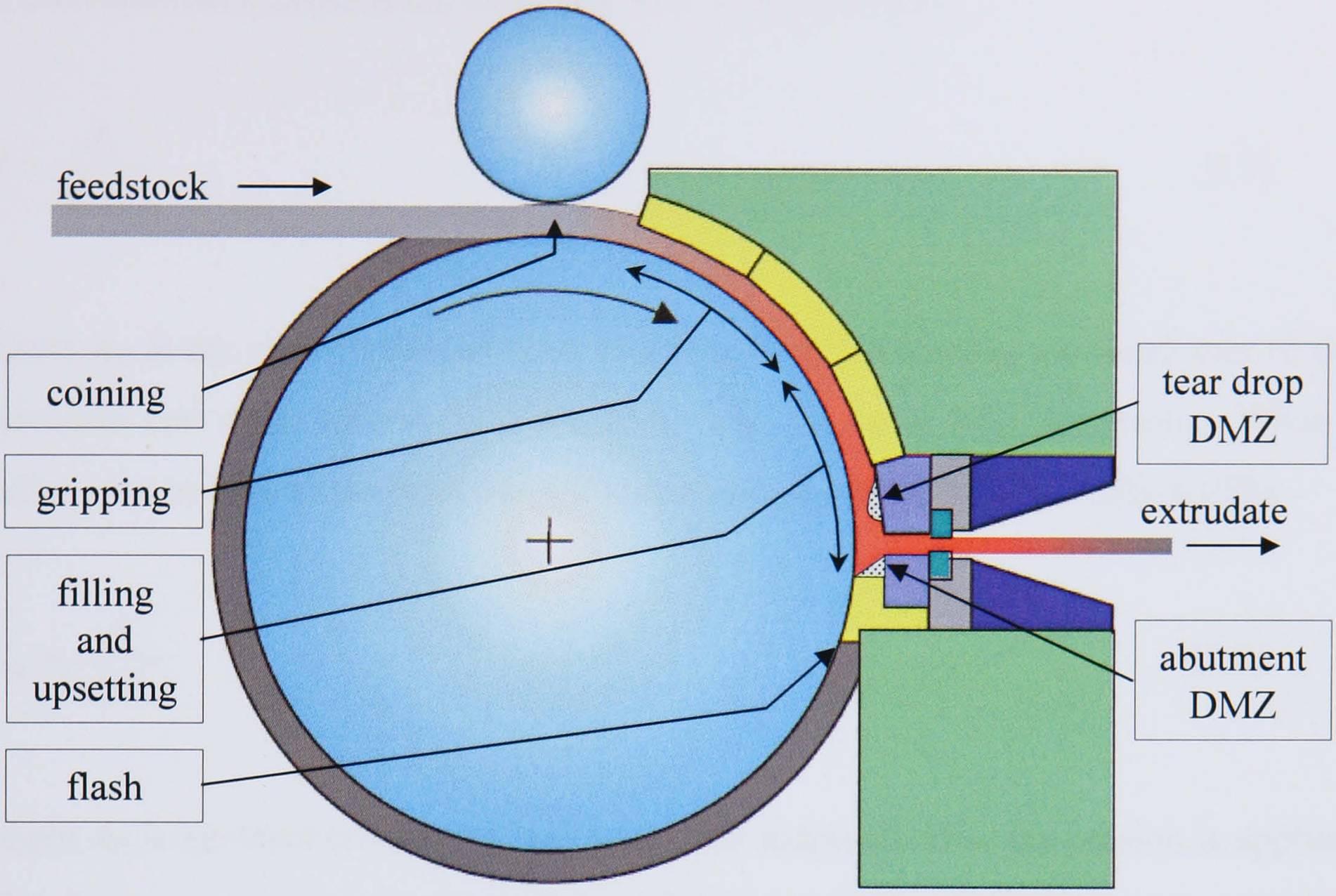

Figure 2.1 Schematic of the flow in Conform

Figure 2.1 provides a schematic representation of the dead metal zones. More detailed information regarding the shape of these DMZs can be seen in Figure 4.33 in section 4.6.4.

As in conventional extrusion (Saha 2000, p.7), the metal flow in Conform is influenced by many factors:

- the type of aluminium alloy,
- the tribology (mostly friction) between the material and the tooling,
- the temperature of the feedstock and the tooling,
- the diameter of the feedstock bar,
- the shape and size of the groove,
- the capacity of the motor / gearbox assembly,
- the wheel angular velocity,
- the type, layout, and design of the die,
- and the extrusion ratio.

2.1.2 Extrusion ratio

In conventional extrusion the extrusion ratio R is defined as:

$$R = \frac{A_C}{n(A_E)} \tag{2.1}$$

where A_C is the area of the container bore, A_E is the total cross sectional area of the extrudate and n the number of holes in the die (for multi hole extrusion). When a puller system is used the modified extrusion ratio R_m is used (Saha 2000, p.159):

$$R_m = \frac{A_C}{n(A_P)} \tag{2.2}$$

where A_P is the final cross sectional area of the extrudate after the tension is applied. The R terms are extensively used in valid theoretical calculations (e.g. pressure, temperature, deformation zones, limit diagram, etc.).

The same expressions would not hold the same validity in the Conform extrusion. In some cases the value can be close to or even less than 1. This could make the term $ln(R)$ a negative value. Parkinson (1988) defined the extrusion ratio for Conform R_c as:

$$R_c = \frac{A_F}{A_E} \tag{2.3}$$

where A_F is the cross sectional area of the feedstock. Obviously the term R_c could be redefined for twin groove Conform systems (Molyneux 1988) and for the double orifice die design (White 1987, p.44).

In both extrusion processes there is a limiting ratio, above which extrusion cannot be achieved because of insufficient pressure. With containers up to 300mm in diameter for large presses (4000 tons) this limiting ratio could be in the region of 1000:1 for conventional extrusion. However, the normal extrusion ratio range in industry practice for soft alloys is from 10:1 to 100:1. Whereas, the limiting ratio for

Conform is nearer 30:1 with feedstock up to 30mm in diameter (400kW machine and 500mm diameter wheel).

2.1.3 Plastic strain and strain rate

The natural strain (or effective strain), $\bar{\varepsilon}$, obtained by integration is a logarithmic function. Therefore, the effective strain in direct extrusion is usually approximated as the fractional cross-sectional area and is defined as follows:

$$\bar{\varepsilon} = \ln \frac{A_C}{A_E} = \ln R \tag{2.4}$$

where A_C is the cross sectional area of the container bore and A_E is the cross sectional area of the extrudate. It is worth noting that when the extrusion ratio is low, the amount of plastic strain is also low. Thus the amount of work done during the extrusion will be less. Therefore, the structure of the extrudate will be similar to that of cast aluminium (i.e. coarse grain) and the mechanical and physical property specifications will be compromised.

It is very difficult to determine the strain rate due to the complex flow pattern in the deformation zone. The material undergoes a rapid acceleration as it passes through the deformation zone. Therefore, a mean equivalent strain rate, $\dot{\bar{\varepsilon}}$, has to be estimated for determination of the flow stress. The original proposal by Feltham (1956 cited Sheppard 1999a, p.28) defined the mean equivalent strain rate as:

$$\dot{\bar{\varepsilon}} = \frac{6 D_C^2 V_R \ln R}{D_C^3 - D_E^3} \tag{2.5}$$

where V_R is the ram speed. Feltham assumed that the deformation occurs in a cone of semi-angle 45°. Tutcher (1979, p.75 and 174) noted that in practice the cone angle varied with the extrusion ratio. After extensive optimisation of the upper band solution, Tutcher suggested the following equation for the mean equivalent strain rate:

$$\dot{\bar{\varepsilon}} = \frac{6D_C^2 V_R (a + b\ln R)(c + d\tan\omega)}{D_C^3 - D_E^3} \tag{2.6}$$

where a, b, c and d are constants and ω is the deformation cone semi-angle with $\omega = i + j\ln R$, where i and j are also constants.

In Conform the determination of the strain and strain rates are too difficult because of the complex flow pattern in the groove, at the abutment and in the die. Furthermore the flow is non-axisymmetric and two different dead metal zones are developed. Carr *et al* (1996) observed that the material in the lower half of the extrudate had clearly been strained to a greater extent than that in the upper half. The minimum strain was not found on the axis of extrusion (as in conventional extrusion), but in an area inside the top portion of the extrudate. By using transverse sections of the product, Carr *et al* demonstrated that the amount of strained material in the extrudate increases with both proximity to the lower surface and distance from the nose (i.e. beginning of the extrusion). Highly strained material also forms a thin surface layer on the upper surface of the extrudate. This layer has been formed from material carried from the tear-drop dead-metal zone. Thus the entire surface of the extrudate is formed from material that has undergone severe deformation. Although Carr *et al's* investigation did not take account of the thermal effects, their findings correlate well with the thermomechanical simulations of the 2D and 3D strains performed by Kim *et al* (2000), and Velay and Sheppard (2000a).

2.1.4 Friction

Friction in aluminium extrusion is a complex and still not fully understood phenomenon. The environment of hot extrusion (i.e. high pressure, high temperature and material flow) prevents efficient experimentation of the frictional interfaces. However, it is well understood that friction determines the billet size (Sheppard 1999a, p.48) and that due to sticking friction the surface of the extrudate is smooth and reflective because its surface is formed by shearing inside the body of the billet. The Conform process makes effective use of the frictional force both to feed the rod to a die entrance and to generate the necessary extrusion pressure. The temperature distribution depends heavily on the frictional heat flux generated at the interfaces

between the tooling and the material. Temperature increases also occur due to intermetallic friction at the dead metal zone interface.

Generally the direct hot extrusion of aluminium alloys is performed without any lubricant. However a small amount of graphite based grease is sometimes used on the face of the die and dummy block (Sheppard 1999a, p.10). If lubricant is used on the surface of the container it could become washed in below the extrudate surface during extrusion. This can lead to surface lamination and blistering (Schey 1983, p.109-110). In Conform it is essential that the feedstock be free from dust, oil, grease and other organic contaminants if quality extrusions are to be produced. In this study only unlubricated extrusions will be considered.

2.1.4.1 Friction in direct extrusion

In direct extrusion (with a flat die) the friction occurs at four interfaces: (a) container-billet, (b) die bearing-material, (c) dead metal zone-material, and (d) dummy block-billet.

Container-billet interface

In most analyses the surface areas of the container and the billet are considered as being perfectly smooth. In reality those surfaces have a relative roughness made of a series of asperities. At the beginning of the extrusion the billet is upset in the container and the surfaces make first contact only at the highest point of the asperities (summits). Consequently due to increasing pressure the contact area is increased. The asperities start to deform and the concentrated mechanical energy required to overcome frictional resistance is converted into heat energy. The concentration of heat and pressure at the asperities raises their temperature above their melting point and accounts for the formation of welded junctions. This eventually leads to sticking friction between the container and the billet and extrusion proceeds by shearing along the container wall. The thickness of the shearing layer is between 40 to 100μm (Sheppard 1999a, p.49; Jowett *et al* 2000a).

Die bearing-material interface

Friction in the die land contributes to the surface quality of the extrusion (Saha 2004). The friction at the die bearing also contributes to the temperature distribution throughout the cross section of the extrusion profile. Therefore, friction is one of the factors influencing recrystallization in the outer band of the extrudate (Saha 2000, p50). Valberg (1996) and Moe *et al* (2003) showed that during extrusion sticking

friction is established in the inlet portion whilst sliding friction occurs towards the outlet of a choked die channel. Abtahi *et al* (1996), Valberg and Pohl (2002), and Saha (2004) developed friction models as a result of their experimental and simulation works. These models defined two regions: a sticking region with constant friction and a slipping region. Abtahi *et al* found that the friction varies according to different die angles.

Dead metal zone-material interface

Friction significantly influences the material flow and it is one of the parameters which defines the dead metal zone semi-angle (Saha 2000, p.8). At the dead metal zone-material interface the material experiences intermetallic friction.

Dummy block-billet interface

Due to a relatively small flow of material and the shearing of the discard, the dummy block-billet interface does not significantly influence the extrusion process.

2.1.4.2 Friction in Conform extrusion

In Conform the friction is complex and it occurs at five interfaces: (a) feedstock-wheel groove, (b) feedstock-shoe, (c) feedstock-abutment, (e) die bearing-material, and (f) flash-tooling (wheel + shoe + abutment). The interfaces (a) and (b) can be divided into three sub-interfaces: (1) biting, (2) upsetting and (3) filling. However in the steady-state process, the energy required for the biting and the upsetting are relatively smaller than those for the other interfaces so that the effects of theses sub-interfaces can be neglected without a significant loss of accuracy (Kim *et al*, 2000). The friction interface between the coining roll and the feedstock can be ignored as the coefficient of rolling friction is expected to be low.

Feedstock-wheel groove interface

The feedstock flows along the circular path of the groove by friction force until it reaches the abutment. Carr *et al* (1996) demonstrated a transverse flow component perpendicular to the shoe with a maximum intensity in the region of the die. They also showed a small region of shear at the abutment near the bottom of the groove. The relatively small area of shear suggests that its effect on the pressure is negligible. Cho and Jeong (2000) demonstrated, with a parametric investigation, that the friction coefficient influences the separation between the material and the wheel (opposite of the die exit) leading to surface defects. These findings suggest that at steady-state, the friction at the upper part of the upset zone is quasi-static (i.e. the feedstock moves

together with the wheel). The friction then fades away when the material reaches the lower part of the upset zone (opposite to the die entrance).

Feedstock-shoe interface

Carr *et al* (1996) suggested that the deformed feedstock initially sticks to the shoe, when first coming into contact with it, but soon begins to slide (kinetic friction). The formation of a dead metal zone (half-teardrop shape) at the upper apex of the die entry on the die/shoe face was also observed. Kim *et al* (2000) achieved good results by using sticking friction (i.e. m=0.95) to model the shoe interface. These results imply that friction interface between the feedstock and the shoe experiences a combination of kinetic friction (at the beginning of the grip length), sticking friction, and intermetallic friction (at the upper apex of the die entry).

Feedstock-abutment interface

Experiments by Tomimatu *et al* (1999) and Carr *et al* (1996) showed the formation of a dead metal zone at the abutment, starting from the side of the wheel up to the bottom of the die entrance. Therefore, the feedstock-abutment interface experiences intermetallic friction (shear of the material).

Die bearing-material interface

The type of friction at the die land is similar to that of conventional extrusion. However, there is a difference of pressure, flow velocity and temperature between the upper part and the lower part of the die land. Therefore, one can expect different friction coefficients (Beherens and Schafstall 1999).

Flash-tooling interface

This interface can be divided into two zones (see figure 2.2). Zone 1 is defined by the gap between the wheel groove and the abutment. Part of the material is virtually extruded through this gap. However, due to the relative affinity between the aluminium and the tool steel, this extrusion stays in the groove and therefore creates a 'seal' after the first few revolutions of the wheel (Khawaja *et al* 2000). The pressure inside the groove (at the top face of the abutment) is equal to the extrusion pressure, but at the bottom of the abutment it is equal to the atmospheric pressure. This suggests that the friction on the side face of the abutment varies from a maximum value (sticking) at the top to a zero value at the bottom. Zone 2 is created due to the dynamic gap between the shoe and the wheel. The material leaks through this gap and will eventually create the flash. As with zone 1, the friction interface between the flash and the shoe will vary from a maximum value (sticking) to zero.

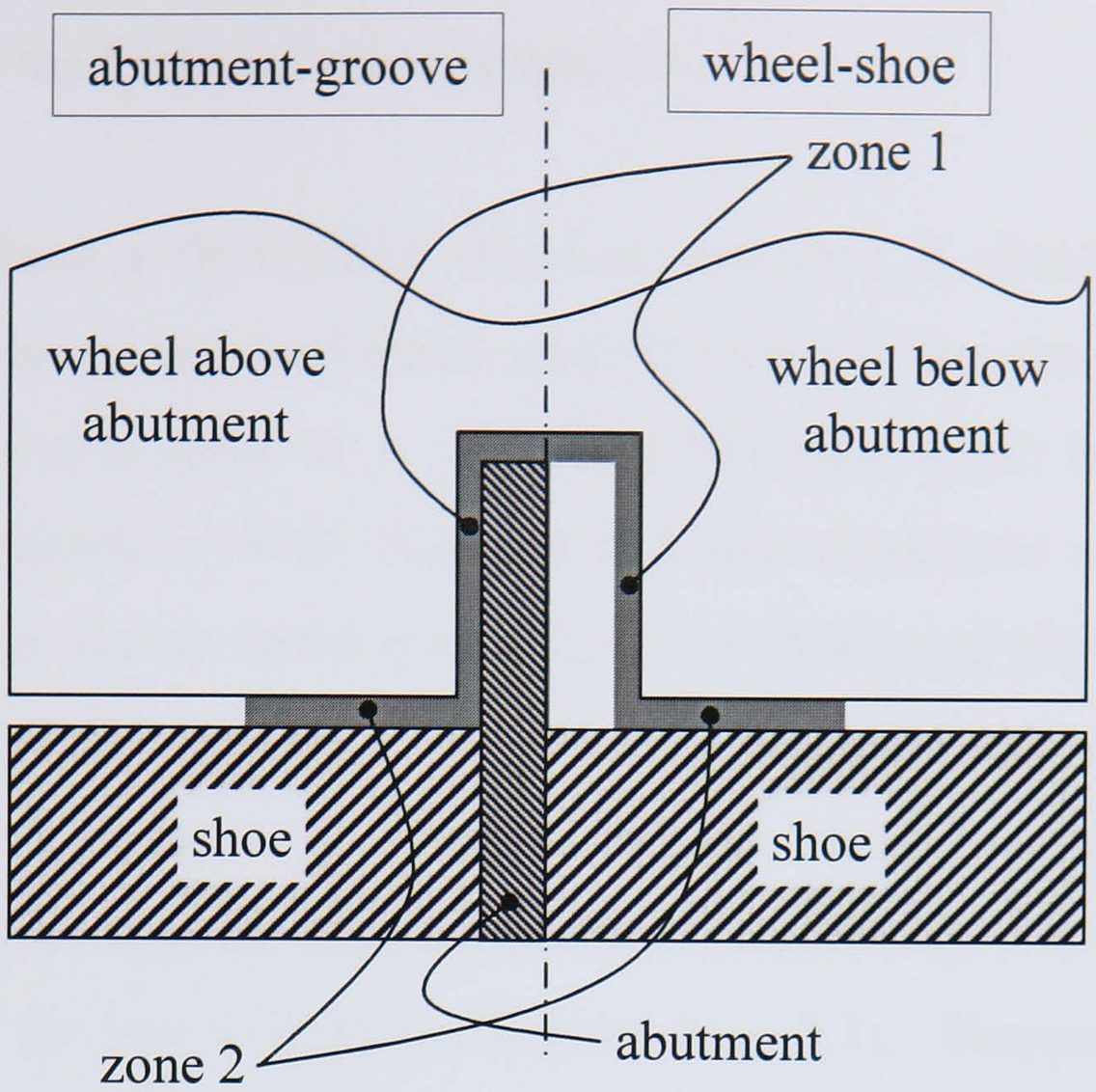

Figure 2.2 Friction interfaces abutment-groove and wheel-shoe

2.1.4.3 Theoretical work

The simple law below, developed empirically by both Coulomb and Amonton, is widely used. It states that the friction stress, τ_F, is proportional to the normal stress (or pressure), σ_N:

$$\tau_F = \mu \sigma_N \tag{2.7}$$

where μ is a constant friction coefficient. If this model is used in the case of very high normal pressures (e.g. in extrusion), then τ_F exceeds the Tresca equivalent yield stress, τ_0. This condition is physically impossible because the friction cannot exceed the shear strength of the material. Wagoner and Chenot (1997, p.317-318) described a Coulomb friction for low pressure, a modified sticking friction for high pressure, and a transitional friction in between. Therefore, τ_F, sometimes called the Tresca friction law, must be limited as follows:

$$\tau_F \leq m\tau_0 \text{ with } \tau_0 = \frac{\sigma_0}{\sqrt{3}} \tag{2.8}$$

where σ_0 is the equivalent von Mises yield stress and m the friction factor (sometimes called the frictional shear parameter).

Friction factor m

Usually m=0 defines a frictionless interface and m=1 a sticking friction. The intermetallic friction (at the dead metal zone) is no more than the shear stress of the material, therefore m is equal to 1. By using FEM and upper bound formulation, Azarkhin and Richmond (1992) demonstrated that conditions of sticking do not always generate the friction factor m=1. Kim *et al* (2000) and Cho and Jeong (2000) both showed that $0.90 \le m \le 0.95$ (for sticking friction) and m=0.3 (for sliding friction) are suitable for the simulation of Conform. Throughout this thesis a limited Tresca formulation is used for high friction coefficients (e.g. 0.9) whilst a Coulomb definition is used for low friction coefficients (e.g. 0.3). Sheppard (1999a, p.144) observed through experiments that m varies between 0.8 and 0.9. Thackray *et al* (2000) listed the variation in m, from 0.70 to 0.92, for different alloys at different temperatures.

From previous research it is clear that the friction factor depends on the interface profile, the rate and type of subsurface deformation, and the boundary conditions outside the subsurface. Beherens and Schafstall (1999) derived a function for the m factor with the use of neural network. The input for this was a combination of experimental work and finite element simulation of a ring compression test. The resultant output for m was shown as:

$$m = f(\sigma_N, v_{rel}, T, \varphi) \tag{2.9}$$

where v_{rel} is the sliding velocity, T is the temperature and φ is the plastic strain. The model shows that m increases with the contact pressure and decreases with the sliding velocity. More recently Flitta and Sheppard (2003) derived a function for m using an axisymmetrical finite element model:

$$m = A_m \alpha n \ln(Z_d / A) + B_m \tag{2.10}$$

where A_m and B_m are fitting parameters; α, n and A are material constants; and Z_d is an averaged temperature compensated strain rate. Although the model provides good

correlation with experimental results, the value of Z_d has only been calculated over a relatively arbitrary rectangular area at the die entrance. For greater accuracy Z_d could be calculated over an area defined by a significant level of strain rate.

Bochmann and Doege (1992), and Hu *et al* (1999) investigated the influence of frictional interfaces by modelling the asperities of the die and/or the workpiece surfaces. In both cases a very fine mesh was used to represent the asperities as a regular triangular shape. It was found that the asperities on the die land have more influence on the deformation than those on the workpiece surface. These results confirm the necessity for polishing the die land.

2.1.5 Extrusion pressure

2.1.5.1 Pressure in direct extrusion

The study of pressure during aluminium extrusion has been extensively reported. The pressure required for the process is the principal consideration in the selection of an extrusion press. The pressure can vary depending on: the alloy and its condition, the extrusion ratio, diameter and length of the billet, temperature of the billet and tooling, ram speed and the shape of the extrudate.

An early estimation of the extrusion pressure, p, was suggested by Siebel and Fangmeir (1931 cited Sheppard 1999a, p.29) in the form of:

$$p = \bar{\sigma} \ln R \tag{2.11}$$

where $\bar{\sigma}$ is the equivalent stress. Unfortunately, this equation underestimates the real extrusion pressure by about 60%. It does not take account the friction, the redundant work and the peak pressure. It is now generally accepted that the extrusion pressure (or the pressure exerted on the ram), p, can be divided into four parts as follows (Sheppard 1999a, p.143-144; and Saha 2000, p.16-19):

$$p = p_D + p_F + p_{RW} + p_B \tag{2.12}$$

where p_D is the pressure required for the plastic deformation of the billet, which is given in the functional form as:

$$p_D = f(\bar{\sigma}, \bar{\varepsilon}) \tag{2.13}$$

where $\bar{\varepsilon}$ is the mean equivalent strain and the flow stress, $\bar{\sigma}$, is defined by:

$$\bar{\sigma} = f(\bar{\varepsilon}, \dot{\bar{\varepsilon}}, T, S_i, P_i) \tag{2.14}$$

where T is the temperature. S_i are the state variables such as grain and subgrain size, stacking fault energy (SFE) and thermomechanical history. P_i are the material properties invariant such as the elastic modulus and the crystal structure. It is important to recognize that S_i also depends on T, $\bar{\sigma}$, $\bar{\varepsilon}$ and $\dot{\bar{\varepsilon}}$.

The pressure p_F is required to overcome the friction mainly at the container wall, the die bearing and the dead metal zone-material interfaces. It is given in the functional form:

$$p_F = f(p_r, m', m'', m''', D_C, L, L', \omega) \tag{2.15}$$

where p_r is the radial pressure, m', m'', m''' are the friction factor at the container-billet, die bearing-material, and dead metal zone-material interfaces, respectively. L is the billet length, L' is the die bearing length (for a solid die) and ω is the semi-dead metal zone angle as a function of the extrusion ratio (see Eq. 2.6).

The pressure p_{RW} is required to compensate redundant or internal deformation work (i.e. forces not directly contributing to the shape change such as the shear forces which occur over much of the cross section of the extrudate). It is given in the functional form:

$$p_{RW} = f(\bar{\sigma}, \omega) \tag{2.16}$$

The pressure p_B is required to overcome the higher number of dislocation density present in the billet before steady-state extrusion is reached (Castle and Sheppard 1976). Therefore, p_B can be written as follows:

$$p_B = f(S_i, P_i) \tag{2.17}$$

From experimental observations and numerical analysis the following formulae can be derived (Sheppard 1999a, p.29; and Saha 2000, p.20-21):

$$p = \bar{\sigma}(a + b\ln R + cL) \tag{2.18}$$

where a is the contribution to the redundant work, b is linked to the semi-dead metal zone angle and c is dependent of the friction coefficients.

Further work by Sheppard (1993) demonstrated the importance of the shape of the extruded product on the extrusion pressure. Therefore the peripheral ratio parameter, λ, was introduced into the pressure equation.

In summary, there are certain interrelations between extrusion pressures, extrusion temperatures, extrusion ratios and ram velocity:

- increase in temperature of the billet reduces the pressure required,
- the higher the extrusion ratio, the higher the extrusion pressure,
- the greater the billet length, the higher the extrusion pressure.

2.1.5.2 Pressure in Conform extrusion

To date very little has been published about the study of extrusion pressure in the Conform process. In publications authors usually refer to the original studies of Green (1972), Etherington (1977a and 1977b) or Gorokhov *et al* (1987 cited Carr *et al* 1996). In all analyses of the mechanics of Conform the important parameters to begin extrusion are primarily the initial grip and the upset zone lengths (see Figure A.1 in Appendix A). These dimensions are directly involved with the friction forces which will eventually create sufficient pressure for extrusion to commence. The lengths are dependent on tool geometry, friction coefficients, material properties and pressure. Plane strain upper bound analyses have been developed by White (1987, p.76-81) and more recently by Kim *et al* (2000). Unfortunately, the deformations present in the Conform process are neither plane strain nor axisymmetric. Therefore, such analyses give limited accuracy.

Both Green and Etherington developed a relationship between the extrusion pressure, p, the length of the initial grip, l_i, and the length of the upset zone necessary for

extrusion to start, l_u (see Figure A.1 in Appendix A). The full demonstration of that relationship is detailed in Appendix A and can be expressed as follows:

$$l_i + l_u = w\left(\frac{2}{\mu} + \frac{p}{\sigma_{cys}}\right) \tag{2.19}$$

where w is the groove width, μ is the coefficient of friction between the groove wall and the feedstock, and σ_{cys} is the compressive yield stress of the feedstock. The extrusion pressure may be determined from general expressions used in conventional extrusion analysis, such as:

$$p = a + b\bar{\sigma}\ln R_{mc} \tag{2.20}$$

where a and b are the contribution to the redundant work and die friction, $\bar{\sigma}$ is the flow stress of the material, and R_{mc} is the modified extrusion ratio for Conform. It is assumed that $R_{mc} = w^2/A_E$ where A_E is the cross sectional area of the extrudate.

Gorokhov *et al* presented a more accurate approach by defining both the angles described by the initial grip, ϕ_i, and the upset zones, ϕ_u (see Figure A.1 in Appendix A). These angles are dependent on friction forces, tool geometries, friction coefficients and material properties. The following equations are derived in detail in Appendix A.

$$\phi_u = \frac{(F + F_d)}{2\mu_u \bar{\sigma}_u w r_g} \tag{2.21}$$

$$\phi_i = \frac{w^2}{2\mu_i x r_g} \tag{2.22}$$

where F is the force required for the extrusion to occur, F_d is the frictional force with the die surface(s), r_g is the radius of the wheel at the groove base, x is the initial contact with the groove wall, μ_u and μ_i are the coefficient of friction between the

groove wall and the feedstock in the upset zone and in the grip length, respectively, and $\bar{\sigma}_u$ is the mean compressive yield strength of the feedstock in the upset zone.

In summary the extrusion pressure in Conform is initiated by the initial grip and upset zone lengths (i.e. the position of the coining roll) and the friction forces (i.e. the wheel rotational velocity and the torque). The torque, T, that must be delivered by the wheel can be determined from:

$$T = F_f r_g \tag{2.23}$$

where F_f is the total frictional force acting toward the abutment (see Appendix A). Thus the corresponding power requirement, P, will be

$$P = \omega T \tag{2.24}$$

where ω is the angular velocity of the wheel.

2.1.6 Heat transfer

Heat transfer is one of the most important phenomena to consider in extrusion as it defines the temperature parameter. This is one of the process variables which can be controlled. Temperature rise and distribution in conventional extrusion have been investigated by many researchers (Lefstad 1988; Pham 1992; Castle 1992; Saha 1996; Libura *et al* 2000; Barron and Larrick 2004) but very little has been published for Conform extrusion (Tomimatu *et al* 1999; Velay and Sheppard 2000a; Maddock 2000). In general it has been shown that variations in temperature are mainly due to the extrusion ratio and ram speed (or wheel speed). The flow stress and therefore the pressure can be reduced if the temperature is increased. However there is a risk of localised incipient melting with high ram velocity.

2.1.6.1 Overall heat transfer

During the overall process heat generation and heat transfer occur in six successive stages which are all interdependent.

Homogenization

Cast billets (or logs) are usually homogenised before extrusion in order to improve their workability. Feedstock, essentially cast rods, are also homogenised (Parkinson, 1988). This heat treatment process partially or completely eliminates undesirable metallurgical effects such as coarse precipitation and dendritic cell segregation, supersaturated solutions of finely dispersed precipitates, and heterogeneous grain and cell boundary precipitation (Jackson and Sheppard, 1996; Saha 2000, p.136-139).

Pre-heat

Pre-heat is important in conventional extrusion to ensure that extrusion will occur, especially for high extrusion ratios. Taper heating or taper quenching billets are used for isothermal extrusion. The initial temperature(s) of the billet will influence the surface finish and structure of the extrudate. Thermal changes in the billet occur after its ejection from the billet heater and prior to the start of the extrusion. There is a small heat transfer from the billet due to convection to the atmosphere and conduction within the container. In Conform extrusion the feedstock is fed directly into the wheel groove with no pre-heating. The necessary heat for extrusion is developed from the friction forces. However, a small amount of heat is transferred to the feedstock before upsetting. This is due to the plastic deformation from coining and the thermal conduction from the wheel to the feedstock.

Extrusion

The heat transfer involved in both the container-die and groove-die volumes are detailed in section 2.1.6.2 and 2.1.6.3 respectively.

Exit

As the extrudate travels on the run-out table heat is lost through radiation, convection to air and quenching loss to water (press quenching), and conduction to the contact surfaces with the run-out table. The extrudate is usually in contact with graphite slats or steel rollers. The contact surfaces are small and so the conduction via the run-out table is assumed to be negligible (Pham 1992).

Stretching

In conventional extrusion the extruded length generally requires straightening. This is done by stretching the extrudate by 1 to 3% of its original length. Such deformation will generate a negligible amount of heat. The majority of profiles extruded by Conform are coiled on the line. Very precise speed control of the coiler is required, which must match the extrusion speed exactly to eliminate any form of

stretching of the relatively 'soft' just extruded profile at the die exit (Bridgewater and Maddock, 1996).

Solution treatment and ageing

The correct heat treatment of soft and medium grade aluminium alloy is important to obtain the required mechanical properties, such as hardness and strength. For all heat treatable aluminium, heat treatment is a two-stage process: solution heat treatment and precipitation hardening (ageing). The fundamental metallurgy behind solution heat treatment and ageing is to allow the hardening constituents into solid solution during solution treatment and subsequent precipitation during ageing (Cramlet *et al* 2000).

2.1.6.2 Heat balance in conventional extrusion

The heat generation and heat transfer that occur during the extrusion are critical because they define the exit temperature of the extrudate. The temperature of the aluminium just leaving the die is important for the product quality (heat treatment, dimensional stability and extrusion defects) and the die life (wear and performance). Castle (1992) and Sheppard (1999b) divided the heat balance between the following processes:

- heat generation due to plastic deformation,
- heat generation due to friction at the container-billet, dead metal zone-material and die land-material interfaces,
- and heat exchange between the billet and the tooling (container, pressure pad, die land).

Heat generation due to plastic deformation

Approximately 90-95% of the mechanical energy is transformed into heat. Therefore the heat generation rate due to deformation per unit of volume, $\dot{Q}_d$, can be written as follow:

$$\dot{Q}_d = \lambda \sigma \dot{\varepsilon} \tag{2.25}$$

where λ is the heat generation efficiency ($0.90 \leq \lambda \leq 0.95$).

Sheppard (1999b) reviewed the different methods available to calculate the temperature changes occurring during aluminium extrusion. The approximate

equations of Stüwe (1968 cited Sheppard 1999b) were introduce in Sheppard's technical note. Stüwe's equations for temperature increase due to deformation, friction at the billet surface, and friction at the die land surface are presented in equations (2.26), (2.27) and (2.28) respectively. Sheppard also introduced the integral profile approach for the analysis of temperature variations in extrusion. With this method the deformation zones are divided into control volumes from which significant heat flows are integrated. The integral profile method, which could be used in real time, proved to correlate relatively well with FEM and experimental results. It was shown that Stüwe's equations can overestimate the temperature rise due to die friction in AA 6063 by as much as 32%.

Stüwe defined the temperature increase due to deformation, ΔT_d as follows:

$$\Delta T_d = \frac{\bar{\sigma} \ln R}{\sqrt{3}\left(\rho_{Al} C_{p(Al)}\right)} \tag{2.26}$$

where ρ_{Al} is the aluminium density and $C_{p(Al)}$ is the specific heat of aluminium.

Heat generation due to container-billet frictional interface

It is assumed that shearing will occur along the boundary of the billet, and that heat transfer is divided equally and uniformly between the billet and the container. Therefore, according to Stüwe, the temperature increase due to friction at the billet surface, ΔT_{bf} , is:

$$\Delta T_{bf} = \frac{\bar{\sigma}}{4\sqrt{3}\left(\rho_{Al} C_{p(Al)}\right)} \sqrt{\frac{V_R L_B}{\alpha_{Al}}} \tag{2.27}$$

where L_B is the billet length, and α_{Al} is the thermal diffusivity.

Heat generation due to die land-material frictional interface

As with equation (2.27) Stüwe gives the following equation to determine the temperature increase due to friction at the die land surface, ΔT_{df} :

$$\Delta T_{df} = \frac{\bar{\sigma}}{4\sqrt{3}\left(\rho_{Al} C_{p(Al)}\right)} \sqrt{\frac{V_E L_D}{\alpha_{Al}}} \tag{2.28}$$

where L_D is the die land length and V_E is the exit speed of the extrudate.

Heat generation due to dead metal zone-material frictional interface

The speed of the flowing material, V_M, at the dead metal zone interface is approximately calculated from the relationship:

$$V_M = \frac{V_R}{\cos\omega} \tag{2.29}$$

where ω is the cone semi-angle of the dead metal zone. The contact length, L_M, is geometrically calculated as:

$$L_M = \frac{D_C - D_E}{2\sin\omega} \tag{2.30}$$

where D_C is the diameter of the container bore and D_E is the equivalent diameter of the extrudate. Therefore one can express the temperature increase due to friction at the dead metal zone, ΔT_{dmf}, as follows:

$$\Delta T_{dmf} = \frac{\bar{\sigma}}{4\sqrt{3}\left(\rho_{Al} C_{p(Al)}\right)}\sqrt{\frac{V_M L_M}{\alpha_{Al}}}$$

$$\Rightarrow \Delta T_{dmf} = \frac{\bar{\sigma}}{4\sqrt{3}\left(\rho_{Al} C_{p(Al)}\right)}\sqrt{\frac{V_R\left(D_C - D_E\right)}{\alpha_{Al}\sin 2\omega}} \tag{2.31}$$

Heat transfer between material and tooling

The heat transfers between the material and the tooling are governed by the law of conduction and convection (if cooling is present). Equations (2.32) and (2.33) represent the temperature gradient due to conduction, ΔT_{cond}, and convection, ΔT_{conv}, respectively.

$$\Delta T_{cond} = \dot{q}_{cond}\frac{d}{kA} \tag{2.32}$$

$$\Delta T_{conv} = \dot{q}_{conv} \frac{1}{h_c A} \tag{2.33}$$

where $\dot{q}_{cond}$ and $\dot{q}_{conv}$ are the rate of heat transfer due to conduction and convection respectively, k is the thermal conductivity, h_c is the convection heat transfer coefficient (film coefficient), A is the area of contact, and d is the thickness of the material through which conduction occurs. Although the thermal conductivity is dependant of the contact stress, in most analyses it is taken as a constant value (Caliskanoglu *et al* 2002).

2.1.6.3 Heat balance in Conform

In Conform extrusion the heat balance is similar to that of conventional extrusion. Heat is generated by the deformation of the feedstock and the different frictional interfaces. Heat is also transferred with conduction and convection. Figure 2.3 shows a flowchart of the heat transfer in Conform extrusion.

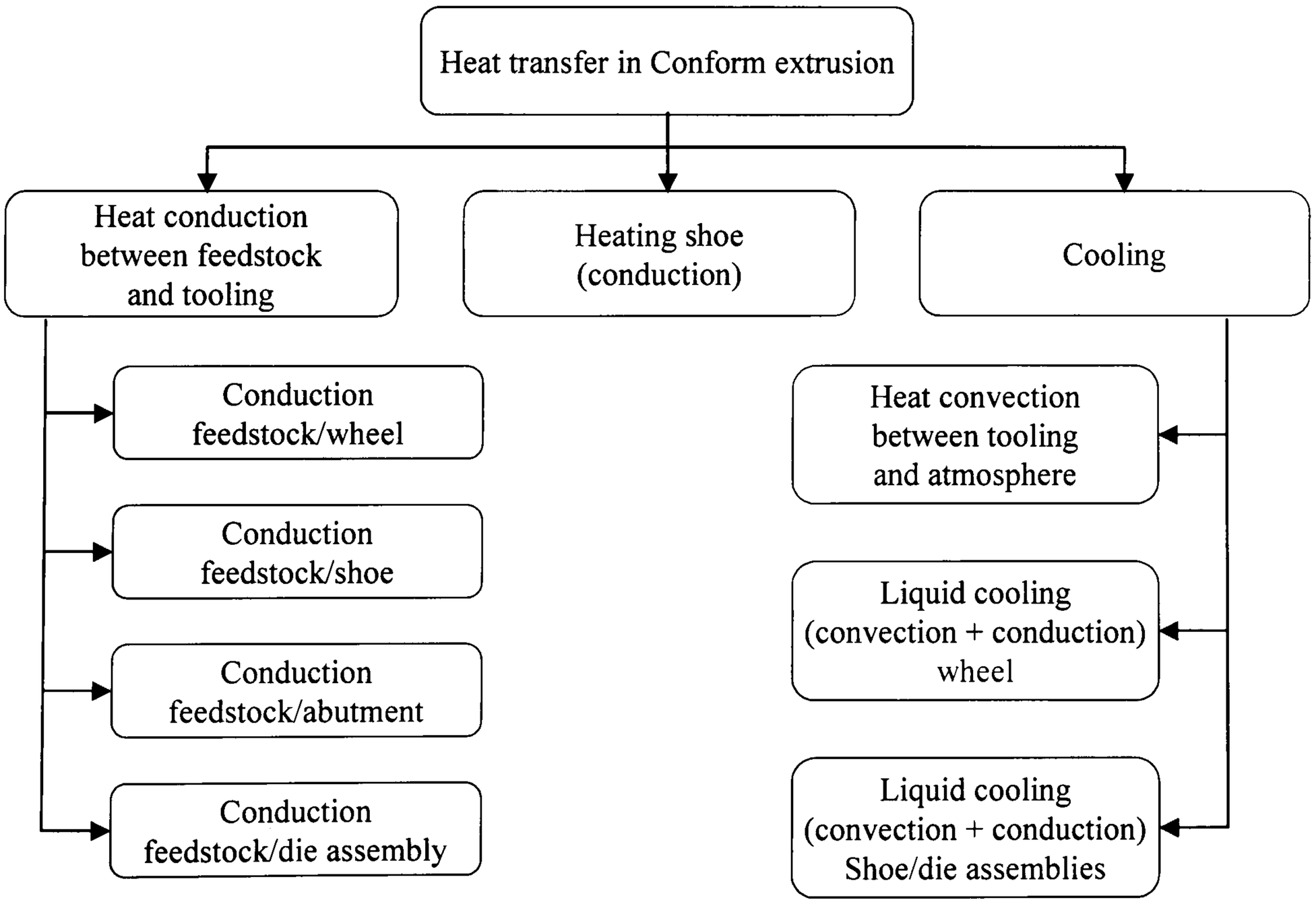

Figure 2.3 Heat transfer in Conform Extrusion

The temperature increase is highly dependant on the rotational velocity of the wheel. Tomimatu *et al* (1999) reinforced the importance of thermal management in Conform extrusion. They reported that there was lower quality extrudate and melting with high wheel velocity. The tooling is relatively small and cooled, which gives rise to an equilibrium temperature in the deformation zone (Parkinson 1988). Wheel cooling (Clode 1992b), die cooling (Tomimatu *et al* 1999) and shoe heating (Bridgewater and Maddock 1996) can be implemented to improve extrudate quality and therefore productivity.

2.2 Constitutive laws

2.2.1 Yield criterion

A yield criterion is a law which defines the limits of elasticity under any possible combination of stresses. It is expressed by:

$$f(\sigma_{ij}) = C \text{ (constant)} \tag{2.34}$$

where $f(\sigma_{ij})$ is called the yield function and σ_{ij} is defined by the Cauchy stress tensor (see Appendix B for more detail). For isotropic materials, such as aluminium alloys, plastic yielding can depend only on the magnitude of the three principal stresses $(\sigma_1, \sigma_2, \sigma_3)$ and not on their directions. Thus any yield criterion can be expressed as follows:

$$f(J_1, J_2, J_3) = C \text{ (constant)} \tag{2.35}$$

where J_1, J_2 and J_3 are the three invariants of the stress tensor σ_{ij} (see Appendix B for more detail). The first invariant $(J_1/3)$ represents the hydrostatic pressure. Although this pressure may increase ductility it does not contribute to deformation. For ductile materials, two different criteria are generally used. The Tresca criterion, which postulates that yielding will occur when the largest shear stress reaches a critical value, and the von Mises criterion which states that yielding will take place

when the second invariant J_2 reaches a critical value. The Tresca criterion provides a practical approximation of yielding, however, the von Mises criterion is usually preferred because it correlates better with experimental data. Both criteria are detailed in Appendix B.

2.2.2 Viscoplastic model

The theory of plasticity adequately describes materials with time-independent behaviour. However the theory of viscoplasticity more effectively defines the material behaviour which exhibits strain rate sensitivity such as in aluminium alloys. During hot extrusion the aluminium alloys properties can vary considerably with temperature. The workpiece (e.g. billet and extrudate) experiences temperature gradients. These temperature gradients are more severe within the feedstock in Conform extrusion. At elevated temperatures, plastic deformation can induce phase transformations and modifications to grain structures. These metallurgical changes can, in turn, modify the flow stress of the material as well as other mechanical properties. Thus, the flow stress, $\bar{\sigma}$, can be expressed as a function of temperature, strain, strain rate, and state variables (see equation 2.14). At very high temperatures $(< 0.9T_m)$, where T_m is the lowest melting point of the material, the influence of strain on flow stress is insignificant, and the influence of strain rate becomes increasingly important. Therefore $\bar{\sigma}$ can be expressed as follows:

$$\bar{\sigma} = f(\dot{\bar{\varepsilon}}, T, S_i, P_i) \tag{2.36}$$

The hot deformation of aluminium alloys is commonly described by the equations shown below (2.37 and 2.38). Initially proposed by Zener and Hollomon (1944 cited Wright *et al* 1996), later modified by Sellars and Tegart (1966 cited Shi *et al* 1997) and then subsequently modified again by Sheppard and Wright (1979). The flow stress is written:

$$\bar{\sigma} = \frac{1}{\alpha} \ln\left[\left(\frac{Z}{A}\right)^{\frac{1}{n}} + \sqrt{\left(\frac{Z}{A}\right)^{\frac{2}{n}} + 1}\right] \tag{2.37}$$

or

$$Z = A[\sinh(\alpha\bar{\sigma})]^n \tag{2.38}$$

where the parameters are defined as follows:

- α is the reciprocal flow stress. Garofalo (1963 cited Hertzberg 1996, p.169) and Ness *et al* (1994) showed that equation (2.37) reduces to a power law when $\alpha\bar{\sigma} < 0.8$ but approximates an exponential relationship when $\alpha\bar{\sigma} > 1.2$.
- n is the inverse of the temperature compensated strain rate sensitivity. It is strongly dependent on α (Sheppard and Jackson 1997).
- A is a constant sometimes termed as the structure factor. It measures the probability deformation occurrences at possible active sites.
- Z is the temperature compensated strain rate parameter also called the Zener-Hollomon parameter. It is given by equation (2.39) below.

$$Z = \dot{\bar{\varepsilon}} \exp\left(\frac{\Delta H}{GT}\right) \tag{2.39}$$

where T is the temperature, G is the universal gas constant (8.31451 $J.mol^{-1}.K^{-1}$), and ΔH is the activation energy for hot deformation. Hertzberg (1996, p.165-166) showed that the activation energy for creep in aluminium increases with temperature up to $T \approx 0.5T_m$ whereupon it remains constant up to the melting point. The constant ΔH at high temperature is equal in magnitude to the activation energy for self diffusion which is approximately 153000 $J.mol^{-1}$ (Sheppard and Jackson 1997).

To be useful in analyses, the flow stresses of alloys must be determined experimentally for the strain, strain rate, and temperature conditions that exist in hot extrusion processes. The most appropriate method, described by Sheppard and Jackson (1997) is the torsion test. It can achieve strain in excess of 20 compared to 0.3 and 2 with tension and compression tests respectively. Table 2.1 lists the flow stress data for both AA1100 and AA6063.

Alloy	α ($m^2.MN^{-1}$)	n -	ΔH ($J.mol^{-1}$)	G ($J.mol^{-1}.K^{-1}$)	$\ln A$ (s^{-1})
AA1100	0.045	5.660	158300	8.31451	24.67
AA6063	0.040	5.385	141550	8.31451	22.50

Table 2.1 Flow stress data (Sheppard and Jackson 1997)

Although the flow stress defined in equation (2.37) is widely used in aluminium extrusion, it does not take into account the evolution of the structure and its subsequent effects. Recently, Marthinsen and Nes (2001) developed a stress-strain relationship for face centred cubic (fcc) metals such as Al-Mg alloys. Their model is based on a statistical approach and it incorporates a general internal state variable description, based on dislocation storage, dynamic recovery of network dislocations, and sub-boundary structures. Effects from grain boundaries, elements in solid solution, and the presence of precipitate particles are also included. Thus the structure morphology of the extrudate may be predicted.

2.3 Quality of the extrudate

The quality of the extrudate can be measured by the degree of internal precision (substructure, grain size, metallurgical structure, precipitates, non-homogeneous metal flow, variation of structure across the extrudate, etc…), external defects (surface finish), geometrical tolerances and mechanical and physical properties. The latter are mostly dependent on the internal structural variations.

2.3.1 Internal defects

Internal defects due to metal flow

Berezhnoy *et al* (1999) studied internal defects caused by the metal flow. They divided the defects into three categories:

- coring, where the metal flows centrally from the dummy block towards the centre part of the extrudate,

- 'top side extrusion defect', where the billet surface near the dummy block flows into the die at some defined point during the extrusion,
- and 'low side extrusion defect', where the defect is created by some material flowing from the container wall to the die.

By optimising the temperature gradient between the billet and the tooling and by controlling the friction Berezhnoy *et al* demonstrated that these surface defects can be prevented. Such defects were also simulated with FEM software by both Thackray *et al* (2000) and Sheppard *et al* (2004).

Internal defects due to macrostructure

During hot deformation of crystals, lattice defects (edge, screw and mixed dislocations) move by different processes known as dislocation climb and cross-slip. Dislocations also multiply according to the Franck-Read source mechanism (Read 1953 cited Hertzberg 1996, p.85-86) and the dislocation density can reach values around 10^{14}-10^{15} dislocation/m^2. In metal with high staking fault energy (SFE), such as aluminium, the dislocation rearrangement process is relatively easy and accelerated. If the crystal contains both positive and negative edge dislocations lying on the same plane, their combination would result in mutual annihilation and the elimination of the two high energy regions of lattice distortion. If two dislocations are of the same sign they repel each other. Dislocations have a tendency to arrange themselves in walls which are roughly equispaced. These walls subsequently form subgrains with a much lower dislocation density (10^{8}-10^{10} dislocation/m^2). This process is termed dynamic recovery and prevents work-hardening during extrusion by balancing the rates of dislocation generation and annihilation. The resultant macrostructure influences the material properties of the extrudate.

Nes *et al* (1994) and Sheppard (1996) developed mathematical models to predict the substructure evolution and the recrystallization kinetics in aluminium rolling and extrusion, respectively. In subsequent work, Marthinsen and Nes (2001) included the effect of grain boundaries, constituent particles and dispersoids. Unfortunately the lack of information regarding strain and temperature distribution in the deformation zones of complex geometry (e.g. shaped bar extrusion), required the user to make assumptions of uniform and isothermal deformation in the extrusion process. Nowadays it is possible to use finite element models to calculate strains, strain rates, stresses and temperatures and subsequently predict the distribution of the

subgrain size, recrystallization kinetics, grain size distribution and other microstructural phenomena affecting the properties of the deformed material.

Furu *et al* (1996) implemented a recrystallization and grain size model into the commercial FEA software Forge 2. The model was validated against experimental work using an axisymmetric cold forward extrusion of AA6010 and AA6082. The FEM results correlated relatively well with the experimental work for the fraction recrystallized and the recrystallized grain size. The model did not include features regarding the nucleation and growth of recrystallization. Dashwood *et al* (1996) implemented a subgrain size model into the Forge 2 software. This empirical model used an average value of the temperature compensated strain rate parameter (Z) with respect to the strain at each node. A relatively good agreement was achieved between the experimental and predicted subgrain sizes. However, this was done at the expense of raising the value of the activation energy, ΔH, to 328kJ.mol^{-1}. The activation energy of aluminium alloys is considered to be a material property and this can vary from between 150 to 160 kJ.mol^{-1} for a 7-series aluminium alloy. Bhattacharyya *et al* (2001) integrated models of crystal plasticity with FEM to study the microstructure of aluminium at the grain-scale (i.e. modelling up to 21 grains with just under 2200 three-dimensional elements). When compared with orientation imaging microscopy (OIM) measurements it was found that the FE model predicted reasonably well the grain orientation produced by deformation. However, the FE model failed to capture the spatial distribution of misorientations. With today's current hardware capabilities, it would be virtually impossible to implement such a model for use with industrial extrusion.

Duan and Sheppard (2002a) incorporated modified physical models proposed by Sellars and Zhu (2000) into Forge 2 to predict three internal state variables: dislocation densities, subgrain size and misorientation between subgrains. Subsequently the values of the state variables were used to update the flow stress of the rolled aluminium at each time step using a model from Marthinsen and Nes (2001). The results from the FEM analyses showed reasonable agreement with experimental observations. Sheppard and Duan (2002b) continued their work on the simulation of rolling with Forge 2 by combining empirical microstructural models from the work of Vatne *et al* 2000. This enabled them to predict the distribution of the volume fraction recrystallized and the recrystallized grain size with aluminium

rolling. A very good correlation between the calculated and experimental results validated the process.

Duan and Sheppard (2003) applied their previous work, mentioned above, to the process of aluminium extrusion. The predicted values (in the two-dimensional domain) fitted well with experimental observations. Recently, both Peng and Sheppard (2004) and Duan *et al* (2004) simulated the metallurgical behaviour of aluminium alloys in hot extrusion in three-dimension (using Forge 3). A good correlation with experimental results was obtained. The author was involved with the work of Duan *et al* (2004) and details of this are shown in Section 5.3 of this thesis.

2.3.2 Surface quality

The visual appearance of extruded aluminium profiles is often very important for commercial products. Anodizing and painting do not always hide surface defects, on the contrary, they sometimes exaggerate them. Sheppard and Clode (1988) investigated the origin and formation of principal extrusion defects. This included pick-up and die lines and also the origin of micro die lines (0.5-2μm) for AA6063. The effects of temperature and temperature compensated strain rate were also established, together with the influence of the die land length and its surface finish. Parson *et al* (1996) studied the effect of die geometry and the role of the process variables (billet temperature and extrusion speed) on the surface quality. Ceretti *et al* (1999) and Sheppard *et al* (2004) simulated surface cracking defects by combining a damage criterion (Cockroft & Latham) with a finite element analysis, both using different two dimensional FEM software.

Sinha and Chia (1988) reported the formation of blisters at the die exit and during heat treatment on products extruded by Conform. They suggested that the main reasons for blistering were due to oil contamination (from the feedstock) and moisture (entrapped air due to high velocity of the wheel). The moisture can react with the newly exposed aluminium to form molecules of hydrogen according to the following reactions:

$$2Al + 3H_2O = Al_2O_3 + 3H_2 \tag{2.40}$$

The entrapped hydrogen expands due to heat and causes blisters on the surface. Similarly in conventional extrusion air can be entrapped in the container during upsetting and cause back-end and front-end blisters. Jowett *et al* (2004) considered the differing of billet-container clearance, temperature differential, and temperature tapers to reduce the air entrapment.

2.3.3 Geometrical tolerances

Based on both theoretical analyses and industrial tests of thin-wall extrusions, Zasadzinski *et al* (2000) found that a geometrical tolerance below 10% is virtually impossible. This work highlighted the importance of die design and manufacture for geometrical quality. Jowett *et al* (2000b) demonstrated that geometrical variations are not primarily due to mechanical deflection of the toolstack, but result from thermally induced distortions in the die. Thedja *et al* (1992), with the use of split die and X-ray micrograph, concluded that the frictional interface at the die land considerably influences both shape accuracy and surface quality of the extrudate. Tashiro *et al* (1992) performed experimental and industrial extrusions with different temperatures for the billet and die. The distortion and variations in the shape of the extrudate was recorded and it was found that these temperatures significantly influenced the geometry of the cross section. Halvorsen and Aukrust (2004) investigated the buckling and waving in fine strip extrusion. It was demonstrated that the flow imbalance created by the variations in feeder geometry can be accurately analysed by FEM techniques.

2.3.4 Mechanical and physical properties

Properties such as strength, electrical conductivity, hardness, fracture toughness, and corrosion resistance can be critical depending on the final application of the extruded product. Sheppard (2000) demonstrated that the mechanical properties of extruded aluminium alloys, such as proof stress, ultimate strength, and percentage of elongation, can be a function of $\ln(Z)$. Sheppard (1996), Parson *et al* (2004), Sweet *et al* (2004) and Van Geertruyden *et al* (2004) observed the formation of peripheral

coarse grain (PCG) in extrusion and suggested approaches to the control of the coarse grain surface layer. These findings suggest a variation of mechanical properties across the cross section of the extrudate due to PCG. Wang *et al* (2004) used FEM and electron backscatter diffraction (EBSD) to study the evolution of PCG. Their results suggested that at high temperatures unstable fine grains coarsen to form PCGs. Røyset *et al* (2004) developed a computer program (Almech) capable of predicting the mechanical properties and the extrudability of 6xxx alloys. The inference engine uses a large database derived from experiments. The prediction models take into account the amounts of undissolved Mg_2Si particles. More consistent mechanical and physical properties can be obtained with isothermal extrusion.

Etherington and Slater (1984) reported the mechanical and electrical properties of a wide variety of alloys in rod and powder form extruded with Conform. The properties were within or close to the required specifications for commercial products as they would be from conventional extrusion.

2.3.5 Limit diagram

Several variables (or combinations of these variables) can influence the occurrence of extrusion defects. These variables are the initial billet temperature and macrostructure, the container and die temperature, the extrusion ratio, the ram speed, the design of the die stack, and the exit temperature. However it is accepted that the quality of the extrudate is mainly influenced by the billet temperature and the speed of deformation (Sheppard 2000). Therefore, for any particular alloy a limit diagram can be generated in order to combine the optimum parameter for productivity. Figure 2.4 shows the limit diagram for AA6063 and the effect of common press variables. The optimum extrusion parameters, in terms of quality, are delineated by three zones: insufficient pressure, inadequate surface and inadequate mechanical properties. For this alloy the ultimate productivity is reached with a billet temperature of around 450°C and an extrusion speed of about $110 m.min^{-1}$.

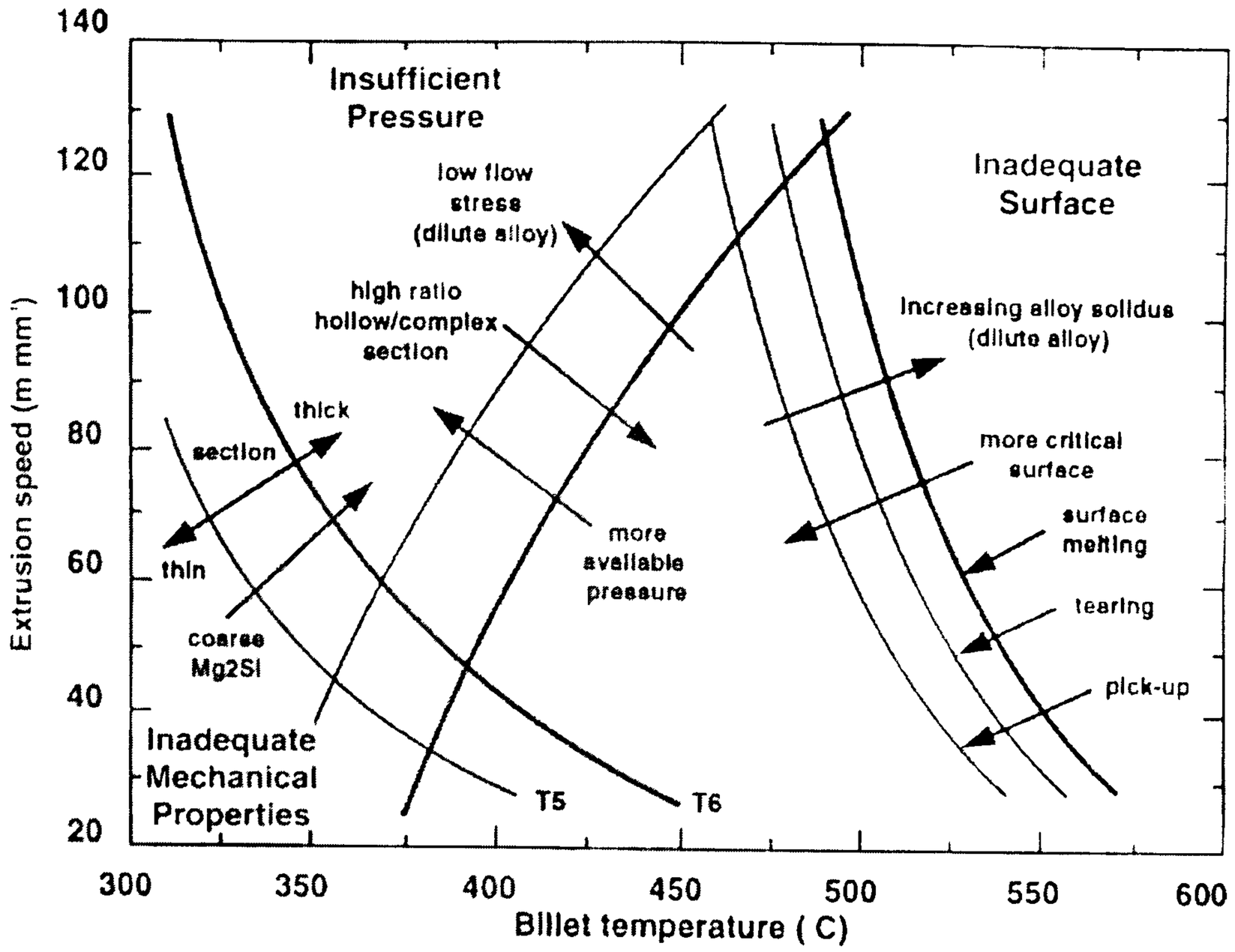

Figure 2.4 Limit diagram for 6063 including common press variable (Sheppard 1999a, p.304)

Using the concept of 'limit diagram' from conventional extrusion, Molyneux (1988) introduced the idea of 'performance envelope' for Conklad extrusion (cladding with Conform). A performance envelope describes an operating zone against the line speed (in $m.min^{-1}$) and the core diameter (mm).

2.4 Tooling in extrusion

As with every metal forming machine, the design and manufacture of the tooling in extrusion plays an important role in the quality of the finished product. In aluminium extrusion the tooling must sustain very high pressures at high temperatures (between 400°C and 550°C). The tooling in contact with the workpiece experiences heat transfer which influences the exit temperature of the extrudate. Both in conventional and Conform extrusion, the design of the die and die stack requires substantial time, effort and expertise. The tool life is predominantly defined by its resistance to wear, fracture and plastic deformation. A poorly designed tool reduces productivity and in the event of a fatal fracture could cause damage to surrounding tooling and threaten

workers' safety. It is therefore essential to optimise the design of the tooling so that the time for extrusion trials is reduced and subsequently productivity is increased.

2.4.1 Die design

The design of the die must allow for uniform flow, stable dimensions and desirable surface quality of the extrudate. With an irregular cross section the material can experience an unbalanced flow at the die exit. The material flows more easily through the thicker sections of the die than the thinner sections. Furthermore, the material from the billet flows easily from the centre and less so from the periphery. Therefore, care and expertise must be applied to the length and angle of die lands in order to achieve a uniform flow during extrusion. The use of recess pocket dies can also help to achieve a balanced flow. For die optimisation it is more practical to update the pocket die by milling than the bearing length by hand grinding. Furthermore, modifications to the pocket would last longer than changes to the bearing length (Lea and Jowett 2004). Unfortunately, more heat is generated by using pocket dies due to the increased length of the flow path along the dead metal zone (i.e. due to the increase of friction).

Extrusion dies are modelled and manufactured with computer-aided design and computer-aided manufacture systems (CAD/CAM). Raggenbass and Reissner (2000) demonstrated that an in-house knowledge based system could improve the design of extrusion die in terms of quality and time. Computerised numerical control (CNC), electrical discharge machining (EDM) and wire EDM machines can then be used to remove the metal in a controlled and accurate manner.

Zhang and Heathcock (2000) used finite element analysis (FEA) to predict the potential flow rate at the die exit and subsequently derive the bearing length. The results agreed well with their experimental observations. Lof *et al* (2000a) developed a two-dimensional FEM model to investigate the influence of profile thickness, bearing length and angle. A design rule was suggested to produce industrial design for bearings and pockets. Lindviksmoen *et al* (1996) and Lof *et al* (2000b) used FEA and statistical design of experiments to calculate the loading on different die mandrel geometries. By minimising the forces on the mandrels, the life length of the hollow die was extended. Recently, Liscomb (2004) confirmed the

suitability of micro-bridge dies for small port, high extrusion ratio and thin walls, by using FEA. Li *et al* (2003a; 2003b) investigated the metal flow and velocity profile in complex shapes by using FEA and experimental methods. A qualitative understanding of pocket design parameters (angle, size and geometry) was presented. Sheppard *et al* (2004) simulated the effect of die land profile on surface quality. It was found that a choked die can significantly reduce the possibility of surface crack initiation.

In the aluminium extrusion industry, AISI 2343 (H11) and AISI 2344 (H13) steels are commonly used for die assemblies and other tools in contact with the hot workpiece (Castle 2000). This chromium-molybdenum-vanadium-alloyed steel is characterised by good resistance to thermal fatigue and thermal shock, hardenability, toughness, machinability and polishability, temper resistance and wear resistance. Tool steels with better resistance to softening, such as QRO 90 Supreme (Sandberg 1988) and Extendo-die (McCaffrey 1988) have been suggested especially for hard alloys and thin-walled profiles.

2.4.2 Tool Wear

Generally in conventional extrusion and certainly in Conform, tool wear is intense because of the sticking friction resulting from non lubrication. In order to extend the performance of the die a surface treatment such as nitriding, chemical vapour deposition (CVD) and physical vapour deposition (PVD) can be used. Nitriding is the most commonly used process. However, Pye (1996) presented the advantages of surface deposition processes against relatively slow diffusion processes such as nitriding. Recently Maier (2004) showed that CVD can now be considered as economical and the demand for this process in industry is growing.

In Conform extrusion the cyclic loads on the die assembly are minimal compared to that in conventional extrusion. This allows the use of material which has more wear resistance and is also more brittle (Bridgewater and Maddock 1996). Materials such as partially stabilised zirconia (PSZ) have been used in Conform for tubes and rods. However this material is not suitable for making dies of complicated shapes due to the unbalanced pressures on the die surfaces (Velay and Sheppard 2000b).

2.4.3 Tool failure

Falk *et al* (1998) simulated the material flow on a cold forging die using FEA. The load distribution on the surface of the die was extrapolated. By investigating different damage concepts, Falk *et al* could estimate the tool material damage and therefore predict the tool life. Hayakawa *et al* (1999) applied continuum damage mechanics and FEA to study the damage and fracture development in extrusion dies. The simulation estimated crack initiation, crack growth and final fracture. Kocańda (1999) demonstrated the effect of cyclic loading and small plastic strain on the fatigue life of extrusion dies. The tool life was predicted with a reasonably high level of accuracy by taking account of the load history and by modelling the die as an elasto-plastic FEM model.

2.4.4 Tool optimisation

The shape of tools can be very complex (e.g. porthole die) and therefore difficult to analyse structurally with traditional methods. Today FEA software and computer hardware are both affordable and easy to use. FEA is therefore recognised as one of the most efficient techniques to analyse and optimise tools (Altan *et al* 1999; Bay *et al* 1999). Modern computers are relatively fast and powerful; i.e. central processing units (CPU) run at frequencies of gigahertz (GHz) units and hard disks have a capacity to store tens of gigabytes (Gbytes). Thus, without compromising efficiency, the discretization (meshing) of the tooling can make use of a large amount of small elements in order to accurately represent the important features of the tool. Unfortunately the application of complex boundary conditions remains a problem and a source or errors. In most metal forming process, the forces and pressures experienced by the tools often vary and are applied with high temperatures and friction. One way to reduce the effort of applying boundary conditions is to perform a coupled analysis where the tooling is modelled as an elastic part (i.e. not rigid) and the workpiece is modelled in the usual way (e.g. viscoplastic) (Lof *et al* 2000a). Sobis *et al* (1992) describe a different method which can be used to reduce computer time. In this second method, the kinematical and mechanical information of the viscoplastic simulation are transferred to the surface of the tool. Hence, the tool is only analysed for the worst loading case. Sarrazin *et al* (2000) used the output of a

2D metal flow in order to input the loading-unloading cycles on a 3D model of a porthole die. It is worth noting that with the fast evolution of software and hardware, the effort of transferring the data accurately may surpass the added computational time for a coupled analysis. Dail (2004) combined FEA with strain-life prediction of fatigue crack initiation to optimise a failed container. It was shown that although FEA expertise is expensive, the cost of tool replacement and the loss of production could ultimately be more costly.

2.5 Feeder plates and expansion chambers

A significant amount of research has been produced regarding the design of pocket dies but very little has been published on feeder plates and expansion chambers. This could be due to the fact that extruders prefer outsourcing a larger press (i.e. a larger container bore) than using a feeder plate. The relatively low number of Conform machines may also explain the lack of research regarding expansion chambers. Therefore very little is known as to how feeder plates and expansion chambers affect important parameters such as the shape of the dead metal zones in the billet, the velocity profile, the pressure and the temperature.

2.5.1 Feeder plates

In conventional extrusion, a feeder plate (sometimes called a feeder die, spreader plate or fishtail plate) is a solid plate positioned in front of the extrusion die in order to produce a shape larger than the billet size. Sometimes ring feeders are incorrectly called feeder plates. Feeder plates should also not be confused with blend rings. A blend ring is put between the container and the die stack to prevent segregation flow. Ring feeders and blend rings are not considered in this study. Figure 2.5 illustrates a feeder plate with a die.

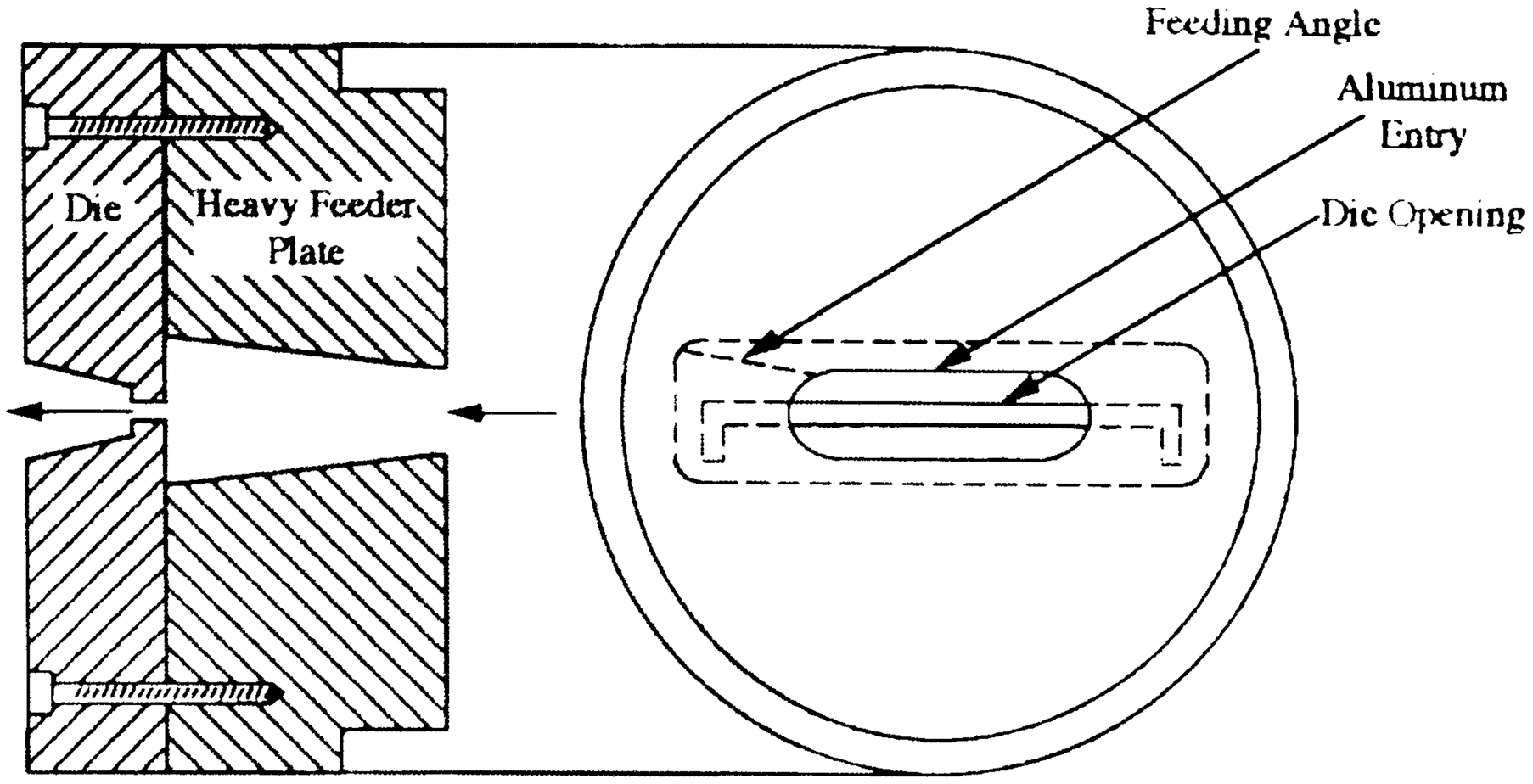

Figure 2.5 Feeder plate and die (Saha 2000, p.98)

Billet scalping may be necessary if the circumscribed circle diameter (CCD) of the feeder entry is very close to the container bore. The feeder plate needs to be thick enough to ensure that the material spreads evenly and smoothly without any abrupt changes in direction. This should limit the risk of streaking on the extruded product (Dion 1988). A large thickness is also required to minimise the internal taper (feeding angle) in order to reduce the reverse pressures which can separate the die from the feeder plate (Mason 1988; Duplancic *et al* 2000).

In Conform extrusion, Etherington and Slater (1984) made use of a different type of feeder plate which was termed a 'stepped feeder plate'. This plate feeds the expansion chamber with a series of steps each comprising a port and a 'mini' abutment. By controlling the port size and the step height the extrusion pressure in the expansion chamber can be balanced in order to extrude flat hollow sections (aspect ratio of 5.5:1) with widths 3.5 times larger than the wheel groove. This type of feeder plate is not investigated in this thesis.

2.5.2 Expansion chambers

In Conform, dies are said to be of two types: direct and indirect. In the direct type the die orifice is placed directly in front of the wheel groove. With the indirect type, the die orifice is fed by an expansion chamber. An expansion chamber (sometimes called expansion shoe) is a cavity placed between the wheel and the die. Its role is to

spread the feedstock, from a primary orifice to the die entrance, in order to extrude larger sections than the feedstock diameter. Thus a wide range of sections and shapes can be extruded from a single feedstock diameter. Figure 2.6 shows a schematic diagram of an expansion chamber.

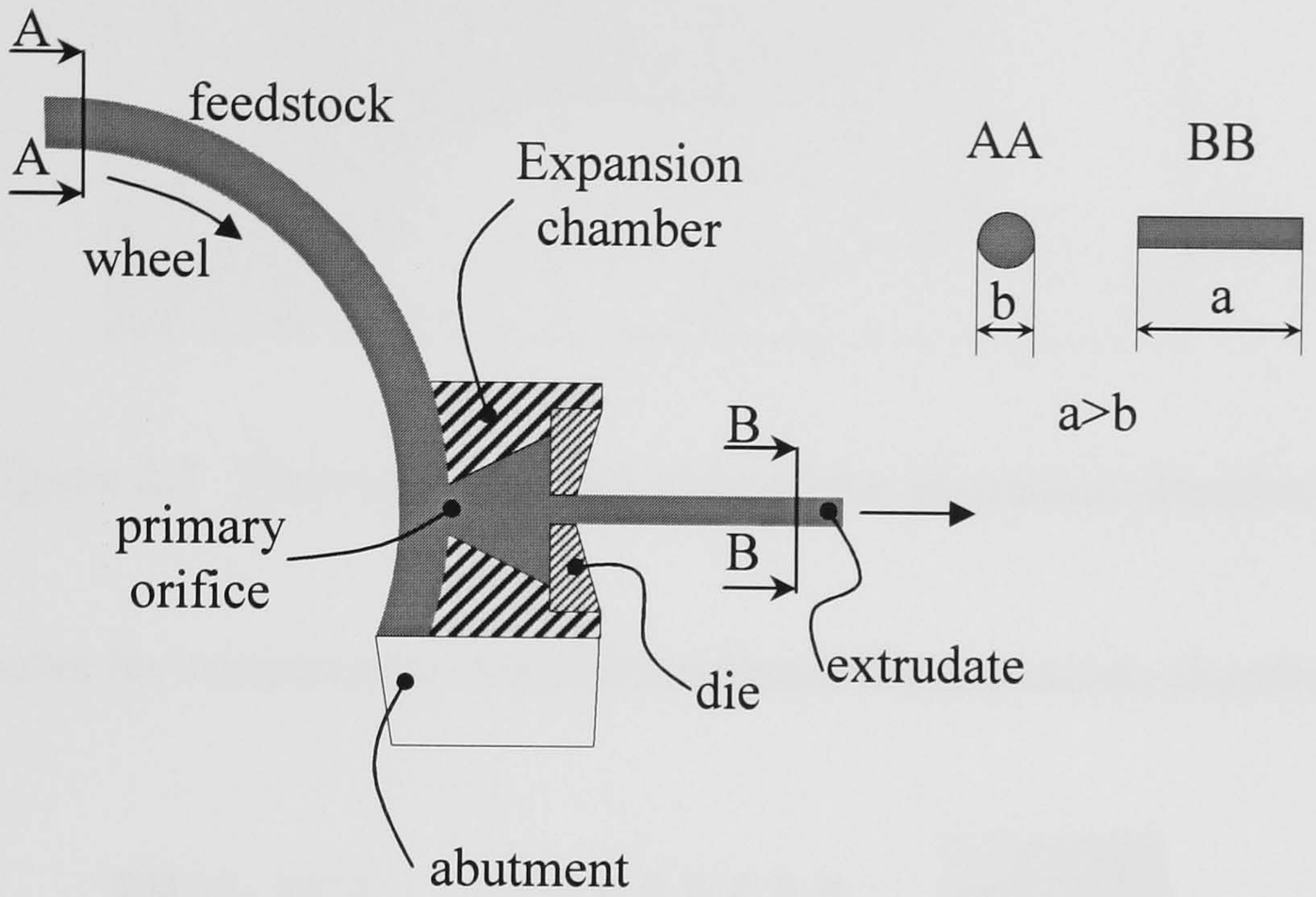

Figure 2.6 Expansion chamber

With the use of macrographs, Sinha and Chia (1988) and Clode (1992b) showed that the material flow in the expansion chamber follows a semi-spherical wave pattern. However, the flow pattern is not axisymmetric because of the pressure differential at the primary orifice (i.e. expansion chamber entry). The creation of dead metal zones at the corners of the expansion chamber was also reported together with a less deformed central layer. Clode (1992b) observed some swirling through the centre zone of the chamber and into the extrudate. Regions of intense shear created the outer annulus of the extrudate which showed some high degree of directionality compared to the swirling microstructure at the centre.

Velay and Sheppard (2000b) used FEM to simulate Conform extrusion with an expansion chamber. Results such as strain and temperature gradients were qualitatively compared between a plane strain model and a three dimensional model. Figure 2.7 illustrates a three-dimensional expansion chamber with (XY) as a plane of symmetry.

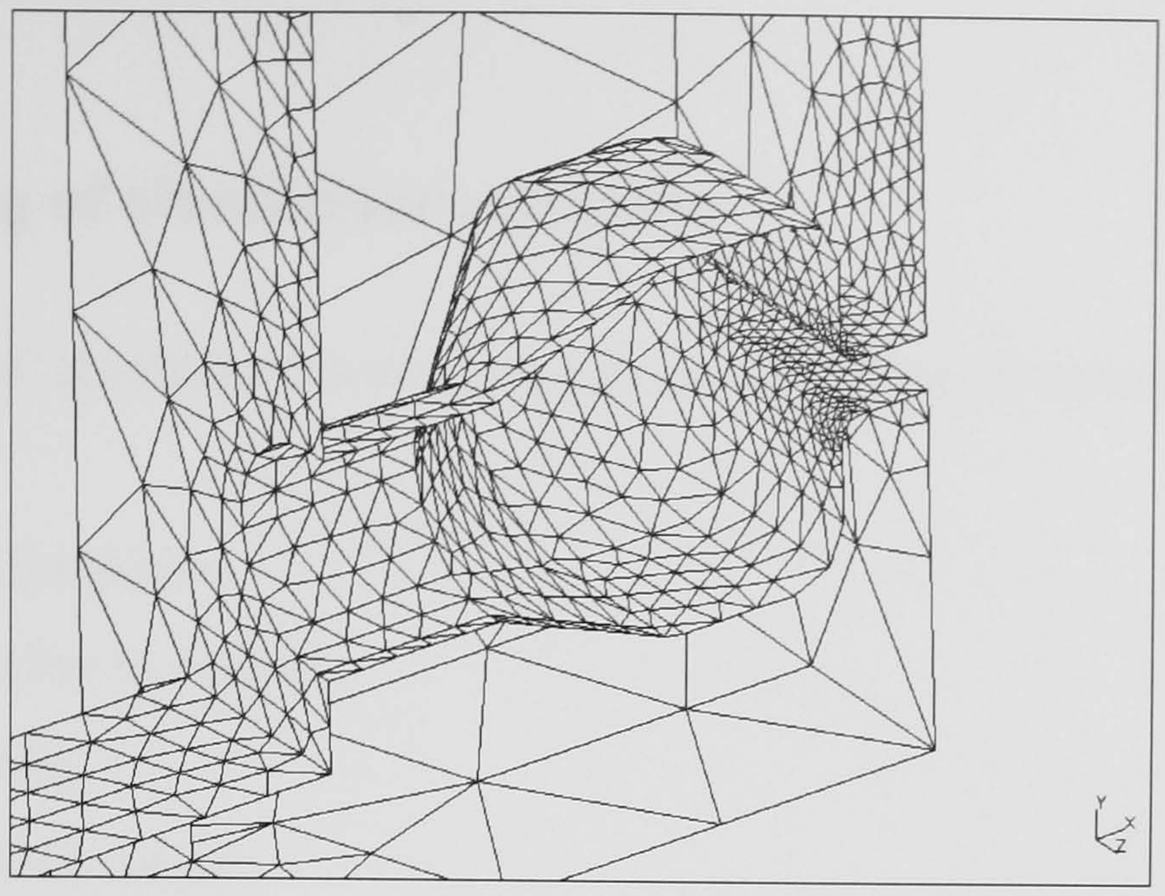

Figure 2.7 Three-dimensional view of the expansion chamber

Figure 2.8 shows the temperature distribution inside the expansion chamber.

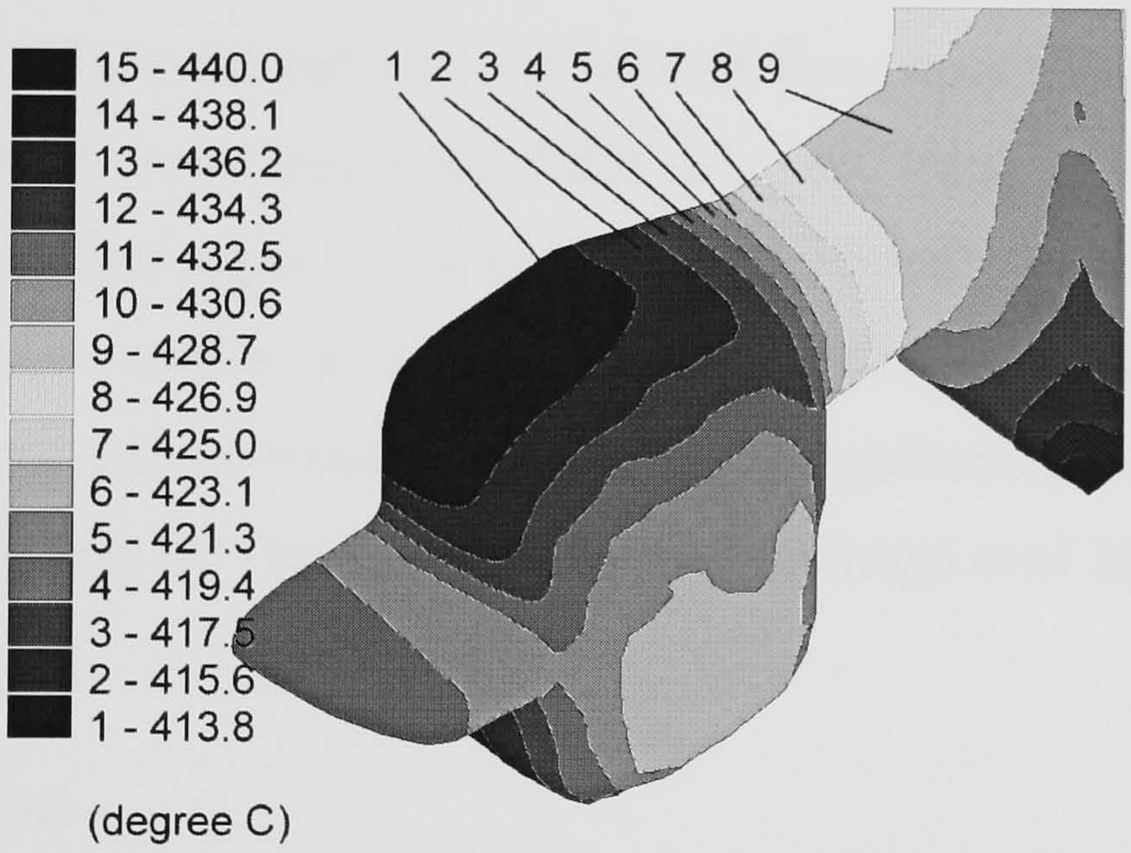

Figure 2.8 Temperature distribution inside the expansion chamber

The results from the 3D model correlated relatively well with observations from experimental works, however some discrepancies were apparent. There were two main reasons for these discrepancies. Firstly, the simulations could not be run until steady state was reached because of the limitations in both computing power and number of iterations available from the FE code. Secondly, the expansion chamber was filled before the start of the analysis, which consequently led to a loss of material history and spatial topology from the initial deformations. The results of these analyses are further detailed in Chapter five.

2.6 Modelling of aluminium extrusion

The mechanics of aluminium extrusion can be modelled in several ways as listed below:

- empirical formulae,
- visioplasticity technique,
- slab analysis,
- slip-line field theory,
- upper bound analysis,
- and finite element method.

The empirical formulae, which are based on experimental results of extrusion, are well documented in section 2.1 of this thesis. The visioplasticity technique is a semi-empirical method where the deformed pattern of flow lines (from a workpiece) is used to determine the stress and strain fields (Lin and Wang 1992). Slab analysis, slip-line field theory and upper bound analysis are all briefly described below. In the past these have been used to numerically investigate the mechanics of extrusion. However, due to the current power of computers and software, most of the analyses are now performed with the finite element method (Bourqui *et al* 2004).

2.6.1 Slab analysis

Slab analysis is also called the free body-equilibrium approach. This method imposes a force balance on a slab of metal of differential thickness. This generates a differential equation where variations are considered in one direction only. This equation is then integrated with relevant boundary conditions to give a solution. Although the effects from frictional interfaces are included in the initial force balance, these do not influence the deformation of the workpiece and the way that the metal flows. Furthermore, this method can only represent plane strain or axisymmetric models. Hosford and Caddell (1983, p.115-119) used slab analysis to define equations for sheet drawings, whilst Sheppard (1999a, p.30-31) used the method for direct extrusion processes.

2.6.2 Slip-line field theory

The slip-line theory is well described by Hill (1950 cited Mooi 1996, p.7-8). The 'slip-lines' represent the planes of maximum shear stress. The workpiece is assumed to be plane strain and rigid perfectly plastic. Thus elastic strains are neglected and the flow stress is a constant (i.e. no work hardening). The effects of temperature, strain rate and time are not considered. A constant shear stress (e.g. sticking friction) can be applied at the frictional interface in the form of a velocity discontinuity. Plane strain extrusion can be analysed by dividing the field into nets of straight lines and centred fans which are composed of α-lines and β-lines (Støren 1993). The slip-line field is represented in the form of a hodograph which is adjusted manually to agree with the physical field. The field and the hodograph can be used to study the deformation of the material by drawing stream lines.

2.6.3 Upper bound analysis

In upper bound analysis hodographs are also constructed to agree with the physical field. In this method the pressure calculated is greater or equal to the exact pressure required for plastic deformation. Johnson and Kudo (1962 cited Tutcher 1979, p.31) made significant progresses with this method. The energy consumed internally in the deformation field is calculated using the appropriate strength properties of the workpiece. The external stresses are evaluated by equating the external work with the internal energy consumption. Constant frictional interface is usually applied and the flow stress does not take into account the effects from strain hardening and strain rate. Only simple geometries, using plane strain models, can be analysed. However axisymmetric upper bound analyses have been used to study extrusion (Jia *et al* 1996; Sheppard 1999a, p.35).

2.6.4 Finite element method

FEM is well accepted as a design and simulation tool in the metal forming industry. Since the mid-90s it has been extensively used for the different modelling tasks of

aluminium extrusion. The use of 3D finite element models is still time consuming and sometimes unreliable. The formulation of FEM can take three forms: Lagrangian, Eulerian or arbitrary Lagrangian Eulerian (ALE). The different formulations of the FEM are discussed in section 3.2 of this thesis.

3 Finite Element Modelling of Aluminium Extrusion

3.1 Introduction

Haepp and Roll (1999) estimated that about 60 finite element (FE) software packages were available for the simulation of forming processes. The simulation of aluminium extrusion demands specific features from a FE package. These features are similar to the ones required in forging as described by Chenot *et al* (1999) below:

- large deformation both in 2D and 3D,
- re-meshing,
- evolving contact and frictional interfaces,
- complicated temperature evolution,
- thermo-mechanical coupling between the workpiece and the tooling,
- possible changes of the microstructure of the workpiece during deformation.

Initially three commercial software packages were shortlisted by the author and his co-worker from a review of both the literature and the commercial documentation. A technical evaluation was also undertaken which included meetings with the vendors. The software packages were benchmarked with a T-shape extrusion, and an assessment against the features listed above was carried out. After a thorough evaluation the French software packages Forge 2 and Forge 3 were selected. Both software packages are commercialised by Transvalor. The initial versions were running on Unix platforms, however, the computer 'power/cost' ratio has increased rapidly since then. The results presented and discussed in this thesis were taken from analyses carried out using the Windows operating system on personal computers (PCs) with parallel processors. The following sections of this chapter consider the suitability of these two programmes for conventional and Conform extrusions.

3.2 The finite element formulation

3.2.1 The Lagrangian form

In the Lagrangian formulation (also called the *material description*) the meshes deform in a way which is geometrically similar to that of the bulk material. In extrusion the workpiece experiences large deformation, thus a Lagrangian mesh rapidly shows severely distorted elements in the region of concentrated strain. The excessive degeneration of the mesh will make the determinant of the transformation matrix negative and subsequently stop the FEA calculations (Yang and Lee 1999). Therefore, in order to be efficient, FE software based on a Lagrangian formulation should incorporate an automatic re-meshing procedure. Such a procedure identifies a critical mesh degeneracy factor when the analysis is temporarily stopped to allow the generation of a new mesh. The meshing algorithm must be robust and efficient especially in the simulation of extrusion where a large amount of re-meshing is required. Before restarting the calculation another algorithm is necessary to transfer the state variables from the distorted mesh to the new mesh without excessively smoothing the gradient of these variables. Both Forge 2 and Forge 3 simulate metal deformation using a Lagrangian description.

3.2.2 The Eulerian form

In the Eulerian method (also called the *spatial description*) the mesh is fixed and the material flows through the mesh. Therefore, no mesh distortion occurs but it is difficult to accurately model the free surfaces of the extrudate after it leaves the die bearing. Richards and Bhattacharyya (1996) modelled the extrusion of metal using an Eulerian code and treated the material as a highly viscous thixotropic fluid. Prediction of velocity, strain and strain rate agreed with experimental data but the results showed that the pressure had been underestimated. Smelser and Thompson (1992) presented the use of Eulerian flow formulation for the simulation of direct and indirect extrusions. It was shown that the Eulerian method is very appropriate for both frictionless direct and indirect extrusion. However, several issues regarding the modelling of direct extrusion with friction remain to be resolved. Problems occur with materials whose constitutive behaviour depends on their history. The Eulerian

equation for this history-dependent quantity is a first order differential equation which requires an initial value. Unfortunately, this initial value and the position of the material (associated with this value) are unknown. Furthermore, the Eulerian formulation raises additional modelling problems with the heat transfer associated with the container and the billet-container interactions. However, the use of Eulerian code for aluminium extrusion process modelling and design can provide useful qualitative information especially for complex hollow profiles (van Rens *et al* 2000). Unfortunately, as mentioned before, the modelling of friction is a very important factor in the extrusion of aluminium alloys with Conform extrusion.

3.2.3 The Arbitrary Lagrangian Eulerian form

This method was developed in fluid mechanics to simulate fluid-structure interaction and to model the motion of free surfaces. Huétink introduced the ALE method for metal forming by formulating his approach as an extension of a Lagrangian formulation with the addition of relatively small convective terms (Huétink and van der Helm 1992). In the ALE formulation, the mesh velocity is not equal to the material and is computed so that the distortion of elements remains as small as possible. Chenot and Bellet (1995) showed that the ALE method significantly decreases the total number of re-meshing steps necessary for a given simulation. Lof *et al* (2000a and 2000b) successfully modelled the hot extrusion of a selection of aluminium alloys using ALE software (DiekA). This software is based on a transient Galerkin formulation in which finite time steps control the discretisation of the analyses. The ALE formulation is applied as a partially decoupled backward ALE algorithm. This means that the state variables, at the start of the next time step, are updated by the displacement from the end of the previous step. This process is repeated for each equilibrium iteration. The mesh topology must remain unchanged as opposed to the method used in traditional ALE formulations. The remapping of the state variables is therefore done with the use of a convective procedure. Furthermore, the computation of the transient thermomechanical equations requires a large number of calculation steps. Often an upper limit for the thermal problem is calculated in order to reduce the number of steps from around 10^7 to less than 50

(Lof and Huétink 2000). The ALE method leads to rather complicated mathematical derivations and results in an unsymmetrical stiffness matrix (Tong *et al* 1992).

3.3 Constitutive equations

Three viscoplastic behaviours were studied: Norton-Hoff, Hansel-Spittel and Zener-Hollomon. The first two are available by default with the software and the latter was programmed via a FORTRAN sub-routine and added into the code.

3.3.1 Norton-Hoff model

This model is based on the Norton-Hoff behaviour law, σ_{N-H}, written in the following stress tensor form (Chenot *et al* 1998):

$$\sigma_{N-H} = 2K\left(\sqrt{3}\dot{\bar{\varepsilon}}\right)^{m-1}\dot{\varepsilon} \tag{3.1}$$

where m is the strain rate sensitivity index which can be a function of the temperature T, such as:

$$m = m_0 + m_1 T \tag{3.2}$$

where m_0 and m_1 are constants. In this study m will be considered as constant.

The effective strain rate, $\dot{\bar{\varepsilon}}$, is expressed in term of the strain rate tensor $\dot{\varepsilon}_{ij}$:

$$\dot{\bar{\varepsilon}} = \sqrt{\frac{2}{3}\sum_{ij}\dot{\varepsilon}_{ij}^2} \tag{3.3}$$

K is the material consistency and depends on thermo-mechanical conditions such as temperature and equivalent strain ($\bar{\varepsilon}$). In Forge 2 and Forge 3 the material consistency can be known as either a *power law* (3.4) or an *exponential law* (3.5) and the equations are defined as follows:

$$K = K_0\left(\bar{\varepsilon} + \varepsilon_0\right)^n \exp\left(\frac{\beta}{T}\right) \tag{3.4}$$

$$K = K_0\left(\bar{\varepsilon} + \varepsilon_0\right)^n \exp\left(-\beta T\right) \tag{3.5}$$

where K_0 is a constant, ε_0 is a constant for strain hardening regulation, n is the coefficient of sensitivity to strain hardening and β is a temperature constant. Since material deformation is a mass transfer process, β must have a value approximately equal to that required for self diffusion. Unfortunately no such limitation is placed on the β value. The term 'power law' is misleading as both equations (3.4) and (3.5) behave exponentially. However, depending on the temperature ranges these laws give a different output. For example, in Figure 3.1 the two different Norton-Hoff flow stresses (equations 3.11 and 3.12) are plotted against a large temperature range (300K to 800K). The stresses were calculated for AA7075 at a strain rate of $5s^{-1}$.

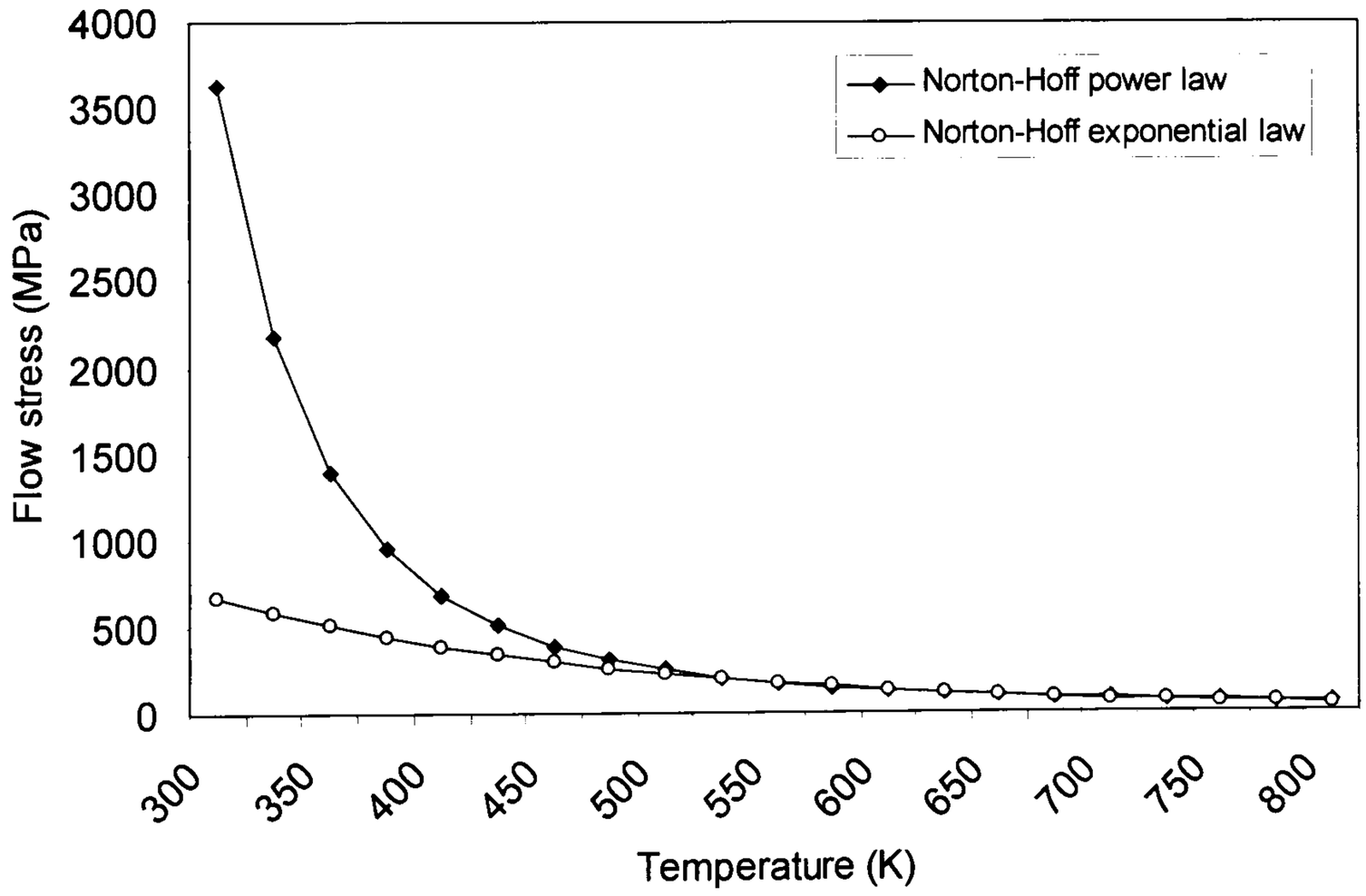

Figure 3.1 Norton-Hoff laws versus temperature

The Norton-Hoff laws diverge noticeably for temperatures below 500K. However in the temperature range of hot extrusion (550K to 800K) both laws give approximately the same output. Figure 3.2 shows both of the flow stresses versus the hot extrusion temperature range.

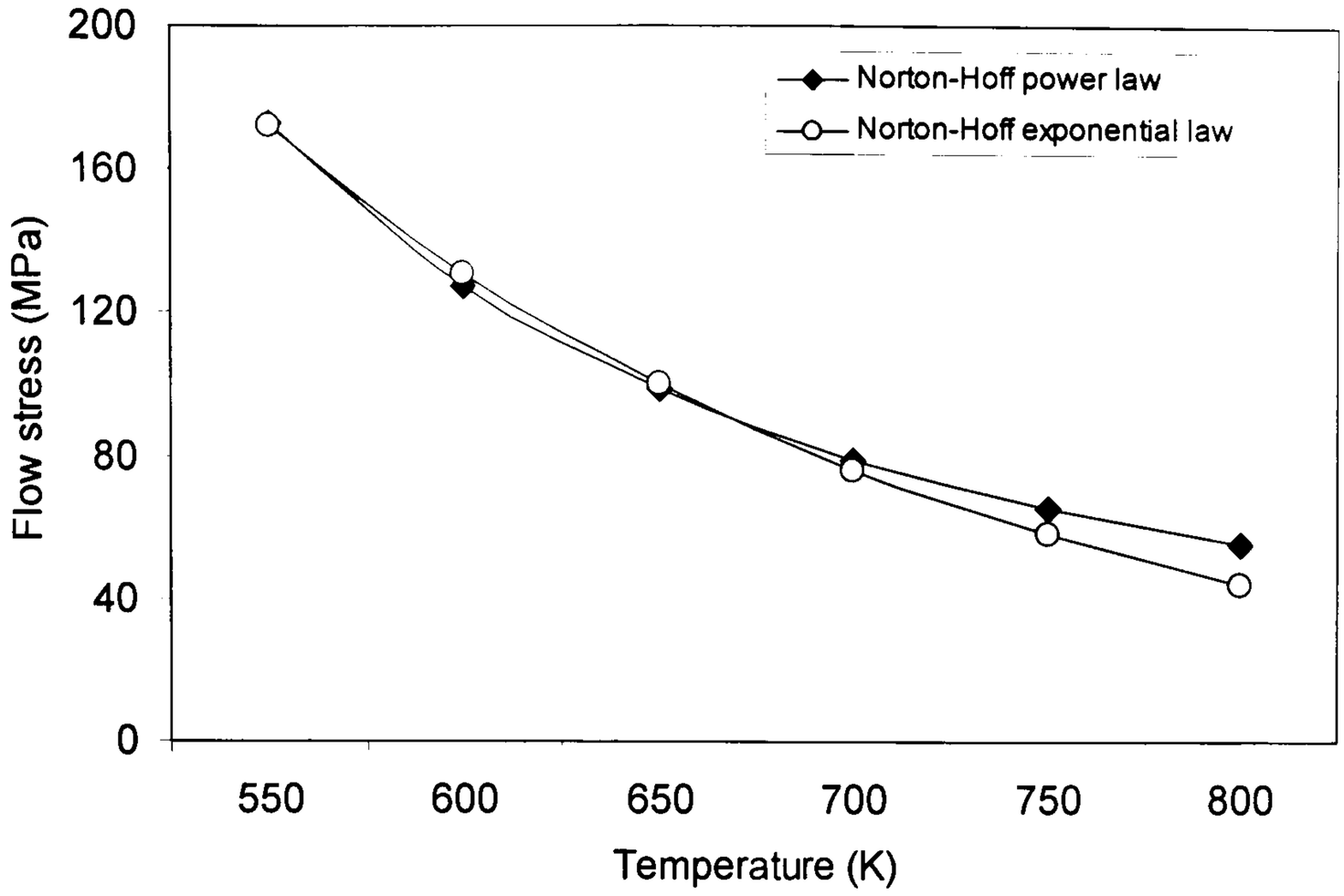

Figure 3.2 Norton-Hoff laws versus extrusion temperatures

At around 675K the exponential law gives a lower value for the flow stress. At 800K the exponential law shows a flow stress which is 20% lower than the power law. The results shown in section 3.3.4 of this chapter show that in general, at higher extrusion temperatures, the Norton-Hoff laws underestimate the experimental flow stress values. Therefore, the Norton-Hoff exponential law will not be considered for the remainder of this chapter.

3.3.2 Hansel-Spittel model

The Hansel-Spittel rheology law, σ_{H-S}, is defined as follows:

$$\sigma_{H-S} = Ae^{m_1 T} T^{m_9} \bar{\varepsilon}^{m_2} e^{m_4/\bar{\varepsilon}} \left(1+\bar{\varepsilon}\right)^{m_5 T} e^{m_7 \bar{\varepsilon}} \dot{\bar{\varepsilon}}^{m_3} \dot{\bar{\varepsilon}}^{m_8 T} \tag{3.6}$$

where A, $m_1 \sim m_5$ and $m_7 \sim m_9$ are regression coefficients. It can be noted that A is acting as the material consistency (K) and m_3 as the stress rate sensitivity index (m). Due to the number of terms present in this formulation, there is always a good regression fit with either good or bad experimental data. However, during hot extrusion of aluminium alloys, the effect of the strain on the flow stress is negligible and therefore the number of terms in the Hansel-Spittel law can be reduced

significantly as demonstrated in equation (3.13). This makes the regression fit more meaningful.

3.3.3 Zener-Hollomon model

The Zener-Hollomon flow stress, σ_{Z-H} has already been defined in equation (2.37) and is represented as follows:

$$\sigma_{Z-H} = \frac{1}{\alpha}\ln\left[\left(\frac{Z}{A}\right)^{\frac{1}{n}} + \sqrt{\left(\frac{Z}{A}\right)^{\frac{2}{n}} + 1}\right] \tag{3.7}$$

$$\text{with } Z = \dot{\varepsilon}\exp\left(\frac{\Delta H}{GT}\right) \tag{3.8}$$

The advantage of this type of formulation is that ΔH represents the energy threshold required to obtain the dynamic balance between work hardening and softening at steady state. In most aluminium alloys the dynamic recovery mechanism is related to vacancy diffusion. The value of self-diffusion in aluminium is close to the value of ΔH (Sheppard and Jackson 1997). Furthermore, the value of A can incorporate the effect of solute contents such as Mg and Si in AA6063. Van De Langkruis *et al* (2000) defined A with the following equation:

$$A = \exp(K_1 - K_2 X) \tag{3.9}$$

where K_1 and K_2 are model parameters and X is the weighted solute content:

$$X = 2[\text{Mg}] + [\text{Si}] \tag{3.10}$$

Finally the temperature compensated strain rate parameter, Z, is a function of the process parameters and can therefore be used efficiently in other relations describing the extrusion process or the behaviour of microstructure (Harris *et al* 2004).

3.3.4 Flow stress influence

Choosing the appropriate flow stress equation is an important factor for accurately calculating workpiece deformation in metal forming. The constitutive equations described above have been compared in terms of both strain rate and temperature commonly present in hot extrusion. Two alloys, AA2014 and AA7075 were selected for this comparison. The derivatives of the flow stresses with the strain rate were also investigated as this is the method by which the stress is updated during the deformation process.

In hot aluminium extrusion the flow stress of aluminium alloys is sensitive to changes of temperature and strain rate. The influence of these parameters is much stronger that the influence of the strain. Thus the constitutive equations can be rewritten as follows:

- Norton-Hoff power law

$$\sigma_{N-H}^{power} = K_0 \exp\left(\frac{\beta}{T}\right)\left(\sqrt{3}\right)^{1+m} \dot{\bar{\varepsilon}}^{m} \tag{3.11}$$

- Norton-Hoff exponential law

$$\sigma_{N-H}^{\exp} = K_0 \exp(-\beta T)\left(\sqrt{3}\right)^{1+m} \dot{\bar{\varepsilon}}^{m} \tag{3.12}$$

- Hansel-Spittel law

$$\sigma_{H-S} = A \exp(m_1 T)\dot{\bar{\varepsilon}}^{m_3} \tag{3.13}$$

- Zener-Hollomon flow stress

$$\sigma_{Z-H} = \frac{1}{\alpha}\ln\left[\left(\frac{\dot{\bar{\varepsilon}}\exp\left(\frac{\Delta H}{GT}\right)}{A}\right)^{\frac{1}{n}} + \sqrt{\left(\frac{\dot{\bar{\varepsilon}}\exp\left(\frac{\Delta H}{GT}\right)}{A}\right)^{\frac{2}{n}} + 1}\right] \tag{3.14}$$

It is clear that equations (3.12) and (3.13) will generate similar flow stresses if they are regressed from the same experimental results. Therefore only the Norton-Hoff power law (σ_{N-H}^{power}), the Hansel-Spittel law (σ_{H-S}) and the Zener-Hollomon flow stress (σ_{Z-H}) were used in the comparisons.

The flow stress parameters for AA2014 and AA7075 were calculated by multi-linear regressions of experimental data from a hot torsion test (Veirod 1983) and a hot compression test (Sheppard and Jackson 1997) respectively. For AA2014 the strain rate was varied between $0.032s^{-1}$ to $29.472s^{-1}$, with the temperature ranging from 573K to 753K. For AA7075 the strain rate was varied between $0.008s^{-1}$ to $80.0s^{-1}$ with the temperature ranging from 533K to 693K. Both sets of data are available in Appendix C. Tables 3.1 and 3.2 list the flow stress parameters for AA2014 and AA7075. Table 3.3 lists the chemical composition of the two aluminium alloys used in the experiments.

Flow stress	Parameters for AA2014 (SI units and MPa)
σ_{N-H}^{power}	$K_0 = 0.4995,\ \beta = 2542.4019,\ m = 0.1812$
σ_{H-S}	$A = 2196.6737,\ m_1 = -0.00584,\ m_3 = 0.18103$
σ_{Z-H}	$\Delta H = 130195,\ n = 3.4716,\ \alpha = 0.0283,\ \ln A = 21.38$

Table 3.1 AA2014 low stress parameters regressed from experimental data

Flow stress	Parameters for AA7075 (SI units and MPa)
σ_{N-H}^{power}	$K_0 = 2.0564,\ \beta = 2009.4698,\ m = 0.1064$
σ_{H-S}	$A = 2866.9973,\ m_1 = -0.00543,\ m_3 = 0.10642$
σ_{Z-H}	$\Delta H = 155136,\ n = 6.4504,\ \alpha = 0.011,\ \ln A = 28.06$

Table 3.2 AA7075 low stress parameters regressed from experimental data

Alloy	*Cu*	*Mg*	*Zn*	*Mn*	*Cr*	*Si*	*Fe*	*Ti*
2014	3.900	0.470	0.020	0.780	-	0.780	0.200	0.013
7075	1.680	2.660	5.890	0.010	0.200	0.030	0.060	0.040

Table 3.3 Chemical composition of AA2014 and AA7075 % wt (balance aluminium)

For each flow stress, the correlation coefficient between the calculated stresses and the experimental stresses was calculated. Figure 3.3 shows these coefficients for AA2014 and Figure 3.4 for AA7075.

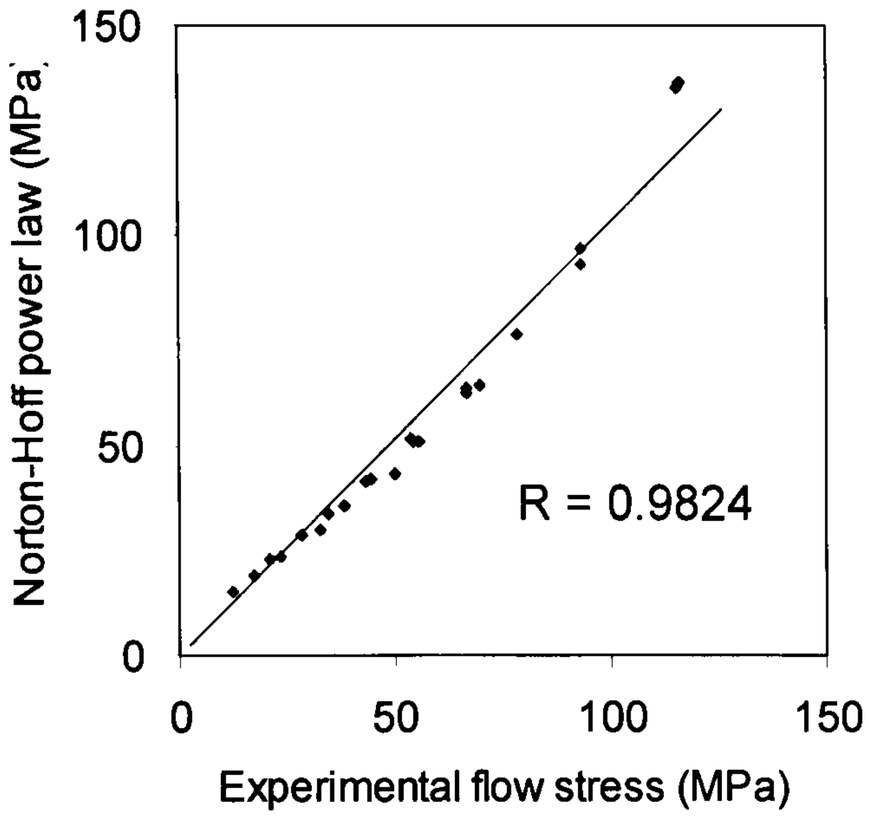

(a)

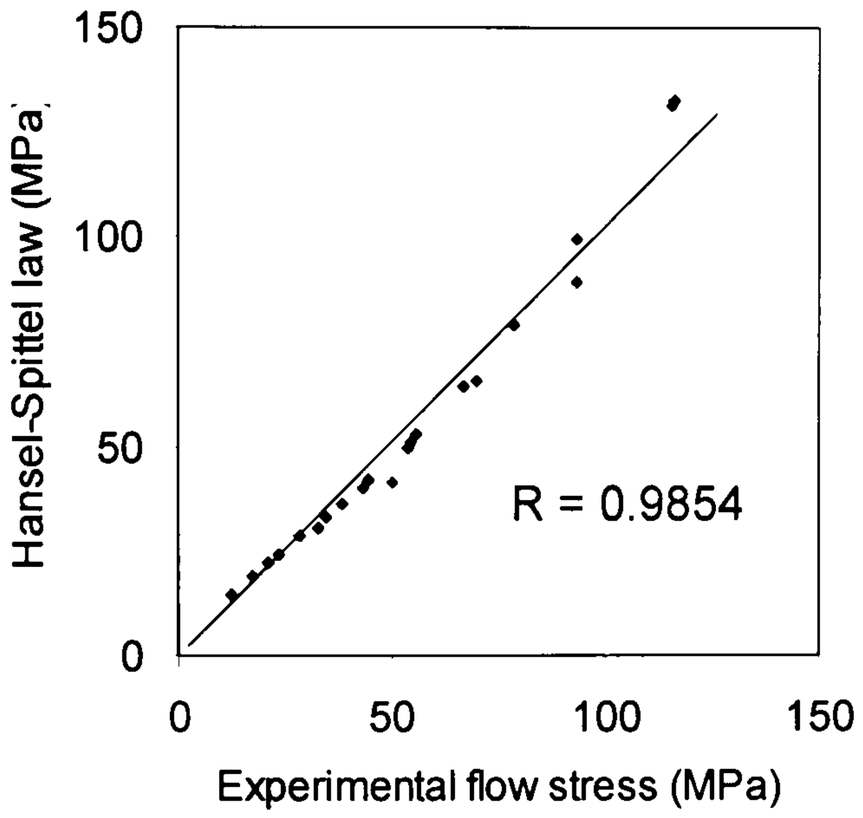

(b)

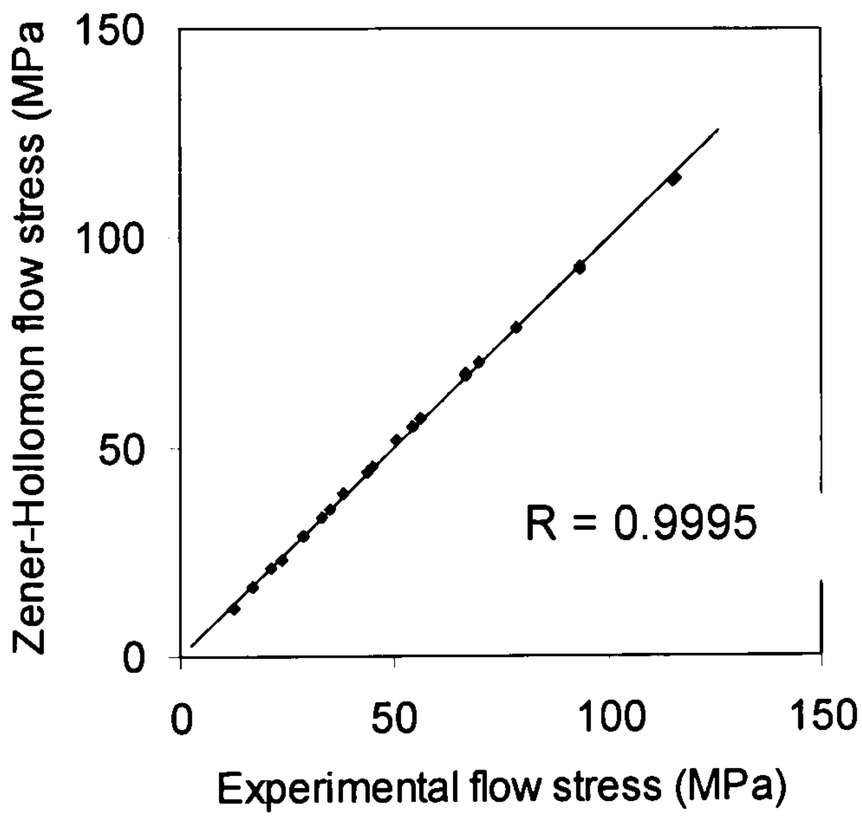

(c)

Figure 3.3 Correlation coefficient for (a) Norton-Hoff power law, (b) Hansel-Spittel law and (c) Zener-Hollomon flow stress with A2014

The correlation coefficient of the Zener-Hollomon function is nearly 1 for AA2014 (see Figure 3.3c) and is just below 0.99 for AA7075 (see Figure 3.4c). The two other flow stress equations, Norton-Hoff and Hansel-Spittel, show a lower correlation coefficient against the experimental data from both alloys.

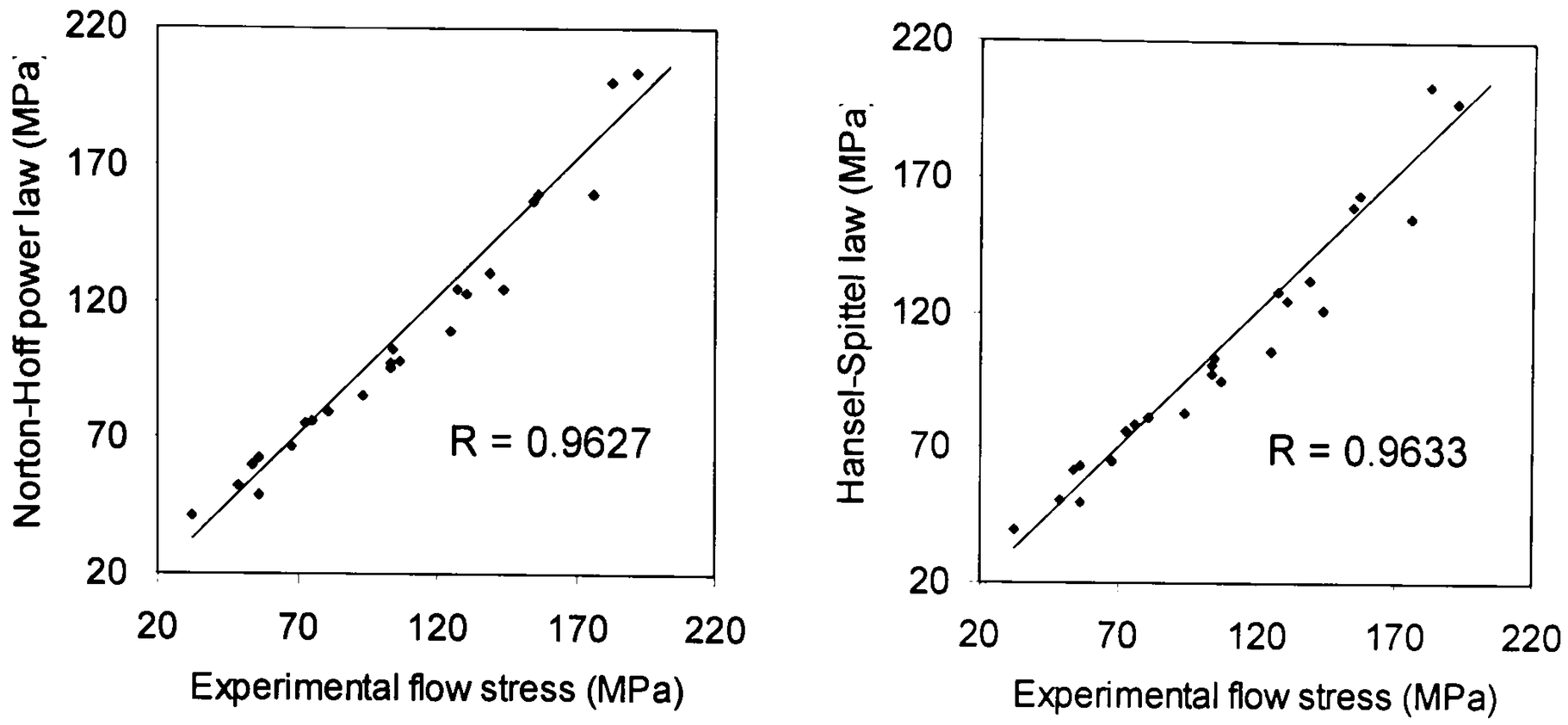

(a) (b)

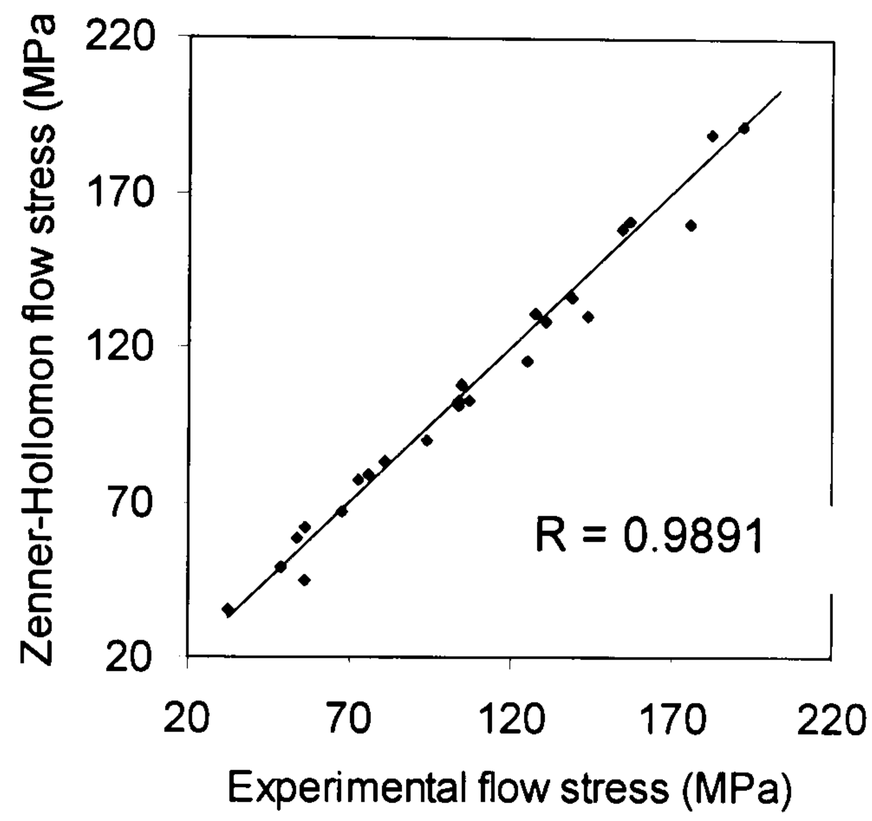

(c)

Figure 3.4 Correlation coefficient for (a) Norton-Hoff power law, (b) Hansel-Spittel law and (c) Zener-Hollomon flow stress with AA7075

Norton-Hoff gives the lowest coefficients with R = 0.9824 for AA2014 and R = 0.9627 for AA7075 (see Figure 3.3a and Figure 3.4a). Therefore the Zener-Hollomon parameters, regressed from experimental data, can be seen to more accurately represent the hot deformation of aluminium.

Figures 3.5 and 3.6 show the three flow stresses plotted against the temperature range (550K to 800K) at three different strain rates ($\dot{\bar{\varepsilon}} = 5$, $\dot{\bar{\varepsilon}} = 25$ and $\dot{\bar{\varepsilon}} = 50$) for both alloys.

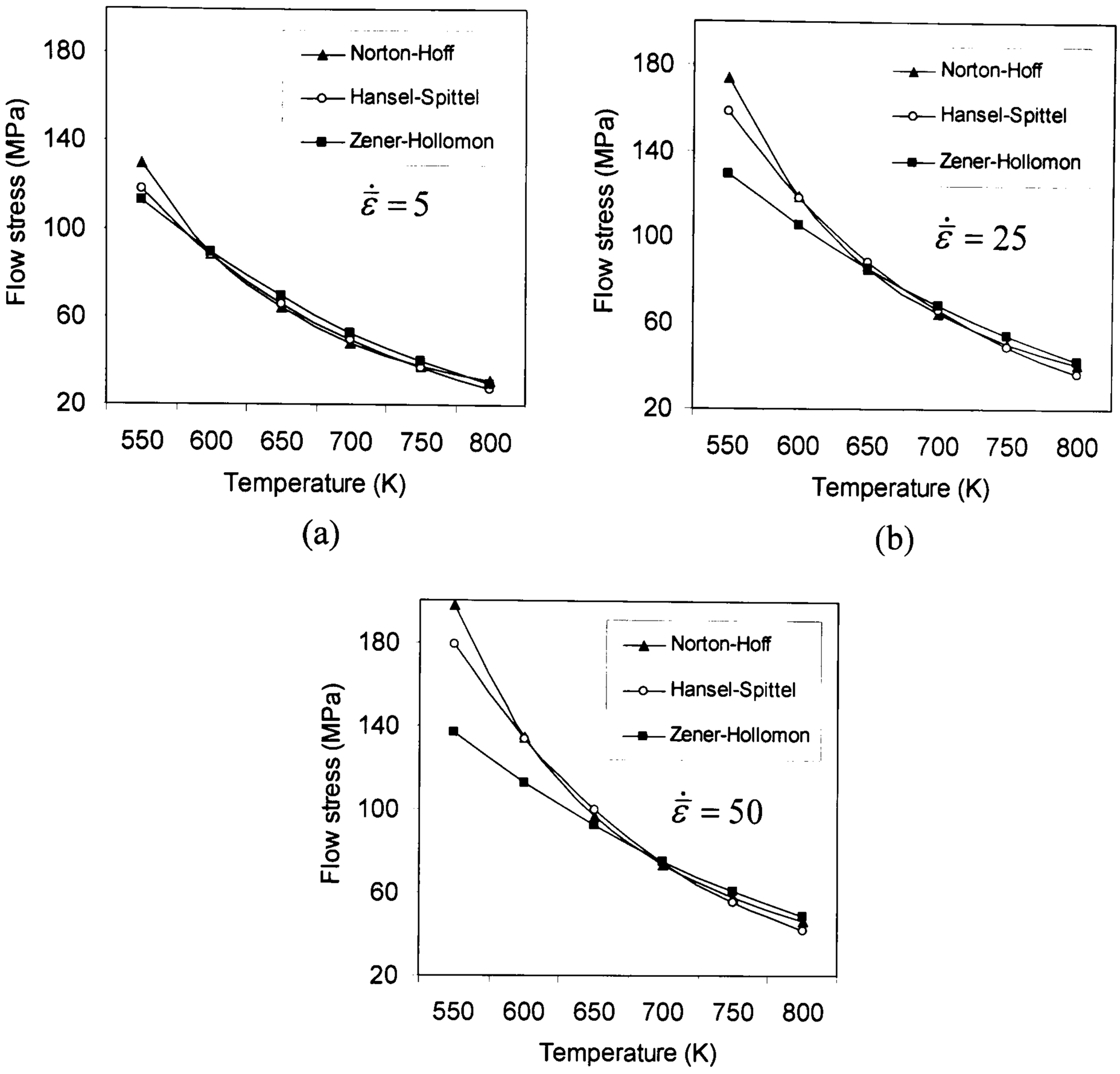

Figure 3.5 Flow stresses versus temperature for AA2014 at different strain rates: (a) $\dot{\bar{\varepsilon}} = 5$, (b) $\dot{\bar{\varepsilon}} = 25$ and (c) $\dot{\bar{\varepsilon}} = 50$

In Figure 3.5 the differences between the flow stress equations for AA2014 are clearly seen. The Norton-Hoff and Hansel-Spittel equations overestimate the flow stress at the low temperature range (i.e. below 650K). Conversely at higher temperatures, the equations slightly underestimate the flow stress. These discrepancies increase with higher strain rates. For example, in Figure 3.5c, at 550K the Norton-Hoff and the Hansel-Spittel flow stresses are respectively 45% and 31% higher than the Zener-Hollomon flow stress.

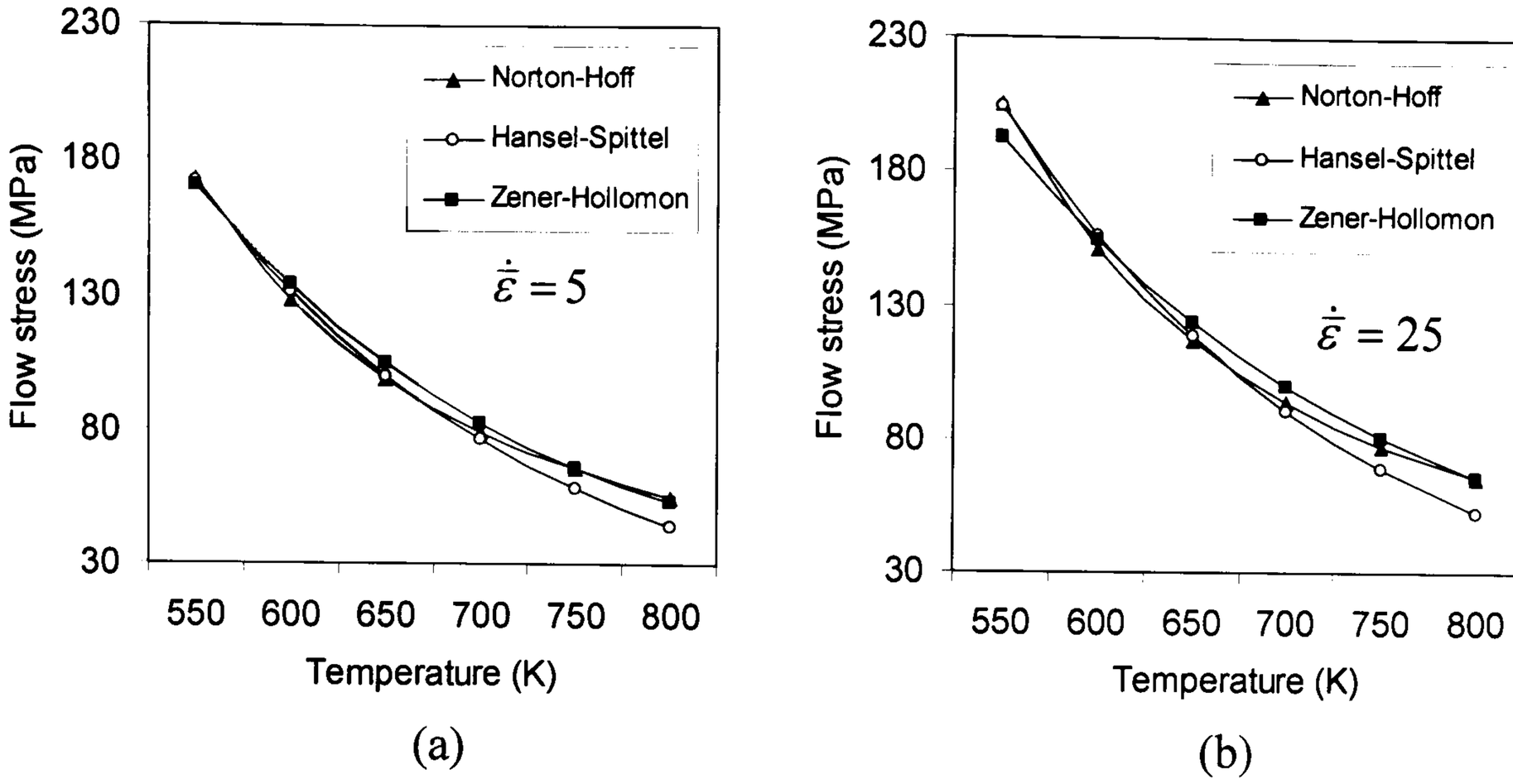

Figure 3.6 Flow stresses versus temperature for AA7075 at different strain rates: (a) $\dot{\bar{\varepsilon}} = 5$, (b) $\dot{\bar{\varepsilon}} = 25$ and (c) $\dot{\bar{\varepsilon}} = 50$

In Figure 3.6 the differences between the flow stress equations for AA7075 are less obvious. One explanation could be that the flow stress parameters for AA7075 were derived from a better set of experimental data than for AA2014 (i.e. six different temperatures at six different strain rates). However the Norton-Hoff and Hansel-Spittel equations still overestimate the flow stress at low temperatures. For example, in Figure 3.6c, at 550K the Norton-Hoff and Hansel-Spittel flow stresses are both 9% higher than the Zener-Hollomon flow stress. Therefore, it seems that the Norton-Hoff and Hansel-Spittel flow stresses can significantly overestimate the flow stress in the lower temperature range.

For FEM calculations the derivative of the flow stress against the strain rate is also used to compute the results (Kobayashi *et al* 1989, p108-110). Equations (3.15),

(3.16) and (3.17) are derivatives against the strain rate, respectively, of the Norton-Hoff, Hansel-Spittel and Zener-Hollomon flow stresses. Details of the derivations are included in Appendix D.

$$\frac{\partial \sigma_{N-H}^{power}}{\partial \dot{\bar{\varepsilon}}} = m \frac{\sigma_{N-H}^{power}}{\dot{\bar{\varepsilon}}} \tag{3.15}$$

$$\frac{\partial \sigma_{H-S}}{\partial \dot{\bar{\varepsilon}}} = m_3 \frac{\sigma_{H-S}}{\dot{\bar{\varepsilon}}} \tag{3.16}$$

$$\frac{\partial \sigma_{Z-H}}{\partial \dot{\bar{\varepsilon}}} = \frac{(\tanh \alpha \sigma_{Z-H})}{\alpha n \dot{\bar{\varepsilon}}} \tag{3.17}$$

The derivatives of the three flow stress equations are plotted against the temperature range at three different strain rates in Figure 3.7 for AA2014 and in Figure 3.8 for AA7075.

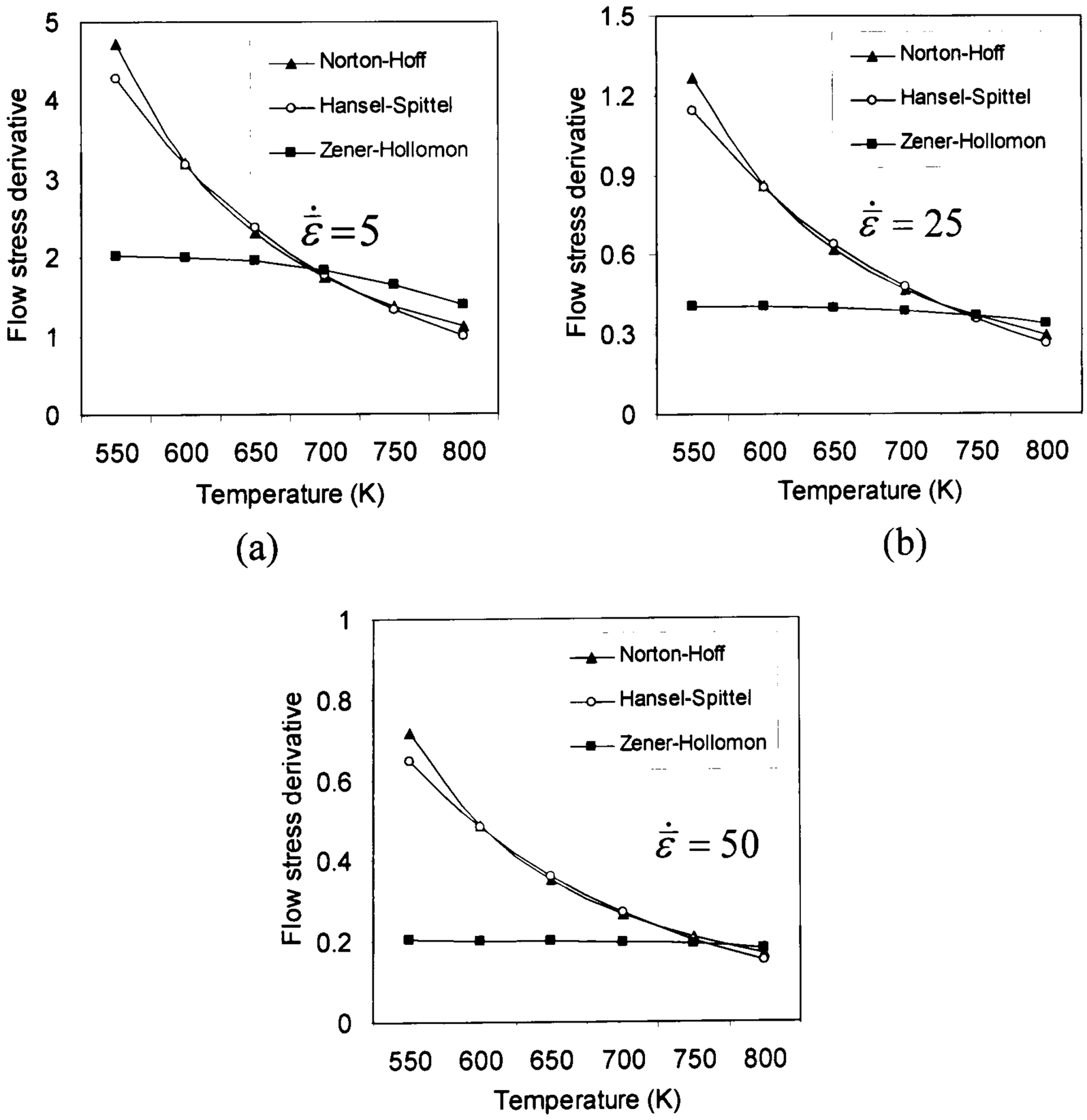

Figure 3.7 Derivatives of the flow stresses versus temperature for AA2014 at different strain rates: (a) $\dot{\bar{\varepsilon}} = 5$. (b) $\dot{\bar{\varepsilon}} = 25$ and (c) $\dot{\bar{\varepsilon}} = 50$

Figure 3.7 shows significant overestimation of the flow stress derivative by both the Norton-Hoff and Hansel-Spittel equations for temperatures ranging from 550K to approximately 700K. For example, in Figure 3.7c, at 550K the Norton-Hoff and the Hansel-Spittel derivatives are respectively 252% and 219% higher than the Zener-Hollomon derivatives.

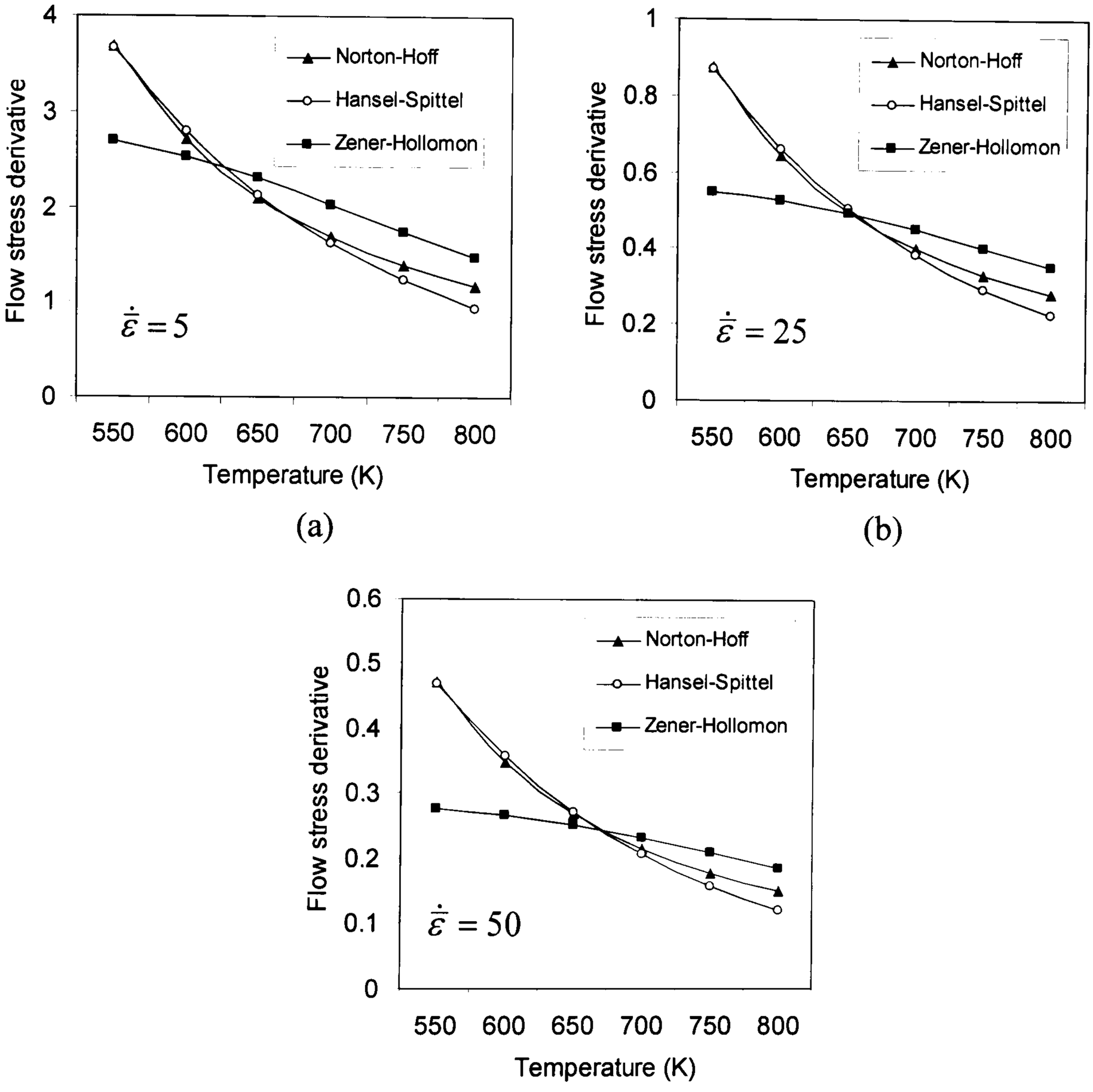

Figure 3.8 Derivatives of the flow stresses versus temperature for AA7075 at different strain rates: (a) $\dot{\bar{\varepsilon}} = 5$, (b) $\dot{\bar{\varepsilon}} = 25$ and (c) $\dot{\bar{\varepsilon}} = 50$

Figure 3.8 also shows a significant overestimation of the derivative by both the Norton-Hoff and Hansel-Spittel equations. However from approximately 650K these equations underestimate the derivative of the flow stress. For both alloys the Zener-Hollomon derivative stays relatively constant within the temperature range. This

was expected as the term $(\tanh \alpha\sigma_{Z-H})$ approaches 1 for high values of $(\alpha\sigma_{Z-H})$. Furthermore, studies have shown that aluminium material is strain rate insensitive at room temperature. Therefore it is surprising to see a distinct variation for the derivatives of Norton-Hoff and Hansel-Spittel flow stresses when they are plotted against the temperature range.

Due to the complex formulae involved in FEM it would be difficult to quantitatively evaluate the contribution of the derivative to the flow stress. Duan *et al* (2004a) simulated the extrusion of AA2024 with FEM. The calculated peak loads were underestimated by 1.8% with Zener-Hollomon and by 6.1% with Hansel-Spittel (or 16.2% with a different source of parameters).

It is evident that the Zener-Hollomon formulation is the most appropriate equation to represent the flow stress in hot extrusion of aluminium alloys using the FEM. However, for the same aluminium alloy, many different flow stress data can easily be found in the literature. The accuracy of the data depends on three major factors: (a) the type of heat treatment (homogenisation) for the testing samples, (b) the testing methods and (c) the person who conducts the experiments. It is therefore important to exercise caution in the selection of flow stress data before the start of any analysis.

3.4 Discretisation

Discretisation is a very important procedure in the simulation of extrusion. The deformations are severe and the part geometry can be complex. Furthermore, the number of re-meshing can be large and mesh regeneration creates some errors such as volume loss and smoothing of solution gradients. Thus special attention must be taken when choosing element type, mesh generation technique, mesh refinement and the re-meshing criterion.

Chenot *et al* (1999) described the finite element discretisation used with Forge 2 and Forge 3 as follows. The velocity field, $[v]$, for isoparametric elements is discretised with the use of the nodal velocity vectors, V_n, and shape functions, N_n:

$$[v] = \sum_n V_n N_n(\xi) \tag{3.18}$$

where ξ is the local co-ordinate vector. The mapping with the physical space is defined by, $[x]$, and is written:

$$[x]=\sum_n X_n N_n(\xi) \tag{3.19}$$

The strain rate tensor, $[\dot{\varepsilon}]$, is computed with the help of the B linear operator:

$$[\dot{\varepsilon}]=\sum_n V_n B_n \tag{3.20}$$

The pressure field, $[p]$, is discretised in term of nodal pressure, P_m, with compatible shape functions, M_m:

$$[p]=\sum_m P_m M_m(\xi) \tag{3.21}$$

3.4.1 Element type

Conform extrusion is a three-dimensional process and is therefore not easily simulated by using equivalent two-dimensional substitute models such as plane strain or axisymmetric. However, with modern computing power it is not always efficient to run 3D analyses. Plane strain studies can produce useful qualitative results of the Conform process as demonstrated in section 5.2.2 of this thesis. Axisymmetric elements are used for the FEM validation in section 4.2.

The use of tetrahedral elements for complex geometries is widely used in the FEM community, especially for its convenience in automatic meshing and re-meshing. In Forge 3 a mixed velocity pressure formulation is used for the elements. Thus the tetrahedral element comprises five nodes for the velocity from which four are interpolated for the pressure. Figure 3.9 represents the finite element interpolation in a tetrahedron.

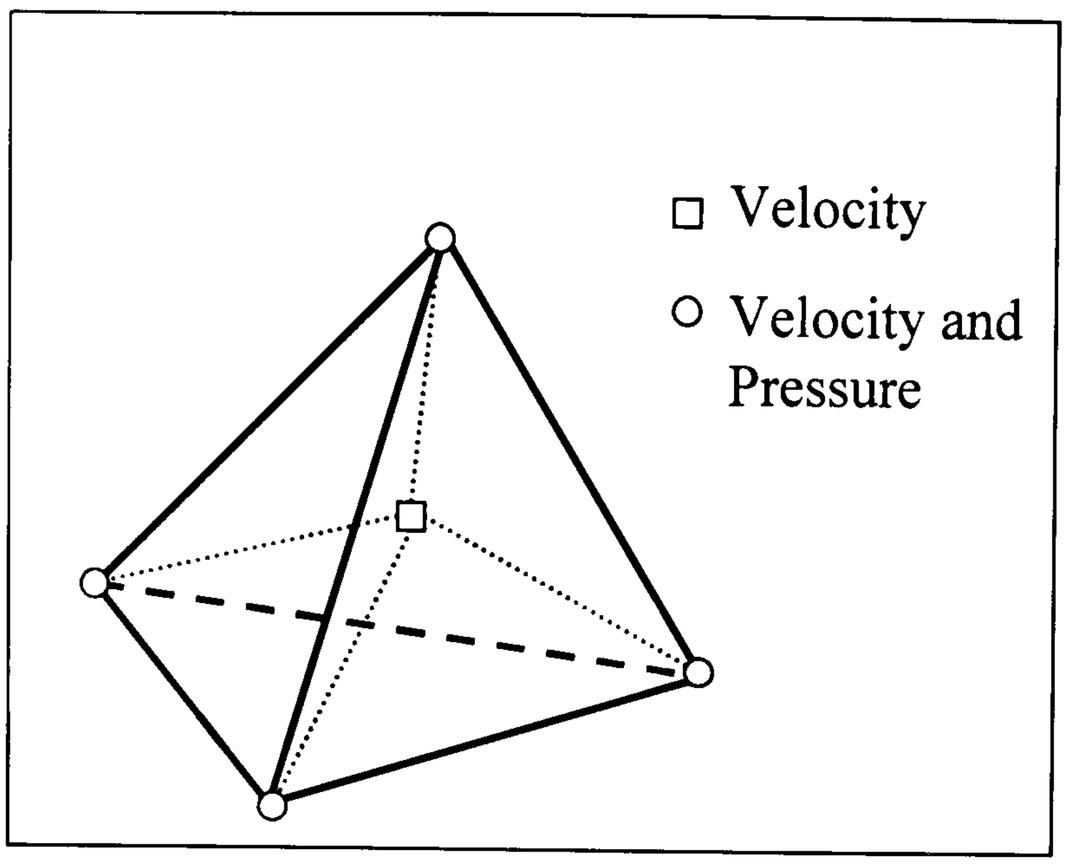

Figure 3.9 Schematic of a finite element interpolation in a tetrahedron

In Forge 2 a seven node triangle with linear discontinuous pressure is used for both plane strain and axisymmetric analyses.

3.4.2 Mesh generation

Currently the most popular approaches for mesh generation are the Delaunay triangulation and the advancing front technique (Yang and Lee 1999). With the latter technique, also called the moving front method, the tetrahedral (or triangular) mesh is progressively generated by creating elements one by one. In this method an active frontal face is selected to define the position of the fourth node in order to create the best tetrahedron. This process is repeated until the whole volume is meshed. Although the advancing front technique generates very good quality meshes in terms of the element shapes, it requires a very large amount of computation time. Therefore this technique is unsuitable for the simulation of extrusion where a large amount of re-meshing is necessary. The Delaunay triangulation generates tetrahedral (or triangular) meshes for a given set of nodes according to the Delaunay criterion (Weatherill and Hassan 1994). In this method the mesh is first generated on the boundaries of the volume (or the surface) and nodes are then inserted incrementally inside the mesh. The tetrahedrons (or triangles) are redefined according to the Delaunay criterion. Generally this method is used with specialised algorithms which force or recover the surface triangulation to match the original geometry. This is known as the 'boundary constrained Delaunay

triangulation' (Weatherill and Hassan 1994). This is the preferred method for generating meshes for the workpiece in extrusion and consequently is the favoured method for the meshing of the feedstock in Conform extrusion.

Two-dimensional mesh

In this thesis 2D geometries (Conform and conventional extrusion) were modelled and meshed using Forge 2. The workpiece (or feedstock) was meshed with plane strain or axisymmetric triangular elements while the tooling was only meshed at the boundary using contact elements. This means that the tooling was considered rigid (i.e. not elastic). It is possible to simulate the deformation of the tooling during extrusion by meshing the internal surfaces. However, by doing so the computational time significantly increases.

Three-dimensional mesh

The 3D geometries (Conform and feeder plate) were modelled and meshed at the boundary using I-Deas (a CAD and FEA package). The surface meshes of the workpiece and tooling were then transferred to Forge 3. The software algorithm generated the internal mesh of the workpiece with tetrahedral elements and the surface meshes of the tooling with triangular elements.

3.4.3 Mesh refinement

Different global mesh edge lengths were defined and applied to the deformable parts (billet or feedstock). Mesh edge lengths were locally adapted depending on the local curvature. Mesh size distributions were imposed during computation by using 'mesh boxes'. These boxes were fixed (i.e. they did not move with the material flow) and a local element length was defined within their surfaces (or volumes).

As with every FEA, a fine mesh is required for those specific areas where accuracy is required. Therefore mesh boxes were implemented at die entries, die exits and sometimes at tooling boundaries. After several analyses, it was found that a minimum of four element edges should be used to define a fillet radius. It was also established that a minimum of 10 elements should be used to represent the extrudate thickness at the die land area.

3.4.4 Re-meshing

Forge 2 and Forge 3 automatically re-mesh the workpiece (or feedstock) at a given frequency or if the mesh has been degenerated. A mesh is considered degenerated if either some of the elements become too distorted, or if the contact surface of the workpiece does not correspond accurately to the tool surfaces. The element distortion is measured by the quality parameter, Q, in terms of the relative Jacobian between the reference element (with $Q = 1$) and the distorted element. The time required to compute the numerical equations is highly dependant on the quality of the mesh. Coupez (1994) suggested that a good strategy with Forge 2 and Forge 3 is to re-mesh as often as possible. However a good quality mesh is costly in terms of computational time and power. Therefore, to perform an efficient analysis, a compromise must be obtained between the degree of discretisation (i.e. use of mesh boxes), the frequency of re-meshing, the computing power and time available.

3.5 Contact conditions and friction models

3.5.1 Contact conditions

In the analyses used for this thesis the tools were considered rigid, i.e. non deformable. The interior of the tools were not meshed and only the boundary surfaces were discretised. The number of equations to be solved simultaneously was therefore greatly reduced. In Forge 2 and Forge 3 the mesh of the workpiece is updated at every step of re-meshing. The midpoint of each element boundary edge is tested. If a midpoint is found inside the tools then a node is created and the element is divided into two elements. Every node found inside the tools is projected onto the surface of contact by an impenetrability algorithm. Figure 3.10 illustrates this contact condition.

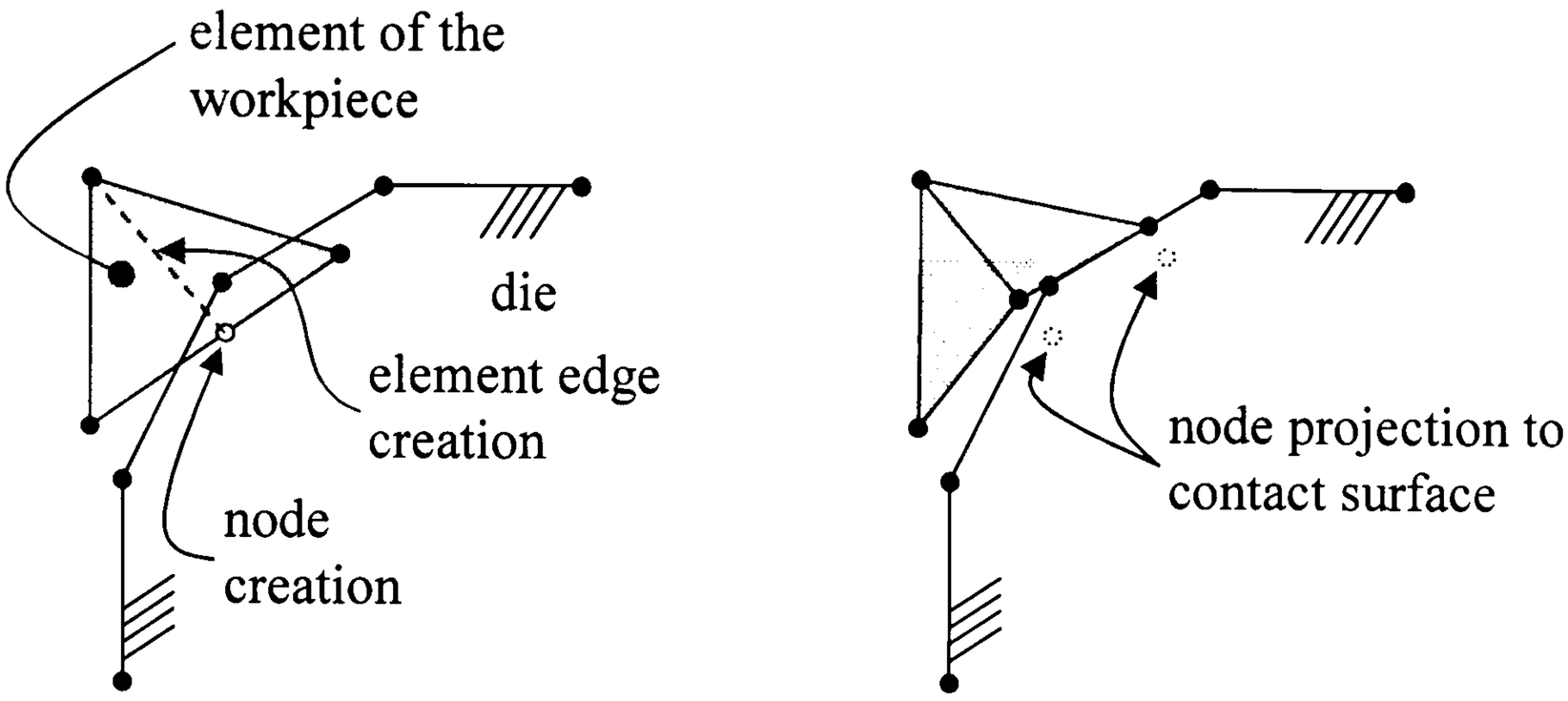

(a) (b)

Figure 3.10 (a) Midpoint penetration and (b) impenetrability algorithm

3.5.2 Friction model

Friction between the workpiece and the surface of the tooling is initiated as soon as contact is established between the two parts. There are three friction laws available with the software: *Coulomb friction law*, *Tresca friction law* and *Viscoplastic friction law*. Velay *et al* (2003) derived the friction coefficients for the three laws by comparing the computed peak load obtained from virtual extrusion with the experimental values measured by Subramaniyan (1989, p.220-231). It was found that the so-called *Coulomb friction law* was one of the most suitable friction laws for aluminium extrusion. This name is misleading however as this law is not a true Coulomb friction, as shown by the definition in Chapter 2. This law limits the friction to a maximum value after a fraction of the normal stress, σ_N, is reached. The friction stress, τ_F, is defined as follows:

$$\left.\begin{aligned} \tau_F &= \mu\sigma_n \text{ if } \mu\sigma_N < \overline{m}\frac{\sigma_0}{\sqrt{3}} \\ \tau_F &= \overline{m}\frac{\sigma_0}{\sqrt{3}} \text{ if } \mu\sigma_N \geq \overline{m}\frac{\sigma_0}{\sqrt{3}} \end{aligned}\right\} \tag{3.22}$$

where σ_0 is the von Mises stress, μ the friction coefficient and $\overline{m}$ is the Tresca friction coefficient. The derived coefficients from Velay *et al*'s study were $\mu = 0.1$

and $\overline{m} = 0.9$. Figure 3.11 illustrates this friction law against the value of the normal stress.

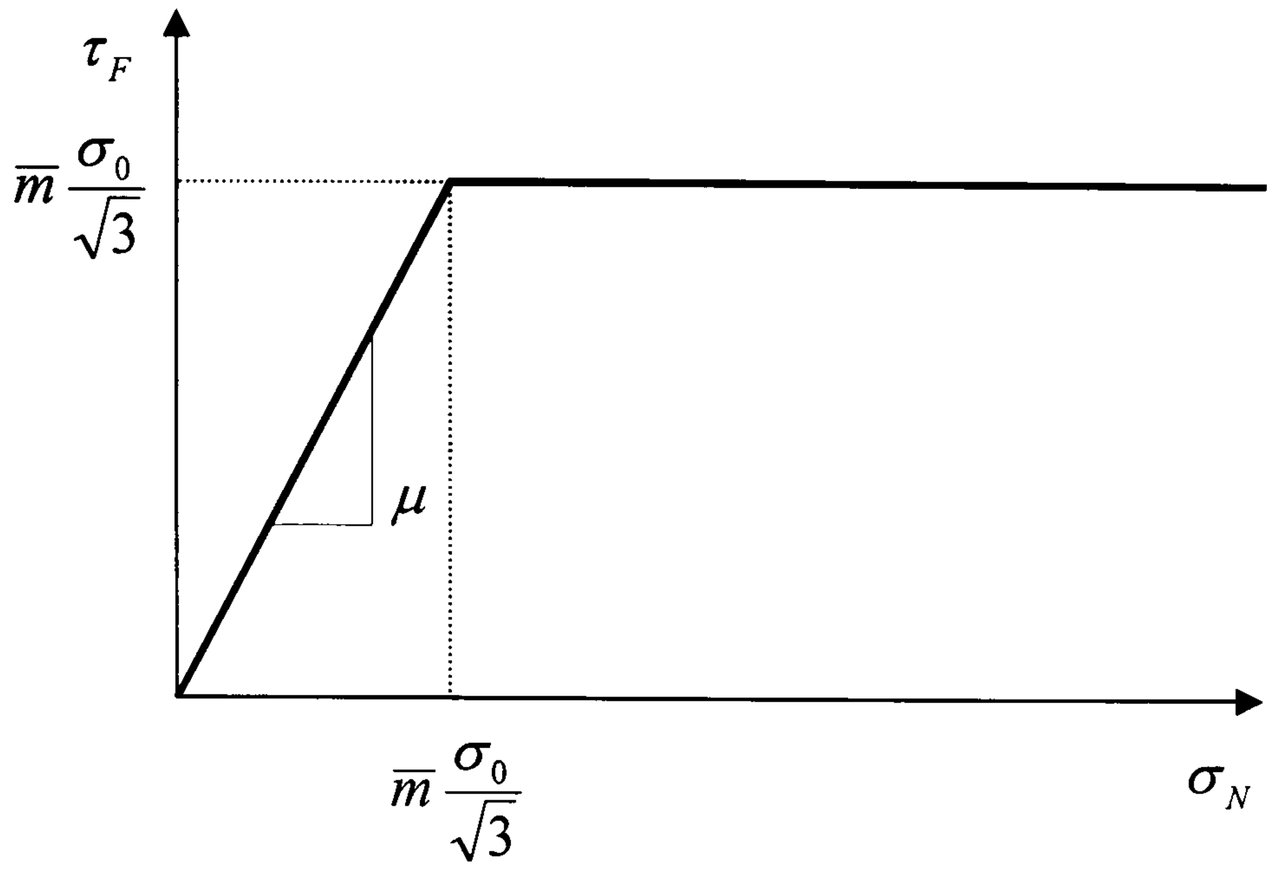

Figure 3.11 Coulomb friction law limited Tresca

3.6 Heat transfer

Every element is subjected to internal heat conduction and dissipation under the constraints defined on the boundary in terms of heat transfer (conduction, convection and radiation) or imposed temperature. This heat balance is represented by the following equation:

$$\rho_{Al} C_{p(Al)} \frac{\partial T}{\partial t} = \Phi_c + \Phi_r + \Phi_{fr} + \Phi_{cst} + \dot{Q}_d \qquad (3.23)$$

where ρ_{Al} is the aluminium density, $C_{p(Al)}$ is the specific heat of aluminium, T is the temperature of the workpiece and t the time. $\dot{Q}_d$ is the heat generation rate (also called the internal dissipation) due to deformation per unit of volume and is described in equation (2.25). Φ_c is the conduction and convection flux, Φ_r is the radiation flux, Φ_{fr} is the friction dissipation flux, and Φ_{cst} is the constant flux. Details of the different fluxes are described below according to Chenot *et al* (1999) and Transvalor (2004a and 2004b).

The conduction and convection flux, Φ_c, combines the rate of heat transfer due to both conduction and convection as defined previously in equations (2.32) and (2.33). This flux is written as follows:

$$\Phi_c = h(T - T_0) \tag{3.24}$$

where h is the global transfer coefficient for conduction and convection and T_0 the tooling temperature.

The radiation flux, Φ_r affects the boundary of the mesh and is written:

$$\Phi_r = \sigma_r \varepsilon_r \left(T^4 - T_{amb}^4\right) \tag{3.25}$$

where σ_r is the Stefan-Boltzmann constant (σ_r= 5.67051.10^{-8}Wm^{-2}K^{-4}), ε_r is the material emissivity and T_{amb} is the ambient temperature. An ambient temperature of 50°C was set for all of the analyses in this thesis.

The friction dissipation flux, Φ_{fr}, at frictional interfaces is shared between the workpiece and the tooling with fluxes relative to their respective effusivity: b_{Al} and b_{Tool}. This flux is written as follows:

$$\Phi_{fr} = \frac{b_{Al}}{b_{Al} - b_{Tool}} \alpha K (\Delta V)^{p+1} \tag{3.26}$$

where α is a friction coefficient, K is the consistency, ΔV is the relative velocity between the material and the tool, and p is the sensitivity to the sliding velocity. The effusivity b_i from a material i is calculated as follows:

$$b_i = \sqrt{k_i \rho_i C_{p(i)}} \tag{3.27}$$

where k_i, ρ_i and $C_{p(i)}$ are the thermal conductivity, density and specific heat of the material i respectively.

The constant flux, Φ_{cst}, is a function of the global transfer coefficients with the air and the tooling.

3.7 Prediction of substructure and properties

Subgrain size has significant influence on the strength and ductility of metals. Modelling of subgrain size evolution is essential for the detailed understanding and control of mechanical properties. In this thesis, the evolutions of microstructure during the hot extrusion of a rod, T-shaped and semi-closed sections were predicted. The empirical and physical equations and FE models are detailed in Chapter 5 together with the presentation and discussion of the results.

3.8 Parallel processing

Most of the three- dimensional analyses presented in this thesis were computed with two processors in parallel. Forge 3 code is parallelised following a Single Program Multiple Data (SPMD) concept (Coupez *et al* 1996). This efficient strategy consists of running compete versions of the code on each processor, thus requiring only a few changes of the initial serial versions of the relatively complex codes. The mesh of the workpiece is divided into sub-domains. Each processor runs a simulation on one sub-domain and its associated set of meshed tools. The re-meshing is performed independently on each sub-domain, whilst also preserving the interfaces. Periodically a parallel repartitioning of the whole domain is activated to transfer the load and to re-mesh the interface. In this way the loading is optimised and each processor shares relatively the same amount of elements. Figure 3.12 has been derived from results obtained by Coupez *et al* (1996) and demonstrates the efficiency of parallel re-meshing and repartitioning of Forge 3 with several processors.

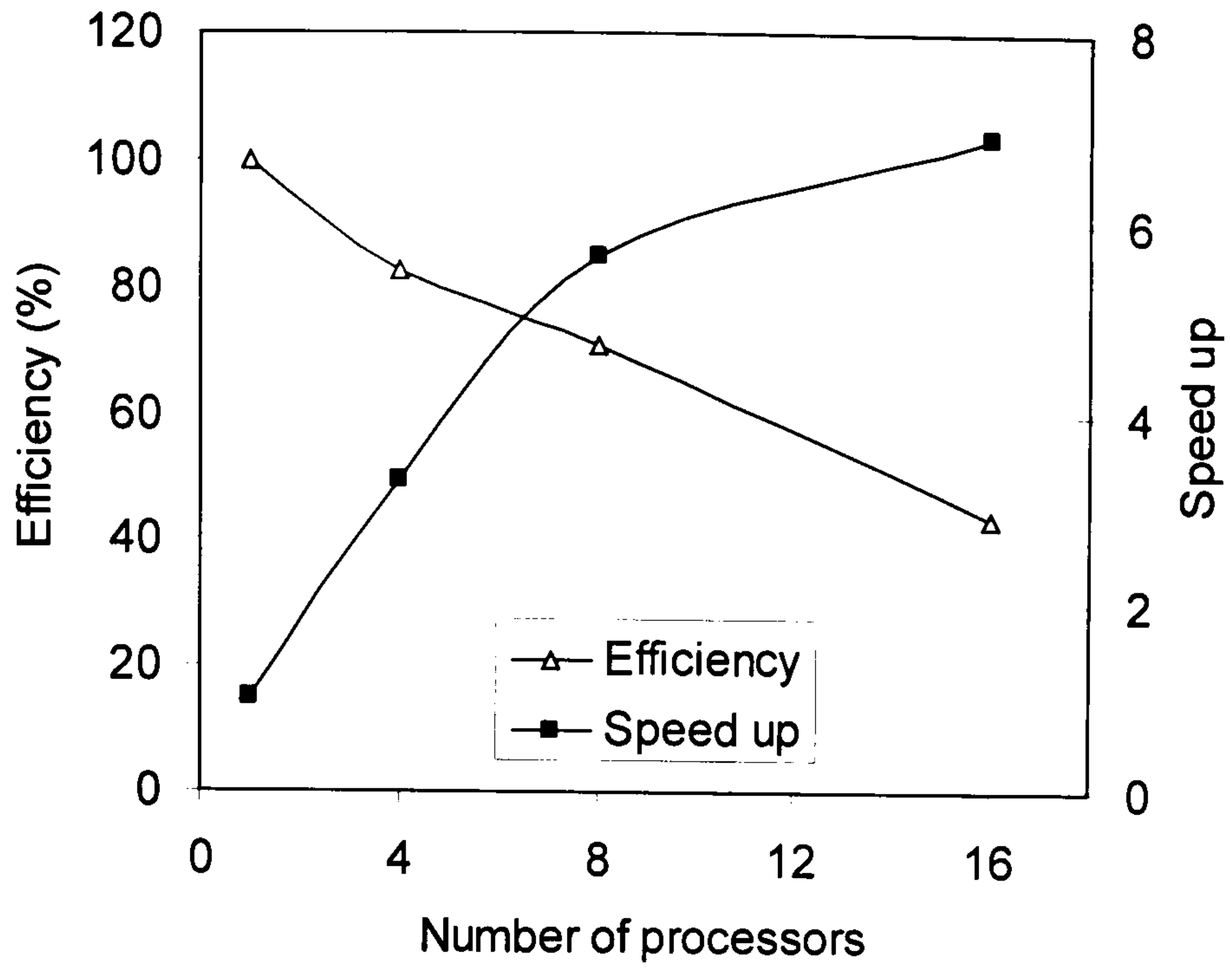

Figure 3.12 Efficiency of parallel re-meshing and repartitioning

As the figure shows, parallel processing speeds up calculations. However, it is clear that increasing the number of processors quickly reduces the efficiency of the analyses.

3.9 Data file

At the start of every simulation the software Forge 2 and Forge 3 read a formatted file with specific syntax (the data file). This file comprises a series of modules each defining the different features of the software required for a successful analysis. Keywords and numerical values are the input parameters for the modules. Forge 2 uses up to 17 different modules while Forge 3 uses up to 18 modules. Details of the modules and their variables can be found in the user guides of the respective software (Transvalor 2004a and 2004b). A copy of the data file created for the simulation of the Conform process (see Chapter 4) is included in Appendix E. The main modules used for the simulations in this thesis are as follows:

- The *Units* module – This defines the system of units for computation. The key word '*mm-MPa-mm.kg.s*' was used. Length terms were defined in millimetres, stress and pressure terms in MPa, thermal quantities in mm.kg.s and the temperature in degrees Celsius.

- The *Rheology* module – This is a very important module as it contains all of the data used for defining the thermo-mechanical characteristics of the workpiece (except for the initial temperature of the material). The contact conditions (friction and thermal exchange) between the different tools and the material as well as the parameters for the Zener-Hollomon flow stress have also been defined in this module.
- The *Increment* module – This imposes an average strain value for one increment. The average strain increment of 1% corresponds to a precise calculation and was the default value used.
- The *Thermique* module – This activates the thermal computations between both the workpiece and tooling, and workpiece and air.
- The *Cinemat_out* module – This defines the kinematics of the different tools.
- The *Boite* module – This defines the mesh boxes in terms of kinematics (fixed or attached to a die), geometry (cylindrical or cuboidal), and size of the elements inside.
- The *Mauto* module – This controls the frequency of the re-meshing of the workpiece.

3.10 FEM validations

Forge 2 and Forge 3 have been validated both quantitatively and qualitatively for hot aluminium extrusion by several authors. Examples of this can be seen in the work of Flitta and Sheppard (2000), Duan and Sheppard (2003), and Velay *et al* (2003). Extracts from Velay *et al*'s work are presented in Chapter four. In that study, Velay *et al* simulated both the peak load and the material flow in the extrusion of AA5456.

3.11 Concluding remarks

In this chapter various results and discussions on different aspects of the simulation of aluminium extrusion with Forge 2 and Forge 3 software were presented. A number of conclusions can be drawn based on the results and discussions.

- The Lagrangian form is the most appropriate formulation to simulate Conform extrusion. However, this formulation is only efficient if it is run together with an automatic re-meshing algorithm on powerful computers.
- The Zener-Hollomon formulation is the most accurate equation to represent the flow stress in hot extrusion of aluminium alloys using FEM. However, caution must be exercised in the selection of flow stress data before the start of any analysis.
- The 'boundary constrained Delaunay triangulation' is the preferred method for generating tetrahedral meshes for complex shapes both in 2D and 3D, and consequently is the favoured method for the meshing of the feedstock in Conform extrusion.
- Adequate mesh refinement is critical for the efficiency and accuracy of the FE analyses. Therefore the use of 'mesh boxes' for areas of interest (e.g. abutment area and die land) and fillet corners (e.g. die entry) is critical for the simulation of Conform extrusion.
- Re-meshing must be triggered as often as possible. Although re-meshing is time consuming, calculating a numerical solution from a poor quality mesh is also time consuming. The right balance between the frequency of re-meshing and the quality of the mesh cannot be quantified efficiently and therefore experience of simulating the Conform process will give an informed judgement.
- The *Coulomb friction law*, which limits the friction to a maximum value after a fraction of the normal stress is reached, is one of the most suitable friction laws for the simulation of aluminium extrusion using Forge 2 and Forge 3.
- The Forge 3 code is very suitable for parallel computing. The loading is constantly optimised and each processor shares relatively the same amount of elements.

4 Thermo-mechanical simulation of Conform

4.1 Introduction

FEM will always produce a solution, however the user must ensure that these results are accurate or at least represent real phenomenon. In this chapter the FEM code is validated by comparing simulated results against experimental work. Of necessity these experiments were taken from work on normal extrusion. The use of scaling (i.e. the use of a smaller workpiece) was investigated in order to reduce the amount of finite element necessary for an analysis. The influence of the coining roll on the feedstock was also studied. Finally, two simulations of Conform extrusion were performed in 3D, one without the production of flash (ideal case) and the other with the flash (industrial case). These results were then compared with experimental work.

4.2 FEM validation

In this section, Velay *et al* (2003) simulated both the peak load and the material flow in the normal extrusion of AA5456 in order to validate the FE software.

4.2.1 Experimental results

The following experiments were performed by Tutcher (1979, p.225-235) and were reported in Sheppard *et al* (1979). The initial billet length was 100mm with a diameter of 73mm. The container diameter was 75mm. A flat-faced die with a land length of 5mm was used. The extrusion ratio was 40:1. The initial billet temperature was 723K. The container, pressure pad and die temperatures were 573K. A constant ram speed of 13mm.s^{-1} was used throughout the complete extrusion process. The

measured peak load was 3.94MN. Figure 4.1 shows the load-displacement locus together with the location of sampling positions for the structural development.

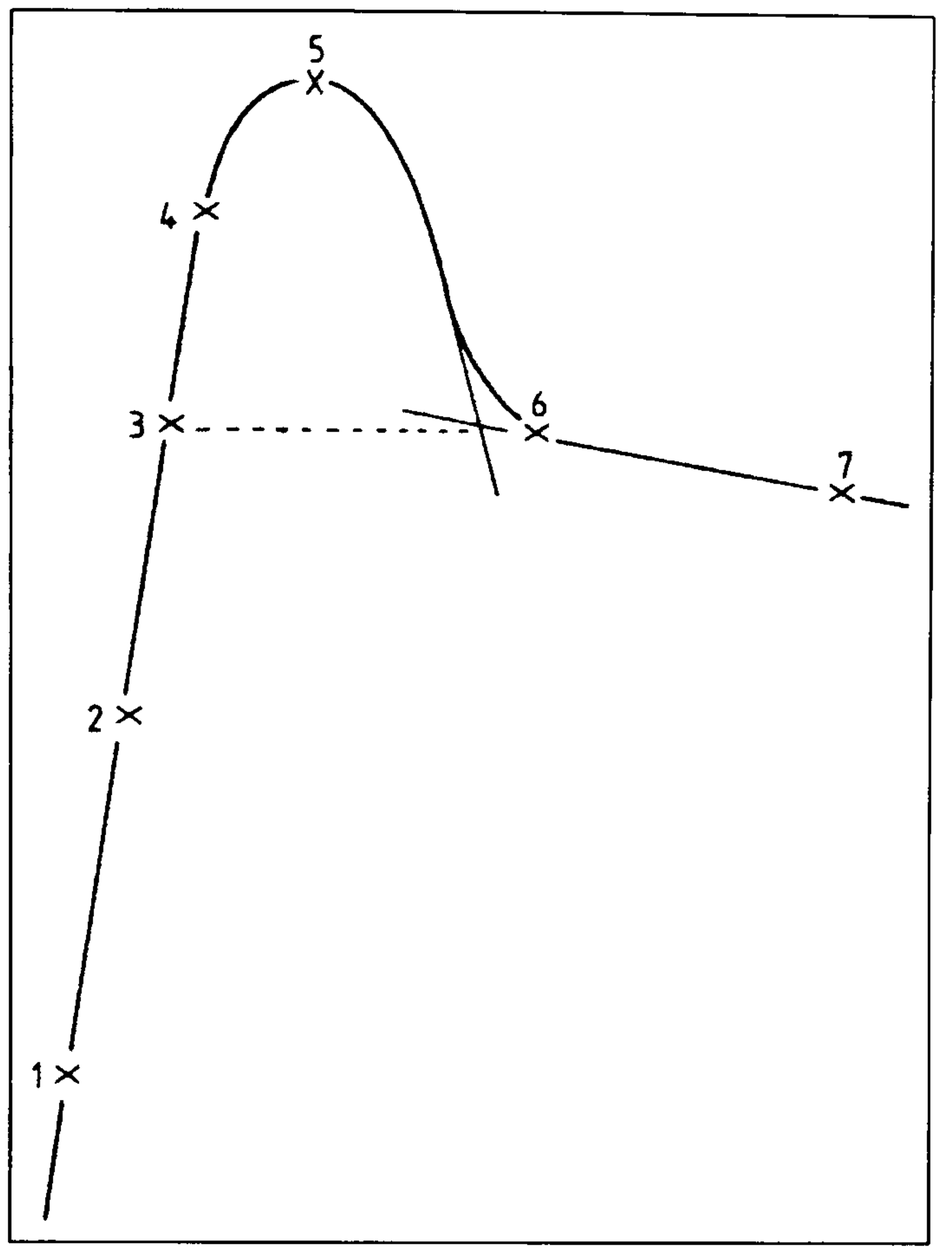

Figure 4.1 Load-displacement locus with sampling positions for macrostructure (Sheppard *et al* 1979)

Figure 4.2 shows the macrostructure and flow pattern of the aluminium in the billet and the extrudate at locations 1 to 6. Figure 4.2a shows the billet during the upset stage. The macrostructure does not change except in the region adjacent to the die entrance where some deformation starts to occur. Figure 4.2b shows the macrostructure of the billet at a latter stage in the upsetting process. The deformation zone adjacent to the die entry is increasing and the grains in this zone are becoming elongated. The grain structure at the periphery of the billet suggests that container/billet shear is occurring due to friction. There is little difference between Figures 4.2b and 4.2c in terms of bulk structure and no dead metal zone is apparent. However as the pressure significantly increases, the deformation zone extends back into the billet, and shearing at the periphery is more pronounced. Although the macrostructure is relatively similar in Figure 4.2d, the extrudate displays a distinct fibrous structure which confirms the increase of deformation. Figure 4.2e, corresponding to location 5 in Figure 4.1, displays the macrostructure at the point of

peak pressure. At this point significant changes are apparent. The fibrous structure of the extrudate extends inside the billet and commences to define the boundaries of the dead metal zones. Furthermore, the layer of material at the periphery of the billet is heavily deformed whilst the material adjacent to the surface of the die plane is far less deformed. This suggests that dead metal zones will form in this area. Finally, a considerable length of material has been extruded and this indicates that the peak pressure does not correspond to the commencement of extrusion. Figure 4.2f shows the macrostructure when the pressure has fallen significantly after the peak pressure and considerable ram travel has occurred as shown in location 6 (Figure 4.1). This location indicates the beginning of the steady state stage. The dead metal zones are clearly identified as well as three regions of intense deformation: the central region and two regions of lesser deformation on either side. More details about the flow pattern during the steady state stage are discussed in section 4.3.2.

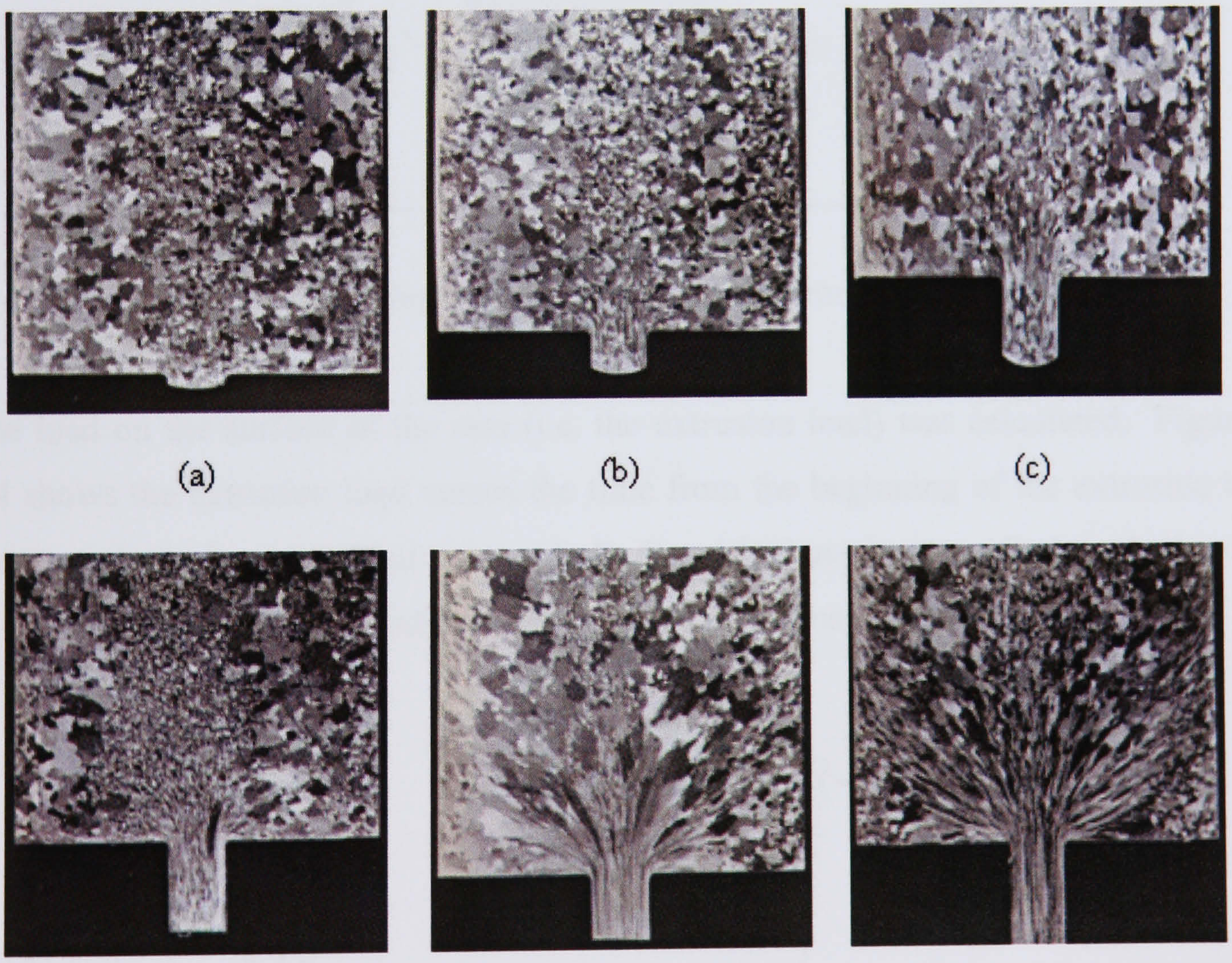

Figure 4.2 Development of macrostructure and flow pattern at (a) location 1, (b) location 2, (c) location 3, (d) location 4, (e) location 5, (f) location 6 (Sheppard *et al* 1979)

4.2.2 FEM results

The experimental variables (geometry, initial temperature and ram velocity) were used as input for the simulation with Forge 2. The billet was meshed using axisymmetric elements. A fine mesh was applied at the contact interfaces, i.e. the billet-ram, billet-container and billet-die interfaces (see Figure 4.3).

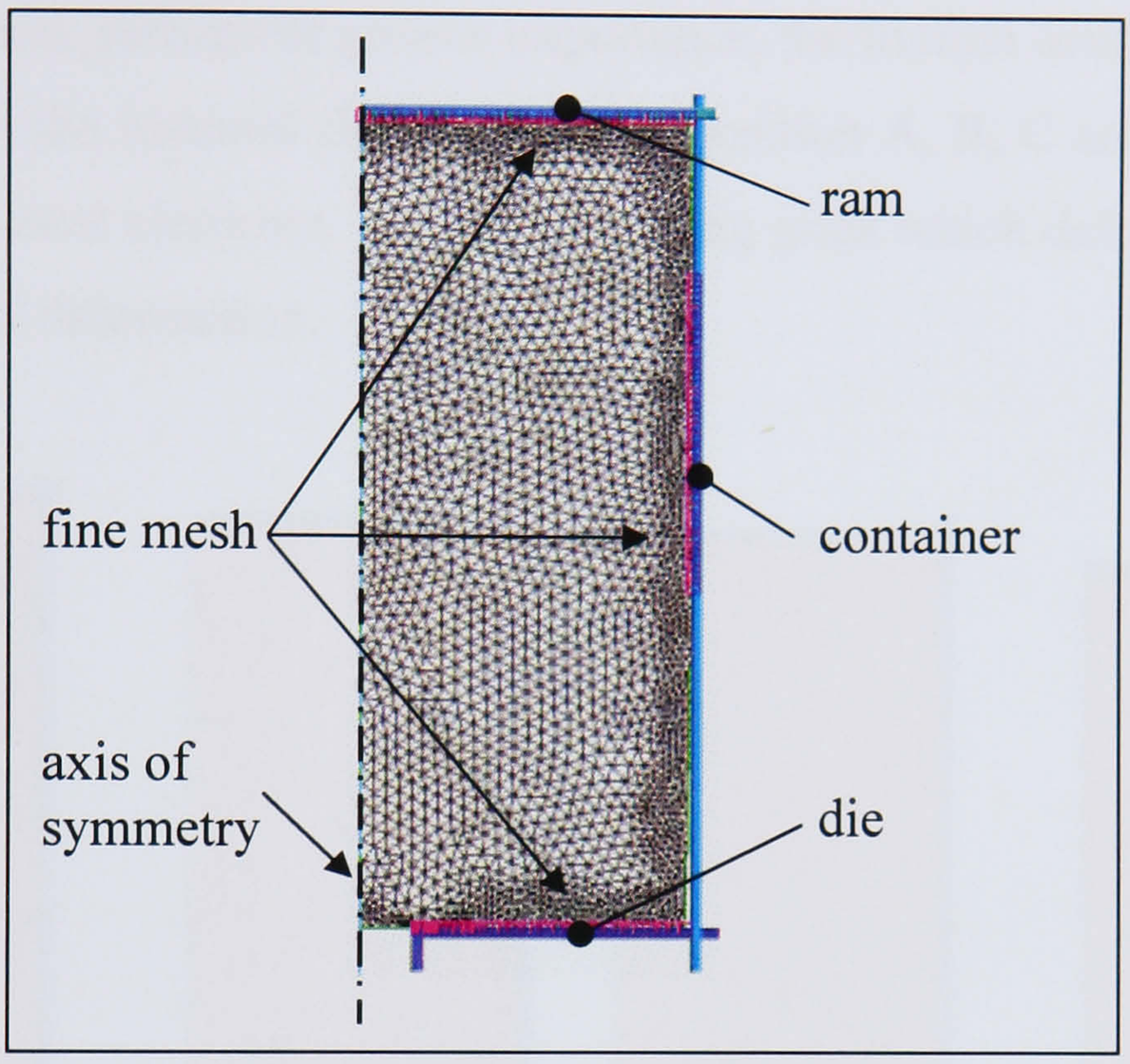

Figure 4.3 Axisymmetric FE model with mesh refinement

The load on the surface of the ram (i.e. the extrusion load) was calculated. Figure 4.4 shows the extrusion load versus the time from the beginning of the extrusion to the start of steady-state. Four points (A, B, C and D) have been marked on the locus of the curve. These points indicate the sampling positions for the flow patterns.

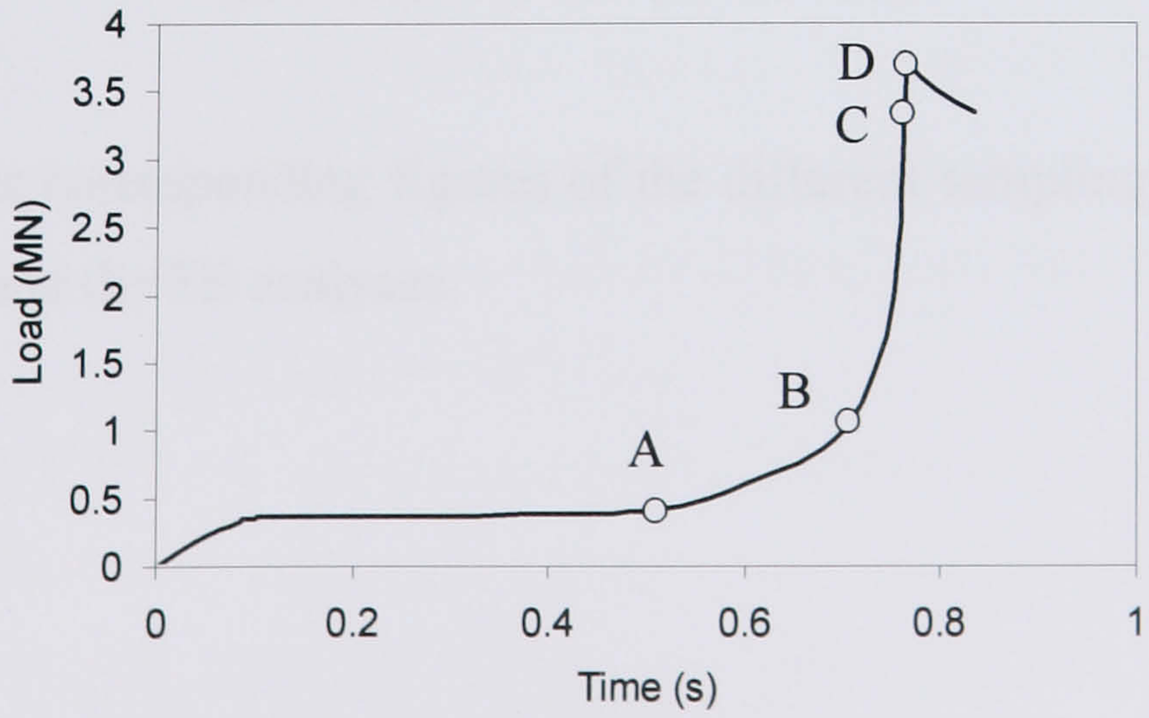

Figure 4.4 Extrusion load versus time

The load curve has been discussed in research papers as a result of both experimental observation (Sheppard *et al* 1979) and finite element analysis (Flitta and Sheppard 2003). The calculated peak load was 3.7MN and therefore the relative error compared with the measured peak load 3.94MN is around 6%. This is an acceptable percentage of error considering the relative accuracy of experimental measurements, flow stress data and, perhaps of greater importance, the friction coefficient values.

Figure 4.5 shows the material flow patterns at position A, B, C and D. The square grids do not represent elements. They are marking grids which deform and distort to represent material deformation.

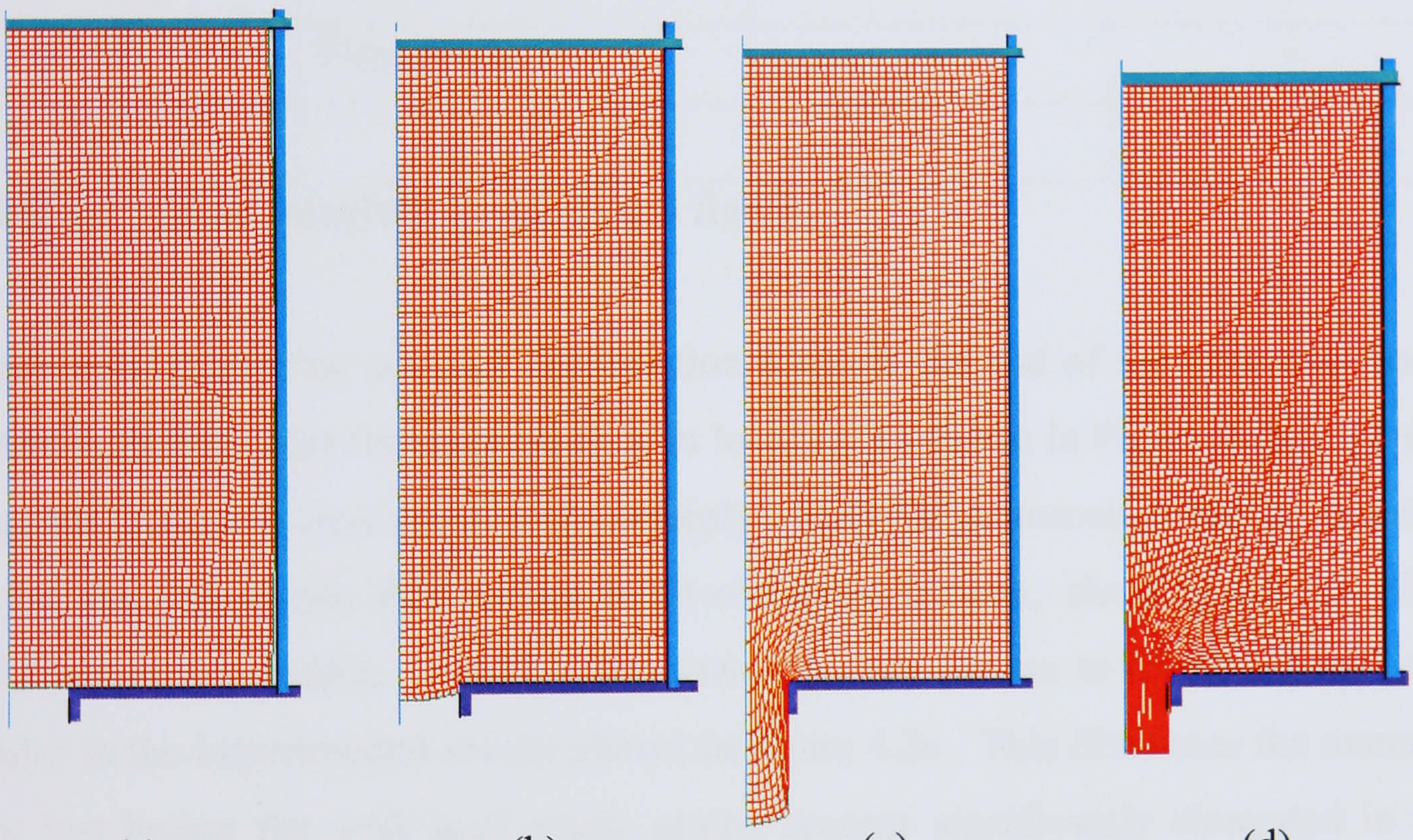

Figure 4.5 Development of material flow pattern at (a) location A, (b) location B, (c) location C and (d) location D

Table 4.1 lists the corresponding figures of the different sampling locations for both the experiments and the FE analyses.

Experiments			FE analyses	
Sampling locations (Figure 4.1)	Flow pattern		Sampling locations (Figure 4.4)	Flow pattern
-	-		A	Figure 4.5a
1	Figure 4.2a	↔	B	Figure 4.5b
2	Figure 4.2b		-	-
3	Figure 4.2c	↔	C	Figure 4.5c
4	Figure 4.2d		-	-
5	Figure 4.2e	↔	D	Figure 4.5d
6	Figure 4.2f		-	-
7	-		-	-

Table 4.1 List of sampling locations and figures

Figure 4.5a shows the material deformation towards the end of the upsetting stage. Figure 4.5b illustrates the material flow at location 1 (shown in Figure 4.2a). At this stage the extrusion load starts to rise sharply. Material deformation can be detected at the die entry and, due to the billet-container friction, shearing at the billet periphery is also visible. Figure 4.5c shows the flow pattern at location 3 and it is similar to the experimental results shown in figure 4.2c. This illustrates the material flow just before the peak load where grains become significantly elongated in the deformation zone adjacent to the die entrance. Figure 4.5d displays the material flow at the point of peak pressure, i.e. location 5 (shown in Figure 4.2e). At this point, the grid pattern near the die entrance takes on a fused appearance due to the high shear deformation occurring. A significant amount of material has been extruded. Significant shear deformations can be seen at the container boundary, whilst less severe deformations are present at the surface close to the die plane. This suggests that the dead metal zone will form in this area.

Figure 4.6 compares the macrograph at location 3 (shown in Figure 4.2c) against the flow pattern at position C (shown in Figure 4.5c). As mentioned previously, this illustrates the material flow just before the peak load where grains become significantly elongated in the deformation zone adjacent to the die entrance. These

elongations can be clearly seen on the grid pattern. Furthermore, the grid pattern also accurately represents the relatively undeformed grains at the tip of the extrudate. The grid provides an almost mirror image of the experimental results.

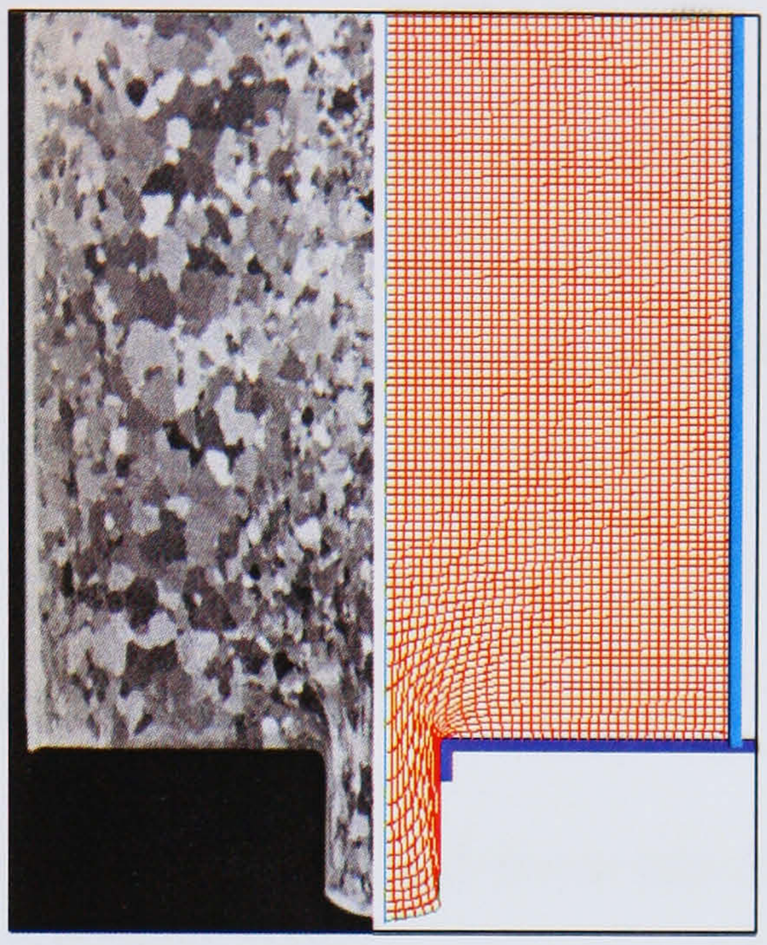

Figure 4.6 Macrograph at location 3 and flow pattern at position C

The results demonstrate that FEM can accurately simulate the velocity field and pressure distribution for the hot extrusion of aluminium. Consequently the temperature, strain and strain rate can be correctly calculated. This is important when the results surrounding the nodal point are extracted to predict the microstructure of the extrudate and eventually its material properties.

4.3 Scaling

The main objective of this section of the thesis was to study whether scaling would be useful for reducing computation time in numerical simulations. This study was conducted in conjunction with Zhi Peng (Peng *et al* 2004) and the author recognises the significant contribution made by his co-worker.

4.3.1 Simulation set-up

Two simulations of a rod extrusion were set-up using Forge 2. The full scale model was based on experiments performed by Veirod (1983, p.196-198). The material

used was AA2014. The initial billet length was 95mm with a diameter of 73mm. The container diameter was 75mm. The extrusion ratio was 20:1. The initial billet temperature was 623K. The temperature for the container, pressure pad and die was 573K. A constant ram speed of 12.4mm.s^{-1} was used throughout the whole extrusion process.

The scaled model used the same boundary conditions (initial temperatures, ram speed and friction coefficients) but the billet was 2.5 times smaller in terms of diameter and height. The die exit diameter was adjusted in the scaled model in order to keep the same extrusion ratio as the full scale one.

4.3.2 Results and discussion

Results such as flow pattern, temperature and strain rate distributions, and sub grain sizes were compared against the experimental data and between the two different FEM models. The computational time for the full scale model was approximately 25 hours and approximately 15 hours for the scaled model. This reduction of time was expected due to the reduction in the number of elements in the model.

Flow patterns

A reference grid pattern, similar to the one shown in Figure 4.5a was adopted to study the material flow pattern. The simulated flow patterns for both rod extrusions are shown in Figures 4.7 and 4.8 for the different positions of the ram. Although the billet sizes differ in these two runs, both flow patterns are similar after the beginning of extrusion. Due to the increase in deformation as the metal approaches the die, parts of the grid pattern are indiscernible (Figures 4.7b-d and 4.8b-d). This deformation can be displayed more clearly by using a contour plot of the equivalent strain as shown in Figure 4.8e. This figure shows the maximum strain at the die entrance and highlights the different regions of deformation.

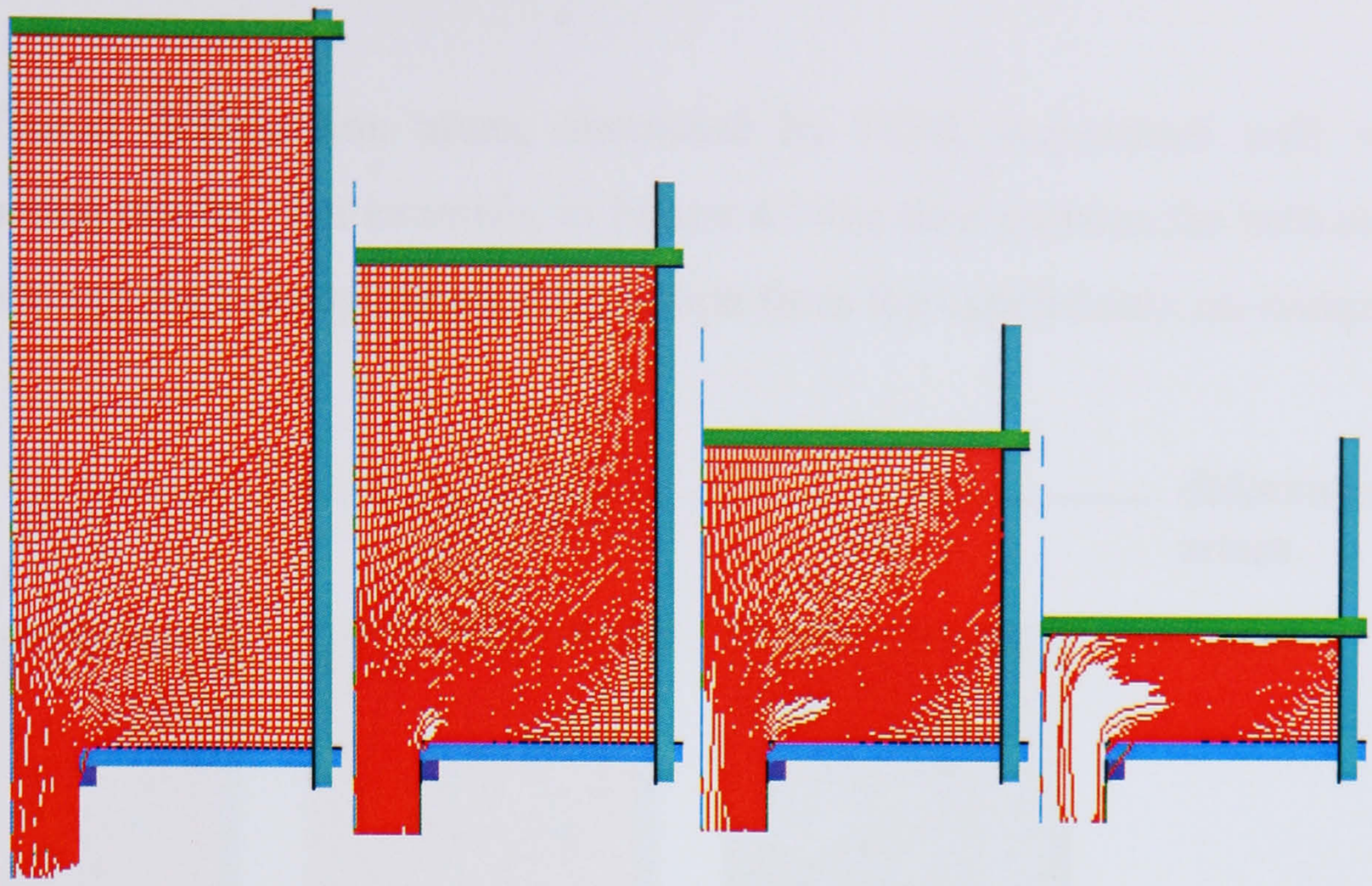

(a) (b) (c) (d)

Figure 4.7 (a), (b), (c) and (d) flow patterns for the full model

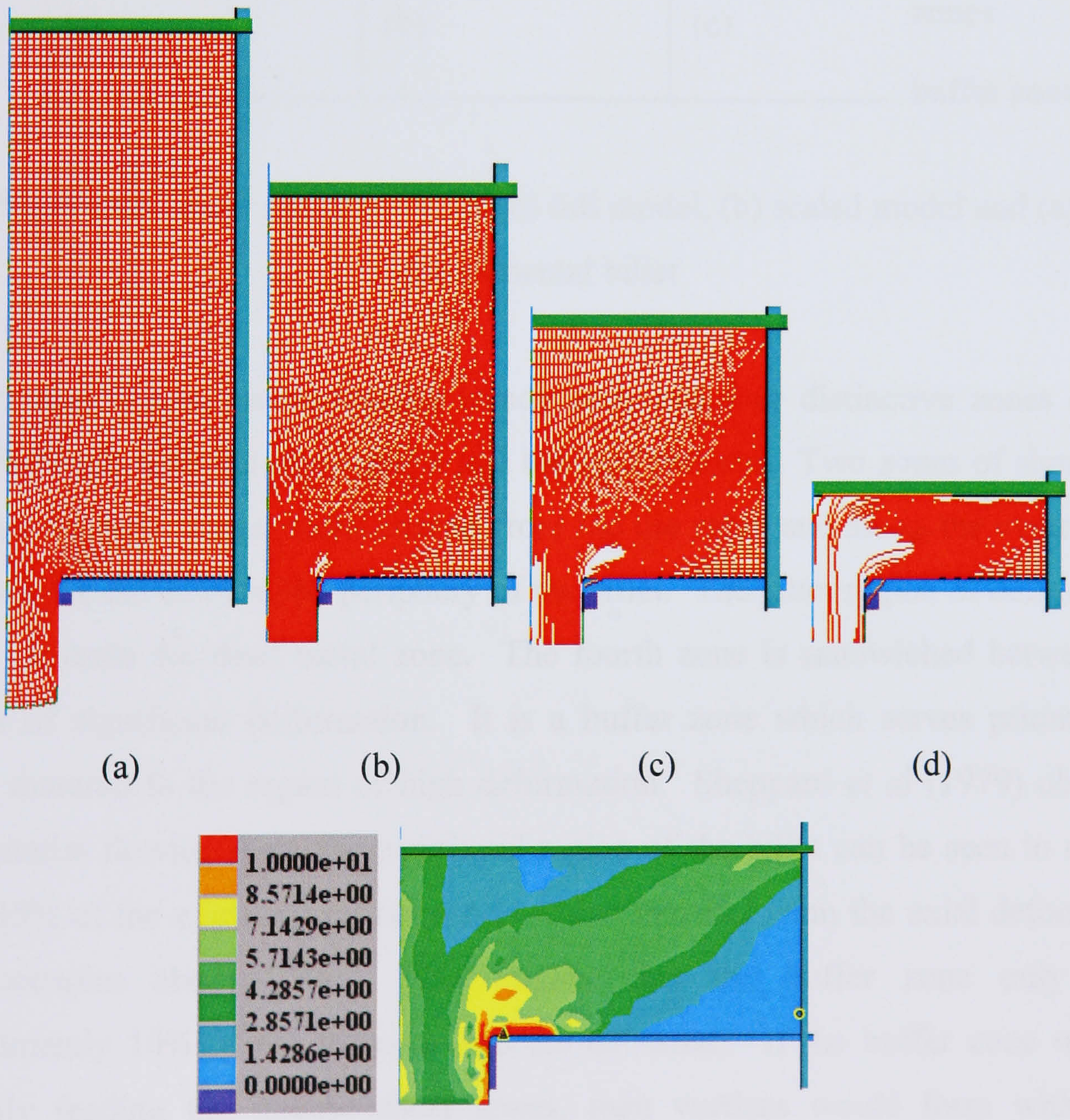

(a) (b) (c) (d)

(e)

Figure 4.8 (a), (b), (c) and (d) flow patterns and (e) equivalent strain for the scaled model

The different deformation areas, simulated by FEM, correspond well with the experimental results. For example, in Figure 4.9 the flow patterns for both simulated extrusions and the corresponding macrograph from the experiments are compared.

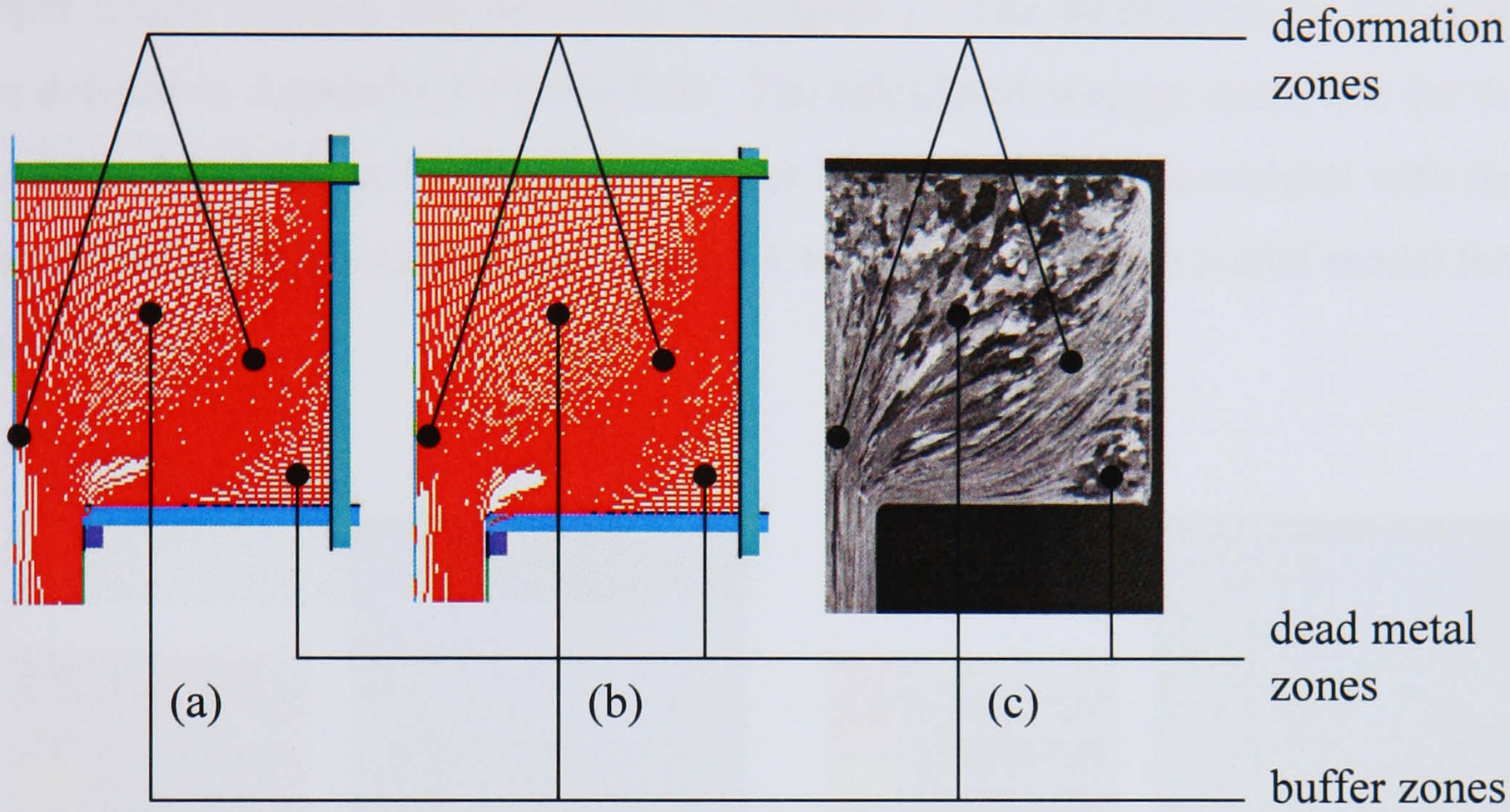

Figure 4.9 Flow patterns for the (a) full model, (b) scaled model and (c) experimental billet

At this stage the extrusion reaches steady state and four distinctive zones can be identified both with the macrograph and the grid patterns. Two zones of significant shear are shown. These zones extend from the die entry and along the central axis and from the die entry to the periphery of the billet. The latter region of deformation clearly delimits the dead metal zone. The fourth zone is sandwiched between the regions of significant deformation. It is a buffer zone which serves primarily to supply material to the region of high deformation. Sheppard *et al* (1979) observed that material flowing from the peripheral region of the billet can be seen to occupy about 35% of the extrudate cross-section whilst material from the axial deformation zone occupies about 55%. This implies that the buffer zone only feeds approximately 10% of the material into the extrudate. If the buffer zone was not primarily feeding the intense shear zones, then vortices would form within the deformation zone due to flow imbalance. This can occur when the dummy block destroys the mass balance of the various deformation zones.

Strain rate

Figure 4.10 shows the distribution of the strain rate for (a) the full model and (b) the scaled model at the same relative position of the ram. The distributions are significantly different and therefore the average strain rates would also be different. The average strain rate can be calculated by the equation (2.6) derived from the upper bound solution and described in chapter 2. The parameters for the equations are defined in Appendix F (Table F.5). The calculated average strain rate for the full model is $5.6s^{-1}$ whilst for the scaled model it is $14.4s^{-1}$. This correlates with the fact that the area of high strain rate in Figure 4.10 is larger with the scaled model than the full model.

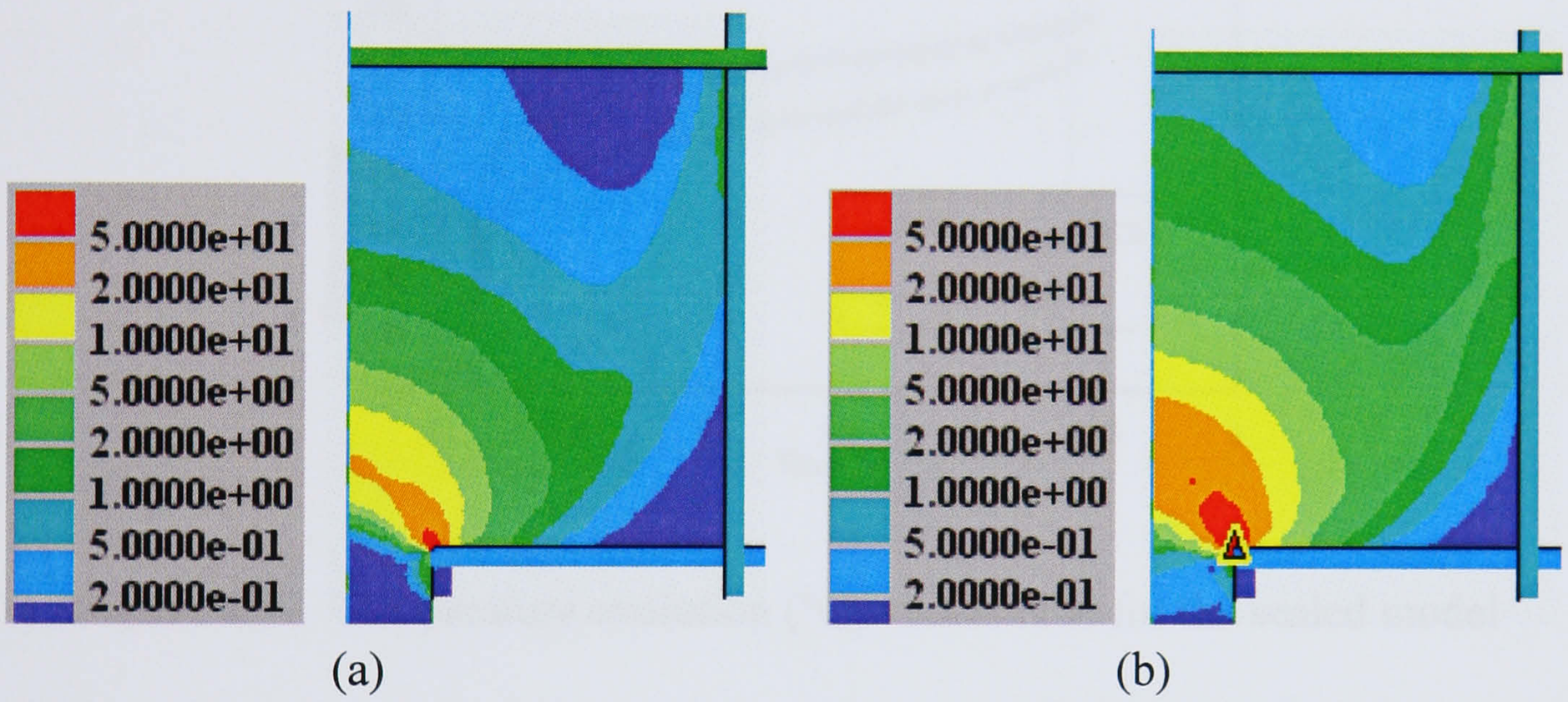

Figure 4.10 Distribution of strain rate for (a) the full model and (b) the scaled model

Temperature

The temperature evolution was recorded at two specific points near the die entrance. The first point was at the centre of the extrudate and the second point at the surface of the extrudate just after leaving the die land. Figures 4.11 and 4.12 show the temperature evolution versus time at both points for the full and the scaled models respectively. In both figures the temperature at the centre increases rapidly towards the end of the extrusion. This is due to the fact that the simulations were carried out to the end of the billet length contrary to industrial extrusions where normally the ram is stopped after about 90% of the billet length is extruded. The dotted lines represent this.

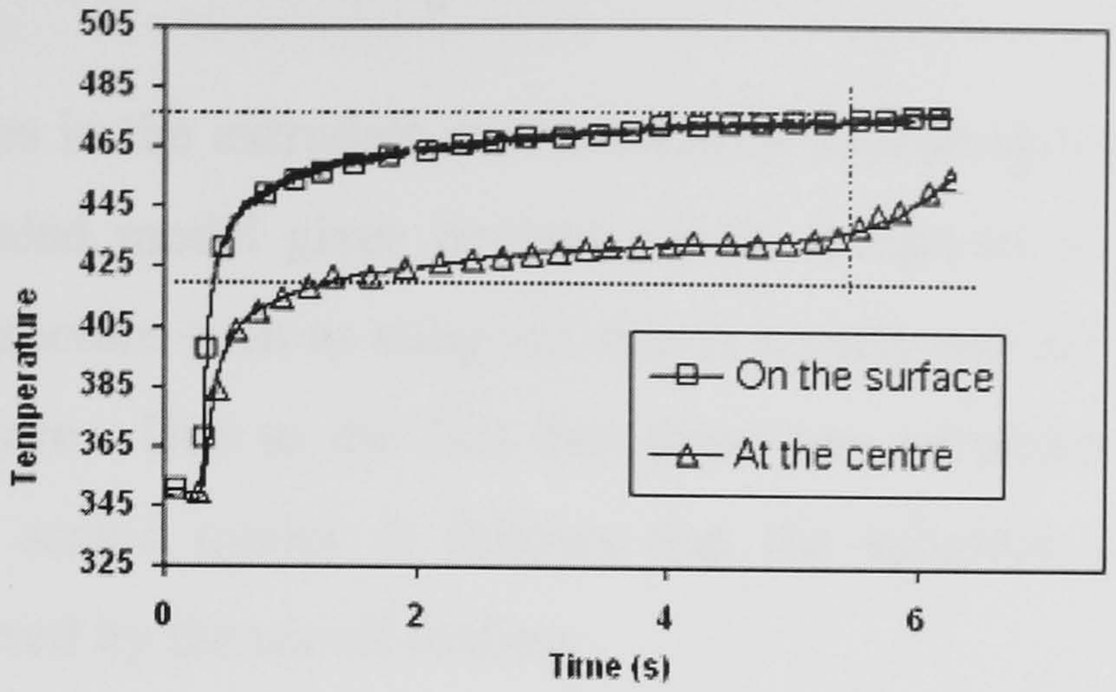

Figure 4.11 Temperature evolution (°C) versus time for the full model

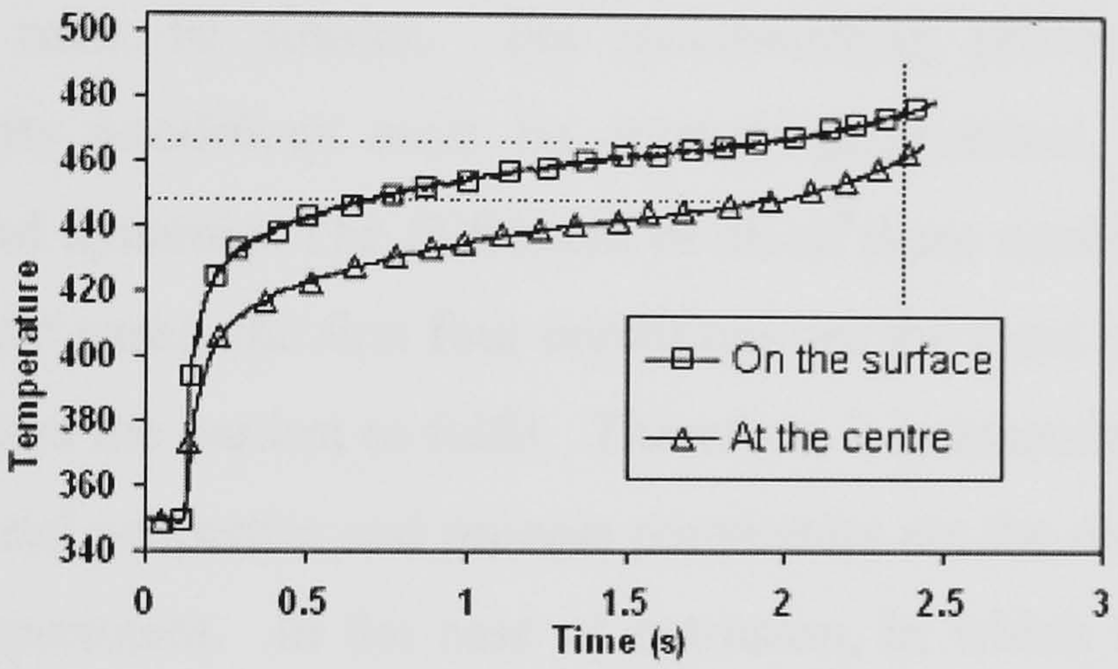

Figure 4.12 Temperature evolution (°C) versus time for the scaled model

The predicted temperatures for the full model correlate relatively well with the temperatures calculated from the experimental data. This latter set of temperatures was derived using the integral profile approach. However, two major differences are found between the two FEM models: the maximum extrusion temperature and the temperature gradient between the centre and the surface of the extrudate. The maximum temperature of the extrudate for the full model is 475°C compared to 466°C for the scaled model. When the extrusions reach steady state, a relatively constant temperature gradient is observed between the surface and the centre of the extrudate as shown in Figures 4.11 and 4.12. However, this gradient is much higher with the full model (43°C) than the scaled model (19°C). Such differences were expected. It is well known that the exit temperature depends on the initial billet temperature, the magnitude of the work carried out during extrusion, and how this is divided between the work needed to overcome friction, and the heat losses to the tooling (Sheppard 1999b).

Subgrain size

The subgrain sizes in the extrudate are reasonably well predicted by the full model. However, the scaled model gives deviant results compared with the experimental data. Material structure such as subgrain size is closely associated to the strain rate and the temperature. Due to the fact that these two variables were not predicted correctly by the scaled model, it follows that the subgrain sizes would also be incorrectly predicted by the use of scaling.

Although scaled models can save a significant amount of computation time and still provide qualitative information for flow patterns, they are unsuitable for the simulation of extrusion. To ensure accurate results and interpretation, the model and the real process must be similar. For metalworking processes the following important similarity conditions must be created: geometrical, plastic, frictional, thermal, elastic and dynamic. The fulfilment of all of these conditions is practically impossible. In most cases, the first four conditions are the most important, although they are also perhaps the hardest to fulfil. Therefore, it is essential to determine and select which material properties and process parameters are the most relevant for the purpose of the experiment. In the case of extrusion, in which temperature rise is significant and strain rate is quite high, more important factors in addition to the material flow need to be considered, for example, the structure evolution. During the extrusion process, the press load, temperature rise, surface quality and extrudate mechanical properties are the most important factors to be considered. If any simulation is applied in extrusion, it has to be effective in predicting all of the above factors. Therefore scaling is not suitable for the study of extrusion and consequently for Conform extrusion where temperature and friction play a major role in the process. It is clear that this major problem will require a solution. An obvious possibility is to introduce a scaling factor as a function of velocity, temperature or both.

4.4 Temperature evolution of the feedstock in the groove

Once the feedstock arrives near the groove of the wheel it is rolled inside the groove by the coining roll. The objective of this process is to create enough friction between the groove wall and the deformed feedstock to initiate the upset zone. This section

of the thesis studies the heat transfer between the feedstock, the wheel, the coining roll and the surrounding air during the coining process until the point when the feedstock reaches the upset zone.

4.4.1 Simulation set up

The study was divided into two stages. The first stage simulated the coining of the feedstock (by moving the coining roll into the groove), the heat generation due to deformation and the heat transfer between all the parts (see Figure G.2 in Appendix G). The second stage simulated the heat transfer between the coined feedstock and the wheel over the griping zone (see Figure A.1 in Appendix A). The simulations used plane strain elements for efficiency purposes. In order to accurately simulate the heat transfer the tools such as the wheel and the coining roll were modelled using deformable dies. This means that the inside of the tools were meshed together with the elastic and thermal properties of tool steel (H13). The dimensions of the tooling, initial temperatures and process variables necessary for the simulations were taken from information provided by Holton Machinery (designer and manufacturer of Conform machines). The temperature of the air inside the groove was calculated by using heat transfer theories (see details in Appendix G). The geometrical parameters are listed in Table 4.2 and the initial temperatures and process variables are listed in Table 4.3.

Description	Value
outer diameter of the wheel	*298mm*
inner diameter of the wheel	*142mm*
wheel thickness	*75mm*
wheel groove height	*13.3mm*
wheel groove thickness	*10.5mm*
wheel groove fillet corner	*4mm*
outer diameter of the roll	*132mm*
diameter of the feedstock	*9.5mm*

Table 4.2 Tool dimensions

Description	Value
initial temperature of the wheel	*384 ℃*
initial temperature of the coining roll	*50 ℃*
initial temperature of the feedstock	*20 ℃*
temperature of the air	*110 ℃*
angular velocity of the wheel	*20rpm*
angular velocity of the coining roll	*43.36rpm*

Table 4.3 Initial temperatures and process variables

Figure 4.13 shows the feedstock, both deformable tools (coining roll and wheel) and the two rigid tools. The lower rigid tool supported the wheel and the upper rigid tool drove the coining roll downwards. The material used for the feedstock was AA6063 and was modelled with the Hansel-Spittel formulation regressed from cold data (i.e. between 20°C and 250°C). A high Tresca coefficient of friction (0.9) was applied between the feedstock and the wheel groove. However a lower Tresca coefficient of friction (0.6) was defined between the feedstock and the coining roll. This simulated the rolling action of the coining roll. A relatively fine mesh was used near the contact surfaces.

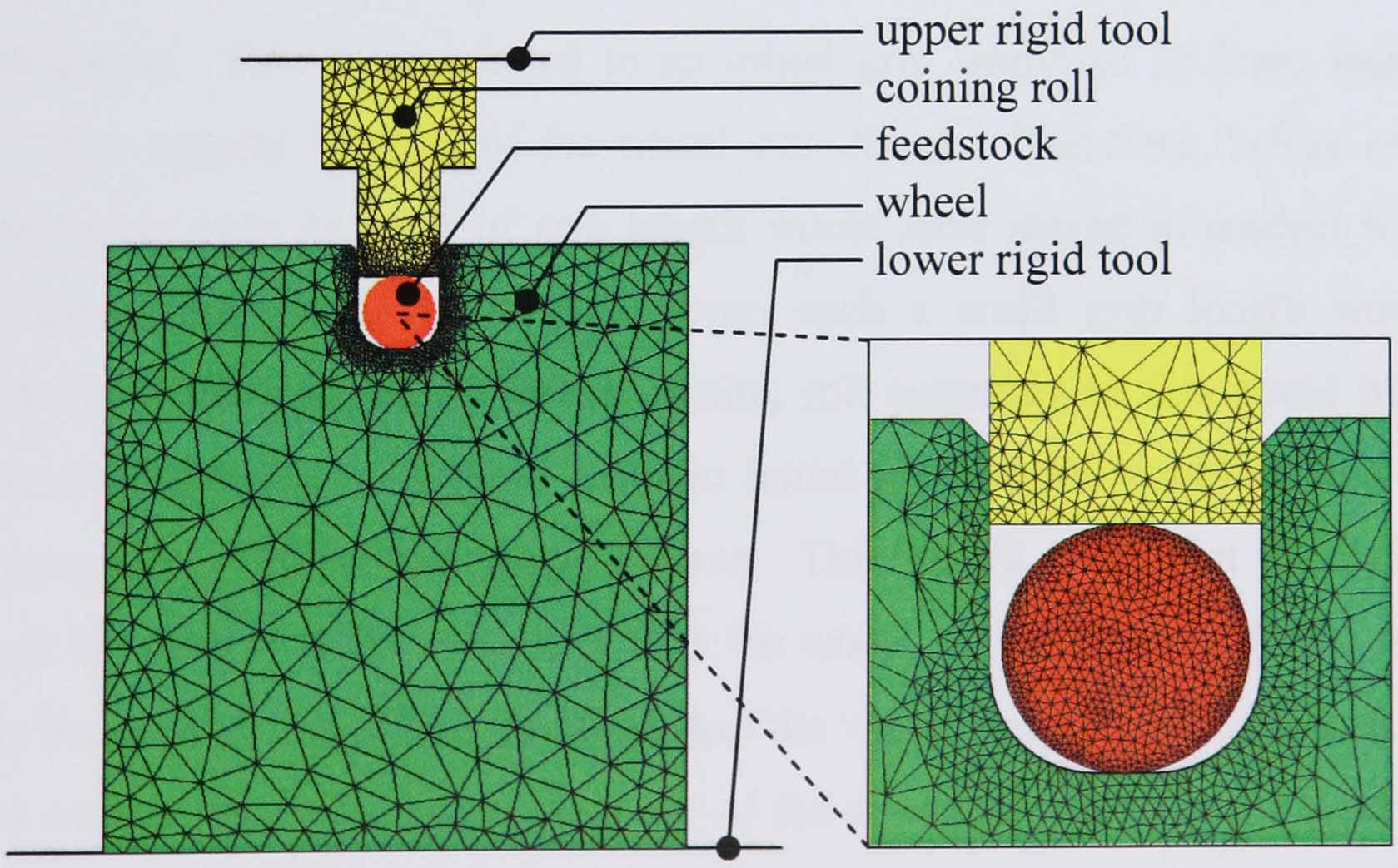

Figure 4.13 Plane strain model of the wheel, coining roll and feedstock

A theoretical value was calculated for the vertical displacement of the coining roll. This value is important as it defines the amount of deformation of the feedstock which subsequently determines the amount of contact between the feedstock and the groove. Consequently this defines the minimum initial grip length and the recommended position of the coining roll relative to the abutment. In practical terms it is convenient to design the coining roll assembly at a fixed point on the Conform machine. A 2.1mm displacement of the coining roll was enough to deform most of the feedstock at the bottom of the groove. Geometrical calculations (described in Appendix G) predicted that a rotation of approximately 10.23° would be sufficient to roll the feedstock from 9.5mm to 7.4mm. The coining roll rotated at 43.36rpm, thus an angular displacement of 10.23° was achieved in approximately 0.04s. Therefore, the feedstock reduction in height of 2.1mm in 0.04s corresponded to a ram speed of $53.4mms^{-1}$.

The initial grip length determined the amount of time that the deformed feedstock was left inside the groove and therefore the amount of heat transfer from the wheel to the feedstock. After the coining simulation, part of the feedstock was in contact with the two parallel surfaces of the groove. The width of that contact was measured at the last increment of the coining simulation. The value was 2.5mm on each side of the groove. The angle of the grip zone was then calculated by using equation (A.19) from Appendix A. With a high coefficient of friction (i.e. 0.9) an angle of 10.21° was calculated. This corresponded to an initial grip length of 25.2mm inside the groove. The angular velocity of the wheel was 20rpm. Therefore, before entering the upset zone, only 25.2mm of grip length would have stayed in contact with the groove for approximately 0.09s. However, such a small grip length would be impractical for the positioning of the coining roll assembly as this could interfere with the shoe assembly. A more realistic initial grip length would be one which could spread over 45° of the wheel groove. This would mean that the deformed feedstock would stay 0.38s in contact with the wheel. Therefore a transient thermal analysis between the deformed feedstock and the wheel was performed over 0.38s in order to estimate the average temperature of the feedstock entering the upset zone. This second simulation used the same parts as shown in Figure 4.13 for the feedstock, the wheel (deformable tool) and the lower rigid tool.

4.4.2 Results

4.4.2.1 Heat transfer due to coining

Figure 4.14 shows the temperature evolution inside the feedstock due to plastic deformation and heat transfer between the wheel, the feedstock, the coining roll and the ambient air. The scale is for Figure 4.14d only. The *h* values define the height of the coining roll. At *h* = 2.1mm (Figure 4.14d), the coining process is finished and the feedstock reaches a maximum temperature of 41.2°C at the surface adjacent to the coining roll and a minimum temperature of 23.3°C at the surfaces adjacent to the fillet corners of the groove.

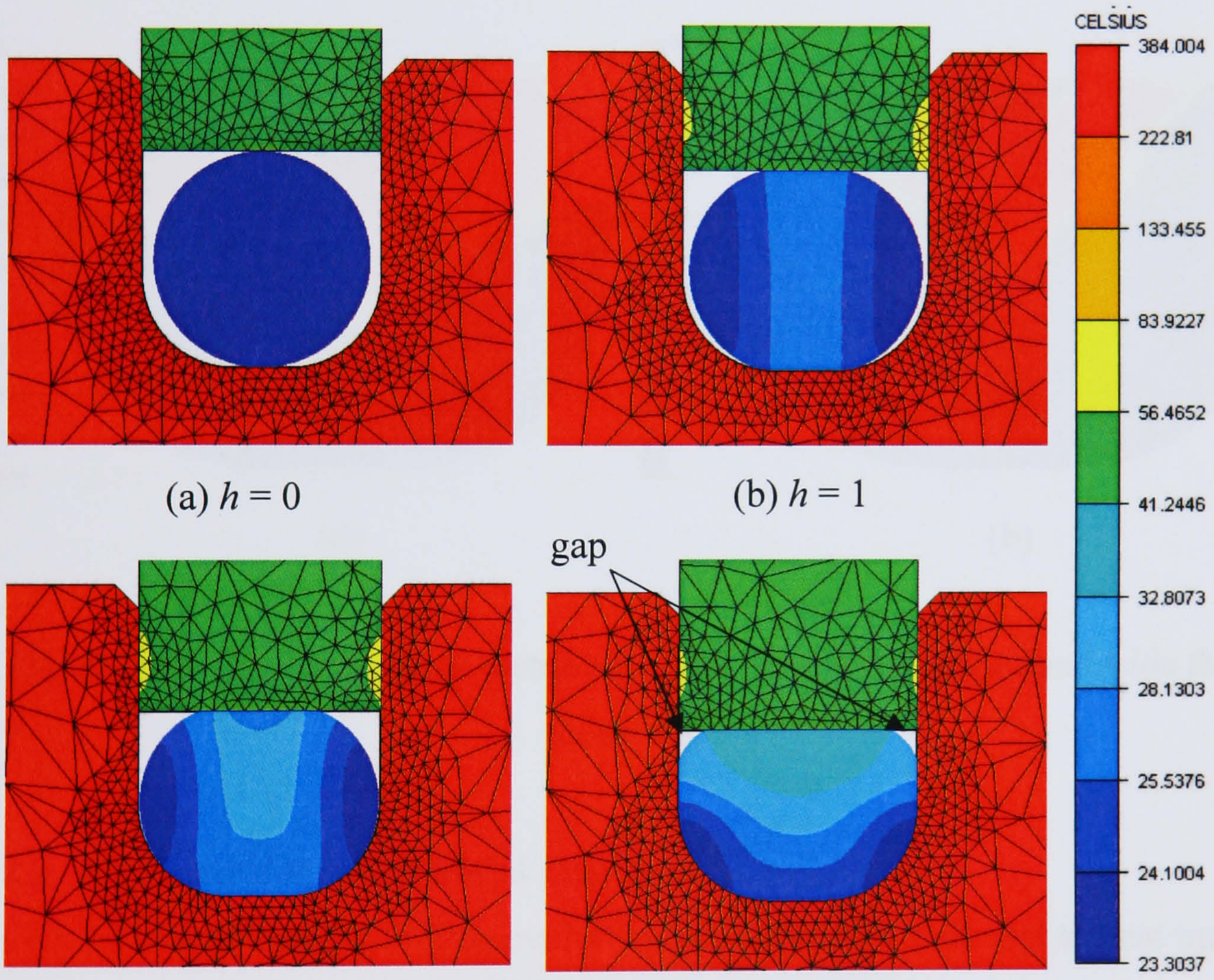

(a) *h* = 0 (b) *h* = 1

(c) *h* = 1.5 (d) *h* = 2.1

Figure 4.14 Temperature evolution of the feedstock at (a) *h* = 0, (b) *h* = 1, (c) *h* = 1.5 and (d) *h* = 2.1

As shown in Figure 4.14d two small gaps are present at the end of the coining process. These gaps are relatively small and represent a total surface of 1.05mm^2. In order to fill the gaps a coining roll with a width of 10.5mm would need to be moved by 0.1mm. The control over such a value would require an advanced and expensive

design for the coining roll. Furthermore, if the coining roll is pushed too far inside the groove there is a risk of back-extrusion of the feedstock, which could generate oxides on its new surfaces. Therefore it was decided that these small gaps could remain for the future simulations.

The temperature increase of 21.2°C (i.e. 41.2°C - 20°C) is mainly due to the heat generated by plastic deformation whilst the temperature increase of 3.3°C at the groove corners is principally due to heat conduction. This reasoning is reinforced by Figure 4.15 which shows a logarithmic distribution of the temperature from 23.3°C to 40.0°C (Figure 4.15a) and the strain distribution (Figure 4.15b) for h = 2.1. The areas of relatively high strain match the areas of large temperature gradients.

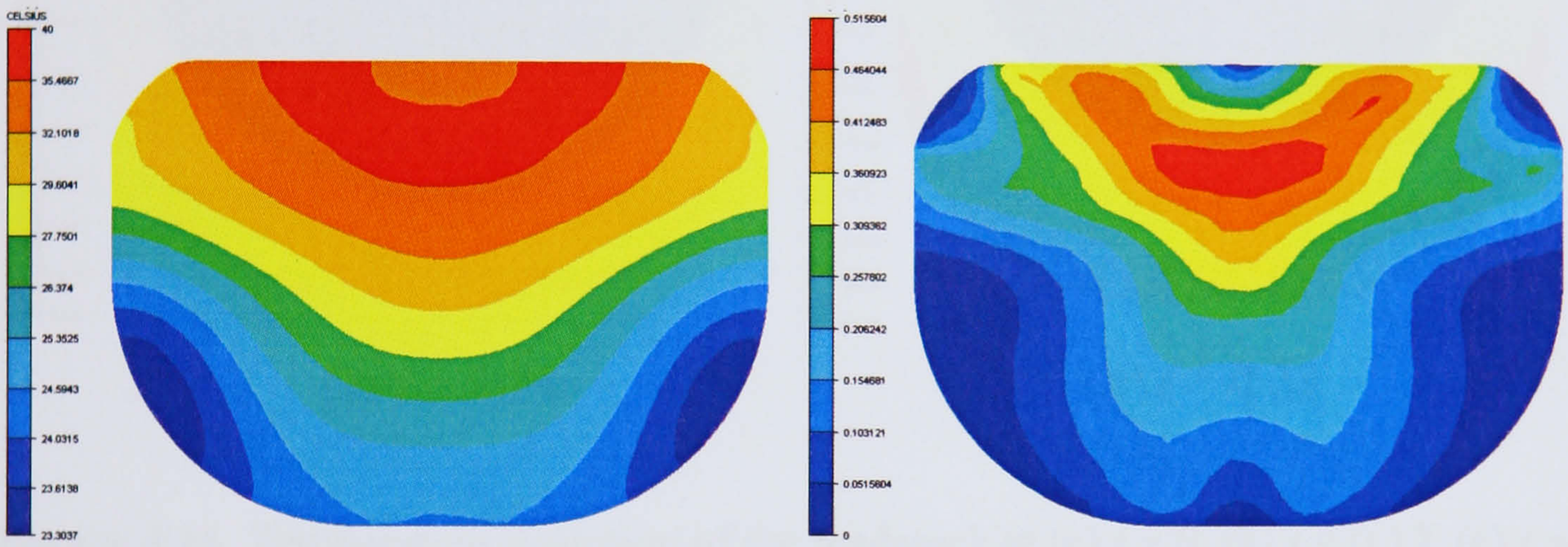

(a) (b)

Figure 4.15 (a) Temperature distribution and (b) strain distribution inside the feedstock

4.4.2.2 Heat transfer in the initial grip zone

Figure 4.16 shows the temperature evolution inside the feedstock due to heat transfer between the wheel, the feedstock and the ambient air. The t values define the time the feedstock stays in contact with the groove before entering the upset zone. At t = 0.38s (Figure 4.16d), the feedstock enters the upset zone with temperatures varying from 162.8°C at the top of the feedstock to 230.5°C at the surfaces adjacent to the fillet corners of the groove. The top surface of the feedstock is cooled by convection from the ambient air whilst the bottom part of the feedstock is rapidly heated by conduction from the wheel.

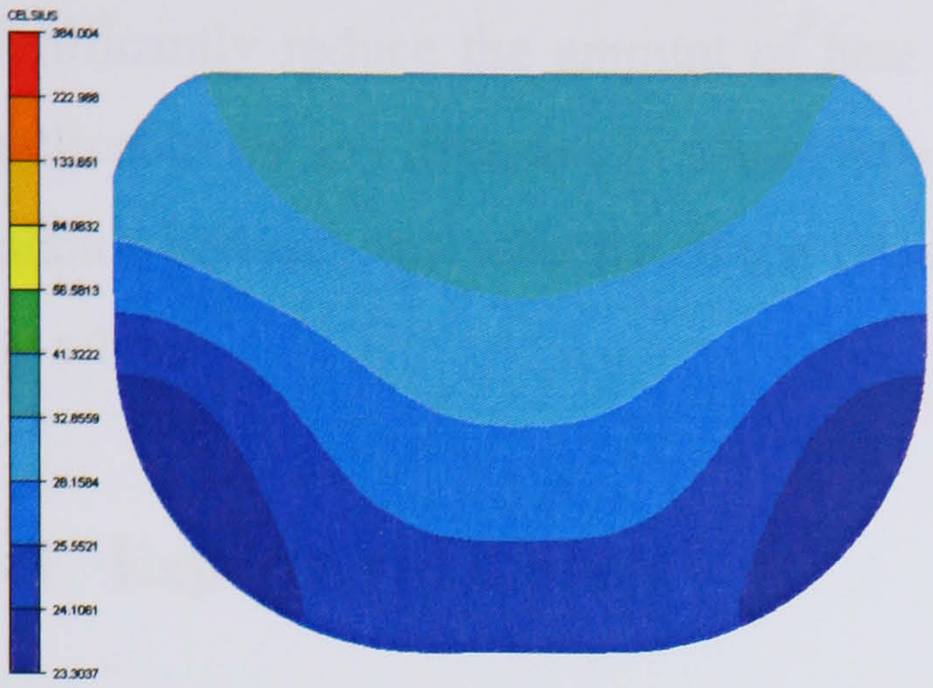

(a) $t = 0$

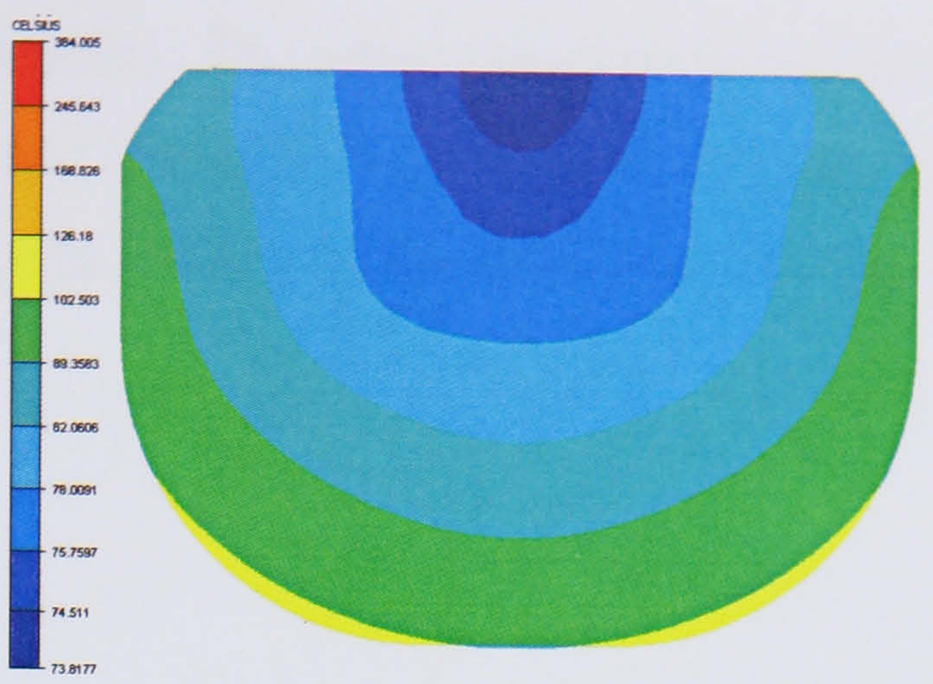

(b) $t = 0.12$

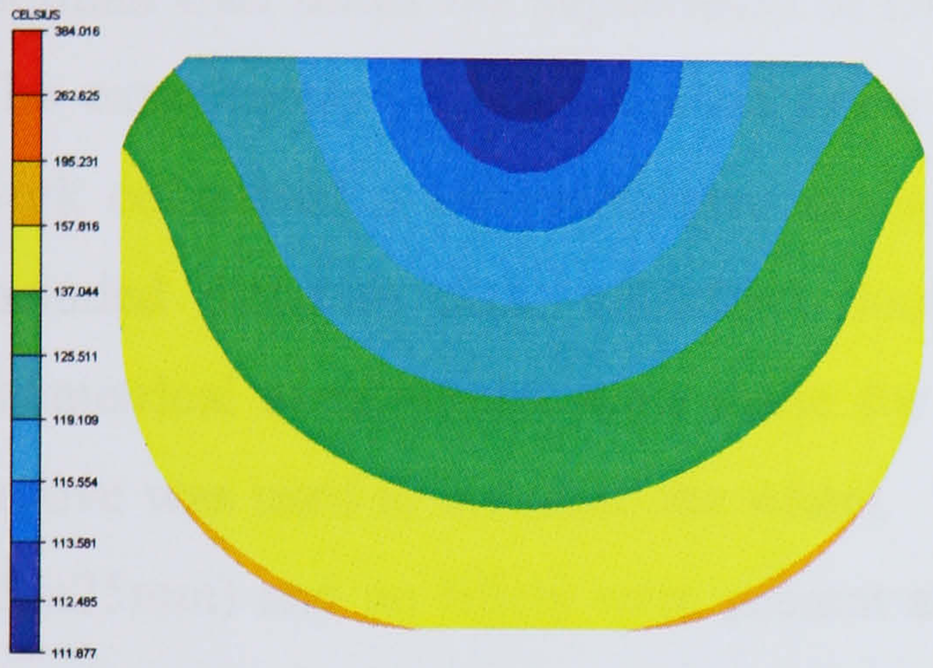

(c) $t = 0.24$

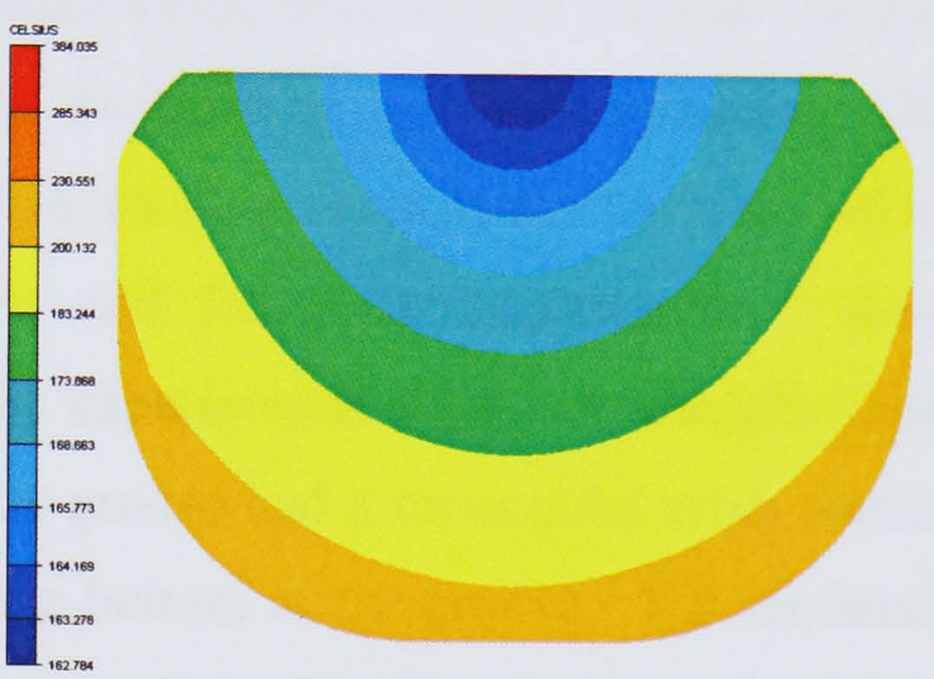

(d) $t = 0.38$

Figure 4.16 Temperature evolution of the feedstock at (a) $t = 0$, (b) $t = 0.12$, (c) $t = 0.24$ and (d) $t = 0.38$

4.4.3 Discussion

These simulations demonstrate that the heat generated by plastic deformation during coining is insignificant compared to the heat transfer from the wheel to the feedstock inside the initial grip length. The study of the temperature evolution within the upset zone requires the use of 3D simulations as shown in Section 4.6. The Conform user would have several ways to control the temperature of the extrudate. An increase of initial grip length would increase the rate of heat transfer to the feedstock and potentially the temperature of the extrudate. However, as mentioned before, it is impractical to vary the position of the coining roll. An increase in the wheel velocity would increase the rate of deformation and therefore increase the extrudate temperature. However, such an increase in velocity would also decrease the time that the feedstock stays in contact with the wheel and this would therefore

significantly reduce the amount of heat transfer. The same reasoning is inversely applicable for any decrease in wheel velocity. Therefore, the user must find the right balance between the velocity of the wheel, the initial grip length and the cooling of the wheel.

4.5 Experimental work

The experimental work for the simulation of Conform extrusion was carried out by Norman Carr under the supervision of Dr Mike Clode from King's College London. The experiments were conducted using the facilities of Holton Machinery. This work comprised a comprehensive series of extrusions (similar to Conform) which included different dies, velocities, tooling and feedstock temperatures. Some geometrical assumptions were made for the experimental work. A straight linear groove was used to simulate the wheel. The groove had a rectangular cross section (22x25mm) and no fillets were present at the bottom of the groove. The feedstock was 430mm long with a rectangular cross section (21x22mm) and was driven towards the abutment by a ram at different velocities. Flashes occurred during the experiments. The extrudate had three different circular cross sections. Several process variables were also recorded before, during and after each extrusion. The variables listed in Table 4.4 describe one of Carr's experimental extrusions. The author's simulation of this extrusion is presented later in the proceeding section.

Variable	Value
Diameter of die orifice	*12mm*
Steady state velocity of the groove	*1.95mms^{-1}*
Initial abutment temperature, initial feedstock temperature	*478°C, 414°C*
Stroke (stroke prior to extrudate formation)	*194mm (3mm)*
Stroke required to achieve steady state	*102mm*
Temperature rise at the abutment during the stroke	*10°C*
Temperature rise at the die during the stroke	*15°C*
Steady state velocity of the extrudate	*6.2mms^{-1}*
Length of the upset	*110mm*
Force on the ram at steady state	*129.1kN*

Table 4.4 Process variables from one of the experimental work.

4.6 3D thermo-mechanical models

Three dimensional analyses using Forge 3 were carried out to simulate Carr's extrusion. The simulations highlighted best practice for efficiently modelling Conform in 3D and included the degree of mesh refinement, boundary conditions and the modelling of different tools. The influence of the flash in Conform extrusion was also studied. The analyses were performed on a PC with dual processors (1.8GHz) and 2Gbytes of memory operating on a beta version of Windows XP 64 bits. Version 6.3a of the software Forge 3 was used.

4.6.1 The ghost die

Initially the simulation comprised only the necessary tools to represent the experiments: i.e. the groove/ram, the shoe, the abutment, and the die (Figure 4.17). In this figure two superimposed surfaces can be seen with the abutment. It is good practice in Forge 3 for the tools to interlock with each other in order to create a perfect fit. This technique is particularly important between fixed and moving tools such as the abutment (fixed) and the ram (moving).

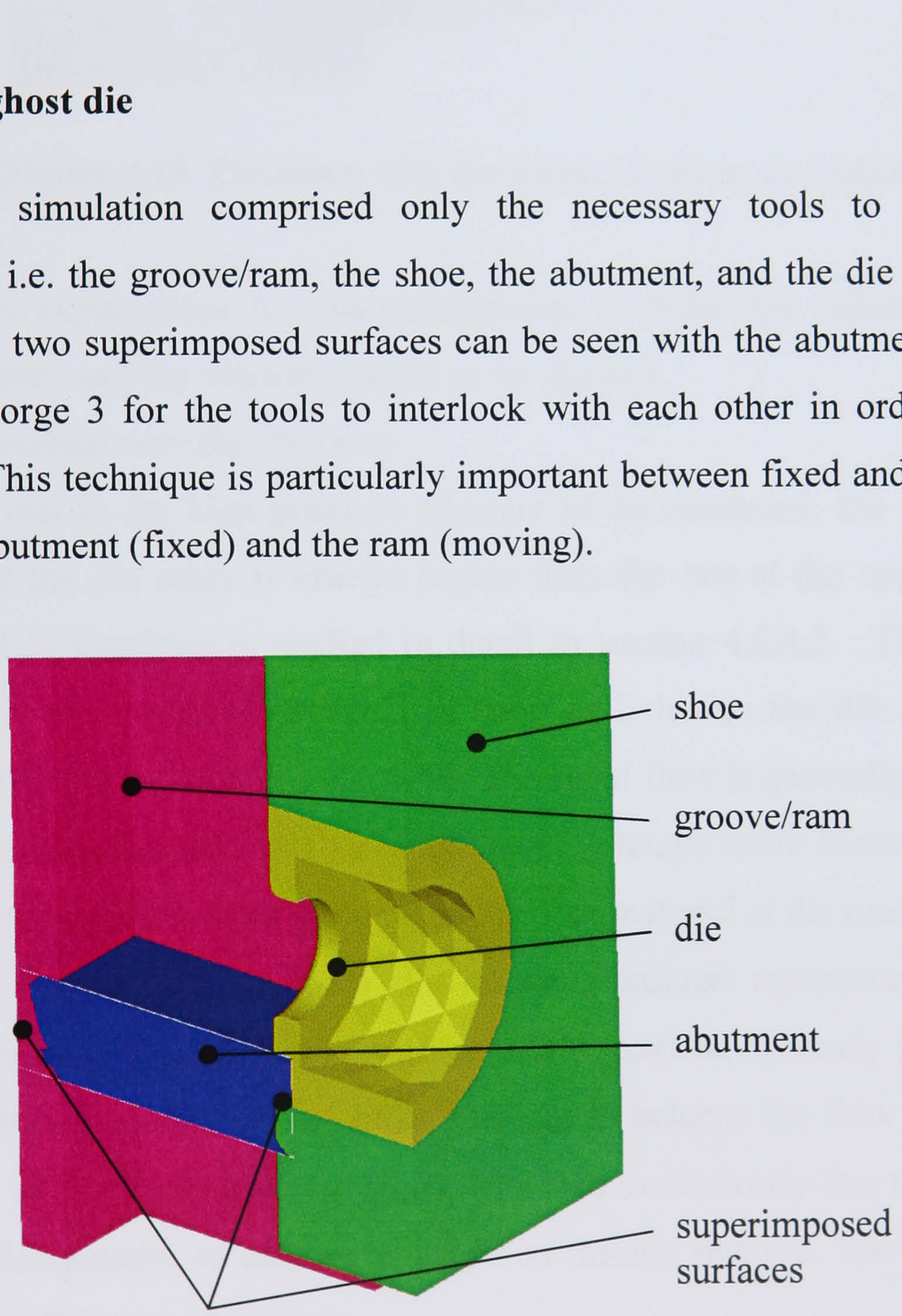

Figure 4.17 Tools with the initial Conform simulation

Unfortunately with this set-up the extrudate bent significantly upwards as shown in Figure 4.18. Eventually this extrudate would curl back towards the tooling.

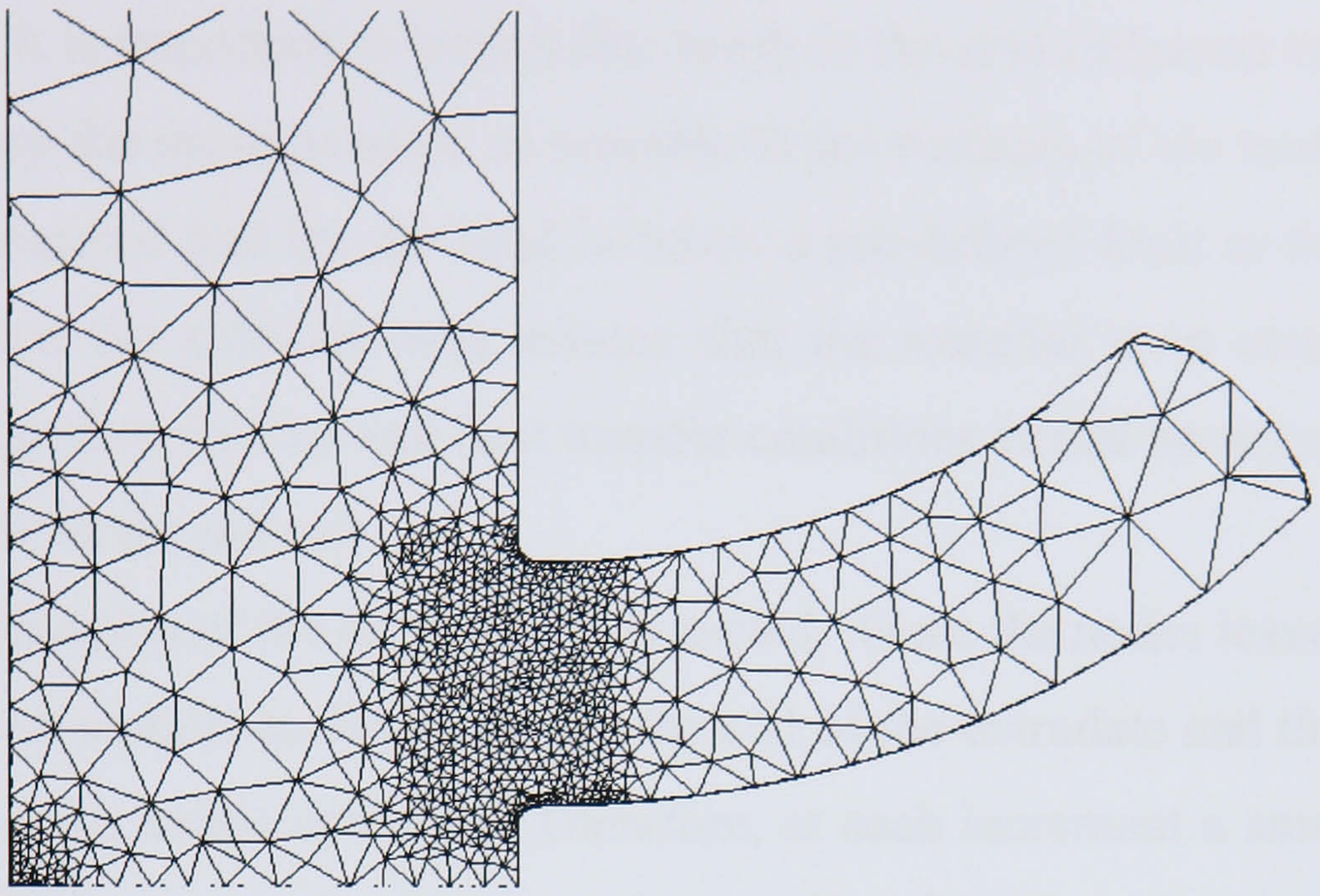

Figure 4.18 Extrudate with the initial Conform simulation

There are two explanations for this phenomenon to occur: the velocity differential near the die entry and the velocity profile at the die exit.

Velocity differential near the die entry

In Conform, due to the high pressure adjacent to the abutment, the velocity at the lower area of the die entry is always higher than the one at the upper area. The velocity field of Conform is studied in detail in section 4.6.4.2. This differential velocity bends the extrudate upwards as soon as it leaves the die land. For the production of shapes with direct extrusion, the metal flow is generally controlled by varying the bearing lengths. With a longer bearing length more friction is generated and the flow of metal becomes more retarded. The material at the centre of the billet moves faster than at the periphery due to the frictional resistance at the billet-container interface. Therefore, the bearing length must be inversely proportional to its distance from the centre of the billet in order to balance the flow of aluminium. Furthermore, with a thinner section the flow moves more slowly due to the small die opening. Subsequently, to balance the flow in thinner sections, the bearing length needs to be smaller, and vice versa.

In previous simulations made by the author, the bearing length had been altered according to industrial practice. For example, in the case of a rectangular strip, the bottom die land was made to be longer than the upper die land. However several

simulations and a relatively fine mesh (10 elements for the length of the bearing) are required for this to simulate the optimum changes in material flow. This technique, if applied to Conform, would lead to a significant increase in computational time. Nevertheless, it is important to keep a fine mesh in the areas adjacent to the die land in order to keep the mesh as close as possible to the surfaces of the tools. If the gap between the material and the die land is below a pre-defined limit at the start of the simulation, then the software will assume that the material is in contact with the tooling and therefore friction and heat transfer conditions would be activated.

Velocity profile at the die exit

The upward direction of the extrudate is expected. Once the nodes leave the die land there is no more contact surface to guide the end of the extrudate and the differential velocity drives the nodes upwards. Therefore, at each increment a small portion of the extrudate is bent upwards. This cumulative effect facilitates the rapid 'curling' of the extrudate. A gravity force can be introduced to the simulation. However, tests showed that due to the relatively small amount of aluminium extruded, the counter balance force generated by gravity does not prevent the bending of the extrudate.

A more efficient way to maintain the extrudate in a straight direction would be to use a ghost die. The term 'ghost' was coined by the author and his co-workers in order to define a die, or tool, which does not exist in a real situation. The ghost die is defined with a null coefficient of friction, is infinitely stiff and has the thermal properties of air. Therefore, it has no influence on either the extrusion pressure or temperature distribution. Figure 4.19 shows a half symmetry of a die and ghost die assembly.

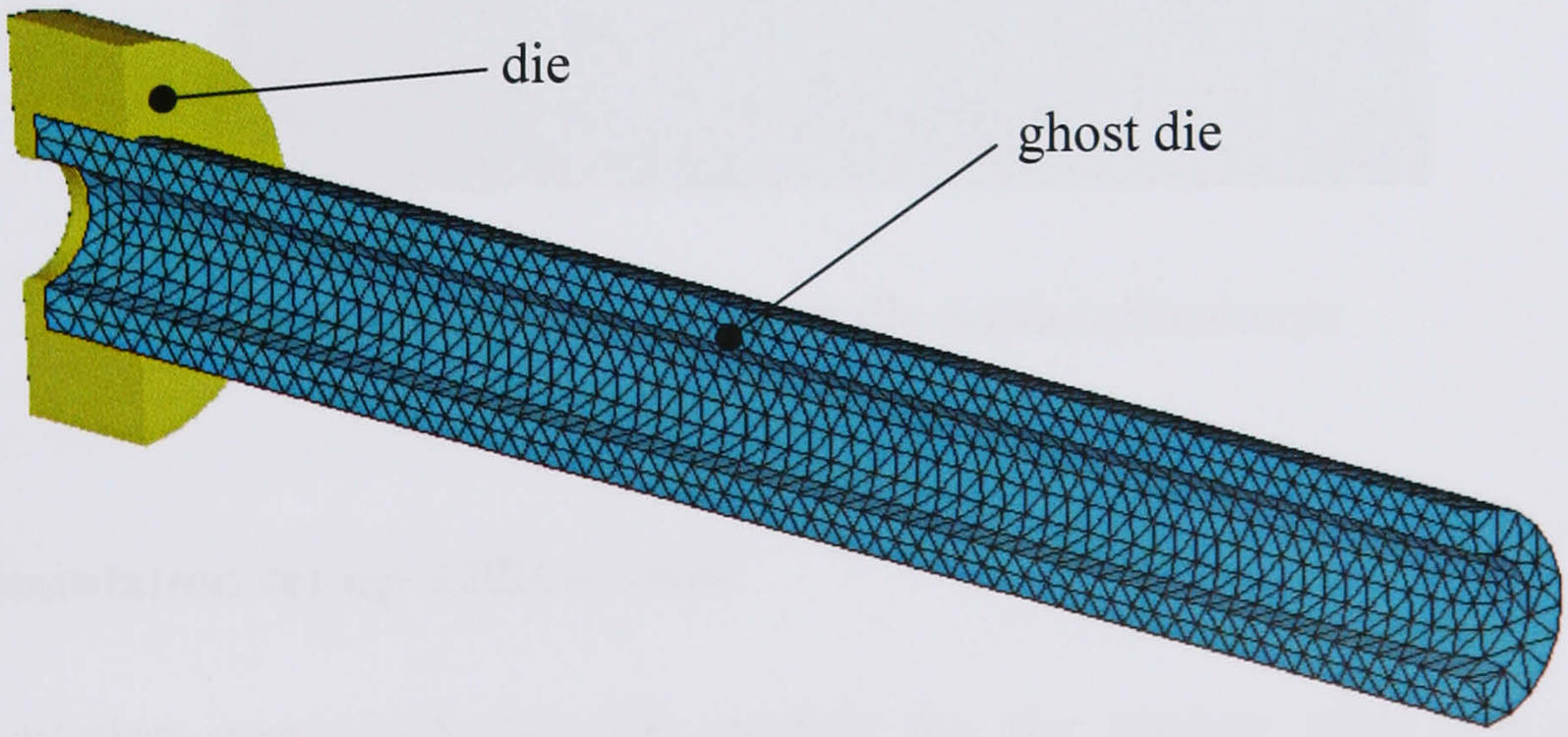

Figure 4.19 Half symmetry of a die and ghost die assembly

There is however a potential problem with the use of ghost dies for the simulation of 3D shapes with curved profiles. If the cross section of the profile is a series of straight lines (e.g. square, rectangle, T-shape, etc…) then it is easy to create a ghost die which matches the exact profile with relatively few elements. However, if the profile uses curved lines then it is very difficult to exactly match the same profile in 3D. In fact there is a risk that a profile will be created which is slightly smaller than the extrudate and which therefore creates a second extrusion (with a very low extrusion ratio) inside the ghost die. In the context of Carr's experiment, where the die orifice is 12mm in diameter, a ghost die with a 13mm diameter was generated in order to control the straightness of the extrudate with an appropriate number of elements. Figure 4.20 shows the different diameters between the die and the ghost die and consequently the different mesh refinements.

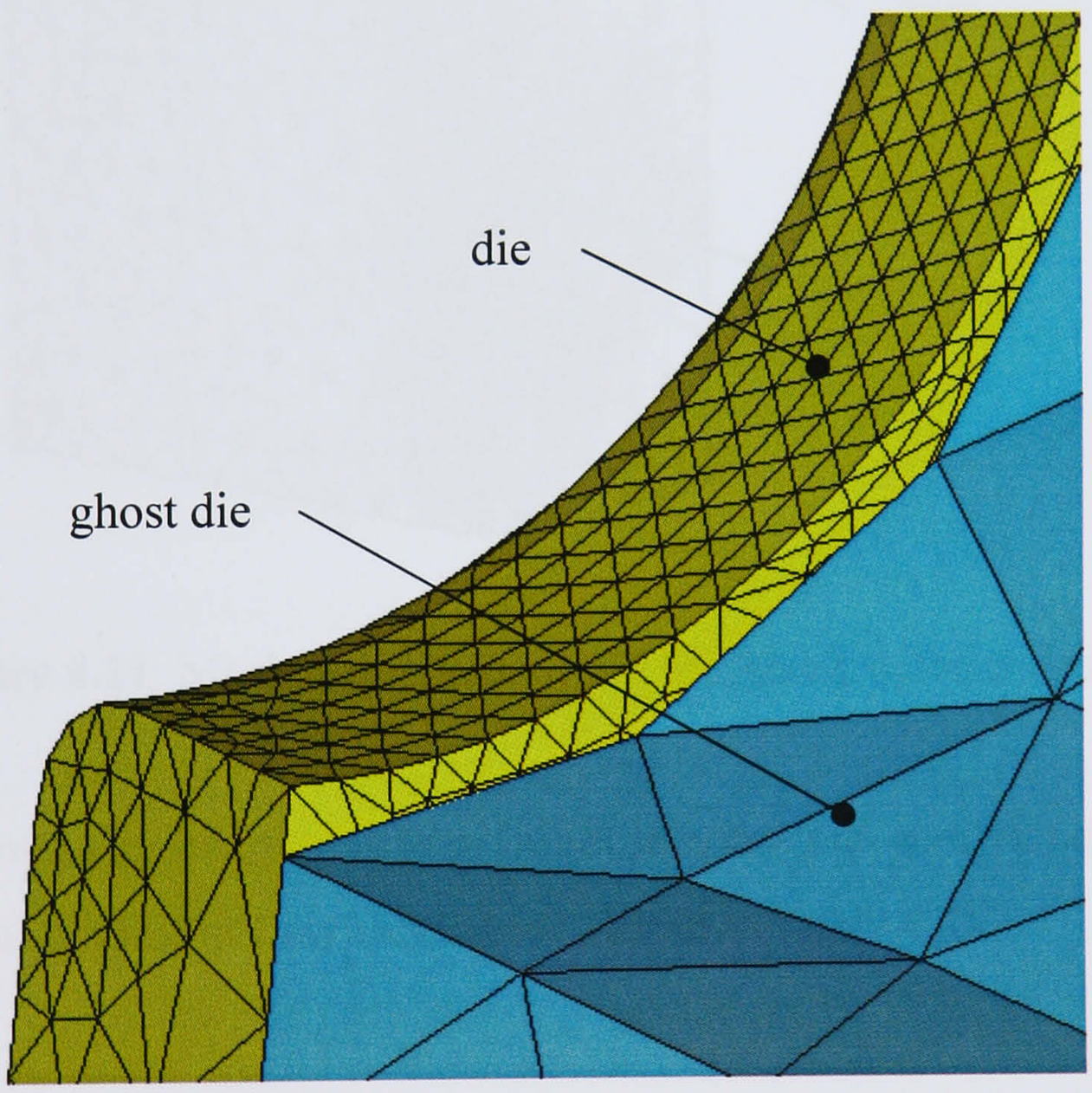

Figure 4.20 Die and ghost die mesh refinements

4.6.2 Simulation set-up without flash

This simulation comprised five FE models for the tooling with one plane of symmetry. The groove/ram, the shoe, the abutment and the die (as shown in Figure 4.17) and the ghost die (as shown in Figure 4.19). A high Tresca coefficient of

friction (0.9) was used for the shoe, ram and abutment models. A lower coefficient of friction was used for the die land (0.4). The mesh of the feedstock (Figure 4.21) with an average element size of 5mm, was refined using two mesh boxes as follows:

- a cylindrical mesh box at the die entrance with elements of 0.4mm,
- a rectangular mesh box at the bottom of the feedstock with elements of 2mm.

The feedstock was discretised with approximately 80,000 tetrahedral elements.

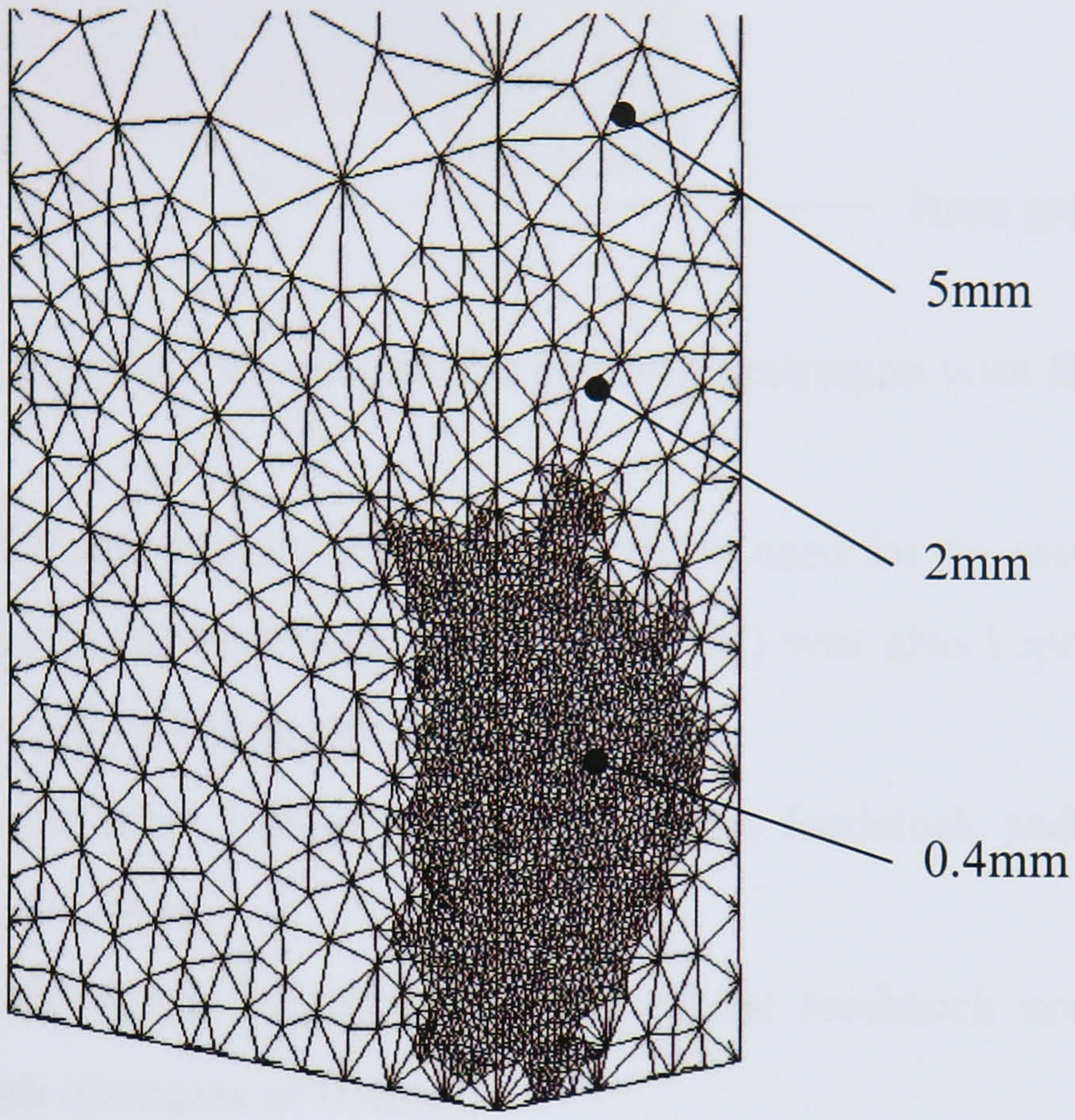

Figure 4.21 Mesh refinement of the feedstock without flash

The remaining boundary conditions (e.g. initial temperature, ram velocity) were kept the same as for those used in Carr's extrusion (listed in Table 4.4).

4.6.3 Simulation set-up with flash

This simulation comprised four FE models for the tooling as shown in Figure 4.22. The models for the shoe and the die remained the same as for the previous simulation. The abutment, ram and feedstock were remodelled to account for the simulation of flash. This was done by leaving a gap of 1mm between both the ram and the shoe and the ram and the abutment.

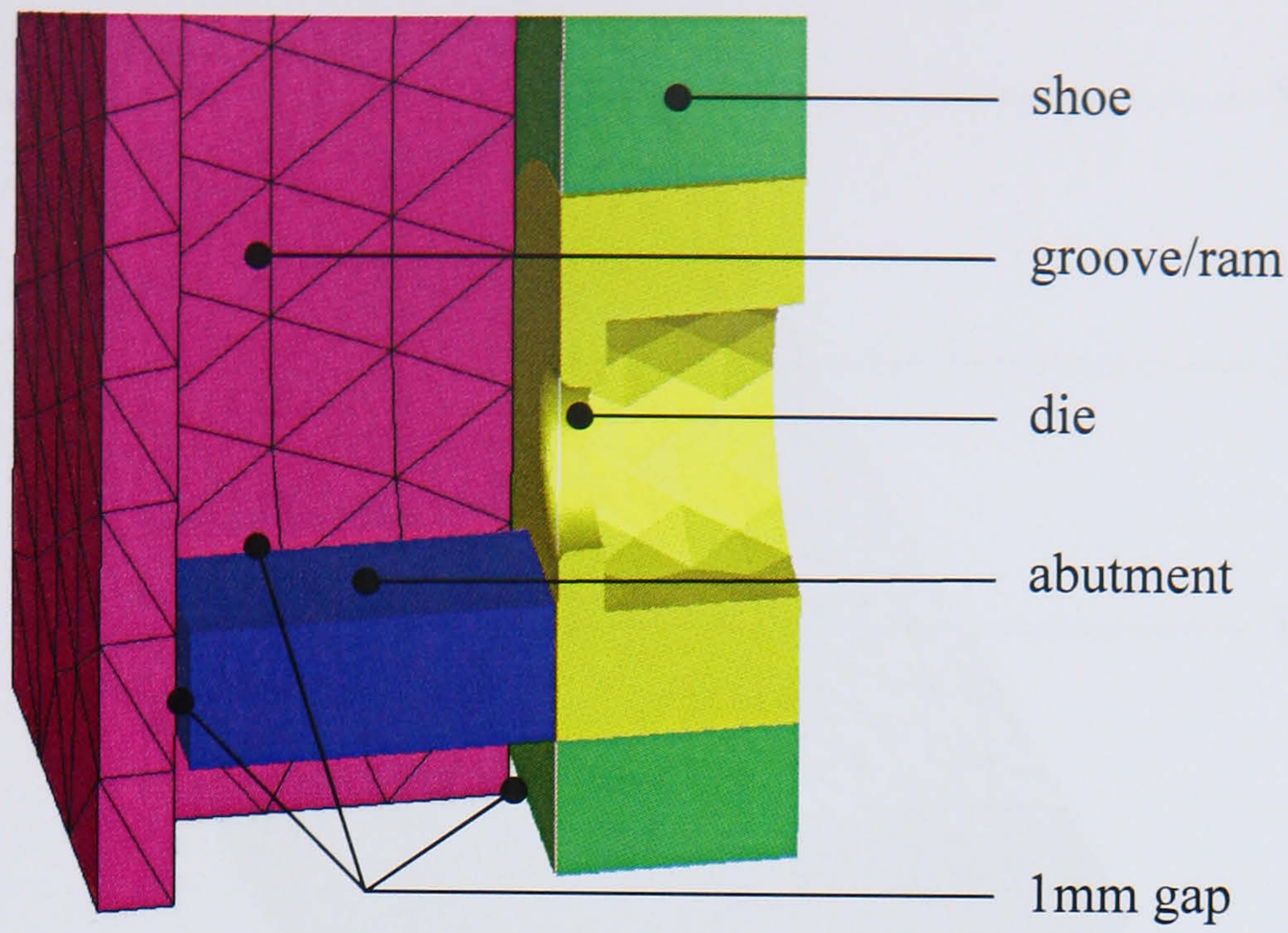

Figure 4.22 FE models for Conform extrusion with flash

The friction coefficients remained the same as those used for the previous simulation. The mesh refinement of the feedstock (Figure 4.23) was also kept the same and in addition three new mesh boxes were also included:

- a rectangular mesh box at the bottom of the feedstock and the groove with elements of 0.4mm,
- a rectangular mesh box at the bottom of the feedstock and the side of the groove with elements of 0.4mm,
- a rectangular mesh box at the corner of the feedstock and against the shoe with elements of 1mm.

The feedstock was discretised with approximately 100,000 tetrahedral elements.

The remaining boundary conditions (e.g. initial temperature, ram velocity) were again kept the same.

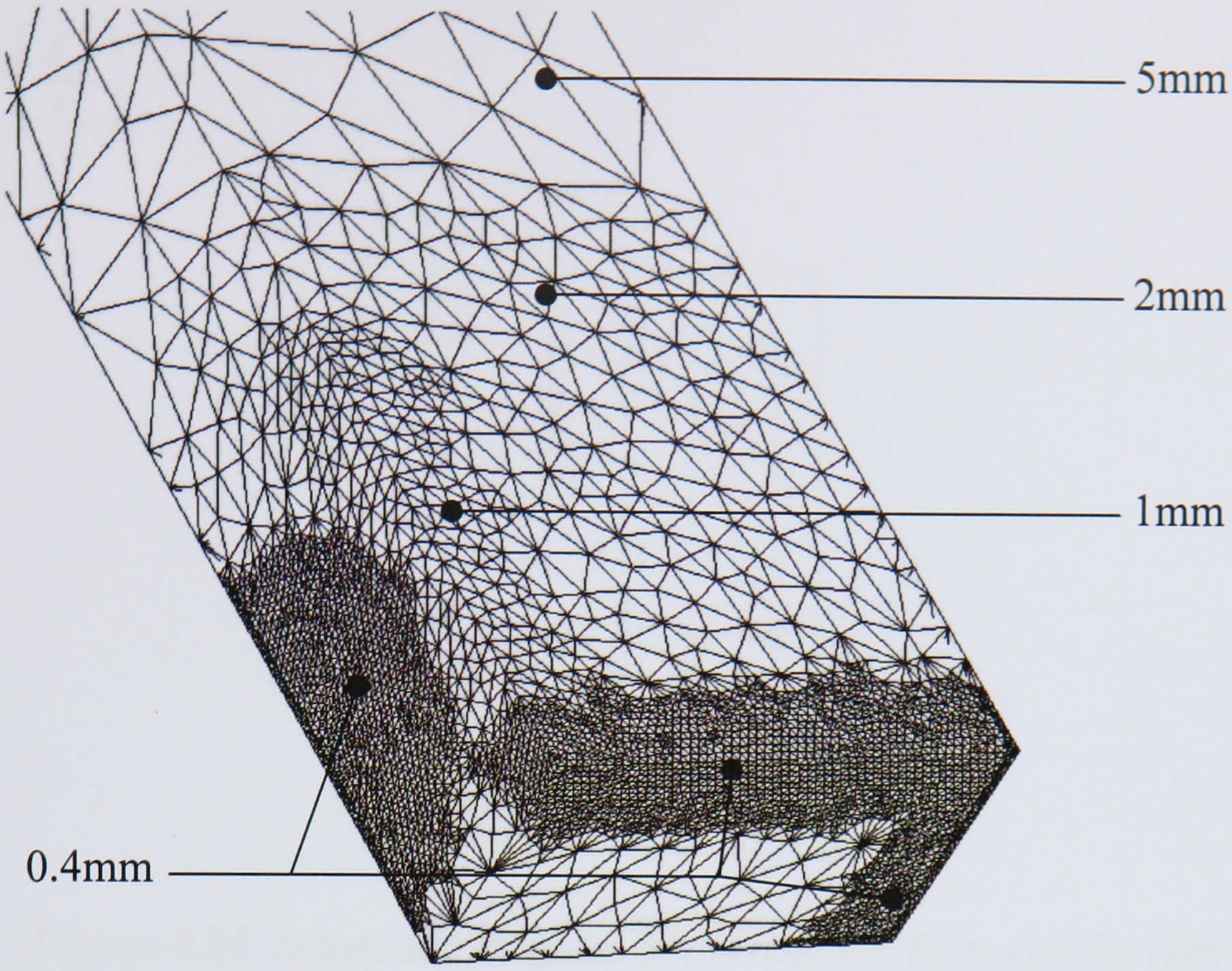

Figure 4.23 Mesh refinement of the feedstock with flash

4.6.4 Results and discussions

Thermo-mechanical FE analyses of 3D models produce a considerable amount of results which the author has displayed in various forms, such as: colour contours, cutting planes, iso-surfaces and graphs. The main results and discussions concerning these 3D simulations are presented in four sections: extrusion load, material deformation, velocity profile and temperature evolution.

4.6.4.1 Extrusion load

The extrusion load is equivalent to the resultant of the reaction forces F_X and F_Y acting on the ram. Figure 4.24 shows a schematic diagram of this. The resultant force, F, is applied at an angle α from the vertical. Therefore the following equations can be written:

$$F = \sqrt{F_X^2 + F_Y^2} \tag{4.1}$$

and

$$\alpha = \tan^{-1}\left(\frac{F_X}{F_Y}\right) \tag{4.2}$$

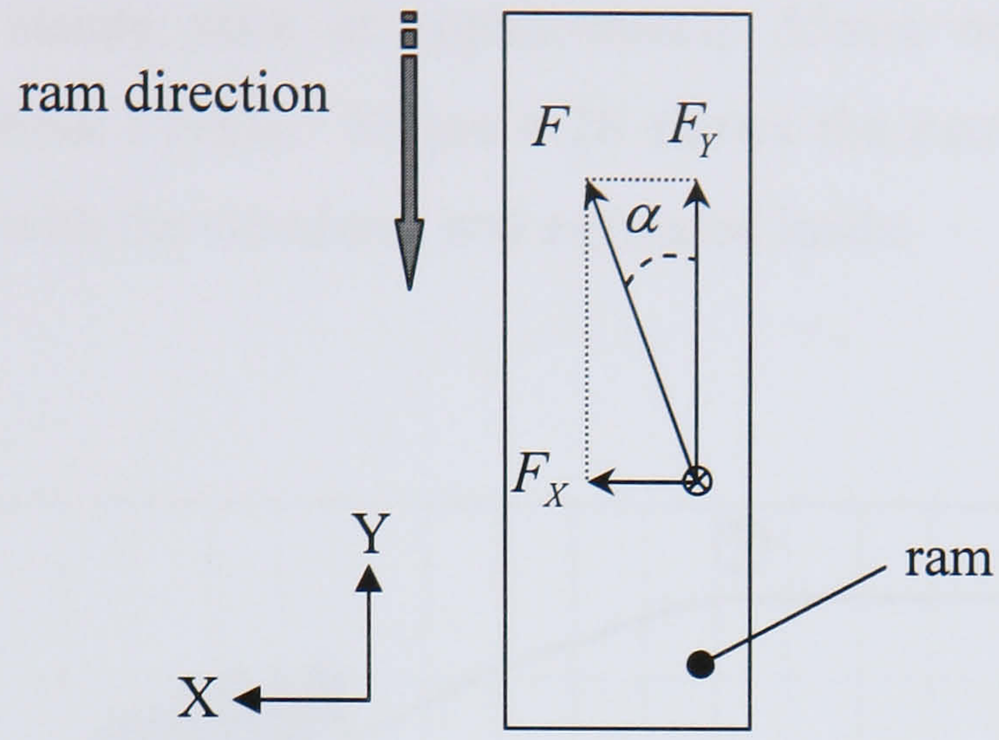

Figure 4.24 Schematic diagram of the reaction forces on the ram

The curves shown in Figure 4.25 display the extrusion load for both simulations (with and without flash) against the ram displacement.

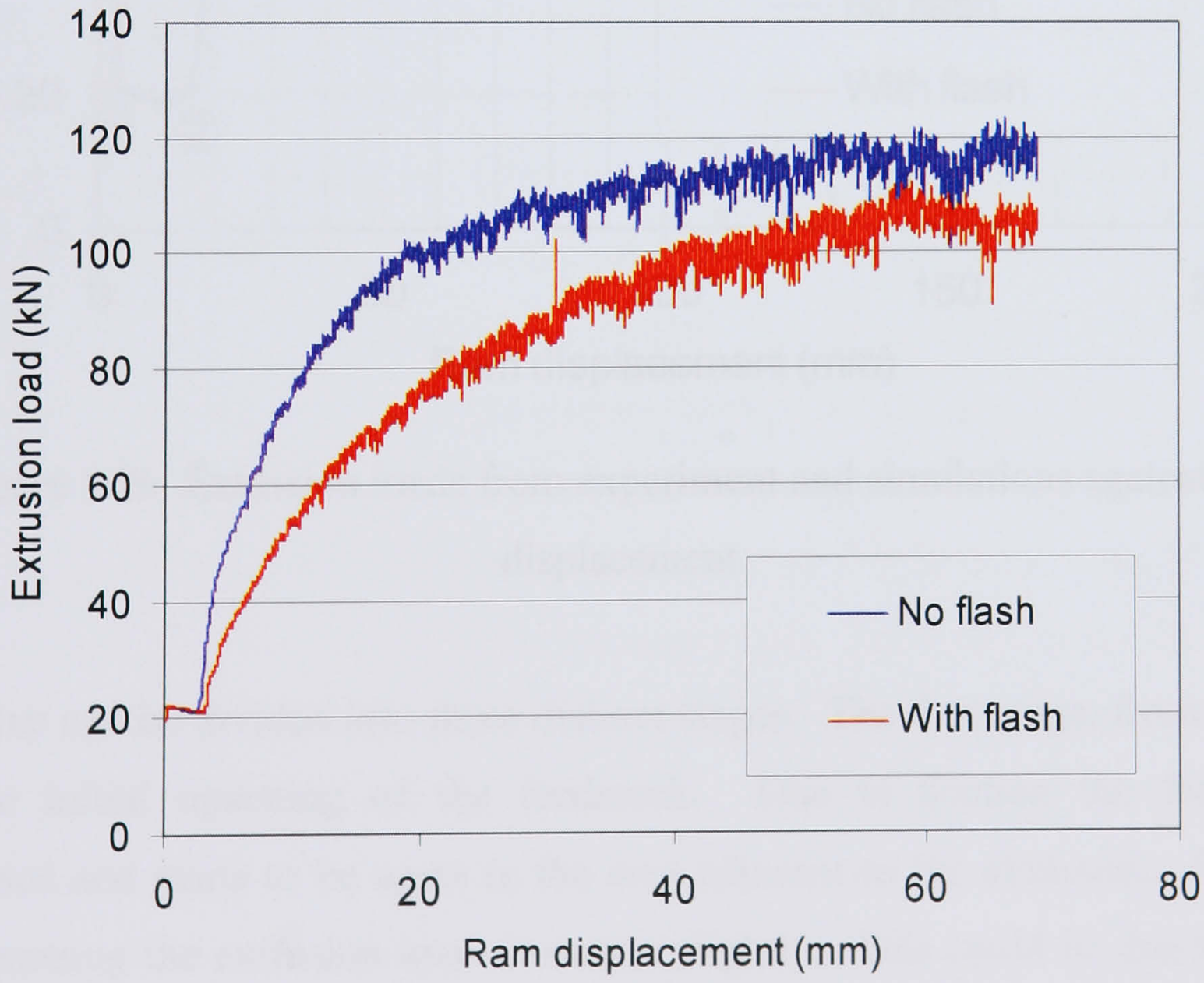

Figure 4.25 Simulated extrusion loads against ram displacement

The extrusion load for the simulation with flash (shown by the red curve) is reaching steady state at approximately 65mm of ram stroke with a maximum load of about 105kN. The extrusion load for the simulation without flash (shown by the blue curve) is reaching steady state at approximately 55mm of ram stroke with a maximum load of about 117kN. Figure 4.26 shows the extrusion loads from the experiment together with the simulated and estimated loads.

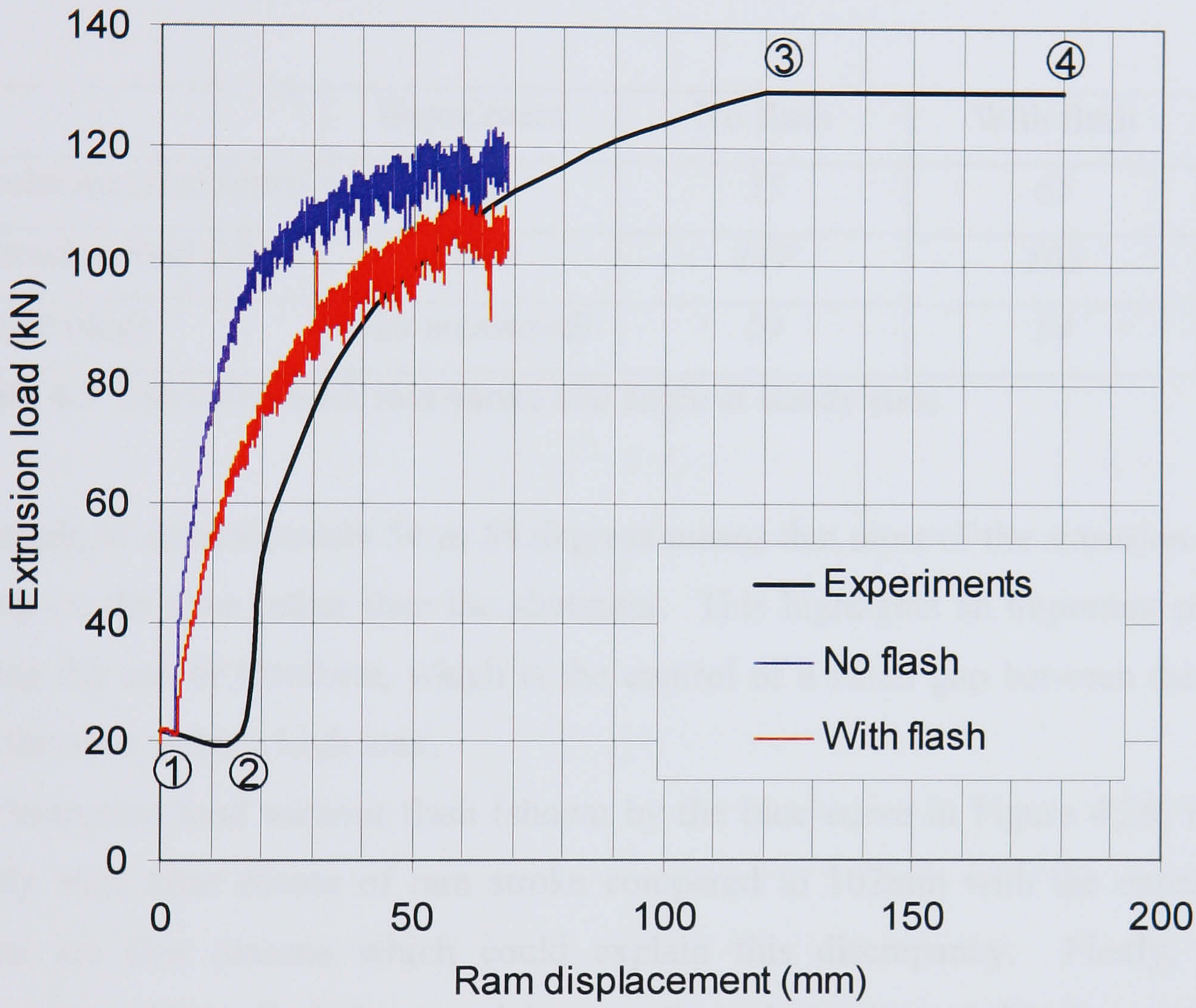

Figure 4.26 Extrusion loads from experiment and simulations against ram displacement

Each curve can be divided into three distinct stages. The first stage, from point 1 to 2, is the initial upsetting of the feedstock. Due to friction the feedstock is compressed and starts to be upset in the area adjacent to the abutment. During the initial upsetting the extrusion load decreases slightly. This could be due to the heat generated by deformation. However it is more probable that the increase of temperature is mainly due to the heat transfer between the tooling (at 478°C) and the workpiece (at 414°C). The second stage, from point 2 to 3, is the formation of the upset length. This occurs when the material begins to enter the die and continues

until steady state is reached. During this stage a significant amount of material is being extruded while the upset zone is still being formed. The extrusion load during this stage evolves according to a logarithmic form. Finally the third stage, from point 3 to 4, is the steady state. In Conform steady state is reached once the upset length is fully established. At steady state the extrusion load remains constant.

Table 4.5 lists the extrusion load at steady state, the ram stroke required to achieve steady state and the angle of the resultant force. These results are shown for both simulations and the experiment.

	Experiment	No flash	With flash
Stroke required (mm)	*102*	*55*	*65*
Extrusion load (kN)	*129.1*	*117*	*105*
Angle (deg)	*(not measured)*	*59*	*54*

Table 4.5 Extrusion load, ram stroke and angle at steady state

An angle of approximately 54 or 59 degrees means that most of the extrusion load is acting on the shoe rather than the abutment. This highlights an important problem during the use of Conform, which is the control of a small gap between the wheel and the shoe under a high load.

The extrusion load without flash (shown by the blue curve in Figure 4.26) reaches steady state after 55mm of ram stroke compared to 102mm with the experiment. There are two reasons which could explain this discrepancy. Firstly, in the simulation without flash the material passes through the die and fills the upset zone. Whilst in the simulation with flash a significant amount of material is passing through the gaps between the wheel and the rest of the tooling. Therefore steady state would occur earlier than if flash was generated. Secondly, it can be seen from the figure that for the simulations extrusion starts shortly after the initial upsetting (≈ 4mm) whilst for the experiment, extrusion only begins after a ram stroke of 16mm (as shown with point 2 in Figure 4.26). The relatively long ram stroke before extrusion is probably due to the experimental set up (e.g. a possible gap between the hydraulic piston and the ram), initial slippage between the feedstock and the ram, and the fact that the ram speed cannot be reached instantaneously as it does with the simulation.

The extrusion load is also 9% lower than the experiment. In addition to experimental errors the following factors can affect the difference between the experimental and the simulated loads:

- The friction coefficient and the type of friction law can underestimate the real friction occurring during the process.
- The fact that flash is not simulated means that the feedstock experiences less friction at the abutment and therefore less load. However, this argument can be counter balanced by the fact that the extrusion ratio is lower with the flash conditions.
- Finally, the flow stress was defined with parameters extracted from the literature. A significant variation could be found between two sets of parameters for AA6063 due to the variation in the composition of this alloy.

The simulation results could be enhanced by using material data extracted from the samples used in the experiments. Furthermore by increasing computing power, the Conform extrusion with flash could be simulated for a longer time period at steady state.

4.6.4.2 Material deformation

The deformation of the feedstock for the simulation without flash is relatively straight forward. The feedstock starts to upset near the abutment and some material travels through the die to form the extrudate. Figure 4.27 shows a series of deformations for different ram strokes. Deformations at $h = 4$, $h = 50$ and $h = 70$ correspond respectively to the points 2, 3 and 4 from Figure 4.26. The upset zone evolves in a similar pattern to that of the extrusion load. This means therefore that the upset zone length increases rapidly, following a logarithmic form, before converging to a maximum length. This maximum value indicates that the process has reached steady state.

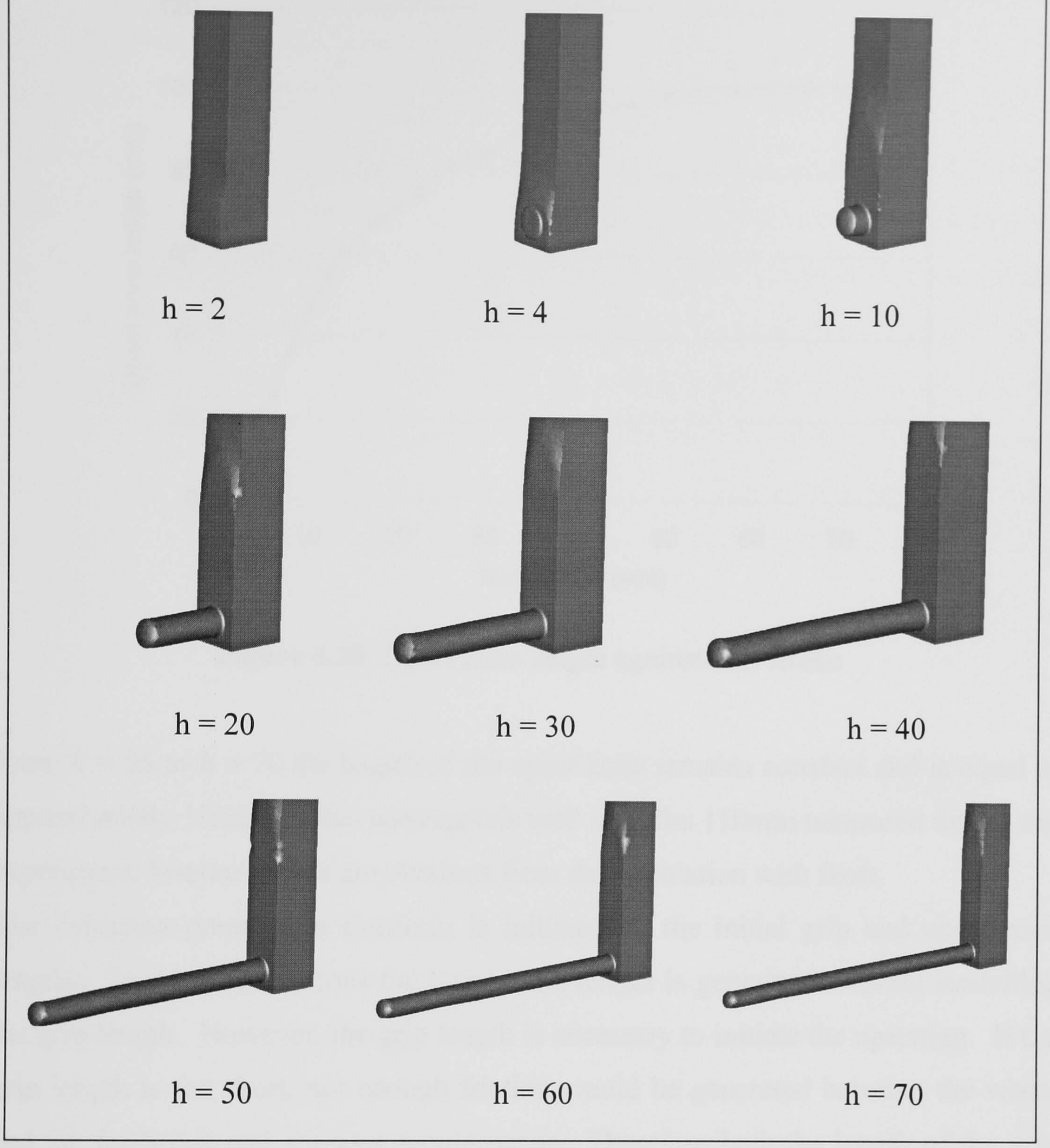

Figure 4.27 Material deformation at different ram stroke without flash

Figure 4.28 shows the increase of the upset zone length against the ram stroke for the simulation without flash. The simulated lengths were taken graphically at 4mm intervals of the ram displacement.

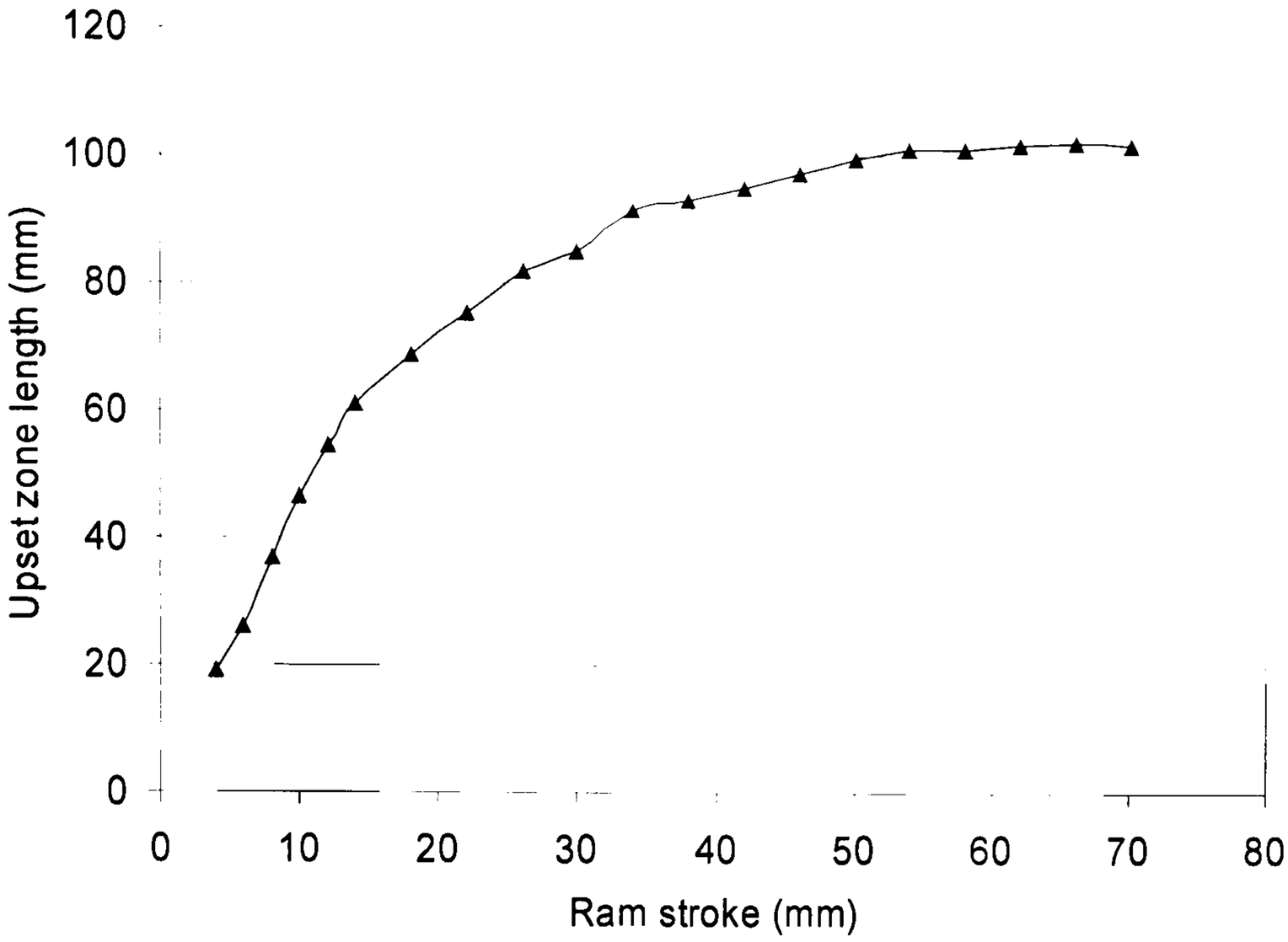

Figure 4.28 Upset zone length against ram stroke

From $h = 55$ to $h = 70$ the length of the upset zone remains constant and is equal to approximately 102mm. This corresponds well with the 110mm measured during the experiment. Similar results are obtained from the simulation with flash.

The extrusion pressure in Conform is initiated by the initial grip and upset zone lengths. In these simulations the upset zone length is generated without modelling the grip length. However, the grip length is necessary to initiate the upsetting. If the grip length is too short, not enough friction would be generated between the wheel and the feedstock and slippage would occur. Therefore both the length of the grip and the upset must be estimated before beginning the extrusion process. This will permit the user to find an optimum position for the coining roll. By using FEM the upset length can be predicted and subsequently the grip length can be calculated by rewriting equation (2.19) as follows:

$$l_i = w\left(\frac{2}{\mu} + \frac{p}{\sigma_{cys}}\right) - l_u \tag{4.3}$$

where l_i is the length of the initial grip, w is the groove width, μ is the coefficient of friction between the groove wall and the feedstock, p is the extrusion pressure, σ_{cys}

is the compressive yield stress of the feedstock (equal to the mean equivalent stress), and l_u is the length of the upset zone necessary for extrusion to start.

Figure 4.29 shows a series of deformations with the flash for different ram strokes. It can be observed that the flash at the abutment occurs before the extrudate is formed. At the beginning of the process the forces acting on the feedstock are mainly in a direction normal to the abutment. Therefore the abutment-ram assembly acts briefly as an indirect extrusion (the abutment being the die). However, after 4mm of stroke some material begins to enter the die and flash starts to form between the ram and the shoe. At $h = 10$ the flash is about to leave the gap between the ram and the abutment. However this does not stop the flash forming at the same velocity as the ram movement. This means that at $h = 28$ the flash is approximately 28mm. Furthermore, a significant amount of flash is created between the shoe and the ram.

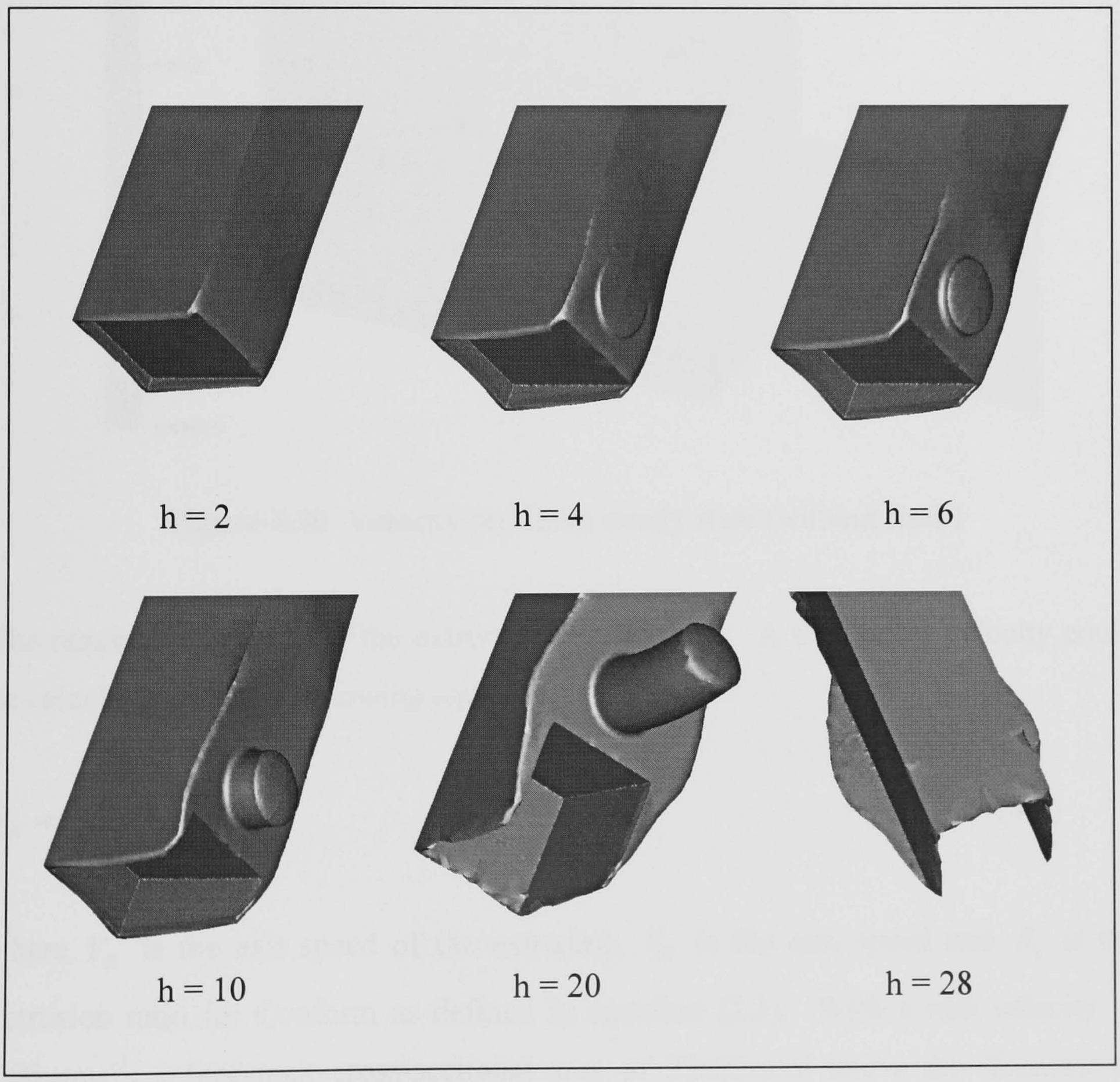

Figure 4.29 Material deformation at different ram stroke with flash

4.6.4.3 Velocity profile

The velocity profile in Conform extrusion is significantly different to the one in conventional direct extrusion. In this section the discussion concentrates on the velocity differential at the die exit and the formation of the dead metal zones.

Velocity differential at the die exit

Figure 4.30 shows the velocity profile for the simulation without flash at steady state.

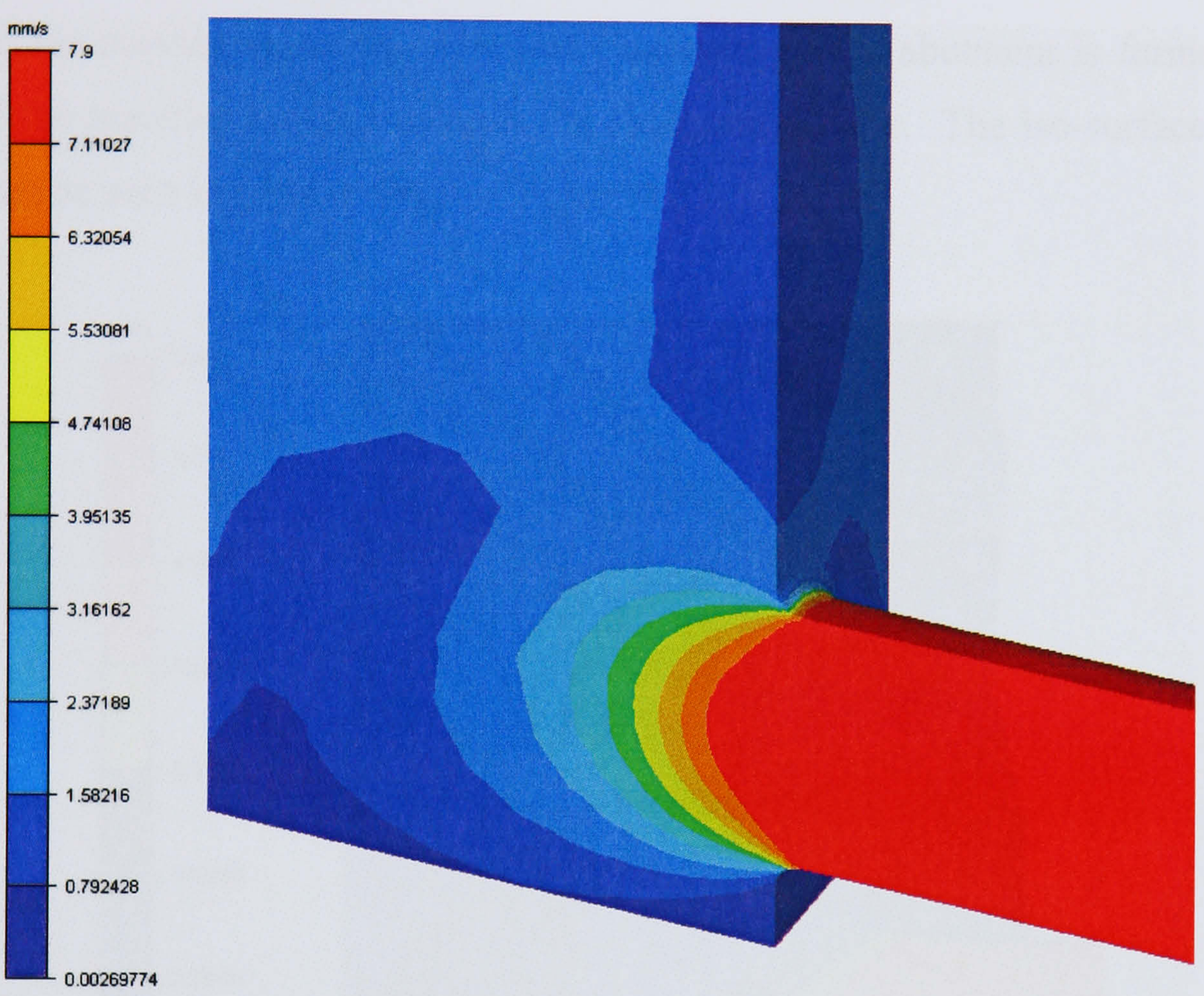

Figure 4.30 Velocity profile at steady state (without flash)

The maximum velocity of the extrudate is 7.90mms^{-1}. A theoretical velocity could be calculated with the following equation:

$$V_E = V_R R_c \tag{4.4}$$

where V_E is the exit speed of the extrudate, V_R is the ram speed and R_c is the extrusion ratio for Conform as defined in equation (2.3). With a ram velocity of 1.95mms^{-1}, a feedstock cross-sectional area of 22x22mm^2 and a die diameter of 12mm, the theoretical extrudate speed would be 8.35mms^{-1}. The difference between the simulated and theoretical velocities could be explained by the loss in volume of

material during the simulation. Over a ram stroke of 70mm the mesh of the material lost a total volume of 600mm^3 from an initial volume of 60500mm^3. This is due to the re-meshing approximations and penetration algorithm (i.e. projection of nodes penetrating the tools).

Figure 4.31 shows the velocity profile for the simulation with flash at steady state. The zones illustrated in dark blue represent the dead metal zones. The DMZ at the apex of the die entry is formed due to the high friction condition between the static shoe and the moving material. The DMZ adjacent to the abutment is formed as a result of the material flowing towards the flash and the die. The iso-surface of the DMZs can be seen in greater detail in Figure 4.33.

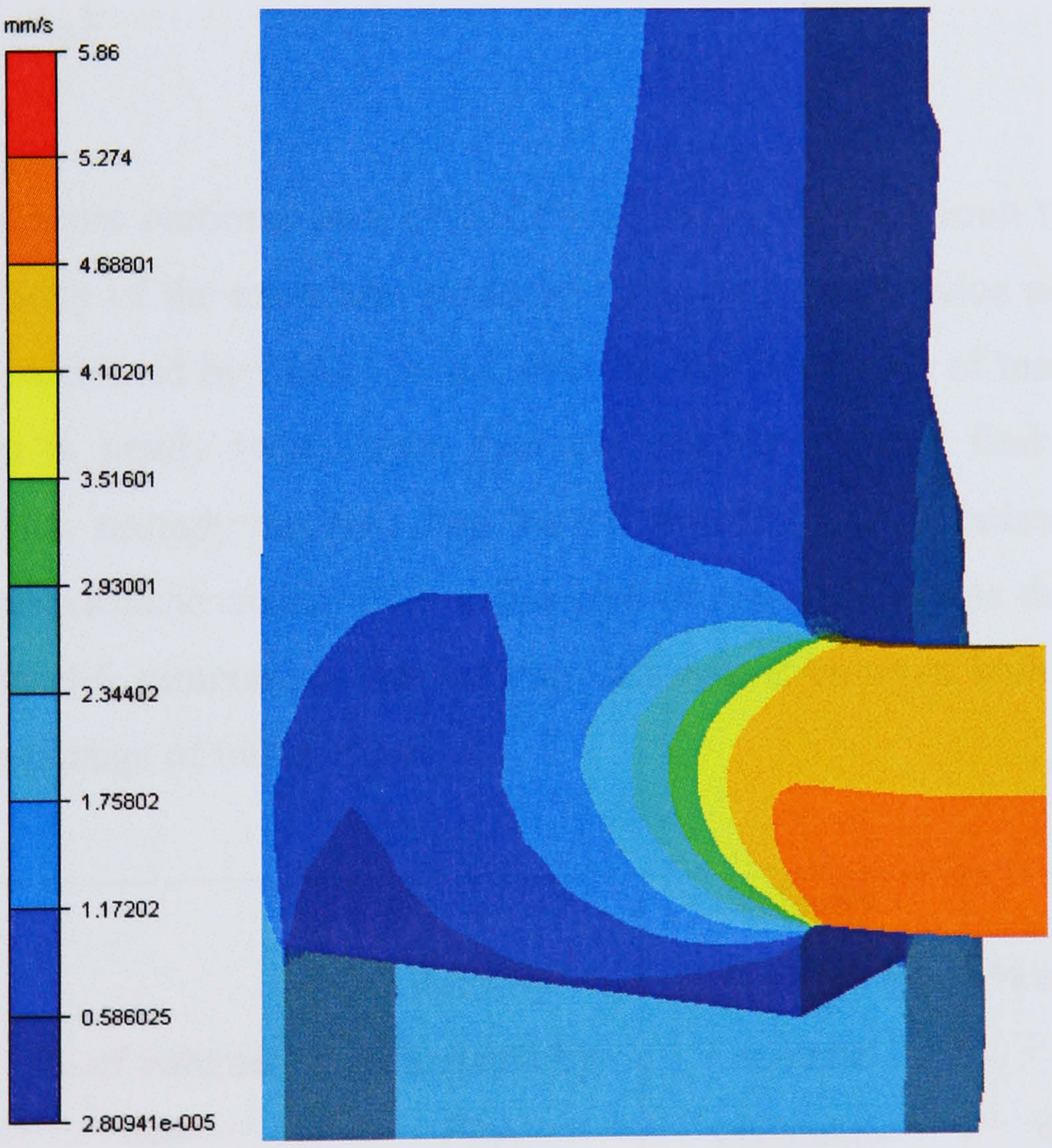

Figure 4.31 Velocity profile at steady state (with flash)

The maximum velocity of the extrudate is 5.9mms^{-1}. Based on a volume constancy relation, a theoretical velocity could be calculated by resolving the following flow balance equation:

$$V_R A_F = V_E A_E + V_{Fl} A_{Fl} \tag{4.5}$$

where V_R, V_E and V_{Fl} are the ram, extrudate and flash velocities; A_F, A_E and A_{Fl} are the feedstock, extrudate and flash cross sectional areas. In the simulation, due to the high coefficient of friction in the groove, there is no slippage between the feedstock and the ram. Therefore the velocity of the flash is equal to the velocity of the ram (i.e. $V_{Fl} = V_R$). The difficult parameter to define is the cross sectional area of the flash. This area is divided into two distinctive zones: zone 1 and zone 2 (see Figure 2.2). The most efficient way to calculate the length of zone 2 is to use FEM. In the simulation with flash the length of zone 2 is approximately 8mm. Equation (4.5) can be rewritten as follows:

$$V_E = \frac{V_R}{A_E}\left(A_F - A_{Fl}\right) \tag{4.6}$$

With a groove cross sectional area of 22x25mm^2 and a flash of 1mm thickness the calculated velocity of the extrudate would be 6.86mms^{-1}. This value is higher than the 5.9mms^{-1} calculated by FEM. In this case the loss in volume of material during the simulation is nearly twice more than the analysis without flash (a total of 1100mm^3). This strongly suggests that the FE simulation underestimates the exit velocity of the extrudate mainly due to this loss of material volume during the FE process. Table 4.6 summarises the velocity differences between both simulations against the percentage of volume lost.

	% of volume lost	Velocity calculated by FEA (mms^{-1})	Velocity Calculated by volume constancy relation (mms^{-1})	% of difference between calculated velocities
Without flash	1%	7.90	8.35	5.4%
With flash	1.8%	5.90	6.86	14.0%

Table 4.6 Extrudate velocities calculated and percentage of volume lost

The difference of 10% between the measured velocity ($6.2mms^{-1}$) and the theoretically calculated velocity ($6.86mms^{-1}$) is probably due to some slippage between the feedstock and the ram during the experiments.

Figure 4.30 does not show any apparent velocity differential at the die exit whilst Figure 4.31 shows a distinctly higher velocity at the bottom of the extrudate. In order to accurately compare the velocity differentials in the extrudate the following procedure was performed. The velocities of the nodes in the plane of symmetry, directly after the die exit, were recorded against their position in the extrudate. This was done for both simulations from the bottom to the top of the extrudate. Figure 4.32 shows a graphical representation of the velocities across the extrudate directly at the die exit.

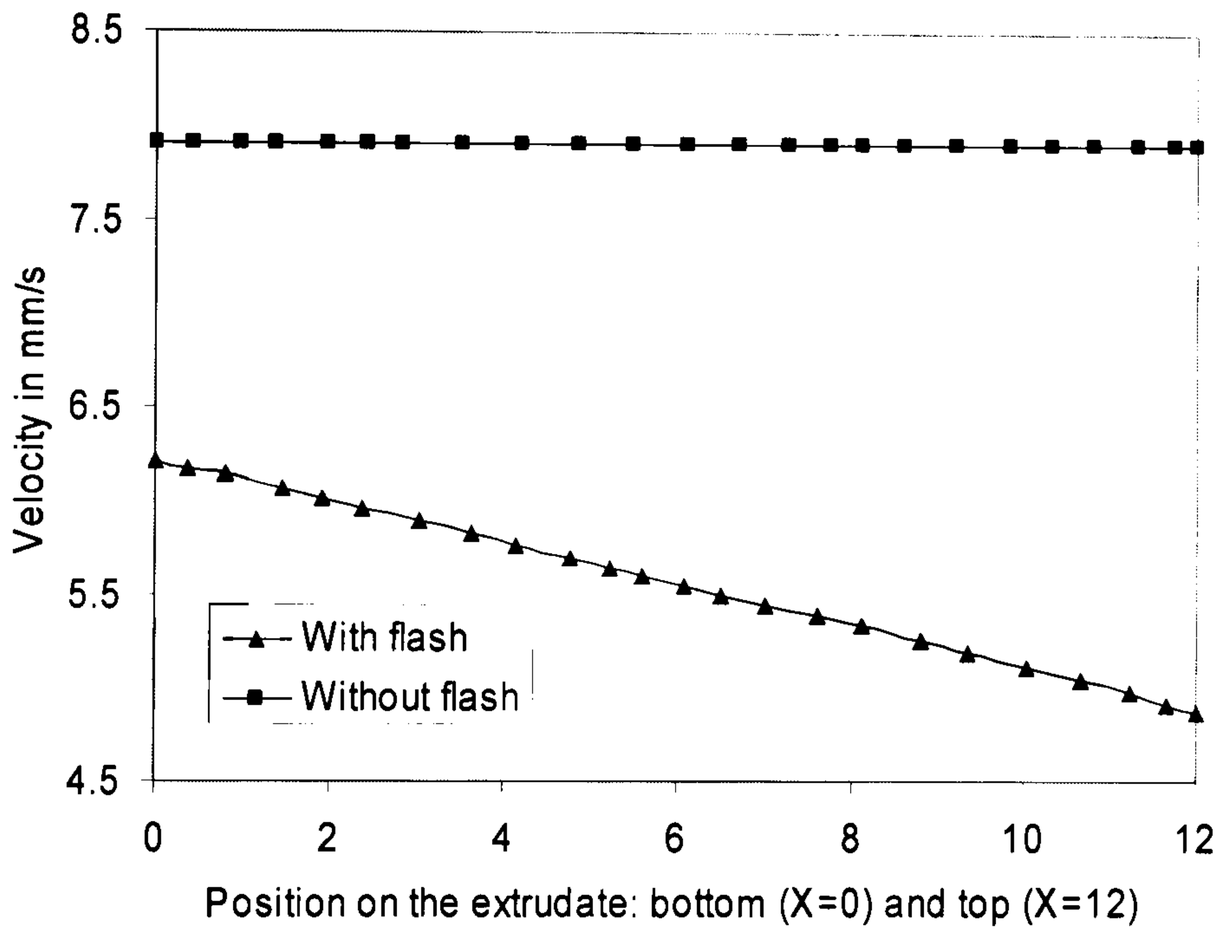

Figure 4.32 Velocities across the extrudate at the die exit (a) without flash and (b) with flash

For the simulation with flash, the velocity at the top of the extrudate is 21% lower than the one at the bottom. Furthermore the velocity decreases linearly across the extrudate. This suggests that the mechanical properties of the extrudate could also vary linearly across the extrudate. However, for the simulation without flash the velocity is constant across the extrudate. Explanations for this could be found in the manner in which the material flows from the upset zone to the die entrance. When the gap is present between the ram and the shoe the material adjacent to the gap flows through it to form part of the flash. Consequently the velocity of the material adjacent to the shoe, and flowing toward the apex of the die entrance is reduced. The

material adjacent to the wall of the groove is driven towards the abutment and forms the flash in the groove. As a result of this, the material at the centre of the upset zone flows faster towards the bottom and centre of the die entrance. However, when no gap is present, the material adjacent to the shoe flows directly to the apex of the die entrance. The bulk of the remaining material in the upset zone flows towards the bottom and centre of the die entrance. It appears that this situation creates an even pressure within the bottom quarter of the upset zone. Subsequently the velocities across the extrudate are equal. This explanation should be taken with caution however. It is possible that different results could be produced with another die profile and differing positions of the die in relation to the abutment.

Dead metal zones

The limits of the dead metal zones for both simulations, at steady state, are represented with the blue surfaces in Figure 4.33. The yellow parts represent the dies and the boxes outlined in blue are the abutments. The abutment in Figure 4.33b (without flash) is oversized in order to interlock with the ram to create a perfect fit.

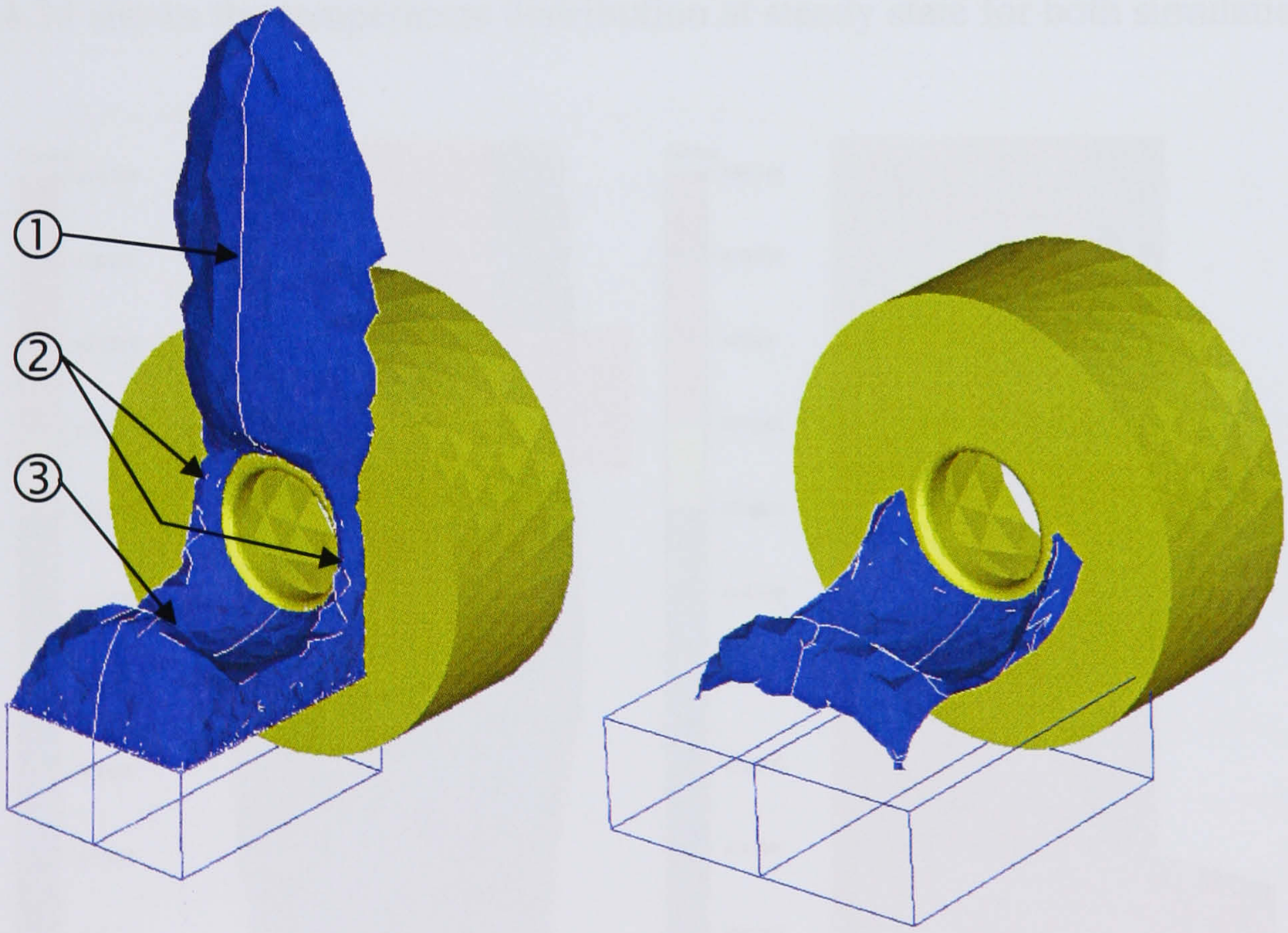

(a) (b)

Figure 4.33 Dead metal zones in Conform (a) with flash and (b) without flash

The dead metal zones, when flash is present, are relatively complex in shape (Figure 4.33a). This shape can be divided into three volumes: 1, 2 and 3. Volume 1 is

delimited by the flow of material through the gap between the shoe and the ram, and the apex of the die entrance. Volume 1 also resembles a half-teardrop. This correlates well with observations made by other researchers. Volume 2 is present on both sides of the die entrance. It is formed by material flowing into the die entrance and towards the gap between the shoe and the ram. Volume 3 is situated above the abutment and is surrounded on its edge by the material flowing through the gap between the abutment and the ram. The profile of the top surface of Volume 3 is probably caused by the relatively high velocity of the centre part of the upset zone. This flow of material hits the abutment in its middle area and forces the rest of the material away before finding its way to the die entrance.

The dead metal zone, when there is no flash, is relatively simple (Figure 4.33b). The volume is created in a similar manner to that of Volume 3. However, in this case, the curvatures of the shape are less pronounced because the edges are not flowing through a gap.

4.6.4.4 Temperature evolution

Figure 4.34 shows the temperature distribution at steady state for both simulations.

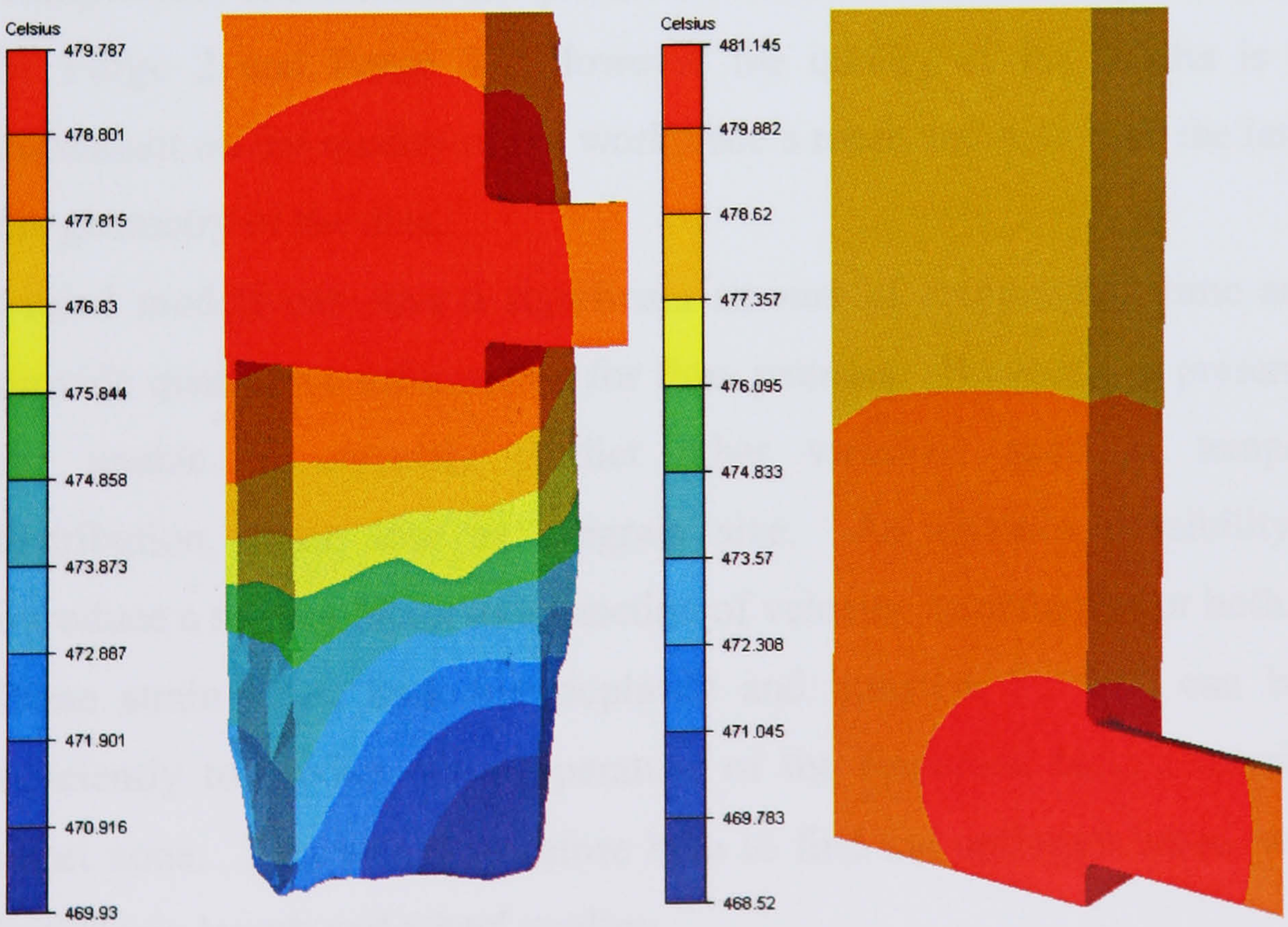

(a) (b)

Figure 4.34 Temperature distribution at steady state (a) with flash and (b) without flash

At steady state, with flash, the maximum temperatures are located at the bottom of the upset zone (Figure 4.34a). There is no significant gradient in temperature in this zone and the temperature across the extrudate is constant. It seems that the temperature rise of the extrudate (from 414°C to 480°C) is caused due to the contact with the tooling (478°C) rather than by the heat generated by plastic deformation. This was expected as the use of rigid dies maintains a constant temperature throughout the simulation. Furthermore, in Conform extrusion the tooling is relatively large compared to the feedstock. It is therefore not unreasonable to assume that in Conform the temperature of the tooling (particularly the wheel, the die and the shoe) controls the extrusion temperature. Similar reasoning is applicable also to the temperature distribution when there is no flash (Figure 4.34b).

4.7 Concluding remarks

Based on the results and discussions of this chapter the following conclusions are suggested:

- Temperature distribution and pressure evaluation are relatively well predicted by Forge 2 and Forge 3. However the quality of the results is highly dependant on the quality of the workpiece's mesh and how well the latter fits the geometry of the dies.
- Scaled models can save a significant amount of computation time and still provide qualitative information for flow patterns. However, at present, they are unable to correctly predict other variables such as temperature distribution, strain rate or subgrain size. An obvious possibility is to introduce a scaling factor as a function of velocity, temperature or both.
- Plane strain FEA, both thermoplastic and transient thermal, can be used efficiently to predict the temperature of the feedstock before entering the upset zone. This would therefore help to find the optimum wheel velocity, initial grip length and wheel cooling.
- An efficient way to maintain an extrudate in a straight direction would be to use a ghost die. Such a die is defined with a null coefficient of friction, is

infinitely stiff and has the thermal properties of air. Therefore, it has no influence on either the extrusion pressure or temperature distribution.

- In Conform the steady state is attained when the upset zone is fully formed. At this stage the extrusion load, temperature, and extrudate velocity converge to their respective maximum values and the dead metal zone is fully formed.
- The velocity varies linearly across the extrudate. This variation can be limited by reducing (or eliminating) the gap between the wheel and the abutment/shoe assembly. Furthermore the exit temperature of the extrudate can be controlled by adjusting the temperature of the tooling in contact with it. For example, to change the temperature of the wheel, the angular velocity and its cooling rate can be adjusted. Accurate control of the exit velocity and temperature across the extrudate can assist in obtaining the desired material properties of the extrudate.
- During the extrusion of complex profiles which require a large number of re-meshing, the loss of volume mesh during the simulation can significantly affect the accuracy of the results in terms of velocity.

5 Expansion chamber and feeder plate

5.1 Introduction

This chapter is comprised of two main studies: the expansion chamber in Conform and the feeder plate in normal extrusion, which can also be utilised in Conform configuration. The former is investigated both in plane strain and three-dimension. Results such as temperature, velocity profile and strain are compared with experimental observations. The feeder plate is investigated by comparing forward extrusion with and without the plate. Results such as temperature, velocity profile, microstructure and pressure distribution are discussed. A section of this chapter describes the simulation of microstructure in aluminium extrusion and its integration into Forge 2 and Forge 3.

5.2 Expansion chamber

5.2.1 Simulation set-up

Hardware and software

The analyses for the expansion chamber were performed on a PC with dual processors (400MHz) and 1Gbytes of memory. The software Forge 2 (version 2.8) and Forge 3 (version 5.2a) were used.

Geometry

The tooling was modelled to simulate a simple Conform extrusion. The groove was linear (rather than a circumferential profile) and its cross-section formed a rectangular U shape of 22mm width by 25.5mm depth. The abutment fitted the groove perfectly (i.e. no flashes were simulated) and was mounted 12mm below the centre point of the expansion chamber circular orifice. Figure 5.1 illustrates half of the expansion chamber in three-dimension with (XY) as a plane of symmetry.

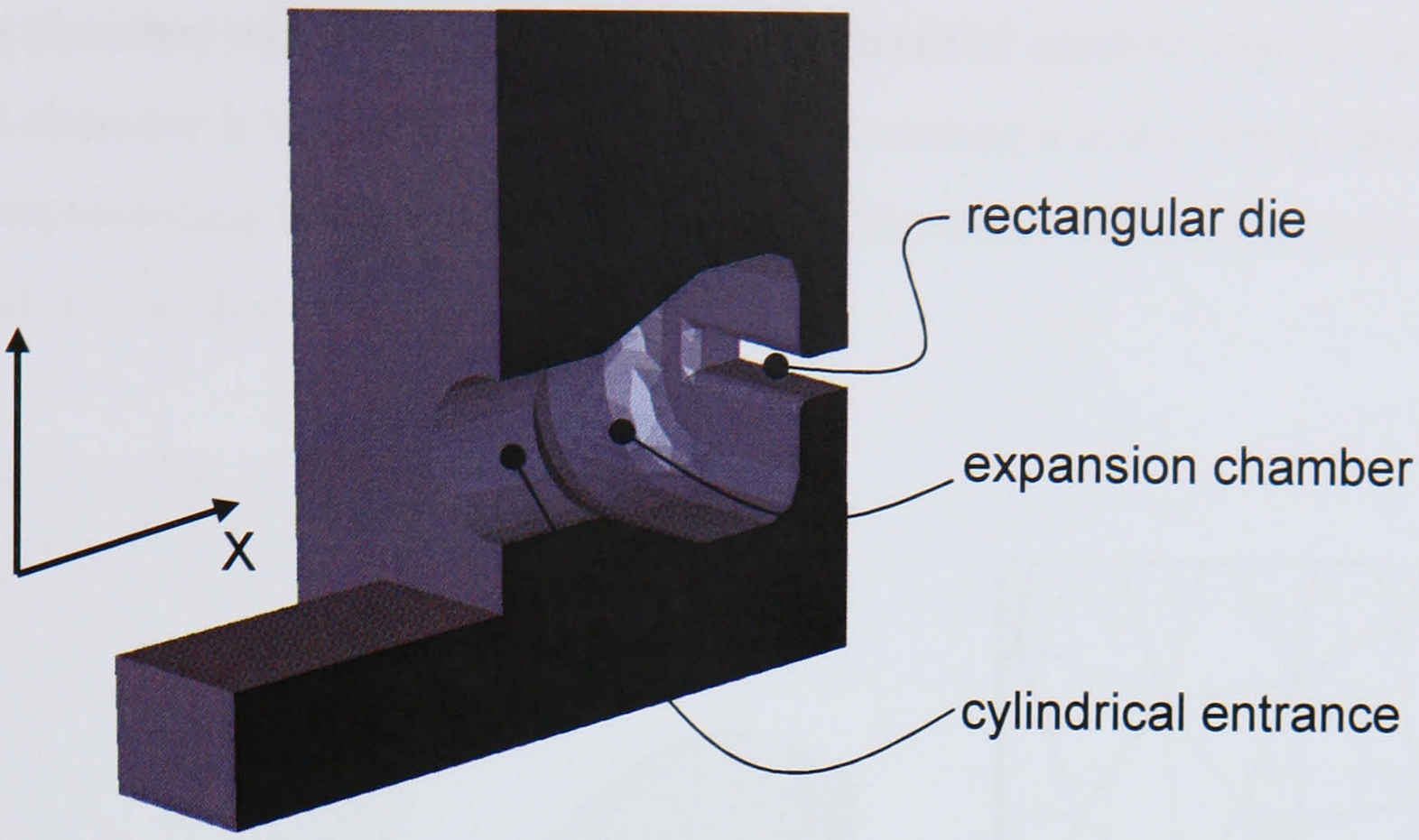

Figure 5.1 Three-dimensional view of the expansion chamber

The material reaches the abutment in the (-Y) direction and then exits towards the (+X) direction. The chamber starts with a cylindrical entrance (10mm x ∅12mm), expands gradually to a rectangular parallelepiped (10mm x 20mm x 32mm with a 3mm fillet radius) and finishes with a rectangular die extrusion (profile of 20mm x 3mm) and a die land of 2.5mm.

Meshing

The Conform process with an expansion chamber involves very high deformations, which lead to large distortions of the elements, particularly in the vicinity of the abutment and die orifice. The distorted elements result in the deterioration of the accuracy of the solution, and in order to maintain numerical stability computational time steps must be shortened. Consequently, a large number of increments would be required to accurately simulate the continuous extrusion process.

During the initial FE simulations for this thesis, a single analysis in 3D could take up to four weeks to produce results. Furthermore the software could only perform a simulation with a maximum of 200 re-meshings. It is important to remember that Forge 2 and Forge 3 were initially developed to simulate forging, a process whereby material deformation is less severe than in extrusion. However, since these initial analyses the software has been updated by the supplier in order to accommodate an unlimited number of re-meshings.

The main problem encountered in the simulations occurred during the filling of the expansion chamber with the material. Once the material reached any surface of the expansion chamber it would come back on itself, creating a self-contact between the elements representing the workpiece. Figure 5.2 illustrates self-contact occurring in the expansion chamber.

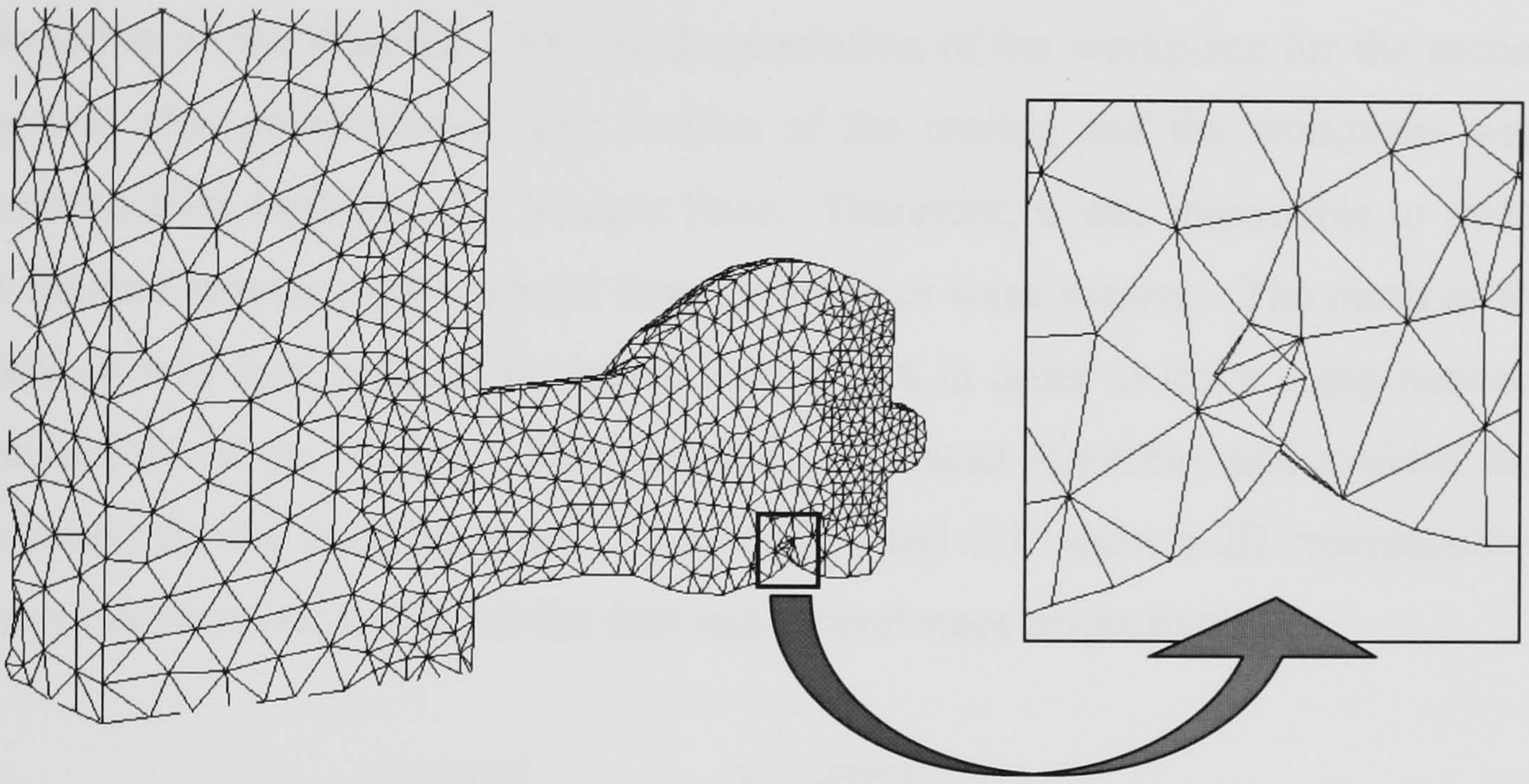

Figure 5.2 Self-contact in the expansion chamber

Although the software included an algorithm for self-contact (in 2D), this was designed to simulate overlaps in forging. The algorithm did not work for the type of self-contact which occurred in the expansion chamber. Consequently the software could not converge to a solution and stopped running. A more appropriate algorithm for this situation would be one which could merge two or more elements depending on the local temperature and compressive stress.

In order to overcome some of the problems mentioned above, the Conform process was simulated in two stages both for the plane strain and 3D models. At first, the commencement of Conform extrusion was analysed. This stage simulated the upsetting of the feedstock and the start of extrusion into the expansion chamber. At the end of the analysis the average temperature was recorded. A second stage, representing the feedstock and the inside of the expansion chamber, was modelled together with the average temperature previously recorded. This stage simulated the start of the extrusion through the die land until the software stopped due to the limited number of increments.

The major disadvantage with this approach was the loss of material history (in terms of velocity, temperature, and pressure) and spatial topology between the first and second stages. In relation to the temperature, for example, the temperature range observed at the end of the final mesh at the first stage needed be averaged to a single estimated value for the whole of the initial mesh at stage two. Therefore the accuracy of the temperature distribution was affected and consequently the deformation of the material. The mesh generation of the workpiece for the second stage was also problematic. The surface of the tooling and the workpiece were discretised with elements, i.e. straight lines. Therefore, it was impossible to match both meshes exactly where curved lines or surfaces were present. The mesh of the workpiece was then reduced by approximately 5% in order to leave a gap between the material and the tooling. This satisfied the contact algorithm and avoided tool penetration for the first increment. Figures 5.3a and 5.3b show a 2D representation of the workpiece and tooling at the first and second stage respectively.

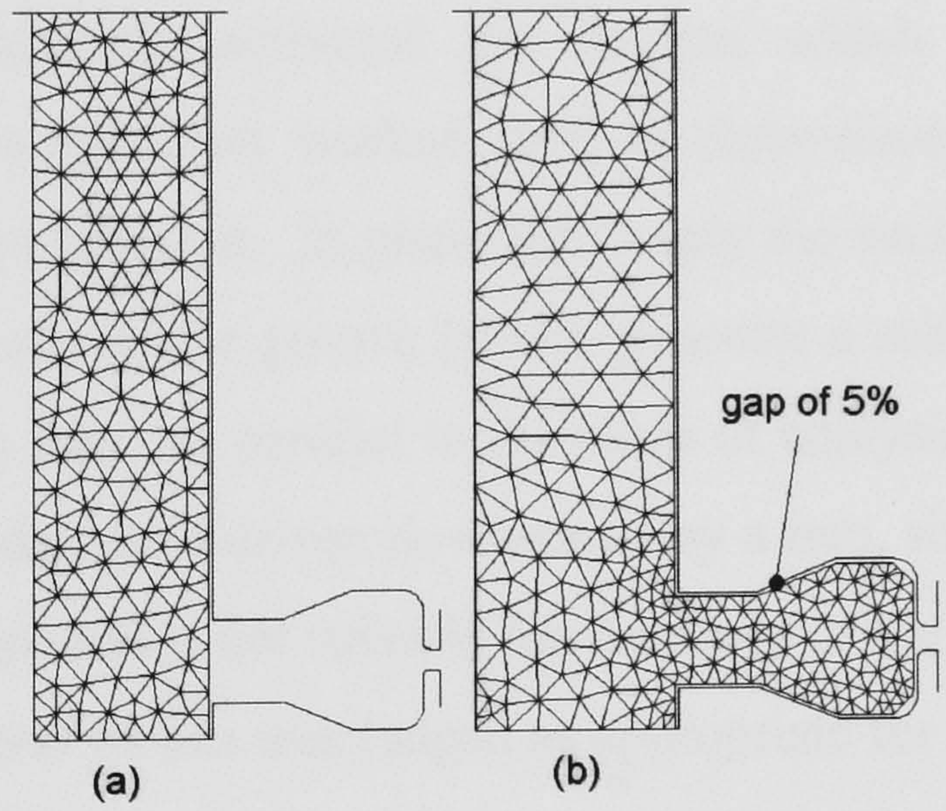

Figure 5.3 Two-dimensional mesh of the workpiece and tooling at (a) the first stage and (b) the second stage

Both tools, in 2D and 3D, were meshed using rigid elements (non-deformable) with tool steel material properties. The heat transfer between the material and the tooling was consequently reduced to a constant heat flux from the tool surface. The flow stress data of AA6063 were used for the workpiece.

Boundary conditions

Sticking friction conditions were imposed between the tooling and the material. Although this was appropriate for the groove surface it was not suitable at the die land. At the time it was thought that reducing the number of tools would reduce the computational time required. Thus the abutment, expansion chamber and die were modelled as one tool and consequently could only have one friction definition. However, further research showed that the computation time is not significantly affected by the number of tools modelled. Therefore subsequent analyses were carried out using different coefficients of friction for the die and the rest of the tooling.

The groove (representing the wheel) was moved downwards at $5mm.s^{-1}$. The friction was initiated by a FE manipulation. At the beginning of the analysis a virtual punch pushed the feedstock against the abutment for the first few increments. The upsetting of the feedstock generated contact stresses normal to the tools' surface. These stresses consequently activated the friction which drove the feedstock downwards. This manipulation worked well in three-dimension but it was not suitable for plane strain analyses. In plane strain only the back of the groove wall is modelled. The two walls of the groove (which generate a substantial friction force) cannot be modelled as they are parallel to the plane of analysis. Therefore, in plane strain analyses the feedstock is driven downwards by a ram, similar to the process in side extrusion. This method is not suitable for the study of the flow in areas adjacent to the abutment, however its use was judged as appropriate for areas in the expansion chamber and die exit.

5.2.2 Plane strain results

Results from the plane strain analyses of the Conform process are difficult to quantify, however qualitative appraisals are possible. Figure 5.4 shows the velocity profile with the use of a logarithmic scale in order to identify stationary material.

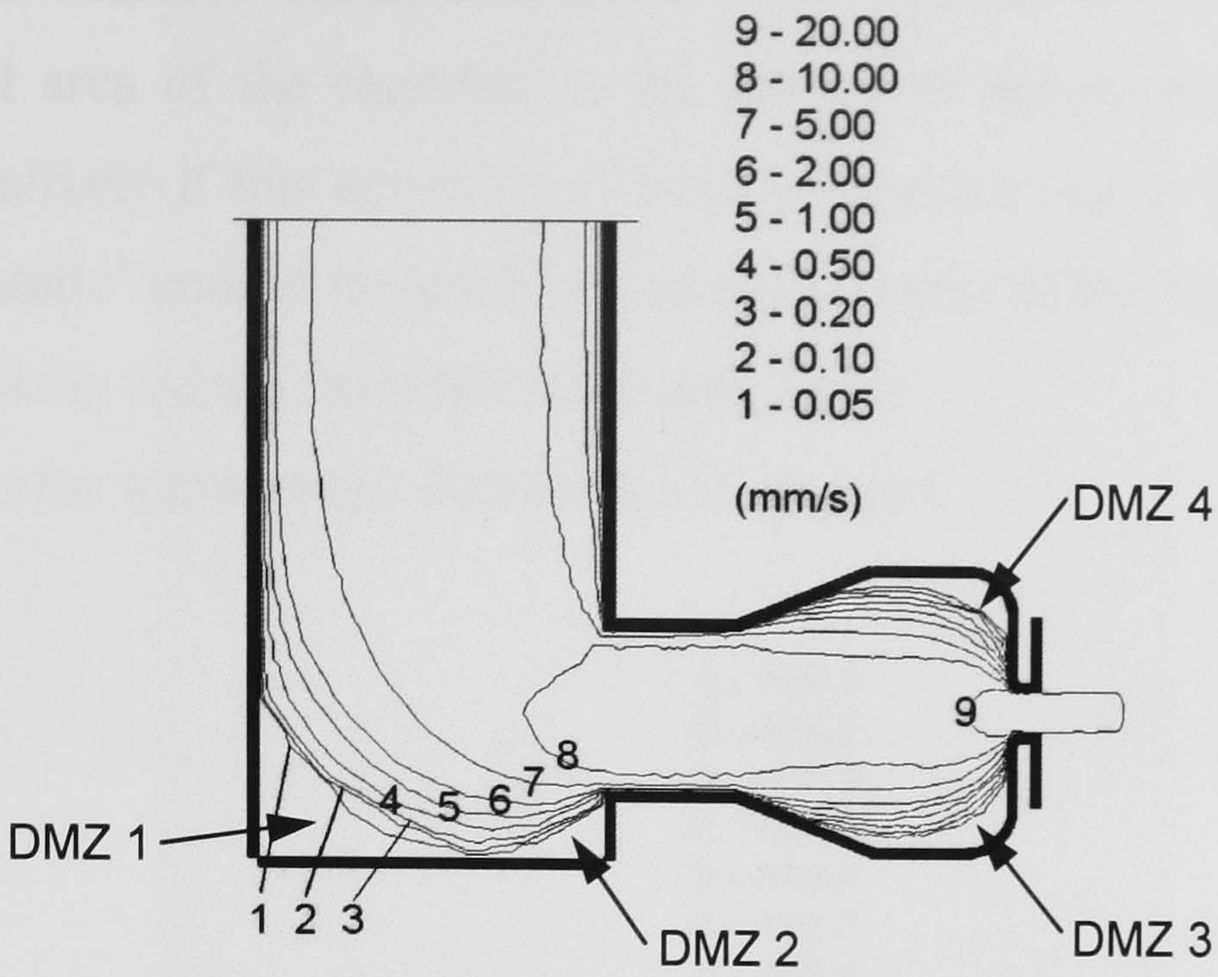

Figure 5.4 Velocity profile

Four dead metal zones (DMZ 1 to DMZ 4) can be clearly identified from this figure. These areas of stationary material developed in a similar manner to that of the dead metal zones found in conventional extrusion processes. Less energy is required to internally shear the worked material than to cause it to flow from the die face to the die land, or from the abutment to the entrance of the expansion chamber. DMZ 1 is not a true feature of the Conform process and was formed due to the boundary conditions applied on the plane strain model. However, DMZ 2 (at the base of the abutment) corresponds very well with the DMZ observed with the Conform experiments from Carr *et al* (1996) and Tomimatu *et al* (1999). DMZs 3 and 4 are located in the expansion chamber and are similar to those formed in forward extrusion with a flat faced die. Both Sinha and Chia (1988) and Clode (1992b) observed similar dead metal zones in the expansion chambers of Conform experiments.

Velocity gradients at the entrance of the expansion chamber are low and the difference between the top and bottom velocity is small. The velocity at the top of the expansion chamber is 5% faster than the bottom one. This does not concur well with experimental results. Sinha and Chia (1988) and Clode (1992) reported a significant difference in velocity between the top and bottom part of the expansion chamber. This unbalanced flow was due to the pressure difference across the expansion chamber entry. Furthermore, it was also reported that the material flow in

the middle of the chamber was of a turbulent nature with an eddying flow observed from the central area of the chamber to the bottom of the extrudate. This latter feature seems unlikely if this condition of constant mass is not to be invoked. It is possible that a 'static' pool of material located at the centre of the expansion chamber could have gradually fed the extrudate with eddy flows.

Figure 5.5 shows the temperature distribution in degree C.

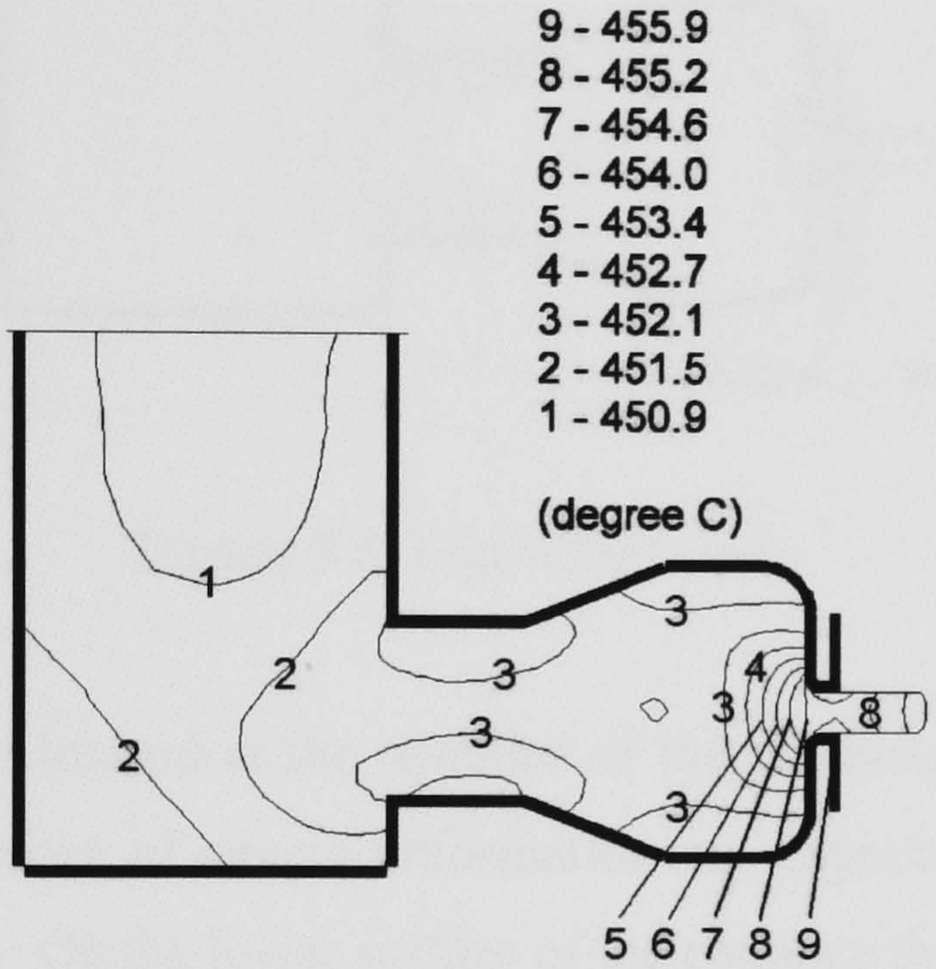

Figure 5.5 Temperature distribution

Although the temperatures at the abutment and the entrance of the expansion chamber are not uniform, the difference between the top and bottom surfaces is insignificant. The maximum temperature is situated at the die exit, where the distribution is symmetrical. As with the velocity profile, the temperature distribution does not give a true representation of the Conform process. For Conform extrusion, Sinha and Chia (1988) reported a difference of approximately 17˚C to 28˚C between the bottom and top surface of a bus bar (the bottom surface having the highest temperature). It was also noted that severe deformations at the die bearing caused a temperature rise of approximately 30˚C to 100˚C. It is important however to remember that the tooling, being rigid, is always at a constant temperature, and that the extrusion is just commencing. Therefore, the heat transfer does not truly represent the exchange between the tooling and the workpiece and the heat balance is not representative of steady state.

Figure 5.6 displays the equivalent strain.

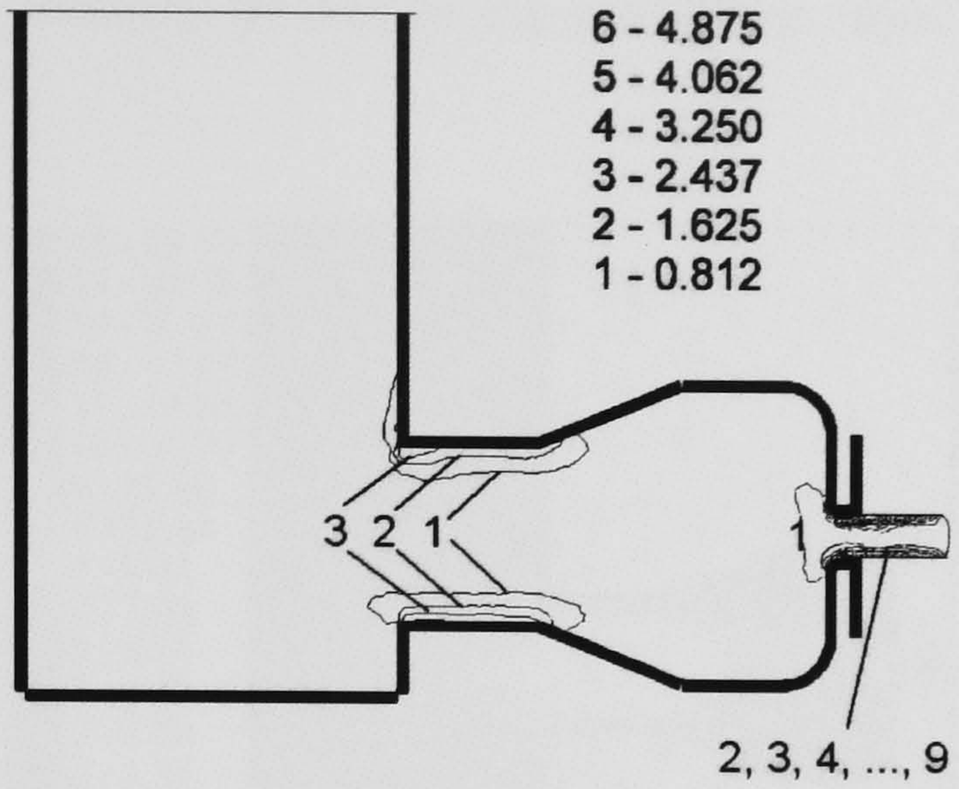

Figure 5.6 Equivalent strain

The highest strains are located at the entrance of the expansion chamber and at the die land, where the zones of severe deformation are expected. The central layer appears less deformed. On the lower surface of the entrance the strain is 22% higher, on average, than it is at the top surface. This strain difference is not clearly visible on the figure. However the strain difference was calculated from the raw data using the 15 nodes along the 10mm long edge. At the entrance of the expansion chamber there is only one dead metal zone situated close to the abutment. Therefore, the material at the lower entrance is strained to a greater extent than that in the upper entrance. The equivalent strain contour reflects phenomenon found in the experimental analyses of Conform. Sinha and Chia (1988) have reported that the shearing strain can be five to seven times higher at the surface than at the centre of the expansion chamber entrance.

5.2.3 Three-dimensional results

A large number of results were produced by the 3D analyses. In addition to 3D views several cross sections can also be generated. However, the plane of symmetry is probably one of the most meaningful cross sections as it is the one displayed by most researchers in their physical experiments. The cross section of the extrudate is

also useful, but in the case of these analyses only a few elements could be utilised across the die exit. Consequently, the results plotted on the cross section of the extrudate were difficult to interpret.

Figure 5.7 shows the velocity profile in the mid-plane from the three-dimensional analyses.

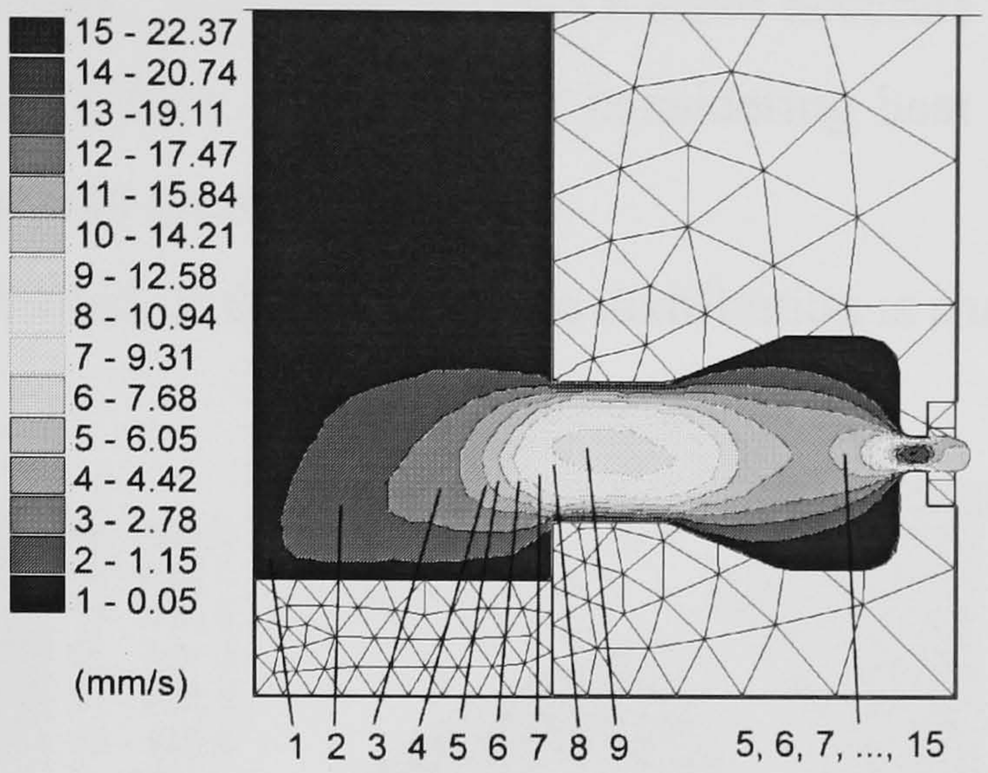

Figure 5.7 Velocity profile in the mid-plane

It can be seen from the figure that in 3D the velocity differential between the upper and lower part of the expansion chamber and die is not accurately represented. This could be due to the relatively coarse mesh at the die entrance. The coarse elements which pass the entrance of the expansion chamber are not capable of accurately representing the material flow. However the dead metal zones are accurately described.

Figure 5.8 shows the temperature distribution in the mid-plane.

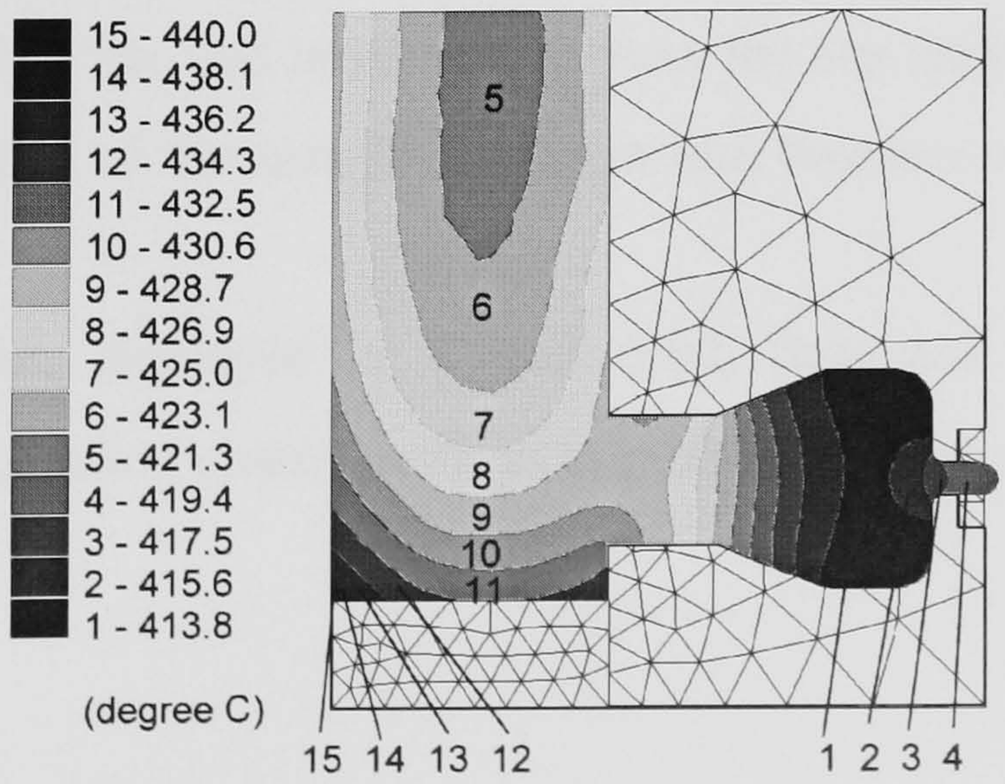

Figure 5.8 Temperature distribution in the mid-plane

The temperature distribution in the 3D model is different to that in the plane strain model. The highest temperature is situated at the abutment near the bottom of the groove. The lower surface of the expansion chamber entrance is 10˚C hotter than the upper surface. The negligible heat gradient at the die exit does not agree with experimental observations. It is believed that a more accurate temperature gradient could be obtained with a finer mesh and by considering heat transfer between the rigid die and the workpiece more accurately.

An interesting phenomenon of the temperature distribution is shown in Figure 5.9.

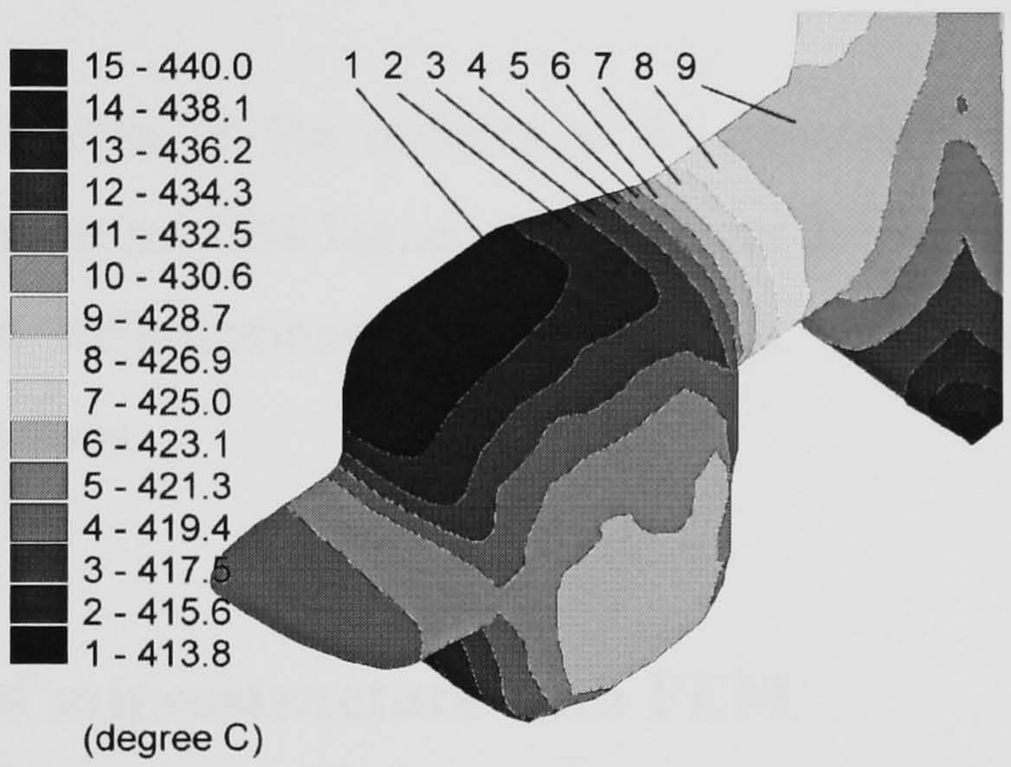

Figure 5.9 Temperature distribution inside the expansion chamber

The lateral surfaces of the expansion chamber are 10˚C hotter than the top and bottom surfaces. This could explain the observations made by Sinha and Chia (1988) regarding the grain size present in the extrudate. They observed that the bottom surface of a bus bar had larger grains than the top surface, and also that the grains towards the edge of the sample are larger and decrease to a minimum size at the centre.

The equivalent strain, displayed in Figure 5.10, does not represent a smooth distribution in the expansion chamber. This is probably due to the coarse mesh used in this area.

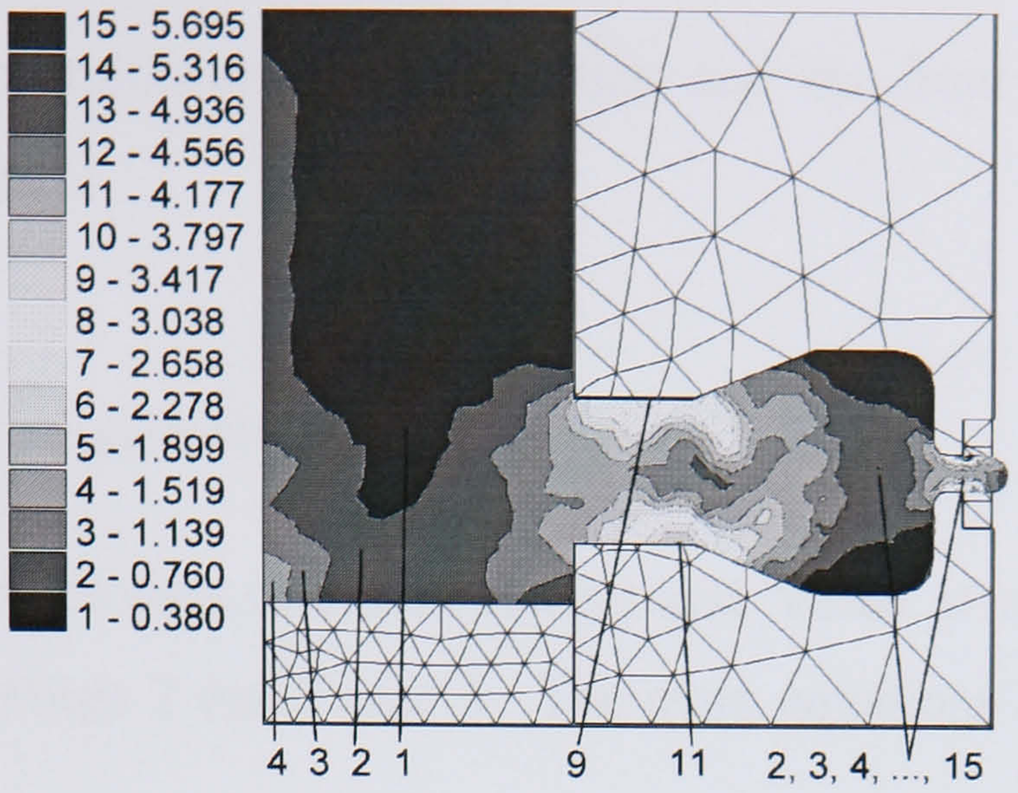

Figure 5.10 Equivalent strain in the mid-plane

After analytical calculation on the surfaces of the expansion chamber, the strain at the bottom was found to be 12% higher than the one at the top. This confirms the formation of severe deformations which occur at the abutment, as noted in experimental observations.

5.3 Prediction of microstructure with FEM

Previous work involving microstructure and FEM (see section 2.3.1) showed that empirical and physical models can be integrated with FE software to successfully predict the microstructural evolution and flow stress of aluminium alloys. Ideally, an accurate modelling of hot extrusion would require an integrated approach, similar to the one suggested by Pauskar and Shivpuri (1999). In this, the microstructural evolution, deformation, heat transfer, and flow stresses are updated at every time step. This integrated approach is schematically represented in Figure 5.11.

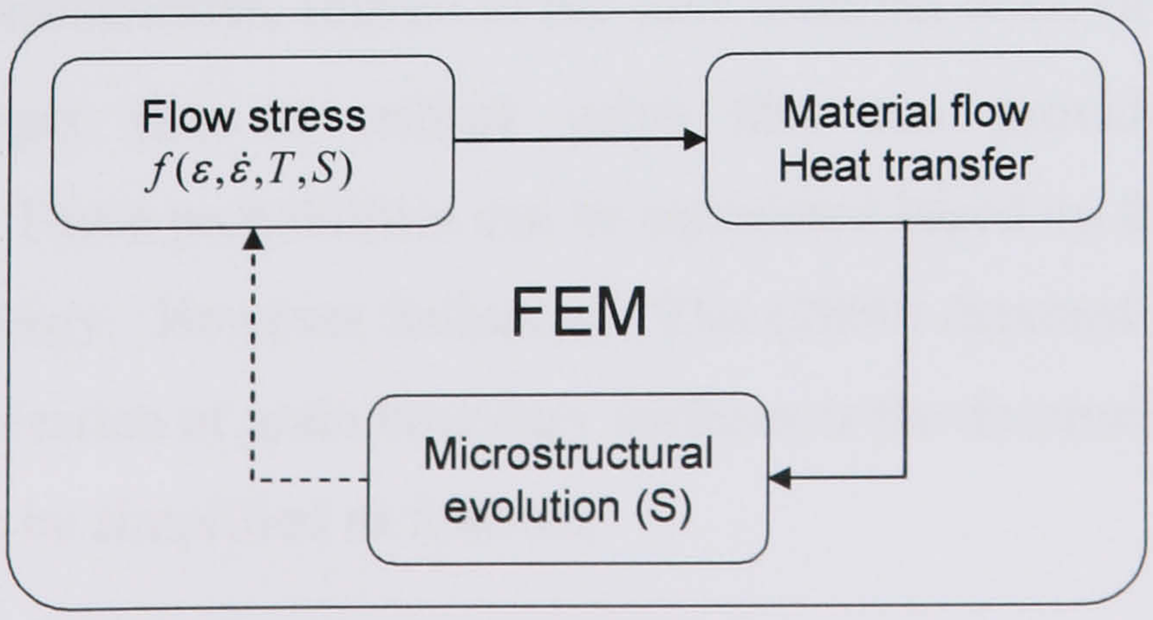

Figure 5.11 Integrated approach for FEM

The link between the microstructural evolution and the flow stress has not been considered in this thesis.

5.3.1 Physical and empirical models

Physical models from Sellars and Zhu (2000) and Vatne *et al* (2000) have been integrated into both Forge 2 and Forge 3. The main equations are discussed in this section.

Recrystallization nucleation density

During deformation nucleation sites occur in places such as grain corners, grain lines, grain surfaces and inside the grain. Consequently the following expression is suggested to evaluate the density of nucleation sites, N_V:

$$N_V = p_1\lambda_1 P_V + p_2\lambda_2 \frac{L_V}{\delta} + p_3\lambda_3 \frac{S_V}{\delta^2} + p_4\lambda_4 \frac{P_\theta}{\delta^3} \qquad (5.1)$$

where P_V is the number of grain corners per unit volume and $P_V = 2.6 \cdot d_0^{-3}$ (d_0 is the initial grain size). L_V is the line length per unit volume and for plane strain compression $L_V = 1.513\left[e^{\varepsilon/1.155} + 0.5\left(1 + e^{-\varepsilon/1.155}\right)\right] \cdot d_0^{-2}$. S_V is the grain boundary surface area per unit volume and for plane strain compression $S_V = \left(0.429e^{-\varepsilon/1.155} + e^{\varepsilon/1.155} + 0.571\right) \cdot d_0^{-1}$. P_θ is the probability of finding sub-boundaries with a misorientation angle larger than a critical value within the grain. $\lambda_1 \sim \lambda_4$ are geometric parameters which can be obtained by statistical analysis. $p_1 \sim p_4$ are the probabilities, related to the four different sites, of finding subgrains with a size larger than a critical value that can provide nucleation for recrystallization. These probabilities can be calculated based on the distribution and average stored energy. However Sellars and Zhu (2000) demonstrated that for large deformations, nucleation at grain boundary surfaces is the dominant term. Therefore equation (5.1) can be simplified as follows:

$$N_V = p_3 \lambda_3 \frac{S_V}{\delta^2} \tag{5.2}$$

Stored energy

The recrystallization is dominated by the total stored energy and its distribution. The total stored energy can be calculated from the total dislocation density, ρ_{tot}, as:

$$\rho_{tot} = \rho_i + \rho_b \tag{5.3}$$

where ρ_i is the internal dislocation density and ρ_b is the boundary dislocation density. ρ_i consists of two parts: the 'random' dislocation density, ρ_r, and the 'geometrically necessary' dislocation density, ρ_g, such as:

$$\rho_i = \rho_r + \rho_g \tag{5.4}$$

$\rho_r \approx \rho_g$ for commercial aluminium alloy (1%Mg) at constant strain rate and temperature. ρ_b can be written as follows:

$$\rho_b \approx C \frac{\theta}{\mathrm{b}\delta} \tag{5.5}$$

where C is a geometric parameter depending on the type of the boundary, θ is the misorientation, δ is the spacing between dislocation walls and b is the Burgers vector.

The total stored energy P_D is approximated as follows:

$$P_D = \frac{G\mathrm{b}^2}{10}\left[\rho_i\left(1 - \ln\left(10\mathrm{b}\rho_i^{1/2}\right)\right) + \frac{2\theta}{\mathrm{b}\delta}\left(1 + \ln\left(\frac{\theta_C}{\theta}\right)\right)\right] \tag{5.6}$$

where G is the shear modulus and θ_C is the critical angle for characterising a grain from a subgrain boundary (approximately 15°).

Recrystallization kinetics

Both nucleation density and growth rate of the nuclei determine the recrystallization kinetics. The model describing this phenomenon is usually based on the Johnson-Melh-Avrami-Kolmogorov (JMAK) equation where the recrystallized volume fraction, X_V, is expressed as a function of the holding time after deformation or the time at solution soak or the annealing temperature:

$$X_V = 1 - \exp\left[\ln(1-0.5)\left(\frac{t}{t_{0.5}}\right)^k\right] \tag{5.7}$$

where t is the annealing time, and k is the Avrami exponent which describes the time dependency of the nucleation and growth rates. $t_{0.5}$ is the time for 50% recrystallization. The equation (5.7) can be re-written as:

$$X_V = 1 - \exp\left[-0.693\left(\frac{t}{t_{0.5}}\right)^k\right] \tag{5.8}$$

There are two models available for the calculation of $t_{0.5}$: empirical and physical (Duan and Sheppard 2003).

The empirical model bypasses the evolution of substructure, and relates the final microstructure with strain, strain rate and temperature by regression of the experimental data. The advantage of this model is that it is easy to integrate into FEM. The empirical model is written as follows:

$$t_{0.5} = A' d_0^a \varepsilon^{b'} Z^c \exp\left(\frac{Q_{rex}}{RT_a}\right) \tag{5.9}$$

where A', a, b', c are constants, d_0 is the initial grain size, ε is the final equivalent strain, Z is the Zener-Hollomon parameter, Q_{rex} is the activation energy for recrystallization, R is the universal gas constant and T_a is the annealing temperature.

The physical model is based on the total stored energy and the density of nucleation sites. This model is defined with the following equation:

$$t_{0.5} = \frac{C'}{M_{GB} P_D} \left(\frac{1}{N_V} \right)^{1/3} \tag{5.10}$$

where C' is a temperature-dependent material constant and M_{GB} is the grain boundary mobility. The physical model generates better results than the empirical model for the simulation of aluminium extrusion (Duan and Sheppard 2003). The physical model was therefore used for the analyses presented in this chapter.

Evolution of subgrain

The evolution of subgrain, δ, is explicitly expressed in a differential form based on the typical theories of work hardening and dynamic recovery:

$$\mathrm{d}\delta = \frac{\delta}{\varepsilon_\delta \delta_{\mathrm{ss}}} \left(\delta_{\mathrm{ss}} - \delta \right) \mathrm{d}\varepsilon \tag{5.11}$$

where δ_{ss} is the subgrain size at steady state. ε_δ is a characteristic strain which determines the rate of evolution of subgrain size and may be related to the deformation conditions (i.e $\varepsilon_\delta \propto Z^{3/4}$). Although equation (5.11) provides a reasonable prediction for the evolution of subgrain during hot deformation at constant strain rate and temperature, it fails to predict the subgrain size for transient deformation conditions (Sellars and Zhu 2000). One explanation is that equation (5.11) was obtained by experiments mainly based on creep or low strain rates. Therefore, only the subgrain size at steady state was implemented into FEM using the following empirical equation:

$$\delta_{ss}^{-m} = A + B \ln Z \tag{5.12}$$

where A, B and m are constants dependant on the material.

The values of the numerous parameters and constants described in this section are listed in Appendix F.

5.3.2 Model validation for aluminium extrusion

The models described in the previous sections were validated using Forge 2 for the subgrain size at steady state. Analyses with Forge 3 validated the prediction of recrystallized volume fraction, nucleation density and subgrain size.

Validation in 2D

The FEM results for AA2014 were compared against experimental results from Vierod (1983). The initial billet length was 95mm with a diameter of 73.5mm. The container diameter was 75mm. A flat-faced die with a land length of 5mm was used. The extrusion ratio was 40:1. The initial billet temperature was 598K. The container temperature was 548K and the pressure pad and die temperatures were 498K. A constant ram speed of 6.7mm.s^{-1} was used throughout the whole extrusion process. Specimens taken at different locations from the deformed material were observed using a transmission electron microscope (TEM) and subsequently the subgrain size was measured for each specimen. Figure 5.12 shows a schematic illustration of the locations of the TEM and FEM specimens.

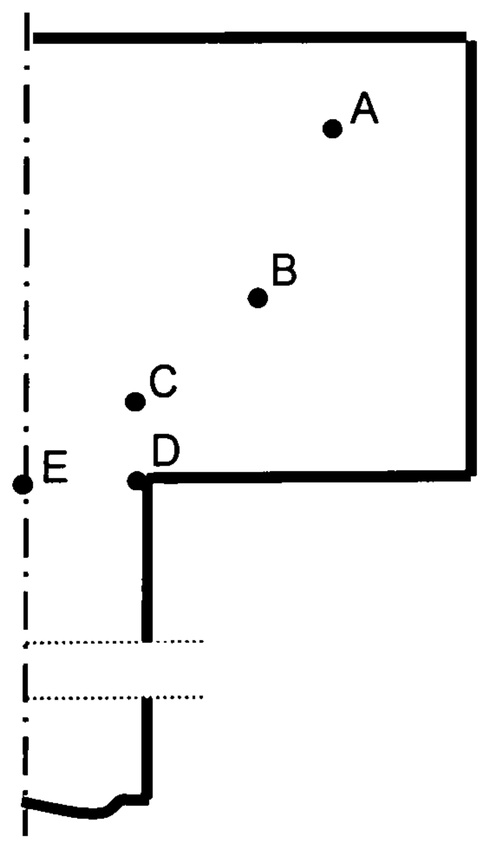

Figure 5.12 Schematic illustration of the locations of the TEM and FEM specimens

Figure 5.13 shows the variations in predicted subgrain size from the centre (location E) to the edge (location D) of the extrudate. The measured and predicted subgrain sizes for each location are listed in Table 5.1. The percentage of error between the predicted and measured values is also listed. More details about the FEM results can

be found in Duan *et al* (2004a and 2004b). It is clear that the predicted subgrain size agrees very well with the measured data.

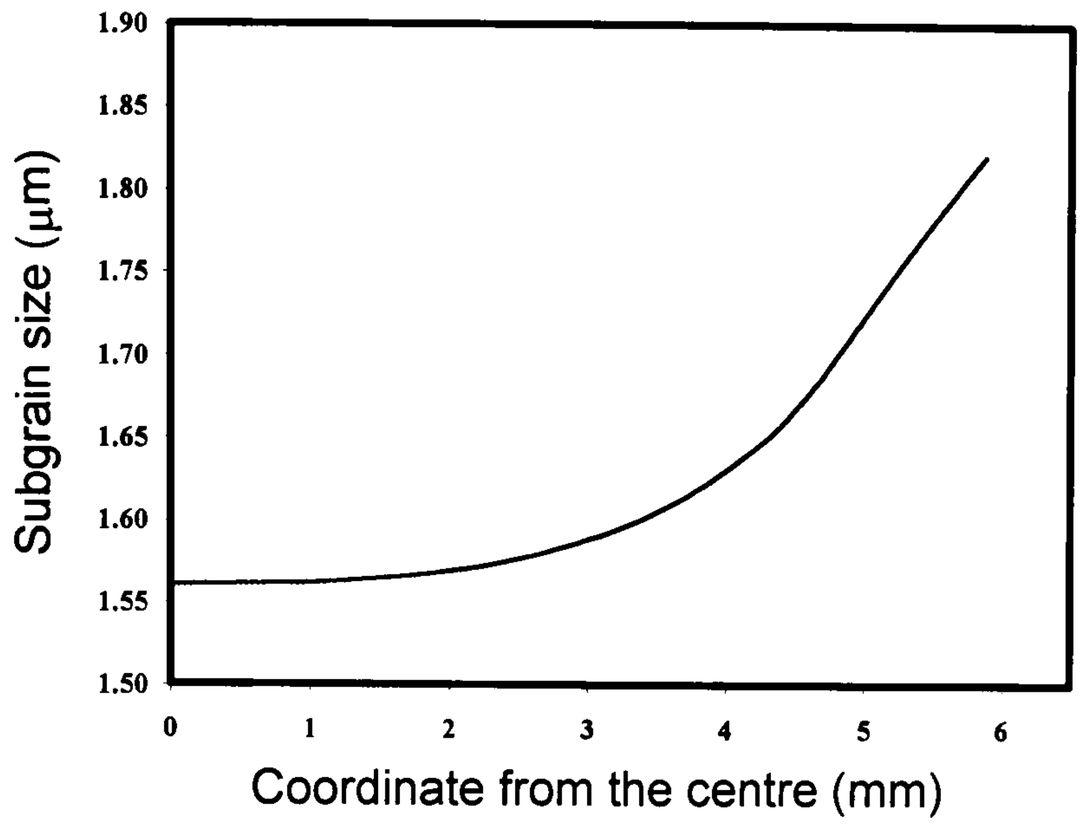

Figure 5.13 Variations of subgrain size along the line ED

Location	Measurement (μm)	Error (±)	Predicted (μm)	Relative Error (%)
A	*1.27*	*0.19*	*1.29*	*1.57*
B	*1.38*	*0.11*	*1.4*	*1.45*
C	*1.36*	*0.21*	*1.44*	*5.88*
D	*1.88*	*0.12*	*1.82*	*3.19*
E	*1.49*	*0.25*	*1.57*	*5.37*

Table 5.1 Measured and predicted subgrain sizes

Validation in 3D

The validation was performed with AA2024 on a T-shaped extrusion. The FEM results from Forge 3 were compared against experimental results from Subramaniyan (1989). The initial billet length was 95mm with a diameter of 73mm. The tooling geometry was similar to the one used for the 2D validation. The initial billet temperature was 613K. The container temperature was 563K and the pressure pad and die temperatures were 513K. A constant ram speed of 7mm.s^{-1} was used throughout the whole extrusion process. The T-shape section had one plane of symmetry as shown in Figure 5.14a. The finite element model of the tooling

comprised the die, container and punch (Figure 5.14b). The radius of all the fillets was 0.5mm.

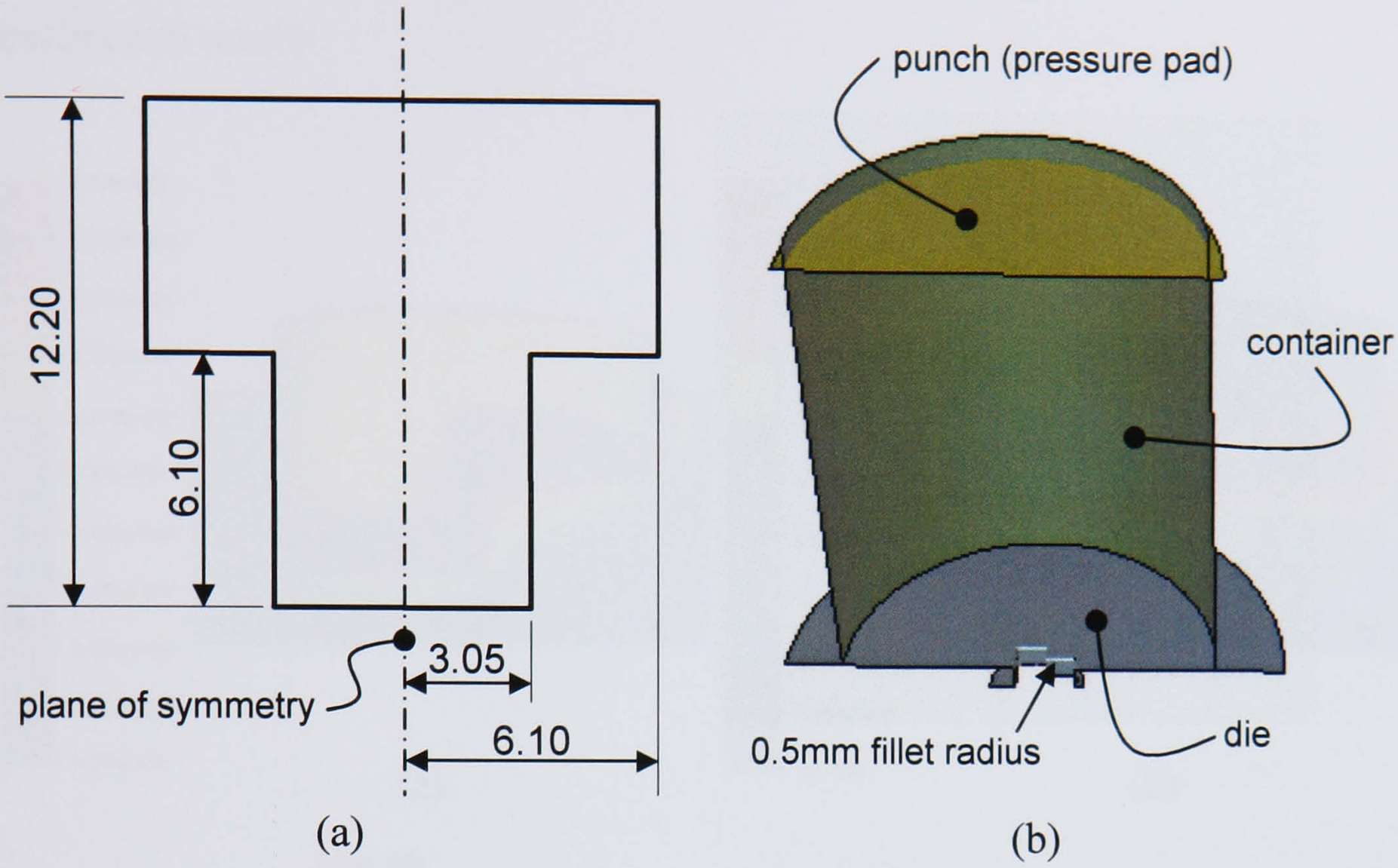

Figure 5.14 (a) Schematic drawing of the T-shaped die (all dimensions in mm) and (b) finite element model of the tooling

In order to be efficient and ensure accuracy in the simulation, four mesh boxes were introduced as shown in Figure 5.15. The minimum element size was 0.18mm (near the die entrance) and the maximum was 10mm (on the periphery of the container). More than 30,000 tetrahedral elements were used for the simulations.

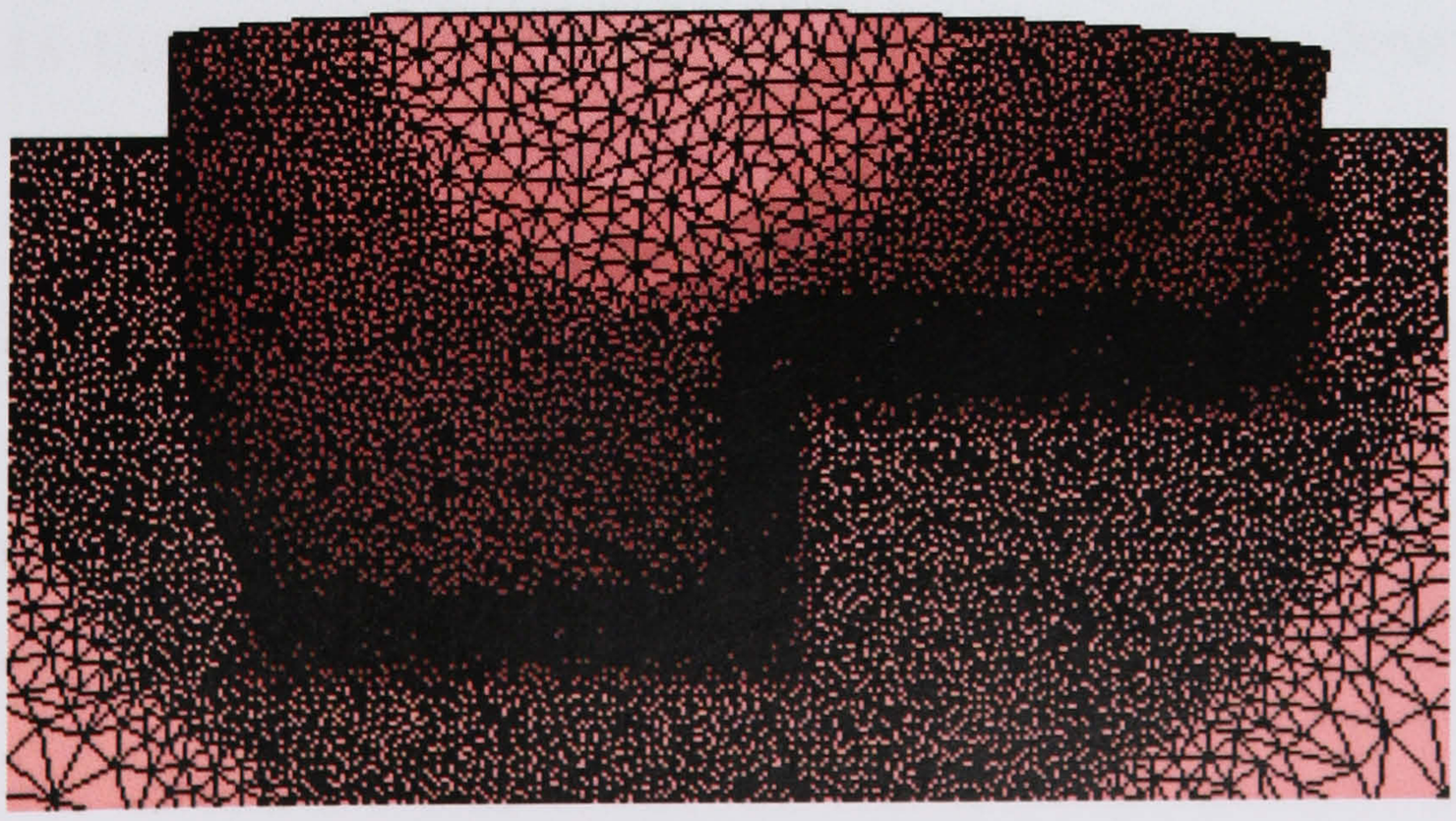

Figure 5.15 Mesh refinement for T-shaped extrusion

Figure 5.16 shows the distribution of (a) subgrain size, (b) nucleation density and (c) recrystallized volume fraction. The latter was compared in detail with the experimental results.

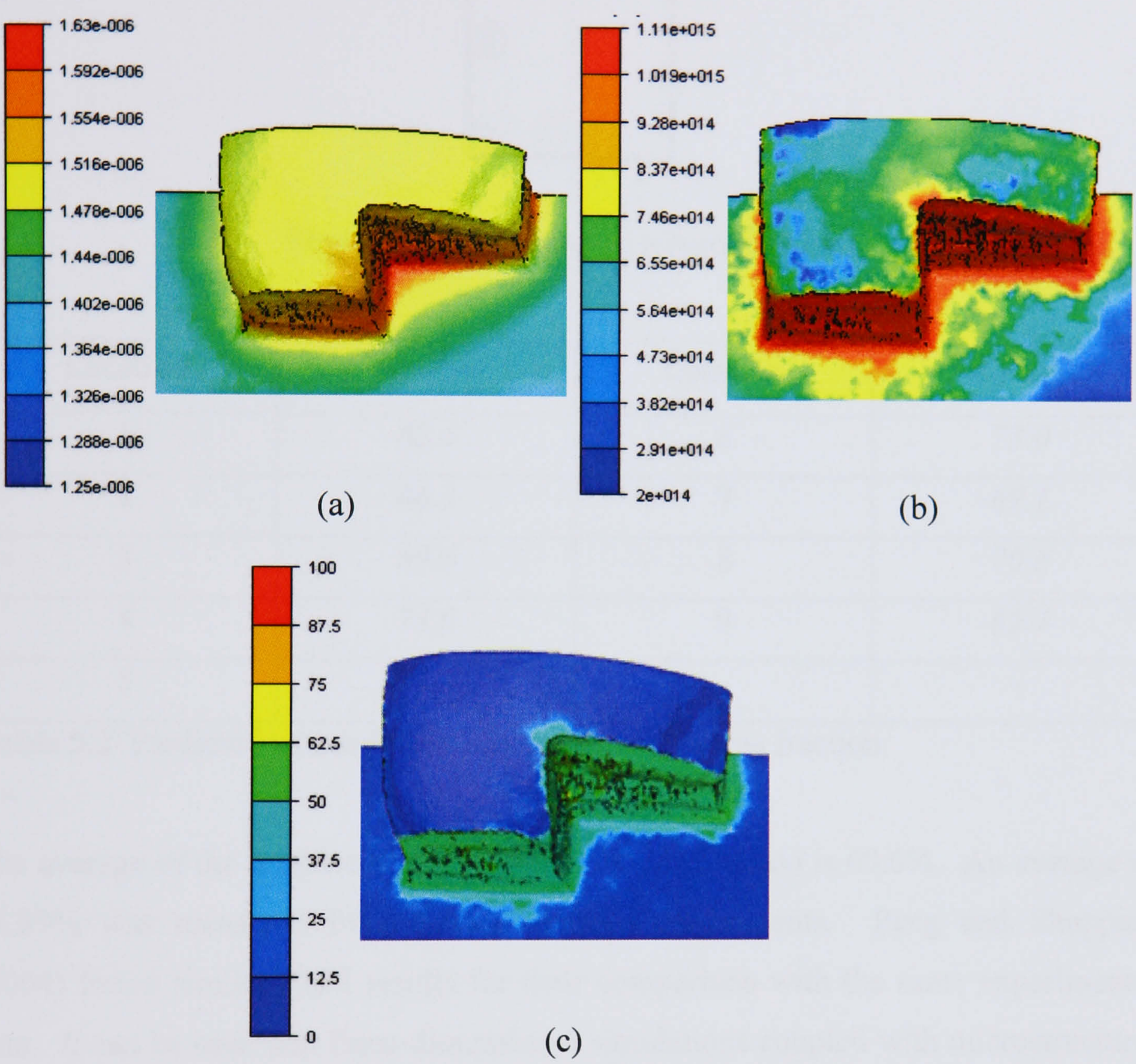

Figure 5.16 Distribution of (a) subgrain size (in *m*), (b) nucleation density (in m^{-3}) and (c) recrystallized volume fraction (in %)

In order to compare the recrystallized volume fractions, a cross-section was extracted from the 3D model (just after the die entrance) and the percentage of predicted recrystallized volume fraction was recorded in 9 locations. Figure 5.17 shows the 9 locations on the cross section and Table 5.2 list the values predicted for these locations.

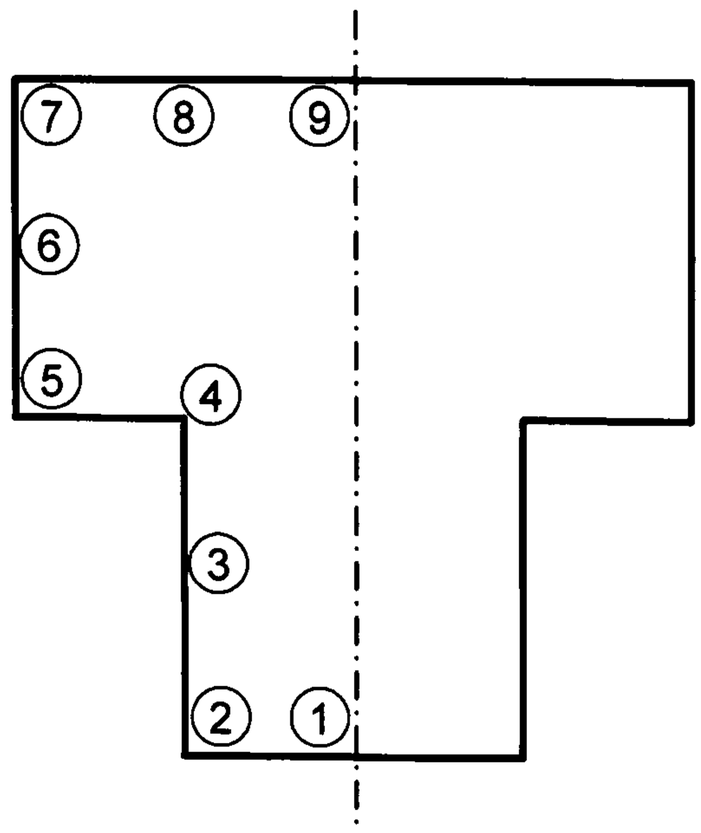

Figure 5.17 Location of recorded values

Location	X_V (%)	Location	X_V (%)
1	*62.4*	6	*73.0*
2	*66.3*	7	*69.1*
3	*69.6*	8	*70.8*
4	*73.6*	9	*65.4*
5	*71.2*	-	-

Table 5.2 Predicted values for the recrystallized volume fraction

The average of the predicted recrystallized volume fraction is 69.0%. An average of 74.89% was measured from Subramaniyan's experiments. Peng and Sheppard (2004) found similar FEM results for their comparison with the same experimental data. It can be seen that three-dimensional simulations coupled with microstructural models can reasonably predict the evolution of microstructure in shape extrusion.

5.4 Feeder plate

In conventional extrusion, a feeder plate is a solid plate positioned in front of the extrusion die in order to produce a shape larger than the billet size. The feeder plate needs to be thick enough to ensure that the material spreads evenly and smoothly without any abrupt changes in direction. A large thickness is also required to minimise the internal taper in order to reduce the reverse pressures which can separate the die from the feeder plate. Therefore, it is important to take into account the elements of feeder plates in the study of the Conform process. Using Forge 3 the

extrusion of a thin wide semi-closed section was simulated with both a feeder plate and a flat faced die. The results for the material flow, distribution of temperatures and subgrain sizes were compared quantitatively and qualitatively for both. Although these analyses were based on an industrial extrusion there were no experimental data recorded by the extruder.

5.4.1 Simulation set-up

The material simulated was an AA6063 and was defined with the Zener-Hollomon flow stress. The following assumptions and simplifications were made in order to reduce the computational time:

- the cross-section of the extrudate was simplified by removing some small features,
- the die land was considered constant at all the die faces,
- the billet was scaled down (in terms of length).

As demonstrated earlier, the scaling of aluminium extrusion is not suitable if accurate values are sought. The last simplification therefore would have affected the values of the results, however scaling was a valid process for the case of the feeder plate as the results were compared between two scaled analyses.

Due to the geometrical symmetry only half of the extrusion needed to be modelled. In this simulation, all tools were assumed rigid. Figure 5.18 shows the tooling set up (a) with the feeder plate and (b) without the feeder plate.

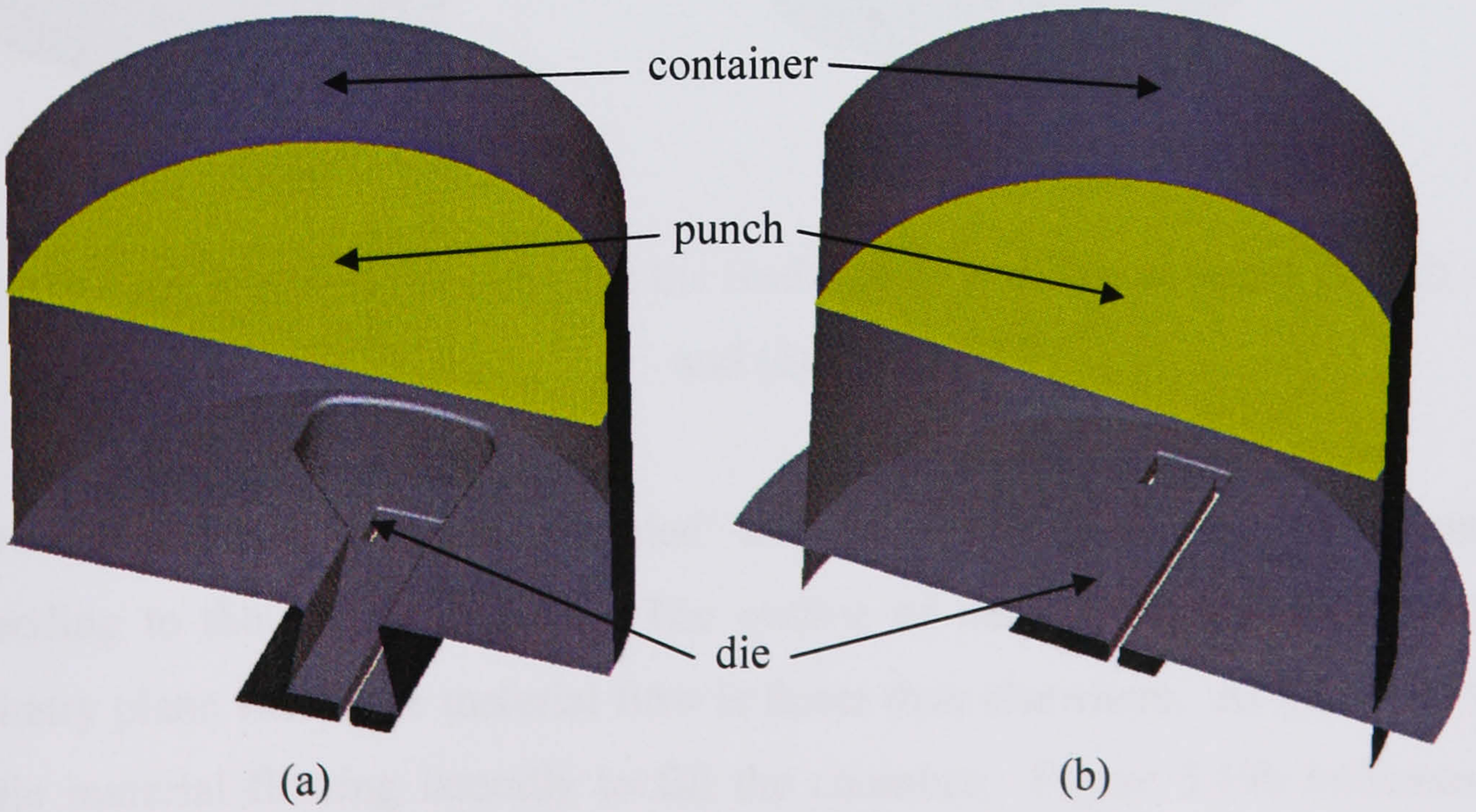

Figure 5.18 Tooling set up (a) with the feeder plate and (b) without the feeder plate

5.4.2 Results and discussion

Material flow

The simulated material flow patterns proceeding through the feeder plate are shown in Figure 5.19a to Figure 5.19d in the sequence of the extrusion process.

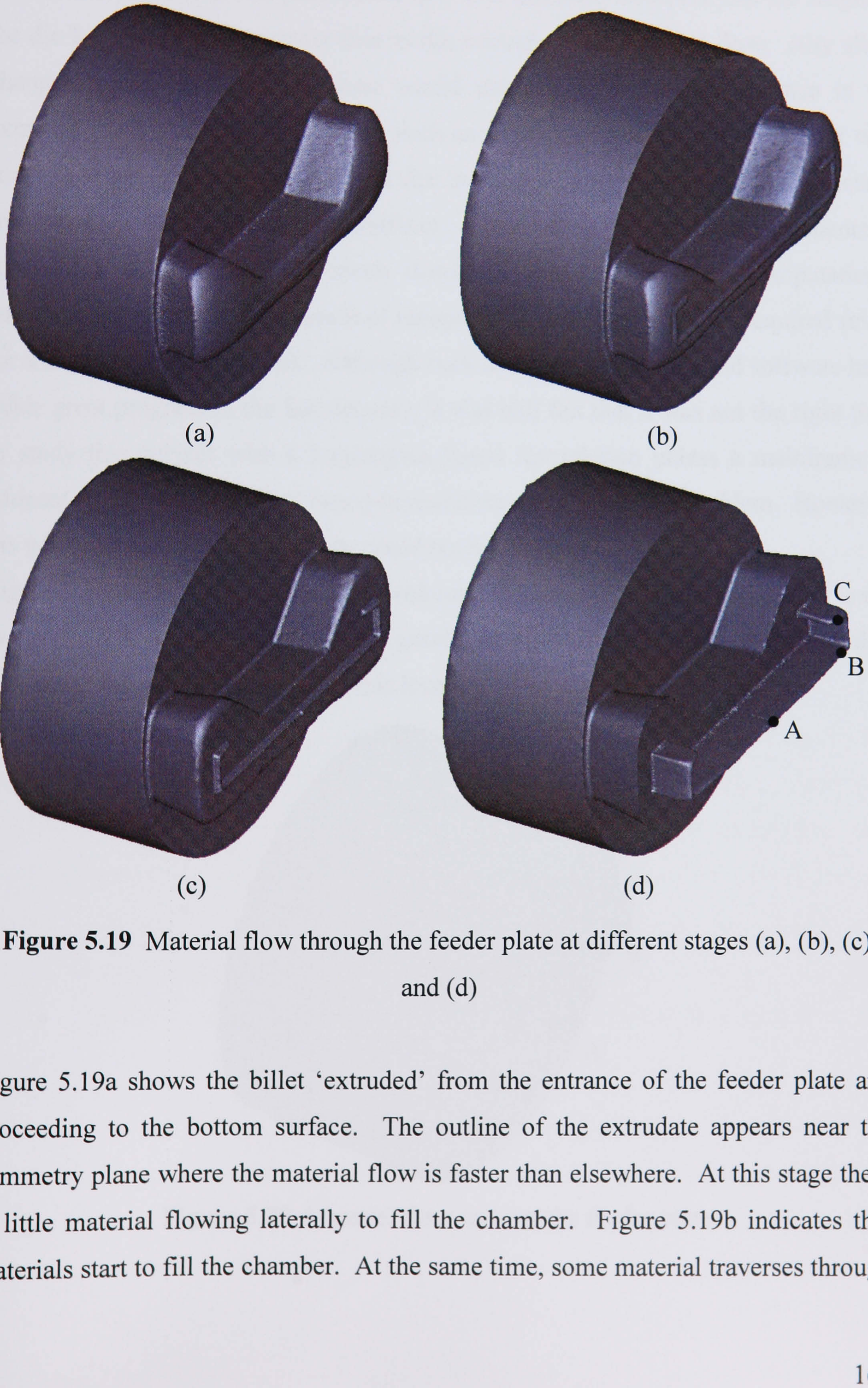

Figure 5.19 Material flow through the feeder plate at different stages (a), (b), (c) and (d)

Figure 5.19a shows the billet 'extruded' from the entrance of the feeder plate and proceeding to the bottom surface. The outline of the extrudate appears near the symmetry plane where the material flow is faster than elsewhere. At this stage there is little material flowing laterally to fill the chamber. Figure 5.19b indicates that materials start to fill the chamber. At the same time, some material traverses through

the die entrance to complete the final shape of the extrudate. In Figure 5.19c only a small volume inside the feeder plate has not been fully filled. In Figure 5.19d the feeder plate is completely filled and the extrudate is advancing in a uniform manner. The extrudate velocities have been recorded at points A, B and C (Figure 5.19d). These are listed in Table 5.3. It should be remembered that the same die land length is used for all the different parts of the die. It is generally accepted that the length of the die land plays an important role in the control of the material flow. Any slight changes in the length of die land would produce an obvious difference in the extruded product shape. Simulating such an important aspect would require a very small time step and very fine element size in order to generate the resultant effects of friction at the material/die-land interfaces. Considering the regular requirements of re-meshing to overcome the mesh distortion and to ensure the computational continuation, a significant amount of computation resource would be required (even for a simple shape extrusion). Although both computing hardware and software have made great progress in the last decades, it was still felt that it was not the right time to study this subject with a Lagrangian based formulation unless a mainframe is adopted. The use of Eulerian based formulation could solve this problem. However, the whole process of material flow could not be visualised.

Figure 5.20 shows the material flow without a feeder plate. The material flow is not uniform. The materials near the die gravity centre flow faster than anywhere else, producing the longest extrusion at this location.

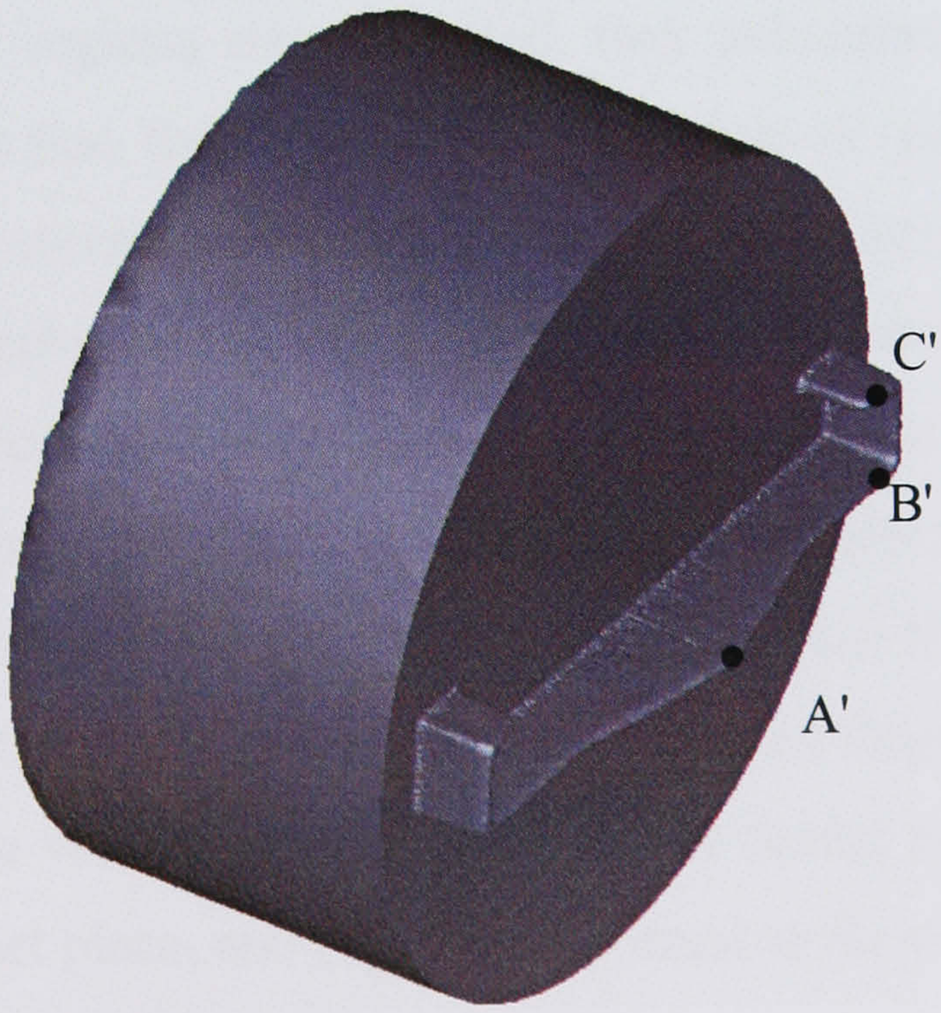

Figure 5.20 Material flow without the feeder plate

The extrudate velocities have been recorded at points A', B' and C' (Figure 5.20). These are shown in Table 5.3.

Point	Extrudate velocity with the feeder plate (mms^{-1})	Point	Extrudate velocity without the feeder plate (mms^{-1})
A	*92*	A'	*108*
B	*94*	B'	*85*
C	*87*	C'	*77*
Maximum velocity difference	*7 (7.4%)*	Maximum velocity difference	*31 (28.7%)*

Table 5.3 Extrudate velocities with and without the feeder plate

The maximum difference in velocities for the extrudate with a feeder plate is $7mms^{-1}$. This indicates that some areas of the extrudate are flowing at a rate which is 6.5% faster than at other areas. The difference in velocities for the extrudate without a feeder plate however, is $31mms^{-1}$. This indicates that the material at the centre of the extrude flows at a rate which is 28% faster than it does at the extremities. This effect is due to the fact that the friction on the container forces the aluminium on the outer region of the extrudate to flow at a slower rate to that at the centre. However, since the outer and central regions are connected, they subsequently interact with each other. This suggests that the centre of the extrudate is 'pulling' the extremities, hence causing tensile stresses in the outer regions. Similarly, the extremities have their own counter-effect on the centre of the extrudate by causing deceleration which creates compressive stresses in this region. Depending on the velocity gradients (i.e. the spatial distribution of the velocity) high compressive stresses could be generated which would lead to buckling. The results therefore show that the feeder plate can contribute to the reduction of flow imbalance in complex shapes.

Figure 5.21 shows the velocity distribution with the feeder plate on (a) the plane of symmetry and an offset place, and (b) a plane normal to the plane of symmetry. The dead metal zones are highlighted.

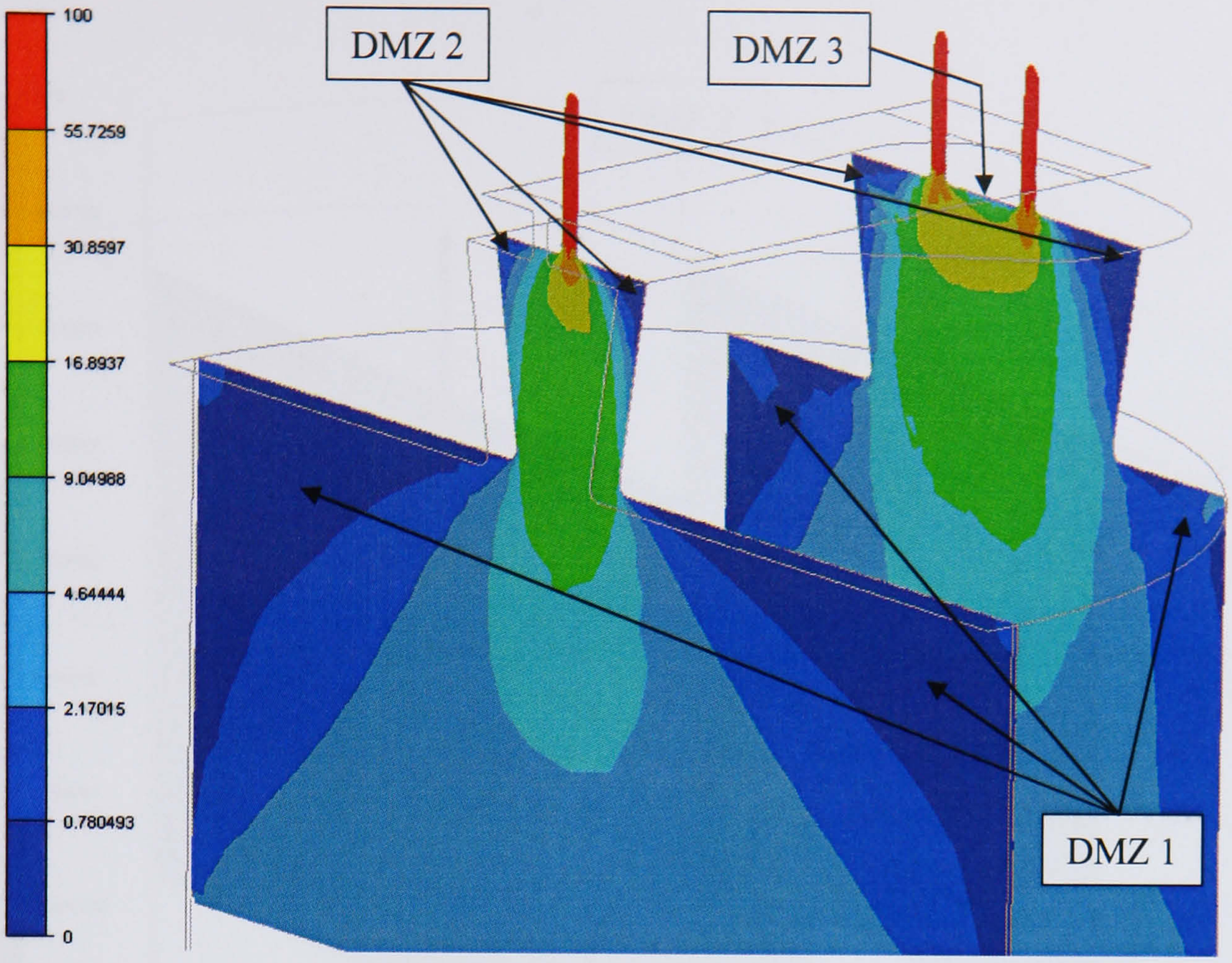

(a)

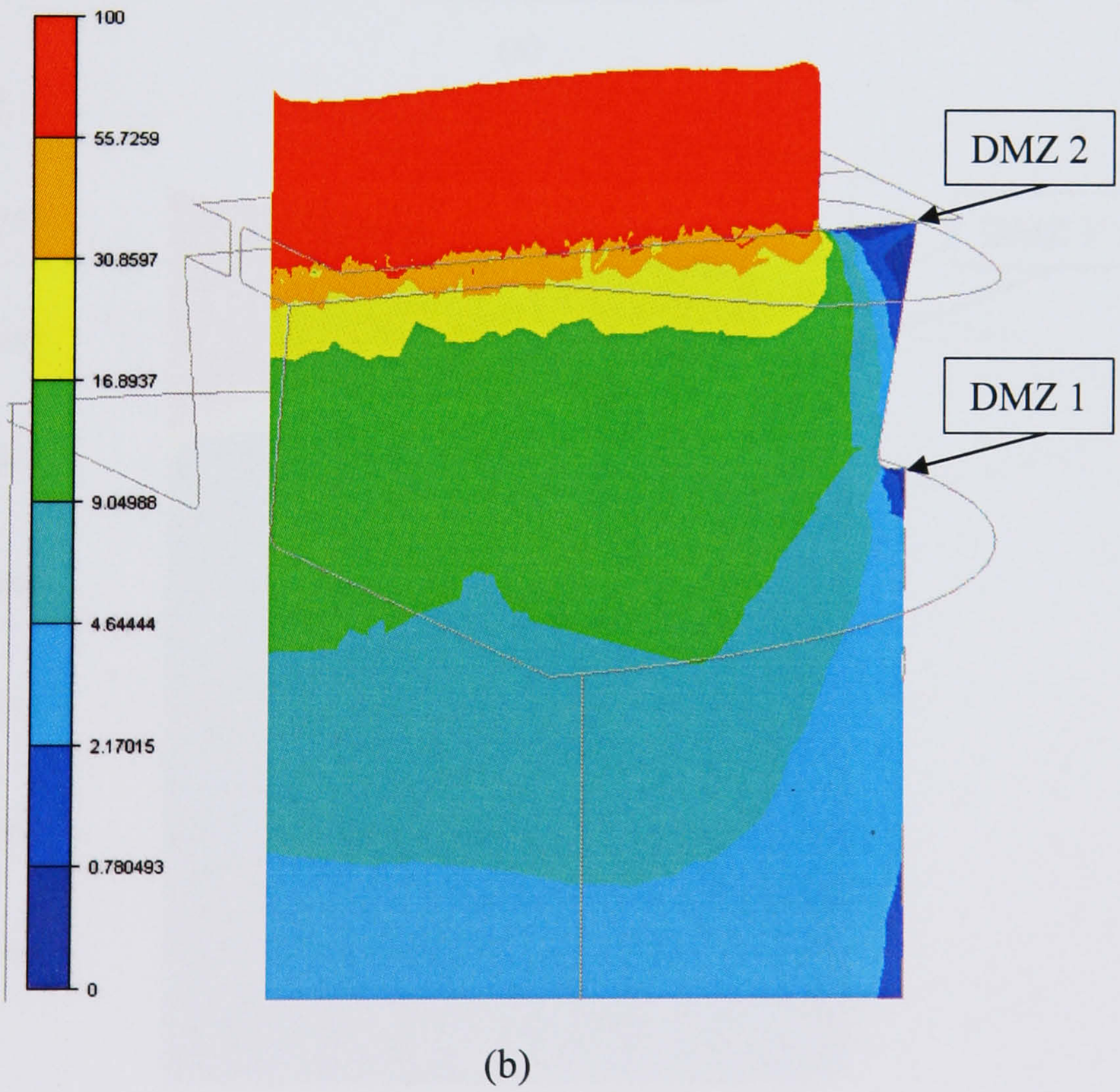

(b)

Figure 5.21 Velocity distribution ($mm.s^{-1}$) and DMZs with the feeder plate on (a) the plane of symmetry and an offset plane, and (b) a plane normal to the plane of symmetry

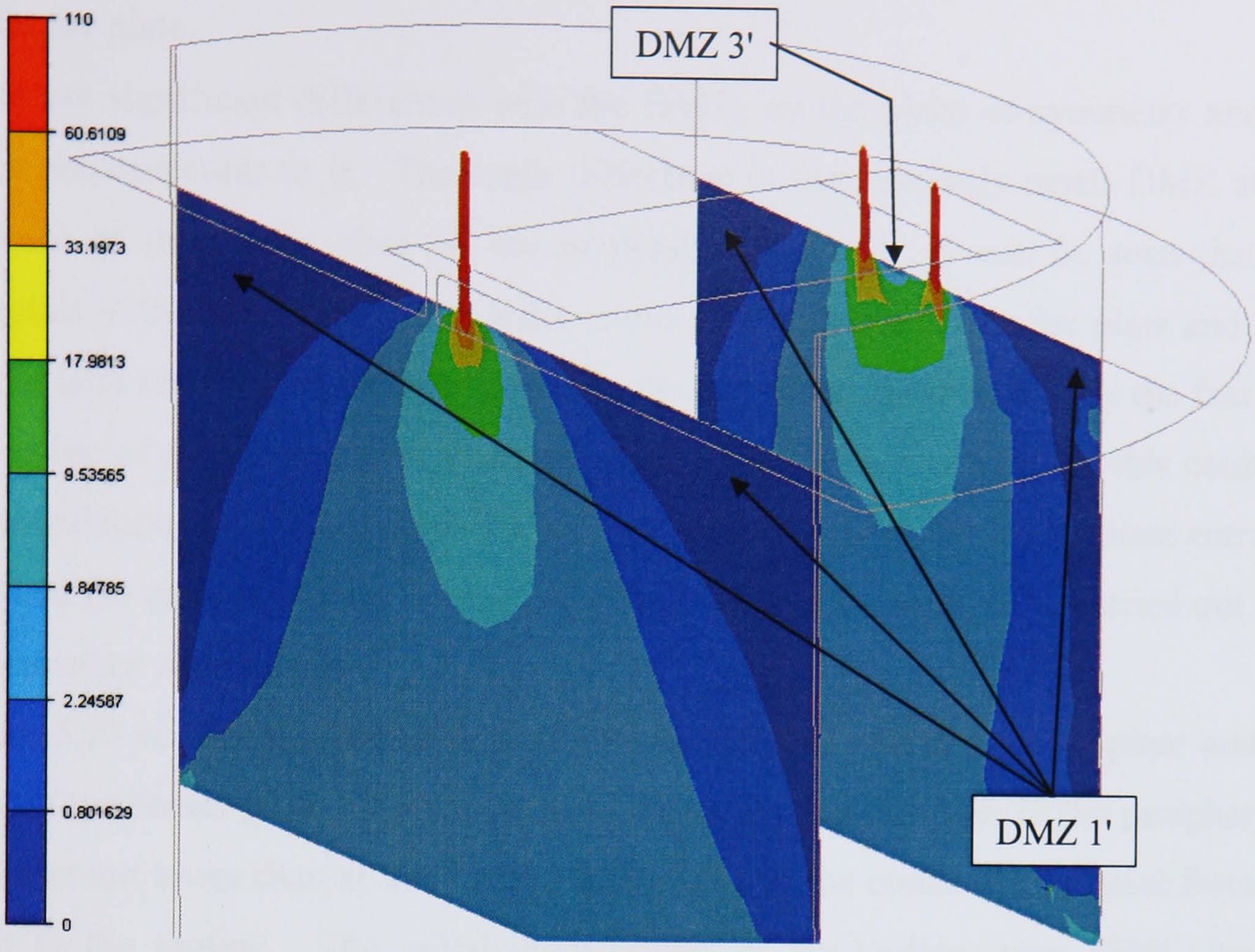

(a)

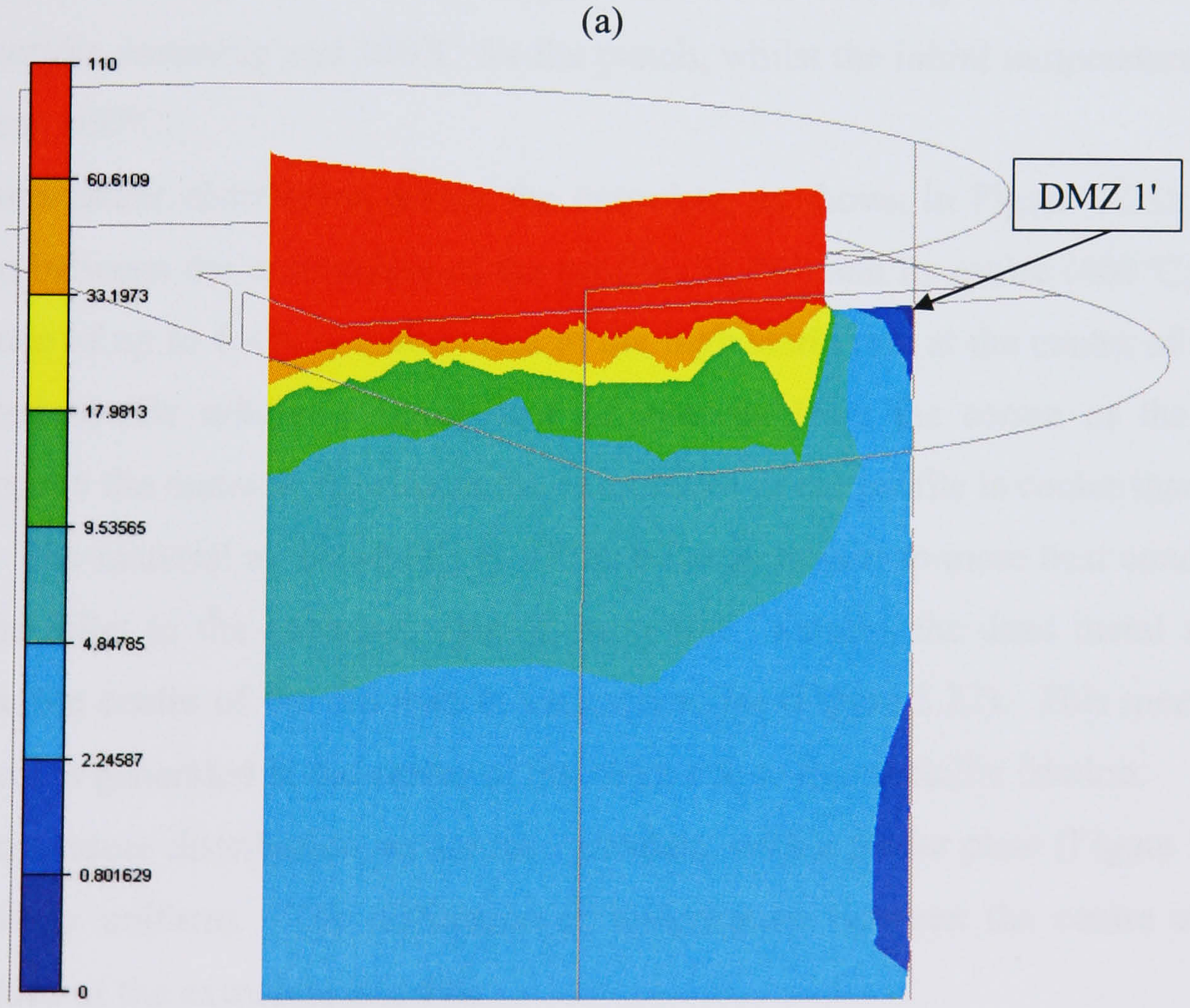

(b)

Figure 5.22 Velocity distribution ($mm.s^{-1}$) and DMZs without the feeder plate on (a) the plane of symmetry and an offset plane, and (b) a plane normal to the plane of symmetry

Figure 5.22 again shows the dead metal zones and the velocity distribution without the feeder plate.

There are significant differences with the DMZs on the plane of symmetry and the plane perpendicular to it. The main difference is the relatively small DMZ at the entrance of the feeder plate on the perpendicular plane. It can be seen that the materials at the periphery of the billet could flow through the feeder plate and then the die land resulting in surface defects in the extrudate. This highlights the fact that the design of a feeder plate is complex. One of the design criteria for this could be the calculation of a critical value for the ratio of the CCD of the feeder plate entrance hole and the container bore. Further work in this area still needs to be carried out.

Temperature distribution

Figure 5.23 shows the distribution of temperature, (a) with the feeder plate and (b) without the feeder plate. With both simulations, the temperatures at the periphery of the billet are lower than at the centre. This is due to the conduction of heat from the billet to the tooling. The initial temperatures of the tooling were 350°C for the container/die assembly and 300°C for the punch, whilst the initial temperature of the billet was 400°C.

The temperature distribution across the extrudate, as shown in Figure 5.23b, is not uniform between the extremities of the profile (382°C) and its centre (408°C). This difference of up to 6.4% is mainly due to the high strain rate at the centre of the die generated by the relatively rapid flow of material from the centre of the billet. Furthermore the material flowing at the extremities of the profile is cooler than at the centre. The material at the periphery of the billet is subject to more heat conduction from the billet to the container than at its centre. Finally, the dead metal zone is larger at the centre of the die than at the extremities (Figure 5.22). This means that more heat is generated at the centre of the billet due to intermetallic friction.

The temperature distribution across the extrudate, with a feeder plate (Figure 5.23a), is relatively uniform. The difference of temperature between the centre and the extremities of the extrudate is 2.4%.

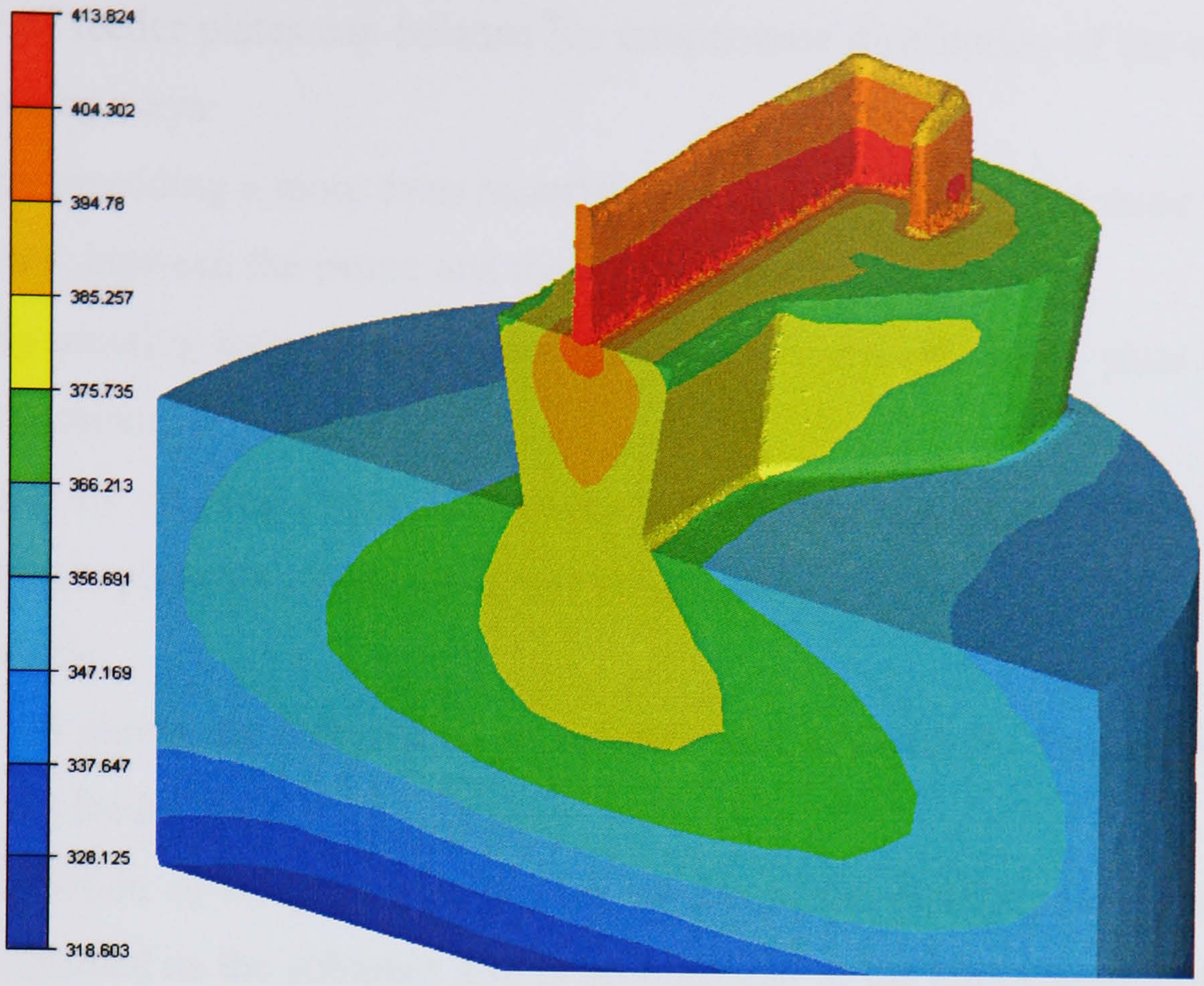

(a)

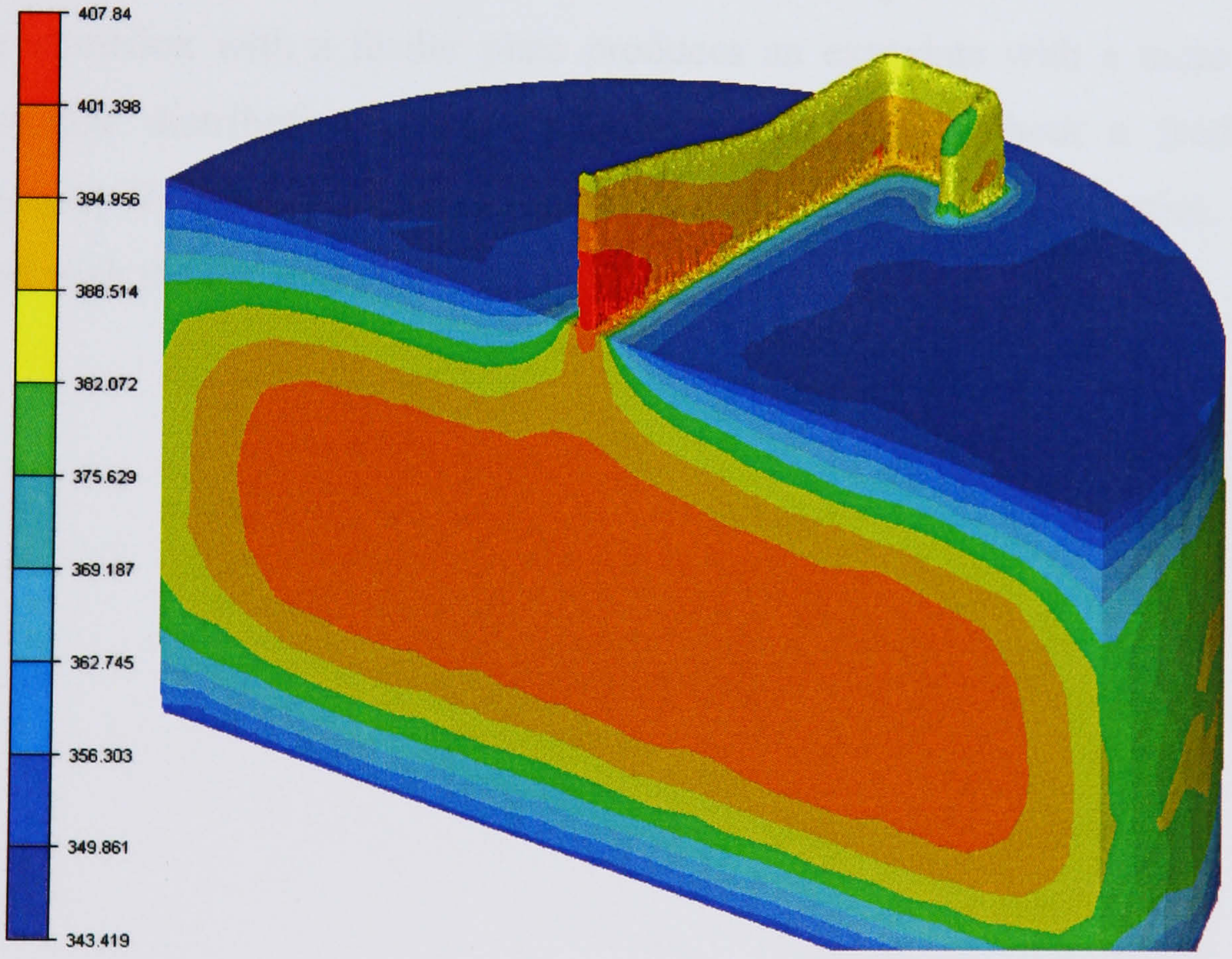

(b)

Figure 5.23 Distribution of temperature (degree C), (a) with the feeder plate and (b) without the feeder plate

The use of feeder plates can balance the temperature distribution of the extrudate in the following ways:

- by providing a more even material flow, and consequently a more even strain rate, between the centre and the extremity of the die,
- by creating more uniform heat conduction inside the feeder plate than in the container,
- and by creating fewer differences between the size of the DMZs inside the feeder plate than those inside the container.

subgrain size

Figure 5.24 shows the distribution of subgrain size, (a) with the feeder plate and (b) without the feeder plate.

The distribution of subgrain size is very similar to the distribution of temperature. This is expected as the subgrain size is proportional to the temperature compensated strain rate parameter Z (see equation (5.12)). Both Figures 5.24a and 5.24b show that the extrusion with a feeder plate produces an extrudate with a more uniform subgrain size distribution across its cross-section than without a feeder plate. Consequently the quality of the extrudate, in terms of material properties, could be enhanced with the use of a feeder plate.

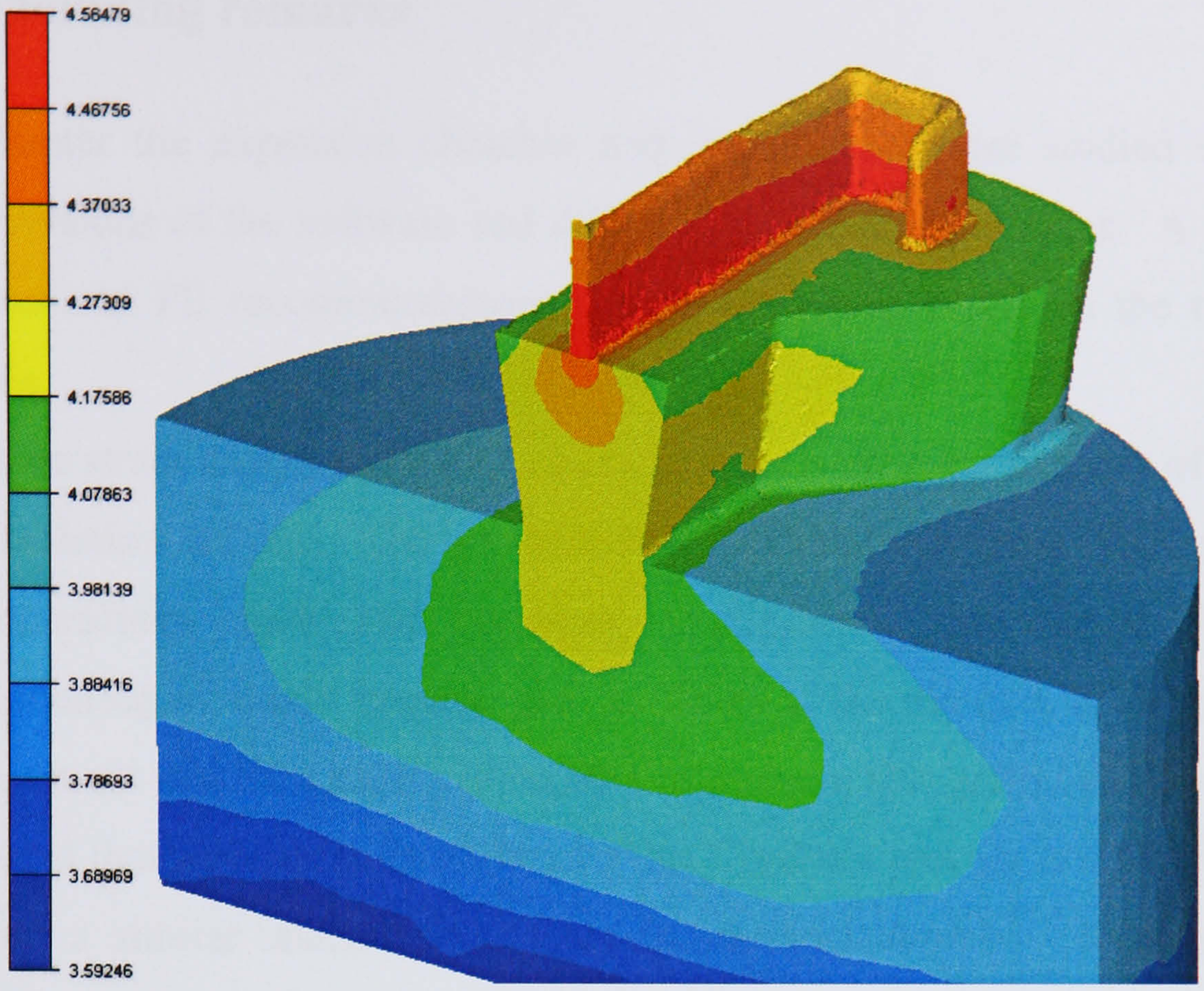

(a)

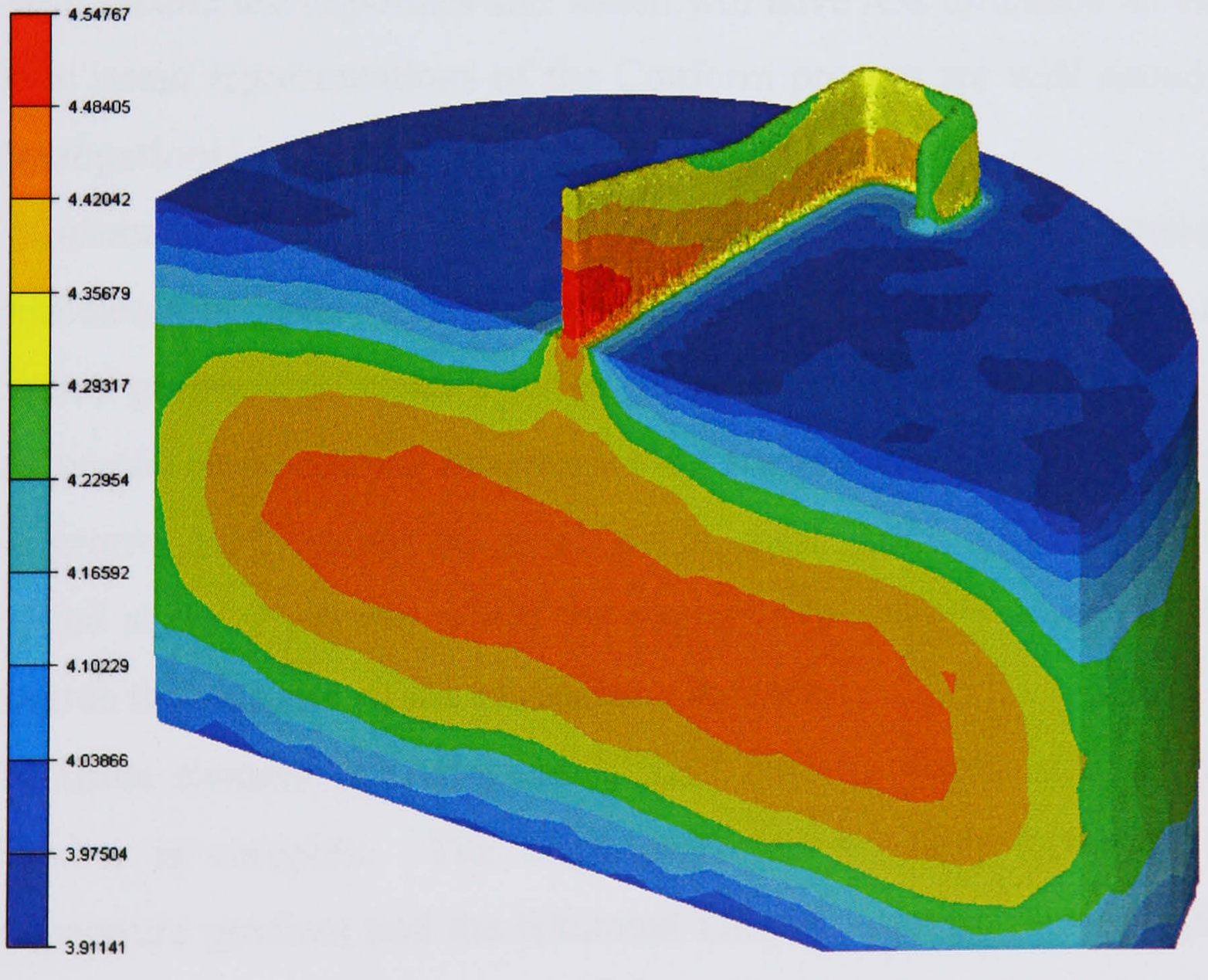

(b)

Figure 5.24 Distribution of subgrain size (μm) (a) with the feeder plate and (b) without the feeder plate

5.5 Concluding remarks

In this chapter the expansion chamber and feeder plate were studied using both different versions of the software and different hardware capabilities. A number of conclusions and FE recommendations can be suggested based on the results and discussions.

- Plane strain analysis of the Conform process is efficient in terms of speed and simulation set up. The pre-processing is relatively easy due to the two-dimensional mesh and boundary conditions. This allows for refined modelling of small features such as fillets at the die exit, gaps between the abutment and the groove, or surface refinement (for grain evolution). It was found that a plane strain analysis of the Conform process is eight times faster than a similar analysis in a three-dimensional domain. When planning a series of simulations, it is crucial to have some basic understanding about which factors are important and which will have less influence on the results. Plane strain representations of the Conform process are well suited for such investigations.
- Unfortunately, it would be wrong to assume that Conform extrusion can be simulated accurately with a plane strain analysis. To some extent a relatively squared groove can be modelled as plane strain due to its geometry, however this would be inaccurate in terms of the friction conditions. The friction on the groove wall cannot be modelled in plane strain. Similar reasoning is applied at the abutment, where the plane strain analogy is rapidly degrading towards the entrance of the expansion chamber.
- The finite element discretisation of the Conform process with an expansion chamber is complex. The large deformations, their locations, the high temperature gradient and the frictional interface require a careful judgement for the mesh refinement, especially within the three dimensional domain. The mesh needs to be refined at the entrance corners of the expansion chamber and in the areas adjacent to the entrance. The mesh at the die entrance should also be refined.
- The evident advantage of three-dimensional modelling of the Conform process is the possibility to simulate precisely the volume and shape of the

material together with the right boundary conditions. From this, 3D phenomenon, such as the material flow, temperature distribution and other variables, can be studied and analysed. The drawback with 3D analyses is the large number of elements required to reach useful results. The finite element equations are numerous in 3D and a mesh refinement from 2 to 1 can increase the analysis time by a factor of 4. Therefore, careful planning is required before complex 3D analyses are performed. Furthermore, the post processing of the results is not straightforward due to the numerous data available at each increment in each direction.

- Both the model proposed by Sellars and Zhu and the model created by Nes and co-workers are available for the prediction of static recrystallization. It is easier to perform numerical analyses using the model created by Nes *et al* due to the fact that the values of the parameters in their model can easily be found in the literature. Also, there are no such problems as non-convergence caused by the inappropriate input of some parameter values. However the model proposed by Sellars and Zhu presents more accurate predictions.
- The evolution of substructure and material properties during the hot extrusion of aluminium alloys can be represented accurately with the Forge 2 and Forge 3 FE codes. However, the use of several tuning parameters for each alloy remains impractical for industrial use.
- The die configuration has a significant influence on the microstructural behaviour and material flow. Based on the study of extruding a thin-walled product it was found that the use of a feeder plate can reduce the degree of non-uniformity in terms of shape and properties.

6 Tool optimisation

6.1 Introduction

For the reliable and economical production of aluminium extrusion an optimum tool life is essential. The main problem confronting Conform's tooling is the failure of the wheel due to high stress and fatigue. The replacement of the wheel requires the dismantlement of several parts including the main driving shaft. It is therefore in the interest of the extruder to predict the life of the wheel or to select the most suitable wheel for a given process. In the first part of this chapter the structural integrity of the wheel is studied using boundary conditions from an estimated linear static load. These results are then compared qualitatively with the stresses obtained from the plastic deformation of the feedstock.

Another very important tool in Conform extrusion, and in all extrusion processes, is the die. The die is the last tool in contact with the workpiece and therefore its design has a great influence on the surface quality of the extrudate. In the second part of this chapter FEM is coupled with the Taguchi method to predict the influence of die profile on the initiation of surface cracks and subgrain size.

6.2 Wheel optimisation

6.2.1 Stresses due to estimated linear static load

A comprehensive study was carried out to evaluate the effectiveness of pre-stressing on different Conform wheels. Different preloads were applied to the wheels via a hydraulic nut in order to reduce the tensile stresses in the wheel during extrusion. The study was commissioned by Holton Machinery Ltd at the early stage of this research and covered six types of wheels. Three wheel diameters were studied, 300mm, 400mm and 500mm, for both aluminium and copper extrusions. The

preload varied from 4.0MN on the 300mm wheel to 12.5MN on the 500mm wheel. Due to the uncertainty of the loading inside the groove, each wheel was loaded with three different extrusion pressures: 400Nmm^{-2}, 600Nmm^{-2} and 800Nmm^{-2}. Table 6.1 lists the different parameters of the study.

Analysis Nb	Wheel Type (mm)	Material to extrude	Preload (MN)	Extrusion pressure (Nmm^{-2})
1	*300*	*aluminium*	*4.0*	-
2	*300*	*aluminium*	*4.0*	*400*
3	*300*	*aluminium*	*4.0*	*600*
4	*300*	*aluminium*	*4.0*	*800*
5	*300*	*copper*	*4.0*	-
6	*300*	*copper*	*4.0*	*400*
7	*300*	*copper*	*4.0*	*600*
8	*300*	*copper*	*4.0*	*800*
9	*400*	*aluminium*	*8.2*	-
10	*400*	*aluminium*	*8.2*	*400*
11	*400*	*aluminium*	*8.2*	*600*
12	*400*	*aluminium*	*8.2*	*800*
13	*400*	*copper*	*8.2*	-
14	*400*	*copper*	*8.2*	*400*
15	*400*	*copper*	*8.2*	*600*
16	*400*	*copper*	*8.2*	*800*
17	*500*	*aluminium*	*12.5*	-
18	*500*	*aluminium*	*12.5*	*400*
19	*500*	*aluminium*	*12.5*	*600*
20	*500*	*aluminium*	*12.5*	*800*
21	*500*	*copper*	*12.5*	-
22	*500*	*copper*	*12.5*	*400*
23	*500*	*copper*	*12.5*	*600*
24	*500*	*copper*	*12.5*	*800*

Table 6.1 List of parameters for pre-stressing study

Analyses 9, 10, 11 and 12, which correspond to the 500mm wheel, have been selected to provide a more in depth understanding of wheel behaviour. The wheel was analysed using commercial FEA software (I-DEAS Master Series) which had been distributed by SDRC.

Model discretisation

The geometry of the wheel, its groove and adjacent parts were provided by Holton Machinery. The feedstock was 25mm in diameter. An extreme temperature of 550°C was assumed for the wheel. The material for the wheel was H13 which at 550°C has a modulus of elasticity of 155000Nmm^{-2}, a Poisson's ratio of 0.29, and a yield strength of 900Nmm^{-2}.

A parameterised solid model was meshed semi-automatically using 3D brick elements in order to obtain a mapped mesh. This was an efficient way to generate the mesh for each different wheel and groove combination. The FE model comprised 2282 elements and 11098 nodes. Planes of symmetry were used where appropriate. Figure 6.1 shows the mesh of the models.

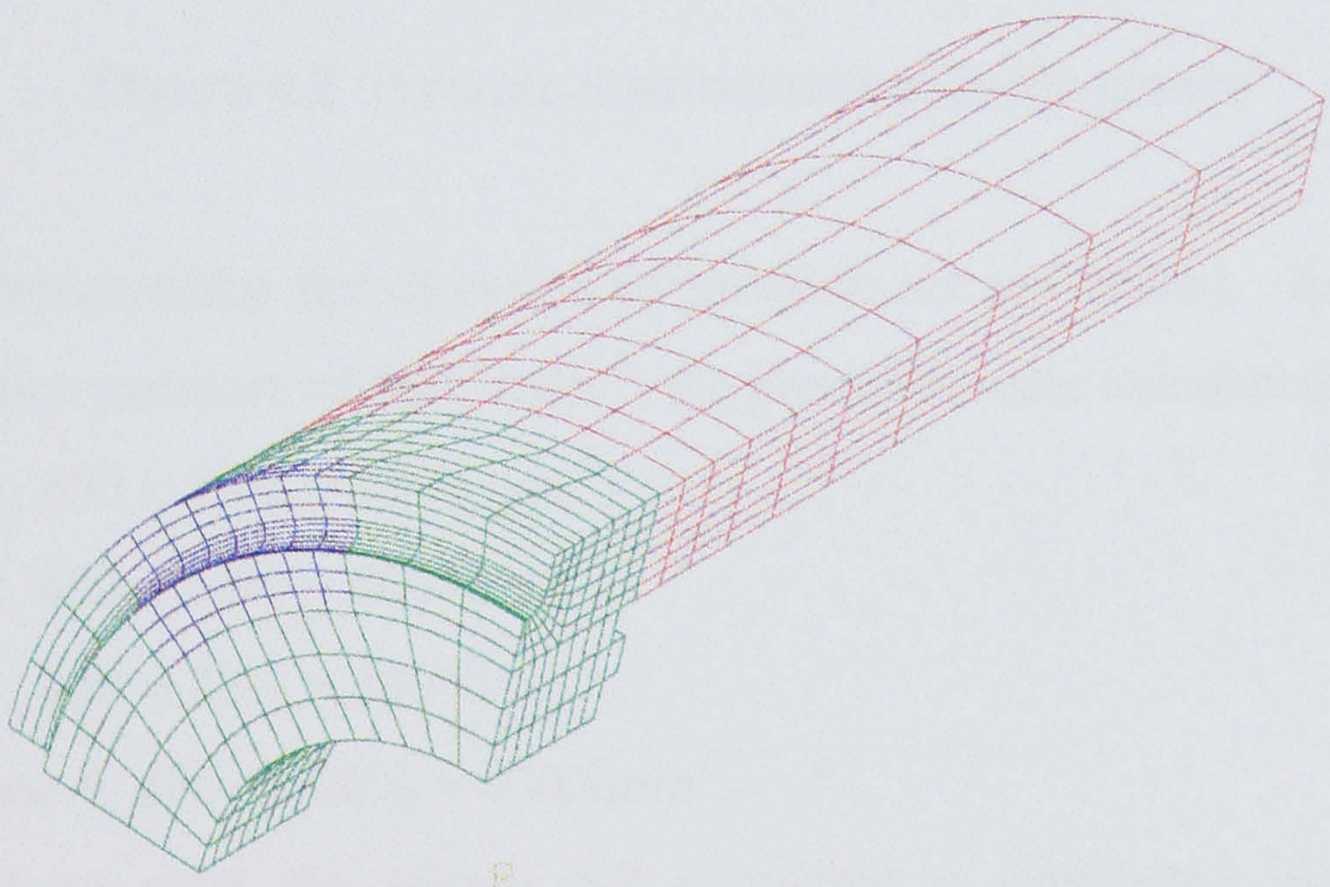

Figure 6.1 Finite element models of the wheel and shaft assembly

The green and blue elements represent the wheel and the red elements the tubular insert which applied the preload. The blue elements also indicate the area of the wheel where the pressure due to extrusion was applied. The length of this area is equal to the length of the upset zone observed in similar industrial trials. In this case the length was approximately 160mm.

Boundary conditions

A preload of 12.5MN was applied at the end of the tubular insert. Three different groove pressures were applied: 400, 600 and 800Nmm^{-2}. Each groove pressure was distributed in four different zones. Each zone was 40mm long increasing from 25% in the first zone to 100% by the fourth. Figure 6.2 shows the four zones of distributed pressure in the groove.

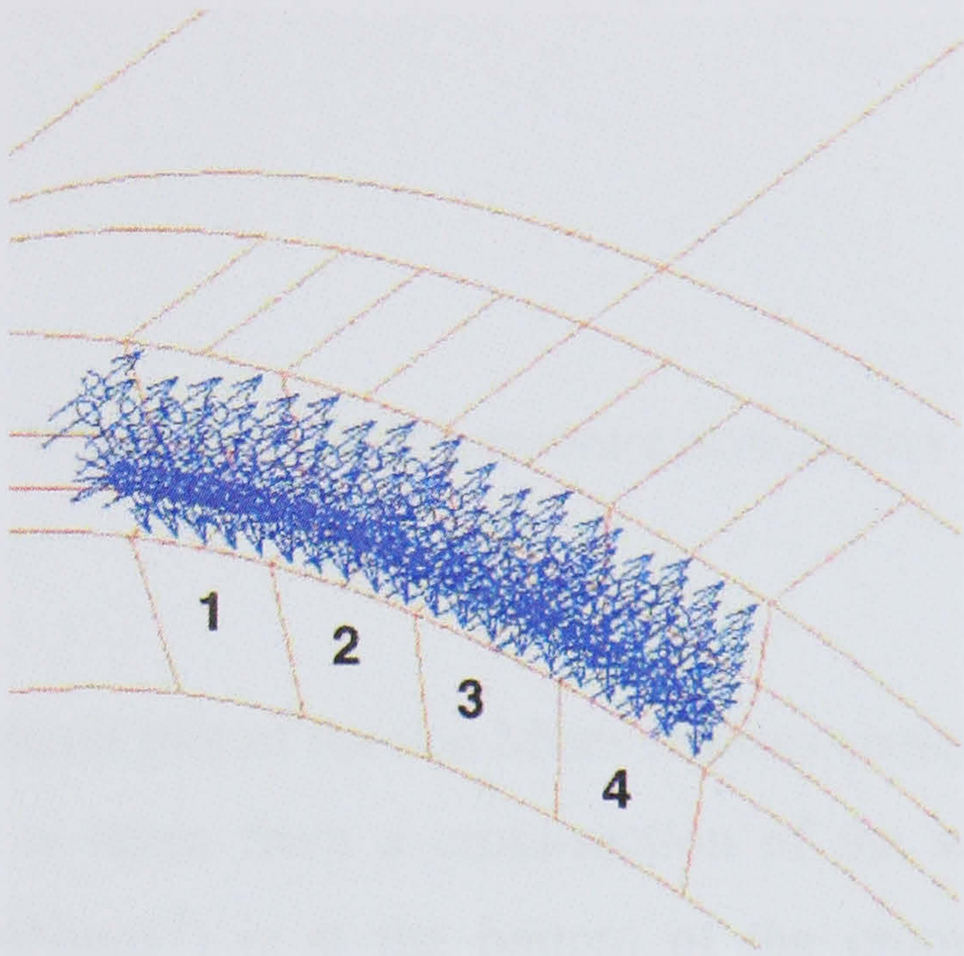

Figure 6.2 Pressure distribution inside the groove

The arrows, representing the direction of pressure are not scaled. As an example, with an extrusion pressure of 400 Nmm^{-2}, the pressures were calculated as follows:

- zone 1, 400 x 25% = 100Nmm^{-2},
- zone 2, 400 x 50% = 200Nmm^{-2},
- zone 3, 400 x 75% = 300Nmm^{-2},
- and zone 4, 400 x 100% = 400Nmm^{-2}.

The methodology used for Figure 6.2 simulated a distributed pressure with a maximum value near the abutment and a minimum value at the other end of the upset zone (i.e. 160mm from the abutment). In addition to the pressure inside the groove a radial pressure was applied to a 20mm wide band on each side of the groove. This radial pressure varied from the groove pressure at the edge of the groove to zero after 20mm. This represents the sealing band pressure created by the flash. Figure 6.3 shows the radial pressure and the four zones. The direction X shows the variation of the pressure from a maximum value at X = 0mm to zero at X = 20mm. The arrows are also not scaled in this figure.

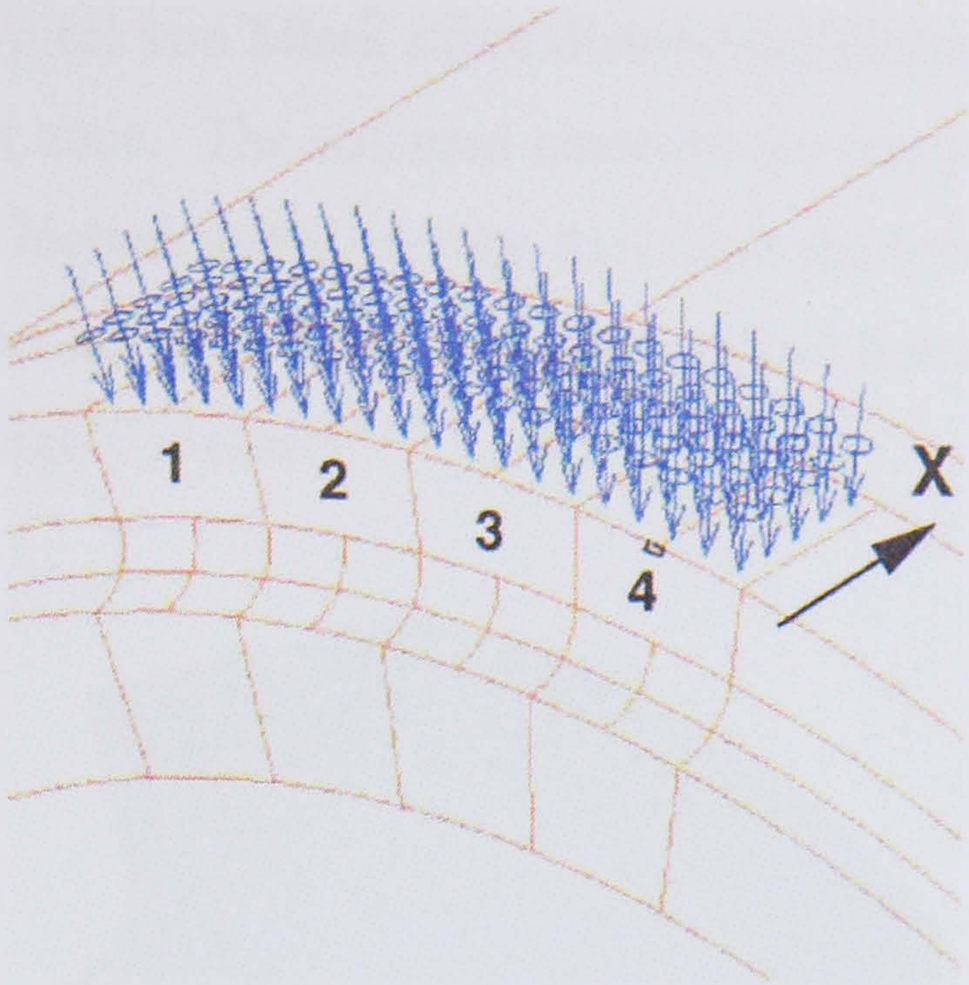

Figure 6.3 Radial pressure distribution

Results

Figure 6.4 shows a contour plot of the von Mises stresses caused only by the 12.5MN preload. The figure is taken from a cross-section of the wheel assembly. The maximum stress (514Nmm^{-2}) is at the bottom of the groove and is due to the compression load generated by the preload.

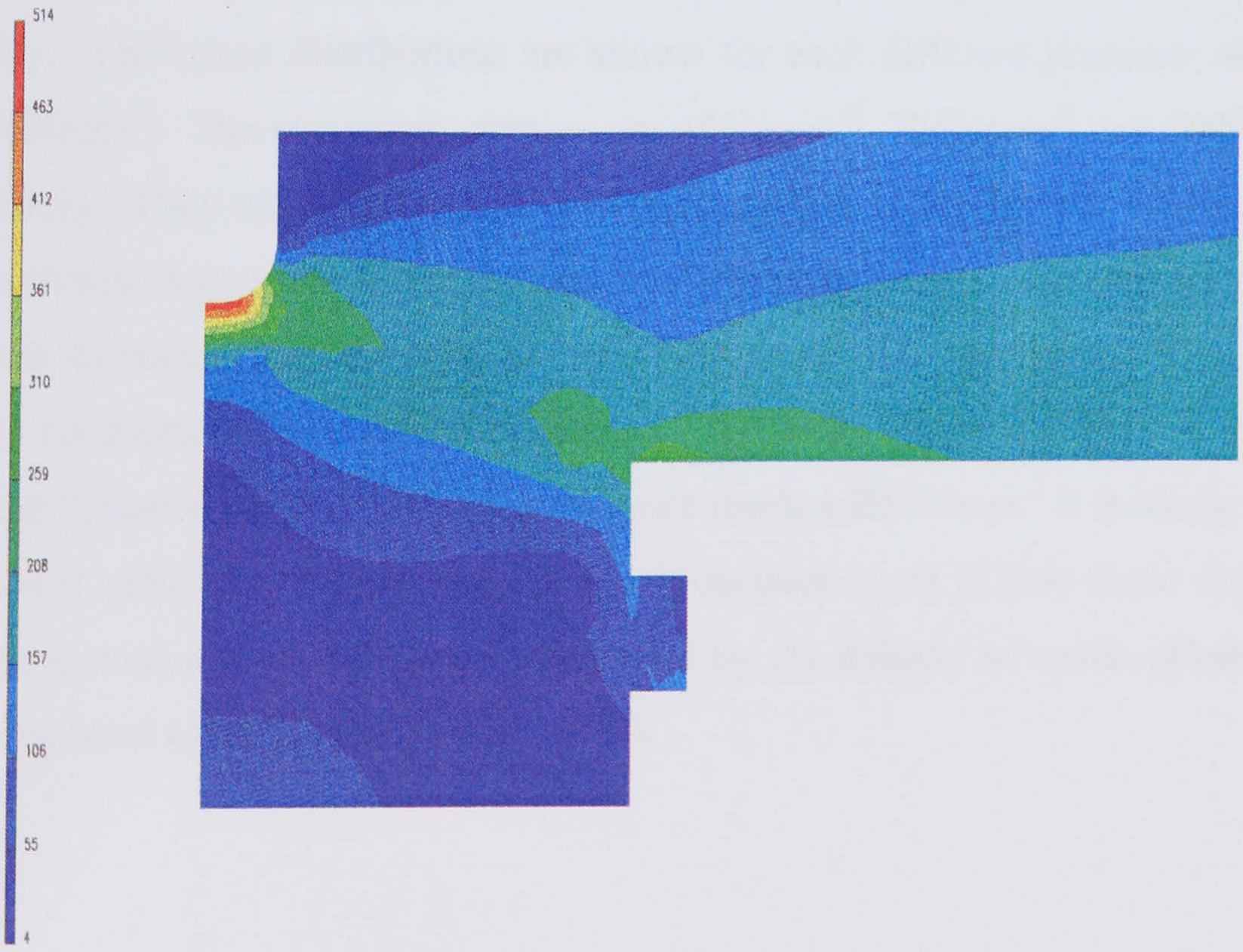

Figure 6.4 Stress distribution with 12.5MN preload only

Figure 6.5 shows a typical von Mises stress distribution in the area of the groove in contact with the upset zone. The coloured contours are not scaled however the red colour represents the highest stress and the dark blue the lowest. As expected the highest stresses are located at the base of the groove and it is noticeable that a large area of the groove is highly stressed.

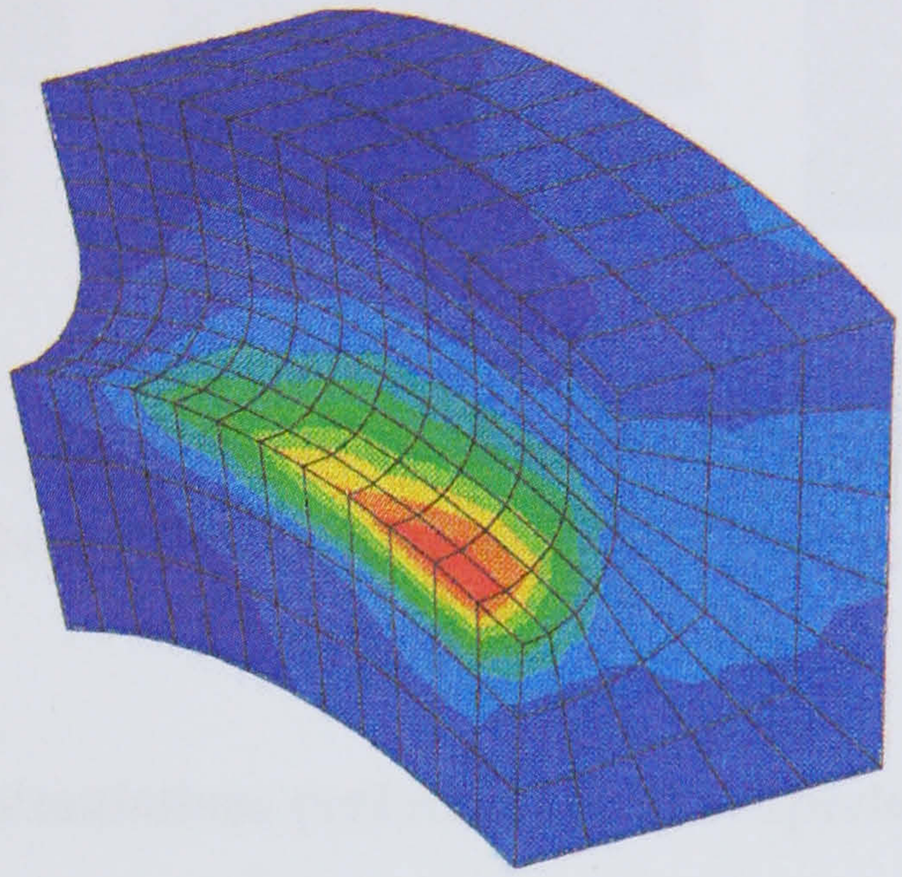

Figure 6.5 General stress distribution inside the groove

Figure 6.6 shows the maximum von Mises stresses in a plane across the wheel assembly. The stress distributions are shown for each different pressure: 400, 600 and 800Nmm^{-2}. The maximum stresses are 481Nmm^{-2}, 725Nmm^{-2} and 1099Nmm^{-2} respectively. They are all located at the bottom corner of the groove. This suggests that the extrusion pressure inside the groove is the main cause of the high stresses. In effect the extrusion pressure tries to 'split' the wheel into two parts. The preload partially counteracts this extrusion pressure. The yield strength of H13 at 550°C is 900 Nmm^{-2}, therefore if the extrusion pressure reaches 800 Nmm^{-2} it is likely that the groove will yield and consequently fail. Groenbaek *et al* (1999) show that crack initiation in tool steel is essentially controlled by the amount of cyclic plastic strain and by the level of compressive mean strain.

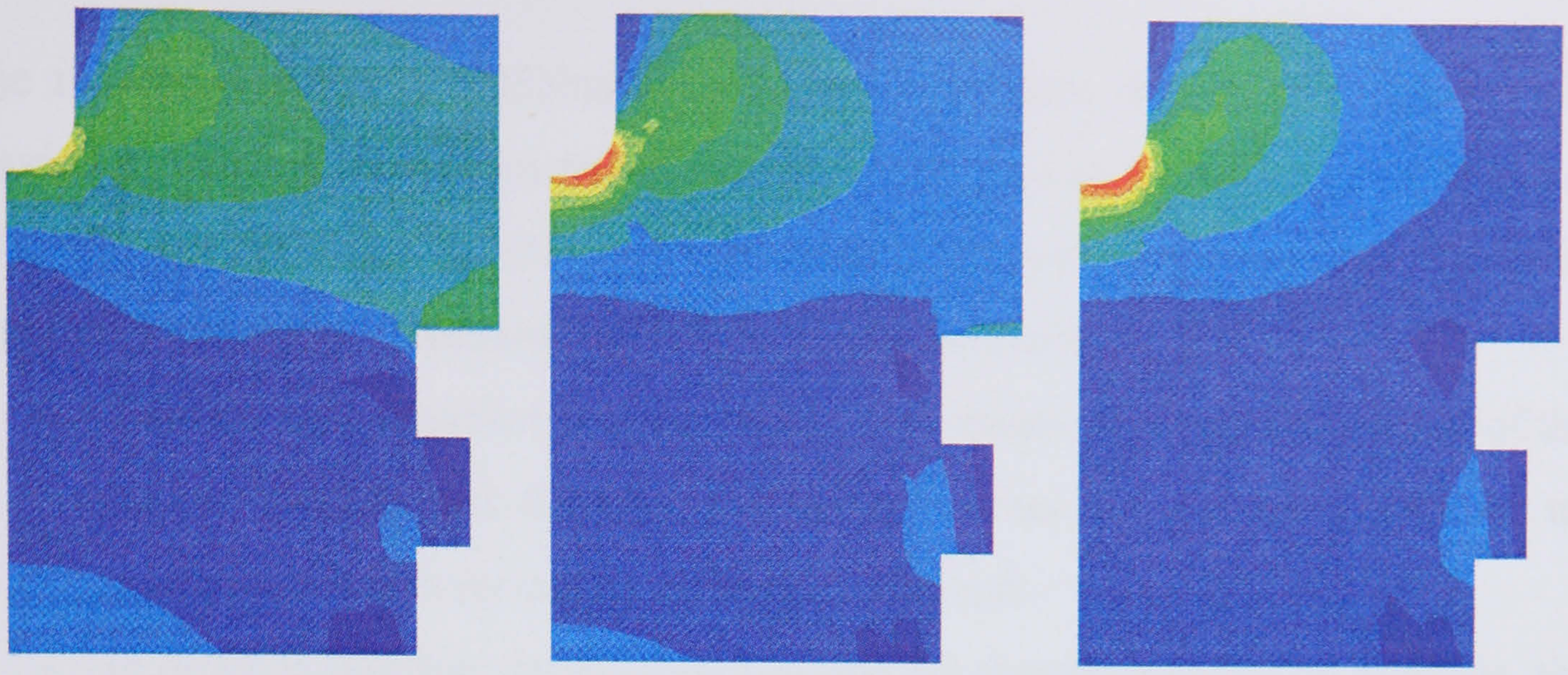

(a) (b) (c)

Figure 6.6 Stress distribution with 12.5MN preload and (a) 400Nmm^{-2}, (b) 600Nmm^{-2} and (c) 800Nmm^{-2} extrusion pressures

6.2.2 Stresses in the simulations performed on the experimental runs

Stresses on the surfaces of the tools were calculated with the 3D thermo-mechanical simulation used in section 4.6.3 (the simulation of Conform experiment). At each increment the pressures on the surface mesh of the feedstock were interpolated to the surface mesh of the tools. This gives an indication of the value of the stress and its distribution on the surface of the tools. Figure 6.7 shows this stress distribution (von Mises stress) inside the ram (near the abutment area) for the simulation with flash at steady state.

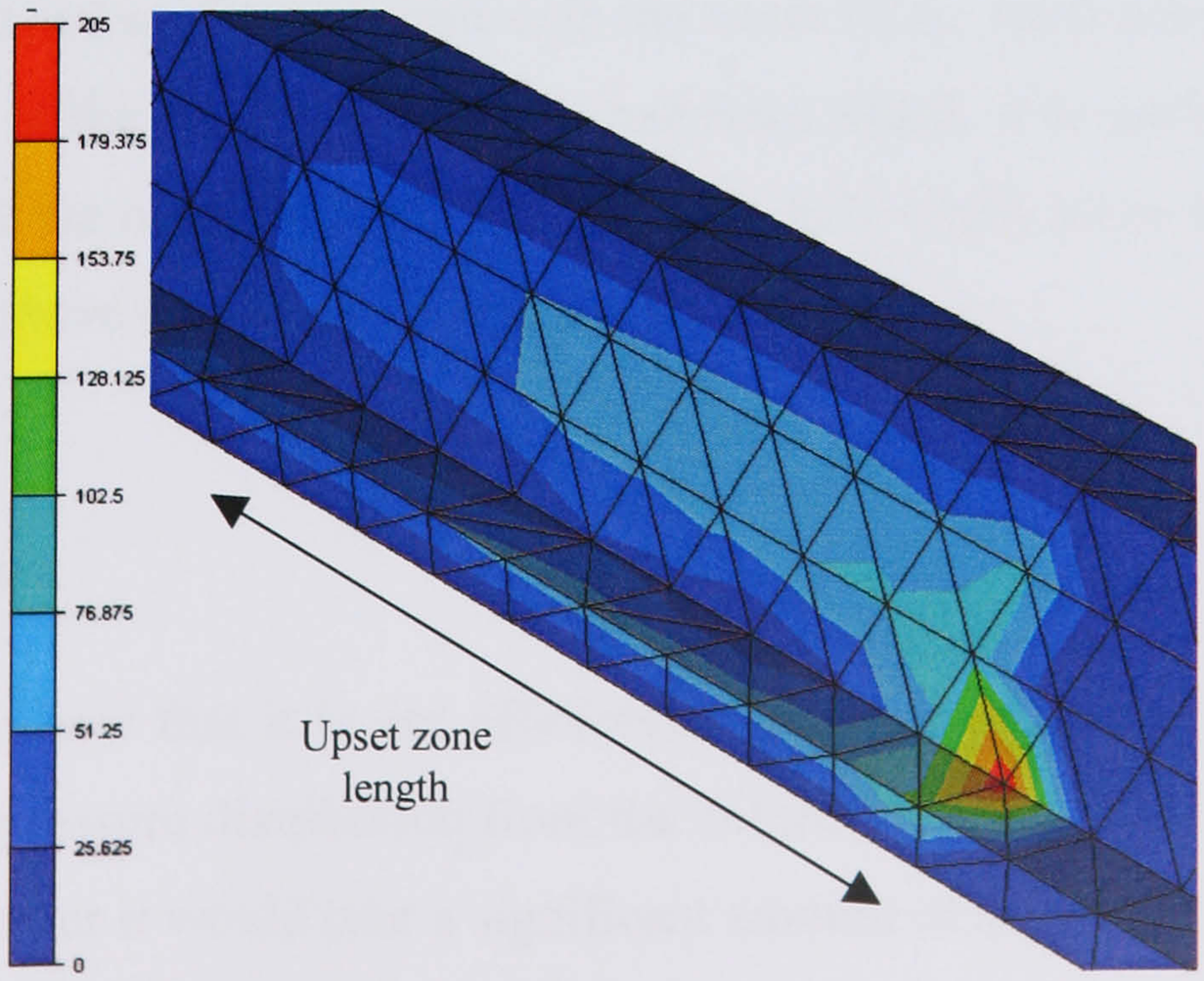

Figure 6.7 Stress distribution in the ram at steady state (Nmm^{-2})

The maximum stress of 205Nmm^{-2} is concentrated near the abutment area. The maximum value is lower than the estimated values used in the previous section (i.e. 400, 600 and 800Nmm^{-2}). However the value of the stress concentration shown in Figure 6.7 should be considered with these practical reasons:

- The ram was modelled as a rigid tool. This means that only the surface of the tool is meshed and therefore no internal stress can be calculated and no modulus of elasticity can be applied to the mesh.
- In order to increase the efficiency of the 3D thermo-mechanical analysis, the mesh used for the ram (and the rest of the tooling) is relatively coarse. Consequently some inaccuracies are generated during the interpolation of stresses from the deformed feedstock (fine mesh) to the surface of the ram (coarse mesh). In fact the ratio between the coarse mesh ($\approx$ 10mm) and the fine mesh ($\approx$ 0.4mm) can be as great as 25:1.
- The groove in the ram has a rectangular cross section (25mm x 22mm) and is without fillets, whilst the groove in an industrial wheel has 10mm fillets at the bottom.

The stress distributions between the static FEA (Figure 6.5) and the thermo-mechanical analysis (Figure 6.7) show similarities. In both simulations the maximum stresses are located near the abutment and gradually decrease toward the end of the upset zone. If a preload had been applied to the thermo-mechanical analysis then it is probable that the stress distribution in the side walls of the groove would have been reduced as occurred with the static FEA. Furthermore, if a preload and some fillets at the base of the groove had been added, it is likely that the stress concentrations at the corners (as shown in Figure 6.7) would move to the middle of the base of the groove (as shown in Figure 6.5).

6.2.3 Discussion

The simulations show that it is not efficient to study the structural integrity of the wheel using the pressure distribution from the deformed feedstock. With the current computational power it would take a significant amount of time to accurately analyse both the feedstock behaviour and the state of stress in the wheel. An efficient way

would be to firstly analyse the deformation of the feedstock, as described in section 4.6, in order to find the maximum pressure in the areas adjacent to the abutment. This pressure could then be transferred to a refined finite element model of the wheel using the four zones of loading as described in section 6.2.1 of this chapter. A simple linear static analysis would provide an accurate distribution of the stresses together with the position of the stress concentrations.

In terms of geometrical optimisation, the increase in fillet radii at the bottom of the groove would significantly reduce the stress concentration. However, this would also reduce those surface areas in the groove which generate the grip between the feedstock and the wheel. Consequently the friction interfaces necessary to drive the feedstock towards the abutment are reduced. Two ways in which these contact surfaces could be increased are as follows:

- The coining roll could be moved further away from the abutment, which would therefore increase the grip length and increase temperature at the abutment.
- A different cross section of the feedstock could be used. For example an oval shape could still be accommodated in the groove and be coined without excessive strain. This would provide more material in contact with the flat faces of the groove. However the fabrication of an oval cross-section could be difficult to cast or to roll.

The stresses acting on the wheel are both tensile and compressive in a repetitive manner. At each rotation of the wheel, just after the abutment, every point at the bottom of the groove experiences a rapid change from tensile to compressive stresses. Furthermore, the wheel is subject to thermal stresses and thermal shock. The main characteristics of H13 tool steel include good resistance to thermal shock and thermal fatigue, good high-temperature strength, good toughness and ductility in all directions and good machinability. Therefore H13 is probably the most suitable material for the design and manufacture of a Conform wheel.

A reliable estimation of the wheel life would require more than just an accurate estimation of the stress-strain distribution. It is essential to evaluate a suitable fatigue model which would accurately represent the initiation of cracks in the wheel. Such a study would require comparisons between different models of fatigue prediction and industrial data. For example Falk *et al* (1998) demonstrated that the 'local energy' approach shows satisfactory results in predicting the tool life of a cold

forging process. This approach takes account of the multi-axial stress conditions which could be suitable for the study of the Conform wheel.

6.3 Die optimisation

Dies must be optimised to produce good shapes, good surface finish, the required structure and a straight profile. In chapter four the straightness and accuracy of the profile was simulated by the use of a ghost die. In chapter five the micro-structure of the extrudate was predicted with FEM. In this section the finite element method is firstly applied to predict the phenomena of surface cracks. These results are then used to evaluate the optimum die profile and to study the influence of the forming parameters both on the subgrain size and the occurrence of surface cracks. The Taguchi method is adopted for the study of the forming parameters. These studies were conducted in conjunction with Xianjian Duan (Duan *et al* 2004b) and the author recognises the significant contribution made by his co-worker.

6.3.1 Prediction of cracks in extrusion

Two types of surface cracks, speed cracks and surface tearing, are often seen in the extrusion of two series of hard aluminium alloys: 2XXX and 7XXX. Speed cracking is caused by the high tensile stresses generated by the intensive friction between the extrudate and the die. Surface tearing occurs when the surface temperature exceeds the temperature of the lowest melting phase. In industrial practice, although various methods have been proposed to reduce the second phase, the elimination of this phase is impossible. Furthermore the distribution of the second phase is non-uniform and discontinuous in nature. Hence, the finite element modelling based on continuum mechanics can not cope with this particular problem. Therefore, surface tearing is not considered in this study.

Void nucleation, growth and coalescence are well accepted as being one of the principal mechanisms of ductile fracture. The fracture toughness of metals depends on the size and space of voids and recrystallized grains nucleating around the second phase particles. Therefore a critical way of controlling ductile fractures is to delay the void nucleation at the particle-matrix interfaces. Several fracture criteria, which

are composed of a form of integration with a combination of stress and/or strain relations, have been proposed to predict the initiation of ductile fracture when the integration reaches a critical value. These criteria can be divided into three categories: void growth model such as the Rice and Tracey criterion (Rice and Tracey 1969); the models based on porous plasticity such as the Gurson-Tvergaard criterion (Tvergaard 1981) and the phenomenological models which are based on experimental observations such as the Cockcroft and Latham criterion (Cockcroft and Latham 1968).

Clift *et al* (1990), Ko *et al* (1996) and Domanti *et al* (2002) have indicated that the Cockcroft and Latham criterion is the best amongst the various existing criteria for the prediction of fracture initiation during extrusion. The normalised form of the Cockcroft and Latham criterion is written as follows:

$$\int_0^{\bar{\varepsilon}_f} \frac{\sigma_1}{\bar{\sigma}} d\bar{\varepsilon} = CL \tag{6.1}$$

where σ_1 is the maximum principal tensile stress, $\bar{\sigma}$ is the equivalent stress, $\bar{\varepsilon}$ is the equivalent strain, $\bar{\varepsilon}_f$ is the equivalent strain to fracture and CL is the critical damage value.

When using the above criteria, the most important task is to ascertain the critical damage value CL or the critical effective plastic strain, $\bar{\varepsilon}_f^p$. For homogeneous materials, this critical value can be considered as a material constant. Ko *et al* (1996) reported that the value obtained from compression testing and tensile testing is different. This difference in values can be attributed to the different deformation history, different stress state at fracture locations and the fracture mode. The differences between surface cracks in hot direct extrusion and cracks occurring in both compression and tensile testing, makes the determination of the critical damage value even more complicated. In compression testing, fractures appear on the free surface at much smaller nominal strains than those in extrusion (equivalent strains are usually greater than 3 on the contact surface). Therefore, the effect of friction on fracture initiation and propagation can be ignored. In tensile testing, fracture does not usually initiate at the surface as it does in hot extrusion and compression testing, and the stress and strain states at the crack initiation site are different. Furthermore,

fracture initiates at much smaller nominal strains than those observed during extrusion.

In this section, aluminium alloy 2014 was studied. The experimental data was taken from the work of Vierod (1983). All billets were scalped to a 73.5mm diameter and extruded from a 75mm diameter container. The billet length was 95mm. The flat faced dies had a die land length of 5mm. The ram speed was 2.9mm/s and the temperatures of the billet, container and die were 475^0C, 425^0C and 375^0C respectively. The simulation used axisymmetric elements.

Figure 6.8 shows the different computed stress components in the extrudate cross section at 1mm before the die exit.

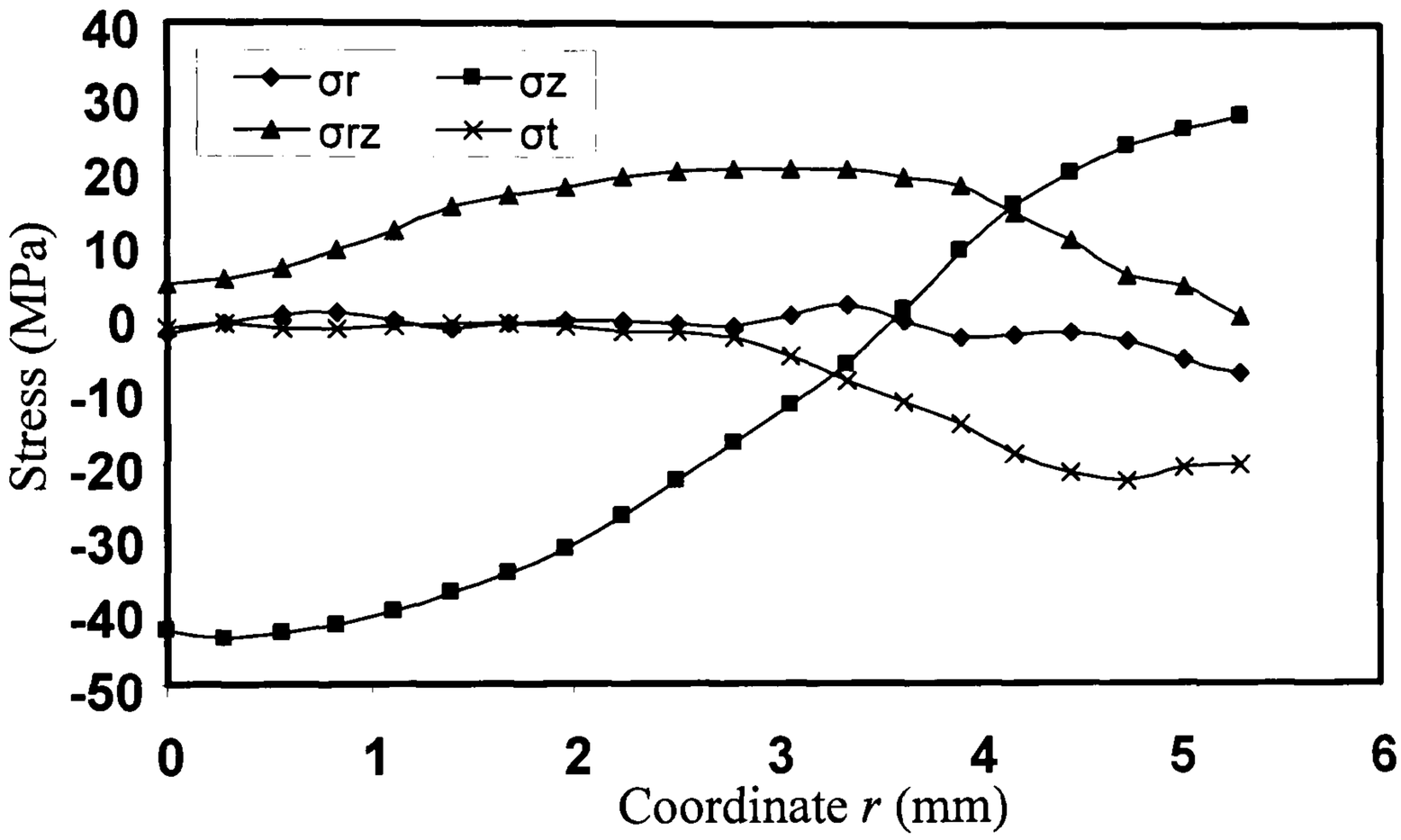

Figure 6.8 Distribution of stress components in the extrudate cross-section

The stress components are defined as follows:

- σ_t is the hoop stress,
- σ_Z is the longitudinal stress (in line with the extrudate) and can be assumed to be the maximum principal stress,
- σ_r is the radial stress and is considered as the minimum principal stress,
- and σ_{rz} .is the shear stress.

The stress σ_Z is negative (i.e. compressive) for $r \leq 3.4mm$, which corresponds approximately to two thirds of the extrudate cross section, and is tensile at the surface. This suggests that cracks will never occur at the centre (three-dimensional

compressive stress state) and would possibly appear at the surface. The longitudinal tensile stress is the major factor causing surface cracks.

The process of crack evolution can be visualised by the use of element deletion techniques. It should be noted that the term 'crack' here is different from its meaning in fracture mechanics which implies a sharp-tip. Since the Cockcroft and Latham criterion was proposed for the prediction of crack initiation, the process of crack growth can not be accurately predicted by the use of this criterion. Also, the surface cracks observed in the hot extrusion of AA2014 are usually caused by the distribution, size and morphology of the second phase particles. Without considering these metallurgical factors, the calculated crack propagation by the use of the Cockcroft and Latham criterion can only be represented as an approximation.

Deleting elements requires the determination of the critical damage value CL. To accurately determine this value, the calculated shape and depth of crack should correspond well with the experimental measurements. An inverse analysis method was used to determine the critical fracture value. FE analyses were iteratively run until the computed location, shape and depth of the cracks satisfactorily matched experimental observations. Figure 6.9a shows an axisymmetric view of the extrudate surface together with the axis of symmetry. Zones 1 to 5 show the different locations where cracks have occurred. The direction of extrusion is indicated. Figure 6.9b, a magnification of zone 2, shows the cracks in detail together with the mesh at the surface of the extrudate. The mesh at the surface is very fine and the length of the elements can be as small as 5μm. The computed surface cracks shown in Figure 6.9 were obtained by using a Cockcroft and Latham criterion equal to 0.235. It can be seen that the surface cracks occur periodically and extend backwards into the extrudate. The direction of the cracks is opposite to the extrusion direction, but follows the same direction as the frictional tensile stresses. It can be concluded that these stresses are the cause of the cracks.

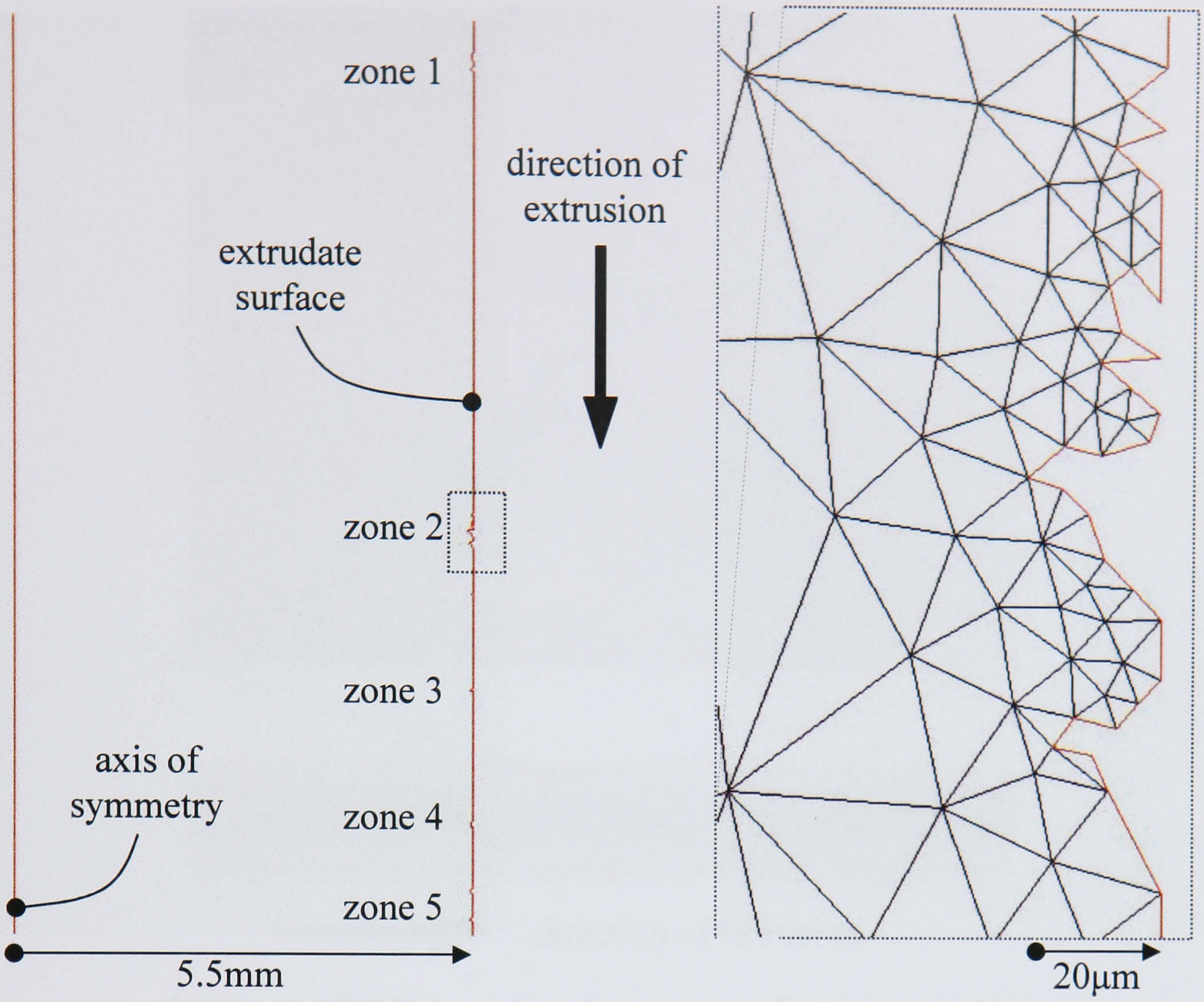

Figure 6.9 (a) Locations of surface crack and (b) crack details

This agrees well with the experimental observations from Veirod (1983) which are shown in Figure 6.10. In this figure the maximum crack length is of the same order of magnitude (35μm) as the one shown in Figure 6.9 (from the inverse analysis).

The results from the simulations agree well with experimental results. The experimental results show both the frequency of the cracks occurring along the surface of the extrudate and that the direction of the cracks is opposite to the direction of extrusion. Therefore, FEM with a *CL* value of 0.235 gives a good prediction for crack formation. However it should be emphasised again that the results in Figure 6.9 should only be treated as a qualitative prediction.

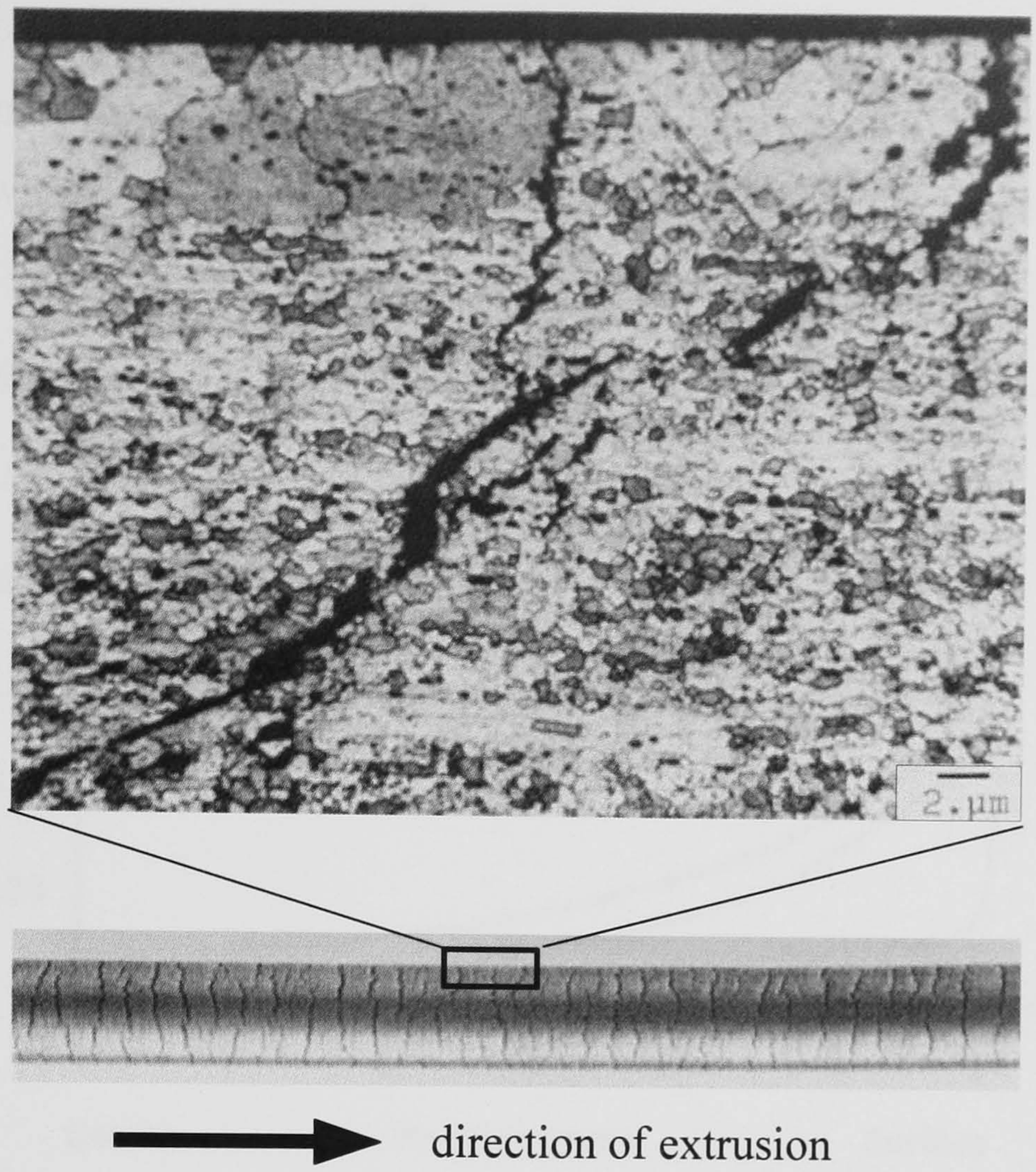

Figure 6.10 Measured surface crack (after Vierod 1983)

6.3.2 Optimum die profile

Four kinds of die configurations, as shown in Figure 6.11, were studied. A friction factor of 0.6 was applied to all the surfaces of the die profiles. A die length of 5mm was assumed for all dies. The angle θ in Figure 6.11b and Figure 6.11c was 10°.

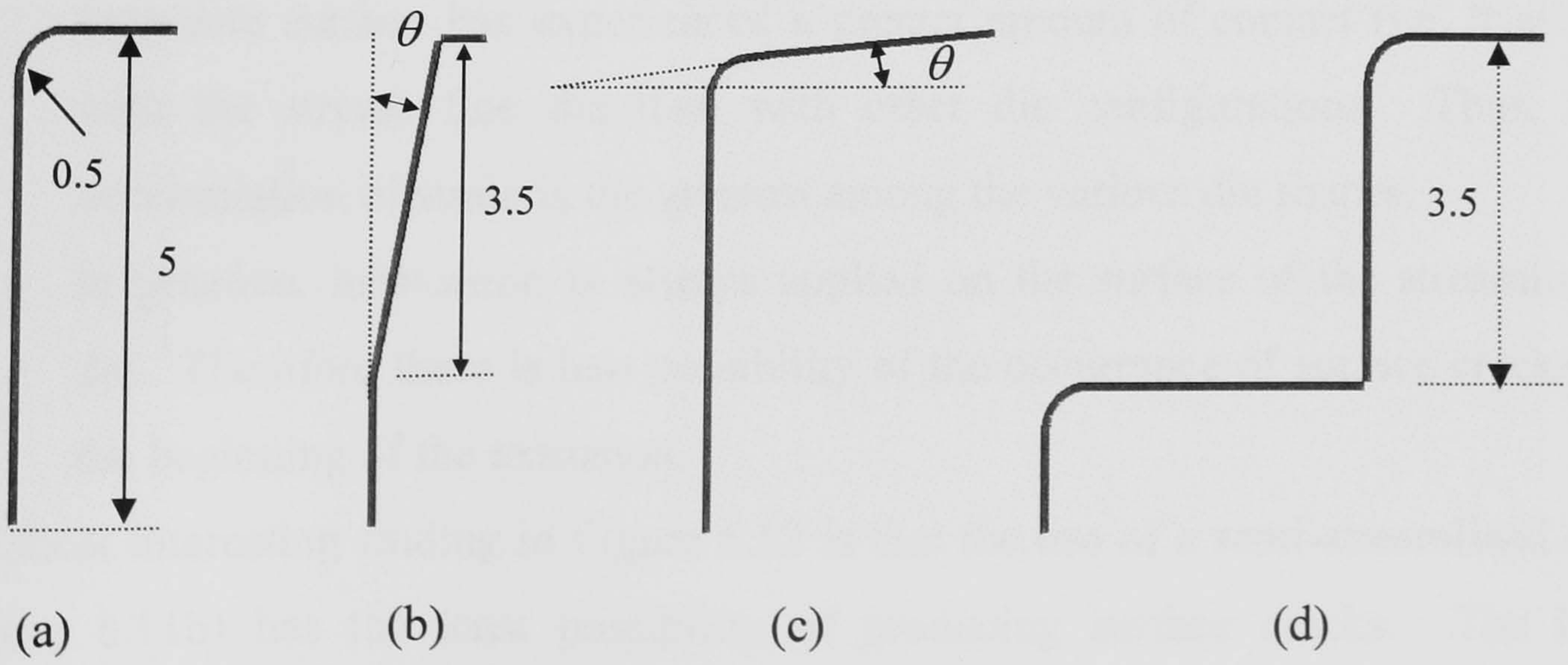

Figure 6.11 Schematic drawing of the various die configurations (all dimensions in mm): (a) flat-faced; (b) semi-streamlined; (c) streamlined; (d) pre-chambered

Figure 6.12 shows the distribution of the Cockcroft and Latham fracture values in the cross section within the die land. The value was calculated at 1mm before the die exit.

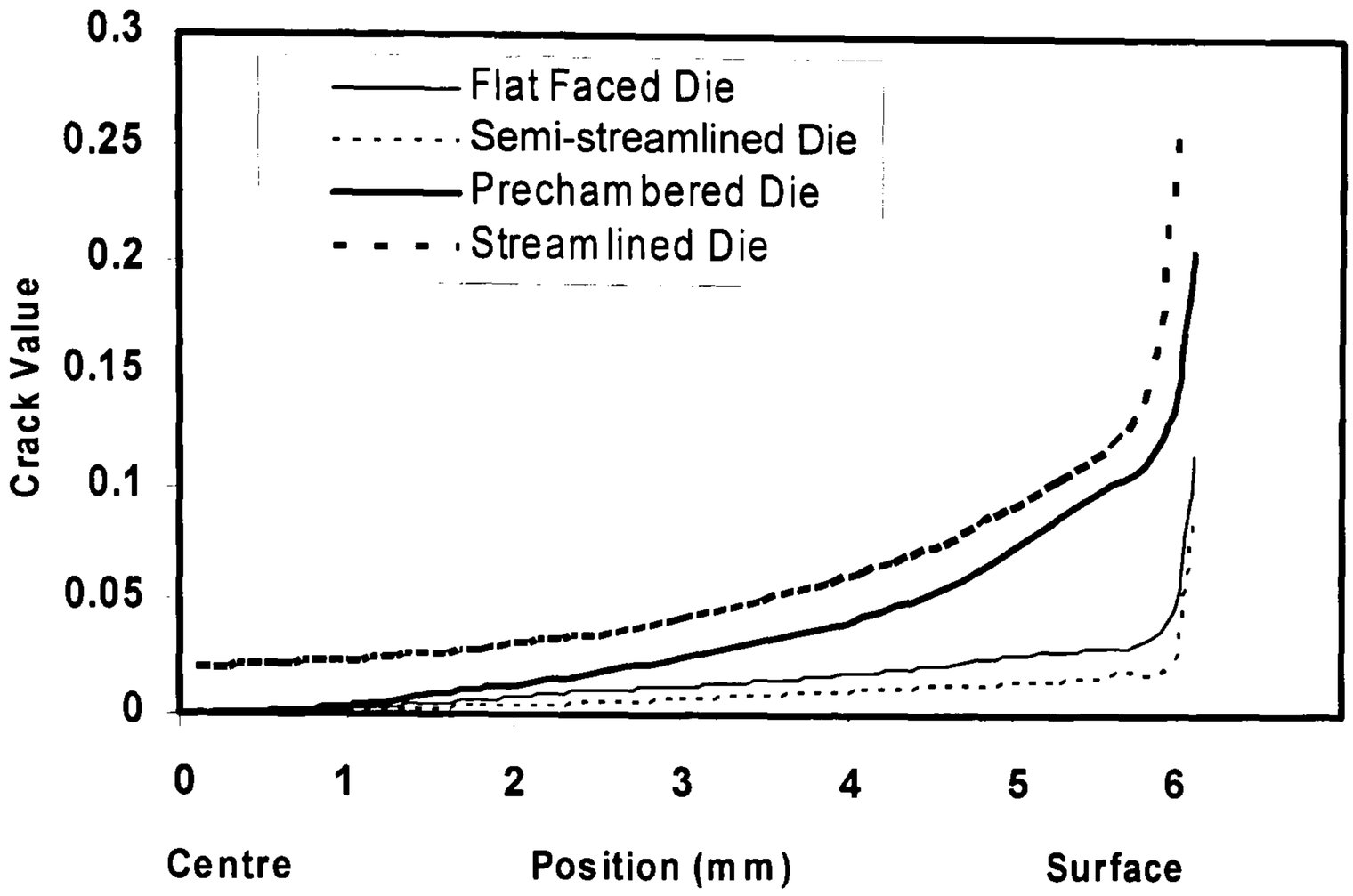

Figure 6.12 Distribution of the Cockcroft and Latham fracture values in the cross section within the die land for each profile

Surprisingly, the stream line die (Figure 6.11c) produces the greatest fracture value. This means that using this die shape tends to generate the surface cracks. This conclusion does not agree with other researchers' work (Domanti *et al* 2002). However, the two following interpretations can be suggested:

- Only a very short ram stroke is simulated. The material which forms the extrudate surface has experienced a greater amount of contact (i.e. friction) with the stream line die than with other die configurations. Thus, the accumulation of strain is the greatest among the various die shapes.
- In practice, lubrication is always applied on the surface of the streamlined die. Therefore there is less possibility of the occurrence of surface cracks at the beginning of the extrusion.

The most interesting finding in Figure 6.12 is that the use of a semi-streamlined die (Figure 6.11b) has the least possibility of producing surface cracks. The key parameters of the semi-streamlined die are the angle θ and the depth of the choke. Jarrett and Parson (1995) gave some useful indications in their patent.

6.3.3 Optimum forming parameters

Four forming parameters were selected to study their influence on the formation of surface cracks. These parameters included the extrusion ratio, the temperature difference between the tool and the billet (ΔT), the extrusion speed and the billet temperature. Each parameter had three levels which are listed in Table 6.2.

Level	Extrusion ratio	ΔT (K)	Extrusion speed (mms^{-1})	Billet temperature (K)
1	*10*	*-50*	*3*	*573*
2	*30*	*0*	*6*	*633*
3	*50*	*50*	*9*	*693*

Table 6.2 Test parameters and their levels

Using a Taguchi method, a three-level series orthogonal array $L9(3^4)$, was set up to investigate the four factors at three levels with only 9 runs (simulations). The Taguchi methods have already been successfully used by the author's co-worker for the study of forming parameters on static recrystallization and final subgrain size during the hot rolling of aluminium (Duan and Sheppard 2002a and 2002b). The $L9(3^4)$ is shown in Table 6.3.

Run	Extrusion ratio	ΔT	Extrusion speed	Billet temperature
1	*1*	*1*	*1*	*1*
2	*1*	*2*	*2*	*2*
3	*1*	*3*	*3*	*3*
4	*2*	*1*	*2*	*3*
5	*2*	*2*	*3*	*1*
6	*2*	*3*	*1*	*2*
7	*3*	*1*	*3*	*2*
8	*3*	*2*	*1*	*3*
9	*3*	*3*	*2*	*1*

Table 6.3 $L9(3^4)$ orthogonal array

The computed contribution of each forming parameter to the fracture value and the subgrain size are shown in Table 6.4.

	Surface crack	Subgrain size
Extrusion ratio	*45.0%*	*8.5%*
ΔT	*8.7%*	*3.8%*
Extrusion speed	*23.2%*	*0.1%*
Billet temperature	*23.2%*	*87.6%*

Table 6.4 Analysis of variance of spread

It can be seen that the extrusion ratio is the dominating variable on the control of surface cracks, followed by ram speed, billet temperature, and tool temperature difference. It is not surprising to see a strong dependence between the extrusion ratio and the extrudate velocity due to the interrelationship between these two variables. The average effect of each parameter level on the fracture value is shown in Figure 6.13.

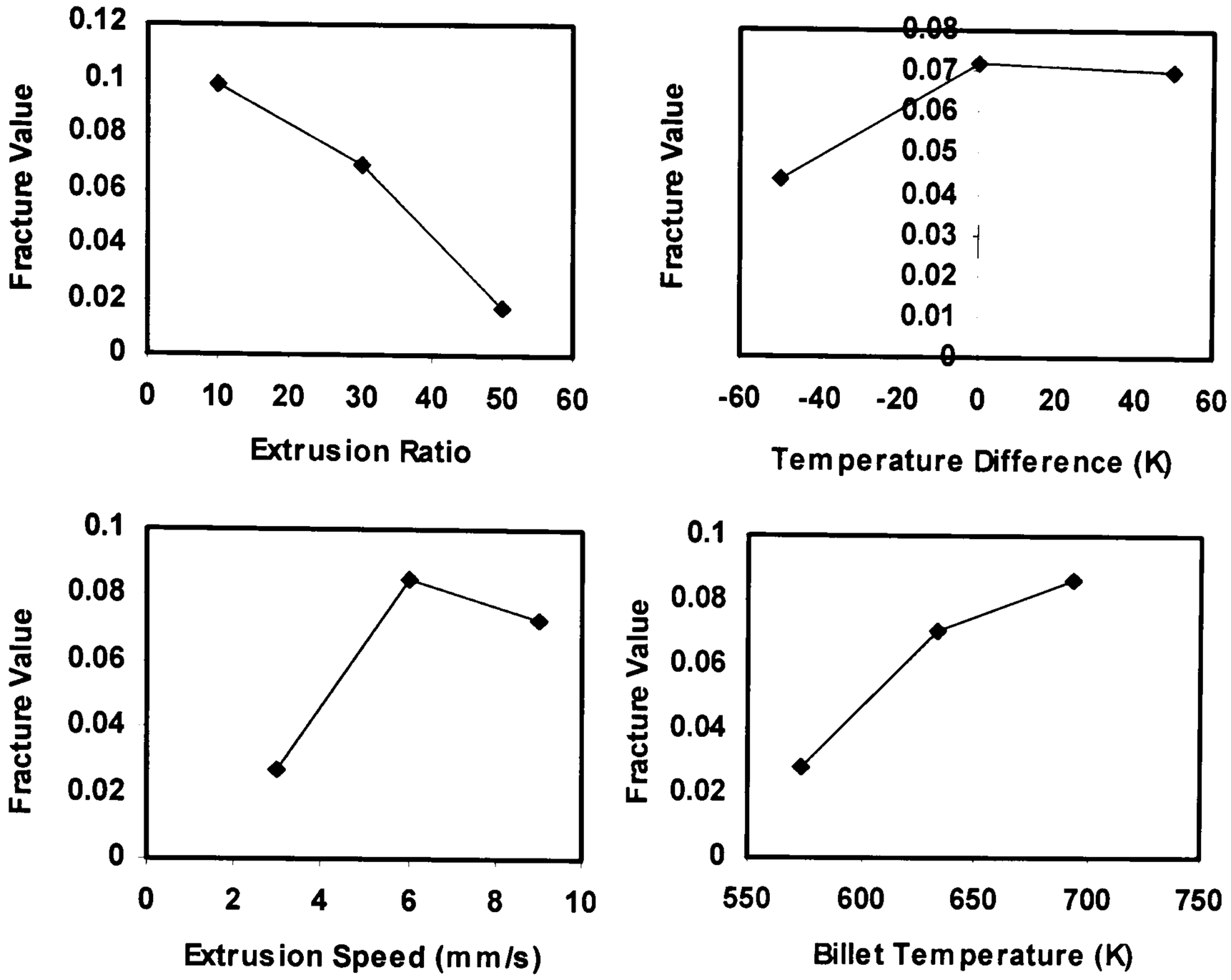

Figure 6.13 Plots of response for each parameter level on the predicted fracture value

Figure 6.13 shows that the fracture value increases with decreasing extrusion ratio, increasing temperature difference (between the billet and tools), increasing extrusion speed, and increasing billet temperature. The predicted fracture value decreasing with the increase of the extrusion ratio was beyond the author's expectation. As shown earlier in Figure 2.4 surface tearing increases with extrusion speed. This therefore indicates that to produce a specified extrudate dimension, the use of a billet with a large diameter is superior to the use of a small billet in terms of preventing the occurrence of surface cracks. However, the use of large billets means that a higher extrusion load is required. The changes in the other three parameters fit well with general experimental observations.

The influences of the four forming parameters on the subgrain size are shown in Figure 6.14 and in the second column of Table 6.4. The billet temperature plays the dominating role in the subgrain size. This was expected and discussed in Chapter 5. Subgrain size is one of the key parameters in the simulation of recrystallization and extrudate structure.

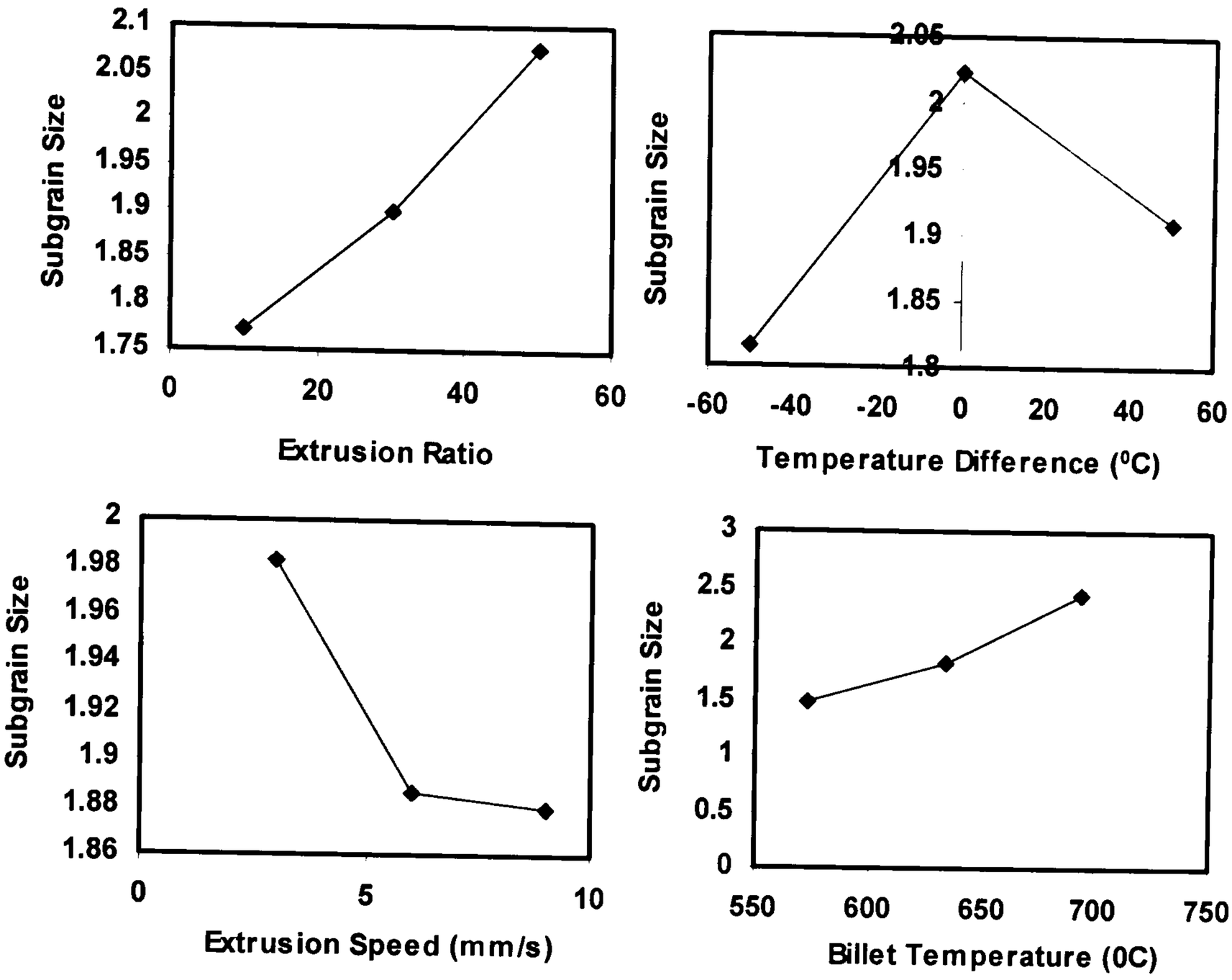

Figure 6.14 Plots of response for each parameter level on the predicted subgrain size (μm)

6.4 Concluding remarks

The finite element method has been successfully applied to study the structural integrity of the wheel during Conform extrusion. FEM has also been used to investigate surface cracks and die design. The following conclusions can be drawn based on the analyses presented:

- An efficient way to study the structural integrity of the wheel in Conform would be to firstly analyse the deformation of the feedstock. This will provide the value of the maximum pressure in the areas adjacent to the abutment. The pressure could then be transferred to a refined finite element model of the wheel using four zones of loading. Finally a simple linear static analysis would provide an accurate distribution of the stresses together with the position of the stress concentrations. Similar procedures could be applied for the study of the structural integrity of the coining roll, the abutment and the die.

- The Cockcroft and Latham criterion is a valid criterion for the prediction of speed cracks. The determination of the critical damage value cannot be solely determined by either compression or tensile testing. The inverse analysis method used in this study is theoretically the best solution. However, this requires several FEM runs and is not considered to be the most efficient use of time for an industrial environment. This therefore highlights the importance of efficient modeling.
- Among the investigated forming parameters (such as extrusion ratio, the temperature difference between the tool and the billet, the ram velocity and the billet temperature), extrusion ratio has the strongest influence on the initiation of surface cracks. The greater the extrusion ratio, the less possibility for the occurrence of surface cracks. The possibility of the occurrence of surface cracks increases with increasing billet temperature, ram speed and temperature difference between the tool and the billet.
- The die configuration has a critical influence on the formation of surface defects. Using a semi-streamlined die can significantly reduce the possibility of the initiation of surface cracks. If no lubrication is added, the streamlined die results in a greater possibility of producing surface cracks in the early stages of the extrusion process.

7 Conclusions and further research

7.1 Conclusions

Several concluding remarks were made at the end of chapters three, four, five and six. The main findings of these are now summarised into the following numbered paragraphs.

1 **On the simulation of the Conform process with FEM**

The simulation of the Conform process is complex and this thesis proposes new techniques to investigate this. The process itself comprises a series of sub-processes such as the coining, the approach and formation of the upset zone, the extrusion of the flash, the fill up of the expansion chamber, and the extrusion of the extrudate. The Lagrangian form is the most appropriate formulation to accurately and efficiently analyse these sub-processes, individually or simultaneously. However this formulation is only efficient if it is run together with a semi-automatic re-meshing algorithm on powerful computers. The discretisation of the workpiece should be performed by the 'boundary constrained Delaunay triangulation' and small features, such as flashes and die corners, should be represented accurately by refined meshes. The quality of the results is highly dependant on the quality of the workpiece's mesh and how well the latter fits the geometry of the dies. Furthermore during the extrusion of complex profiles, which require a large number of re-meshing, the loss of volume mesh during the simulation can significantly affect the accuracy of the results in terms of velocity. The Zener-Hollomon formulation is the most accurate equation to represent the flow stress in extrusion of aluminium alloys using Conform. However, caution must be exercised in the selection of flow stress data for the

simulation of the coining where the feedstock is relatively cold. The use of parallel processors or cluster computers is strongly recommended.

2 On the innovative procedures for the simulation of some of the Conform sub-processes

The evident advantage of three-dimensional modelling of the Conform process is the possibility to precisely simulate the volume and shape of the material together with the right boundary conditions. From this, 3D phenomena, such as material flow, temperature distribution and other variables, can be studied and analysed. However, plane strain FEM, both thermoplastic and transient thermal, can be used efficiently to predict the temperature of the feedstock before entering the upset zone. This process helps to find the optimum wheel velocity, initial grip length and rate of cooling. An efficient way to maintain an extrudate in a straight direction in simulation would be to use a ghost die both in 2D or 3D. Such a die is defined with a null coefficient of friction, is infinitely stiff and has the thermal properties of air.

3 On the important features of Conform extrusion

In Conform steady state is attained when the upset zone is fully formed. At this stage the extrusion load, temperature, and extrudate velocity converge to their respective maximum values and the dead metal zone is fully formed. Furthermore, the velocity varies linearly across the extrudate. This variation can be limited by reducing (or eliminating if possible) the gap between the wheel and the abutment/shoe assembly whilst still maintaining the aluminium surface in the wheel groove. The exit temperature of the extrudate can be controlled by adjusting the temperature of the tooling in contact with it or by varying the velocity. Accurate control of the exit velocity and temperature across the extrudate can ensure the desired material properties of the extrudate. The ideal material properties could also be obtained by ensuring consistency across the extrudate with the use of an optimum design of the expansion chamber, feeder plate and die.

4 On the optimisation of wheel design

An efficient way to study the structural integrity of the wheel in Conform would be a preliminary analysis of the deformation of the feedstock. This will provide the value of the maximum pressure in the areas adjacent to the abutment. The pressure could then be transferred to a refined finite element model of the wheel using four zones of loading. Finally a simple linear static analysis would provide an accurate distribution of the stresses together with the location of stress concentrations.

5 On the prediction and modelling of macrostructure

Both the model proposed by Sellars and Zhu and the model created by Nes and co-workers are available for the prediction of static recrystallization. It is easier to perform numerical analyses using the model created by Nes et al due to the fact that the values of the parameters in their model can be more easily found in the literature. However the model proposed by Sellars and Zhu presents more accurate predictions. Nevertheless, the requirement of several tuning parameters for each aluminium alloy renders both models impractical for industrial use, which justifies the use of simulation by FEM.

6 On the optimisation of die design and extrudate surface quality

The Cockcroft and Latham criterion would appear to be a valid criterion for the prediction of speed cracks. The determination of the critical damage value cannot be solely determined by either compression or tensile testing. Therefore, the inverse analysis method is theoretically the best solution. However, this requires several FEM runs, ideally with finer meshing, and hence is not considered to be the most efficient use of time for an industrial environment. The extrusion ratio has the strongest influence on the initiation of surface cracks. However it is important to note that the extrusion ratio and velocity of the extrudate are strongly interlinked. The possibility of the occurrence of surface cracks increases with increasing billet temperature, ram speed and temperature difference between the tool and the billet. The die configuration has a critical influence on the formation of surface defects. Using a semi-streamlined die can significantly reduce the possibility of the

initiation of surface cracks. If no lubrication is added, which is not feasible in this process, the streamlined die results in a greater possibility of producing surface cracks in the early stages of the extrusion process. The use of a feeder plate can reduce the degree of non-uniformity in terms of shape and properties.

7.2 Further research

This thesis engages in several fields of science and engineering using modern software and computers. It is therefore not surprising that a number of recommendations can be made for further research. The main recommendations are summarised into the following numbered paragraphs.

1. **On the simulation of the overall Conform process**

   Affordable computing power (parallel processors or clusters) is now at a stage where the simulation of the whole Conform process could be undertaken. This would involve a 3D model analysing the coining of the feedstock, the formation of the upset zone, the 'extrusion' of the flash, the feeding of the feeder plate or the expansion chamber, and finally the extrusion of the profile. Such a model would include a minimum of six tools (coining roll, wheel, shoe, abutment, expansion chamber, die) of which two would be rotating: the wheel and the coining roll. In order to obtain an accurate temperature distribution it would be necessary to mesh the interior of the tools. One challenging issue would be the definition of the flow stress. The feedstock enters the Conform machine with a temperature of approximately 20°C and exits at about 450°C. Therefore suitable flow stress formulation would have to be found to deal with such a range in temperature. An ideal solution would be to use a physical model based on dislocation density, subgrain size and misorientation, to calculate the value of the flow stress at each increment of the analysis.

2. **On scaling down the size of the mesh**

Scaled models can save a significant amount of computation time and still provide qualitative information for flow patterns. However, at present, they are unable to correctly predict other variables such as temperature distribution, strain rate or subgrain size. An obvious possibility is to introduce a scaling factor as a function of velocity, temperature or both. However the scaling of a feedstock is not as straightforward as the scaling of a billet. More fruitful research could therefore involve investigation of a 'dimension scaling factor'. Such a factor would ideally be able to scale up results from a 2D plane strain analysis to a 3D analysis. With such increased efficiency in the simulation of Conform, it should therefore be possible to create an expert system for Conform extrusion. This system would optimise control parameters and process variables and would be the foundation for the integration of knowledge based systems and FEM. Such integrated approach would lead to significantly shorter lead times, better extrudate quality and consequently more cost effective design and production (Tisza 1999).

3. **On the use of Conform for unusual extrusion**

Industrial demands for curved profiles are increasing. The conventional process comprising extrusion, stretching and bending has been recently complemented by new concepts (Birkenstock *et al* 2004, König and Muschalik 2004 and Buntoro and Müller 2004). Due to the 'natural' curvature of the extrudate in the Conform process it could therefore be possible to enhance this to produce the requisite curved profiles for industry. In the area of advanced profiles, reinforcing elements such as high strength steel wire are embedded into an aluminium alloy during direct extrusion using a modified die (Kleiner *et al* 2004). Due to the success of the Conform process for the cladding and sheathing industry, it would seem likely that Conform could also be applicable for reinforced profiles and this would therefore merit further investigation. Furthermore within the automotive industry, there is a growing requirement for economical thin-walled sections. Conform could offer a competitive solution for this.

4. On the use of the Eulerian formulation for feeder plates and expansion chambers

The simulation of feeder plates and expansion chambers with a Lagrangian formulation is very resource intensive. At steady state, the chambers are continuously filled and therefore the Eulerian approach has been shown to be a much more efficient method. The expert system suggested above may be able to provide information on both the shape of the flash and height of the upset zone. This predicted data would subsequently allow for a model of the workpiece at steady state to be simulated using only the Eulerian method. The reader should be aware that the Conform process runs at a steady state for long durations; a further factor supporting Eulerian analyses in parts of the simulation.

5. On innovative finite element modelling procedures

During the simulation of Conform those meshes which have passed the die land and the bottom of the extrudate subsequently become redundant. Unfortunately, they are still part of the overall stiffness matrix of the workpiece and are therefore still included in the numerous and time consuming calculations at each increment. One solution to reduce the computing time is to use a cut-off sub-routine. Such a sub-routine deletes a portion of mesh below a predefined plane. Unfortunately this can easily create mesh instability. After deletion of the elements below the plane, the end of the workpiece is left with a jagged surface. Every re-meshing procedure includes one step where nodes are 'regularised'. This means that the position of the node is moved against the neighbouring nodes (e.g. diagonal inversion, node centring) in order to improve the local mesh topology. The node regularisation on the jagged surface frequently produces poor elements. Consequently, a wrong computation of the velocity field is calculated resulting in incorrect thermo-mechanical calculations. This problem could be reduced or possibly eliminated by two actions. The first action would be to reduce the internal mesh size. For example in Forge 2 and 3 the refinement of the internal mesh is controlled by a parameter ('volumic size factor') written inside the FE code. The second action would be to create a specific buffer zone around the cutting plane enabling the software to pre-

detect nodes which would approach the cutting plane. The nodes inside this zone would then be exempt from the regularisation at each re-meshing. This would allow the jagged surface to remain as it is without causing the analysis to stop.

6. On the study of frictional interfaces

The influence of friction within the Conform process is significant. However every metal forming software to date has defined friction in a relatively simplistic manner. The friction laws are not able to accurately describe the contact between the workpiece and the tools. Further research is therefore necessary to develop a physical friction model which could take into account the deformation of the asperities, surface topography, pressure, friction conditions, lubricants (if necessary) and the influence of temperature.

Appendix A

Analyses of Conform extrusion mechanics

Figure A.1 and A.2 represent an idealised geometry of the wheel-shoe-abutment section and the wheel groove-shoe section respectively.

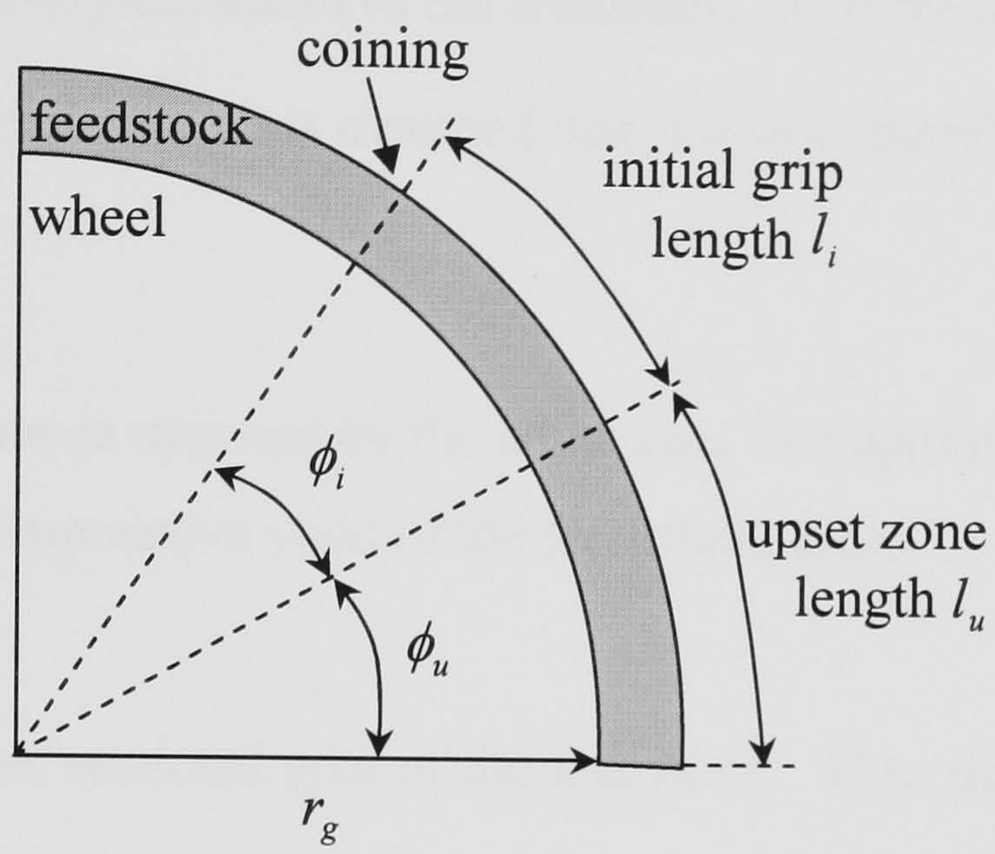

Figure A.1 Schematic of the wheel-shoe-abutment section

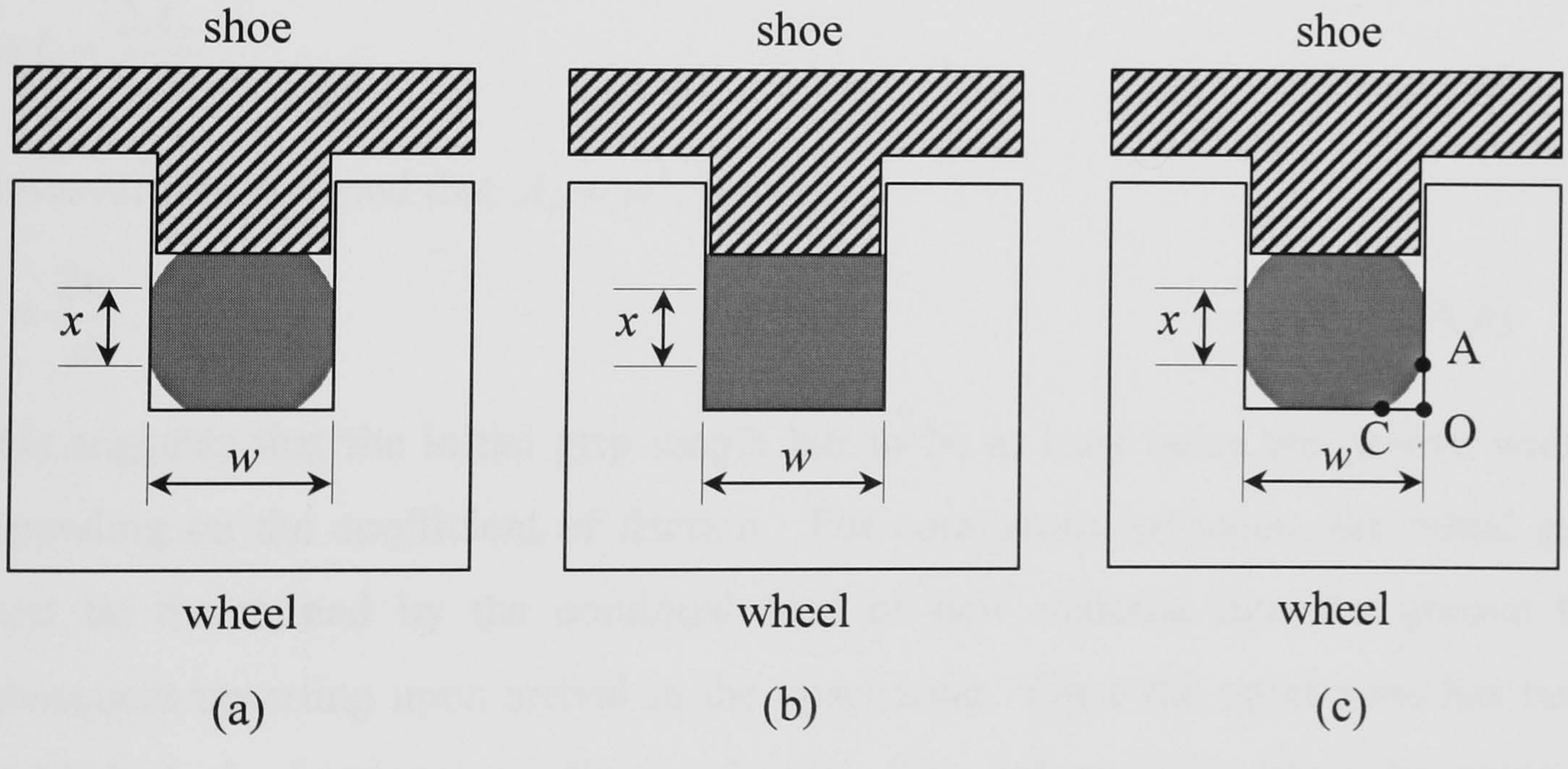

Figure A.2 Schematic of the wheel groove-shoe section (a) initial grip contact, (b) upset zone contact and (c) Initial grip not in contact

Analysis from Green and Etherington

It is assumed that the feedstock deforms during the initial grip is such a way that the initial contact with the groove wall, x, is a quarter of the groove width, w (see Figure

A.2a). The frictional force between the feedstock and the groove wall transmits the wheel torque to the feedstock. The frictional force between the stationary shoe and the feedstock opposes the circumferential motion of the feedstock. The net tangential force, F, acting on the abutment is thus:

$$F = 2\mu\sigma_{cys}A_i = 2\mu\sigma_{cys}xl_i \qquad \text{(A.1)}$$

where μ is the coefficient of friction between the groove wall and the feedstock, σ_{cys} is the compressive yield stress of the feedstock, A_i is the area of initial grip, and l_i is the length of initial grip. It is assumed that $x = w/4$, therefore:

$$F = \frac{\mu\sigma_{cys}wl_i}{2} \qquad \text{(A.2)}$$

The net frictional force is opposed by the abutment. For upsetting, this force must be sufficient to cause compressive yield of the feedstock, thus:

$$F = \sigma_{cys}A_F \qquad \text{(A.3)}$$

where A_F is the cross sectional area of the feedstock. Thus the following equations can be written:

$$\sigma_{cys}A_F = \frac{\mu\sigma_{cys}wl_i}{2}$$

$$\Rightarrow l_i = \frac{2A_F}{\mu w}$$

However it is assumed that $A_F \approx w^2$, hence:

$$l_i = \frac{2w}{\mu} \qquad \text{(A.4)}$$

This suggests that the initial grip length has to be at least twice the groove width, depending on the coefficient of friction. For continuous extrusion, the initial grip must be maintained by the continual feed of new material into the groove for subsequent upsetting upon arrival in the upset zone. Once the upset zone has been established, the frictional conditions change. The deformed feedstock becomes in contact with the entire surface of the groove and the shoe (see Figure A.2b). The interface thus experiences shear instead of sliding. It is in this region that sufficient pressure must be generated for extrusion to occur. This is expressed in terms of an overall extrusion pressure required to overcome homogeneous and redundant deformation and friction at the die. By using a similar process to that which was used for equation (A.4) the following equations can be derived:

$$pw^2 = 2\tau_{ys} w l_u \tag{A.5}$$

where p is the extrusion pressure, τ_{ys} is the yield strength of the feedstock in shear, and l_u is the length of upset zone necessary for extrusion to start. Thus:

$$l_u = \frac{pw}{2\tau_{ys}}$$

However if the Tresca's yield criterion is applied ($\sigma_{cys} = 2\tau_{ys}$), then l_u can be expressed as follows:

$$l_u = \frac{pw}{\sigma_{cys}} \tag{A.6}$$

By combining equations (A.4) and (A.6) the total length (initial grip + upset zone) can be written with the following equation:

$$l_i + l_u = w\left(\frac{2}{\mu} + \frac{p}{\sigma_{cys}}\right) \tag{A.7}$$

Finally the extrusion pressure may be determined from the general expression used in conventional extrusion analysis. As seen in section (2.1.5.1) of this thesis, this can take the simplified form:

$$p = a + b\bar{\sigma} \ln R_{mc} \tag{A.8}$$

where a and b are the contribution to the redundant work and die friction, $\bar{\sigma}$ is the flow stress of the material, and R_{mc} is the modified extrusion ratio for Conform. It is assumed that $R_{mc} = w^2 / A_E$ where A_E is the cross sectional area of the extrudate.

Analysis from Gorokhov *et Al*

In this analysis a radial section is considered through the feedstock and tooling. It is suggested that the contact area over the initial grip can be more strictly determined by reasoning that the feedstock sectional area will remain constant. Therefore the following equation can be written:

$$\pi r^2 = w^2 - 4A_{AOC} \tag{A.9}$$

where r is the radius of the original (un-deformed) feedstock, and A_{AOC} is the cross sectional area of unfilled groove (see Figure A.2c). AC can be assumed to be an arc. thus:

$$A_{AOC} = \left(1 - \frac{\pi}{4}\right)\frac{(w-x)^2}{4} \tag{A.10}$$

Substituting in equation (A.9) and rearranging:

$$x = w - \sqrt{\frac{w - \pi r^2}{1 - \frac{\pi}{4}}} \tag{A.11}$$

Now the contact areas of the feedstock with the groove and the shoe can be determined in terms of the angles described by the initial grip, ϕ_i, and the upset zones, ϕ_u (see Figure A.1).

For the initial grip the following equations can be calculated:

The contact area with the shoe, A_{is}:

$$A_{is} = x(r_g + w)\phi_i$$

where r_g is the radius of the wheel at the groove base.

The contact area with one groove side, A_{ig}^{side}:

$$A_{ig}^{side} = x\left(r_g + \frac{w}{2}\right)\phi_i$$

The contact area with the groove base, A_{ig}^{base}:

$$A_{ig}^{base} = xr_g\phi_i$$

Hence the total area with the groove, A_{ig}:

$$A_{ig} = 2A_{ig}^{side} + A_{ig}^{base} = x(3r_g + w)\phi_i \tag{A.12}$$

By similar reasoning, the upset zone relations can be calculated:

The contact area with the shoe, A_{us}:

$$A_{us} = w(r_g + w)\phi_u$$

The total area with the groove, A_{ug}:

$$A_{ug} = w(3r_g + w)\phi_u \tag{A.13}$$

The total frictional force acting toward the abutment, F_f, is given by:

$$F_f = F_{fu} + F_{fi} \tag{A.14}$$

where F_{fu} is the frictional forward force generated in the upset zone, and F_{fi} is the frictional forward force generated in the initial grip length. These are defined as follows:

$F_{fu} = \mu_u A_{ug} \overline{\sigma}_u$ and $F_{fi} = \mu_i A_{ig} \overline{\sigma}_i$

where μ_u and μ_i are the coefficients of friction between the groove wall and the feedstock in the upset zone and in the grip length, respectively. $\overline{\sigma}_u$ and $\overline{\sigma}_i$ are the mean compressive yield strength of the feedstock in the upset zone and in the grip length, respectively.

During the steady state extrusion, the frictional force will be balanced so that:

$$F_f = F_a + F_s + F_d + F \tag{A.15}$$

where F_a is the reaction force of the abutment on the feedstock, F_s is the opposing frictional force at the feedstock and shoe interface, F_d is the frictional force with the die surface(s), and F is the force required for the extrusion to occur. With:

$F_a = w^2 \overline{\sigma}_u$, $F_s = \mu_i A_{is} \overline{\sigma}_i + \mu_u A_{us} \overline{\sigma}_u$, $F_d = \mu_d A_d \overline{\sigma}_u$ and F can be represented as a general extrusion pressure equation.

By applying force balances in the initial grip length and upset zone, the angles ϕ_i and ϕ_u can be calculated. In the upset zone the following equilibrium is present:

$$F_{fu} = F + F_d + F_{su} \tag{A.16}$$

where F_{su} is the frictional force generated in the upset zone at the feedstock and shoe interface and $F_{su} = \mu_u A_{us} \overline{\sigma}_u$. Therefore, equation (A.16) can be written as follows:

$$\mu_u A_{ug} \overline{\sigma}_u = (F + F_d) + \mu_u A_{us} \overline{\sigma}_u$$
$$\Rightarrow \mu_u \overline{\sigma}_u w(3r_g + w)\phi_u = (F + F_d) + \mu_u \overline{\sigma}_u w(r_g + w)\phi_u$$

which gives:

$$\phi_u = \frac{(F + F_d)}{2\mu_u \overline{\sigma}_u w r_g} \tag{A.17}$$

The angle described by the initial grip, ϕ_i, is derived from the requirement that the length of the initial grip must generate sufficient frictional force to cause upsetting when the feedstock first impinges on the abutment. Hence:

$$F_{fi} = F_a + F_{si} \tag{A.18}$$

where F_{si} is the frictional force generated in the initial grip zone at the feedstock and shoe interface and $F_{si} = \mu_i A_{is} \overline{\sigma}_i$. Therefore, equation (A.18) can be written as follows:

$$\mu_i A_{ig} \bar{\sigma}_i = w^2 \bar{\sigma}_u + \mu_i A_{is} \bar{\sigma}_i$$

$$\Rightarrow \mu_i \bar{\sigma}_i x(3r_g + w)\phi_i = w^2 \bar{\sigma}_u + \mu_i \bar{\sigma}_i x(r_g + w)\phi_i$$

which gives (assuming that $\bar{\sigma}_i \approx \bar{\sigma}_u$):

$$\phi_i = \frac{w^2}{2\mu_i x r_g} \tag{A.19}$$

Appendix B

Cauchy stress tensor, invariants and yield criterion

The Cauchy stress tensor

The Cauchy stress tensor $[\sigma_{ij}]$, where $i, j = 1,2,3$ or x, y, z, is symmetric and is represented by nine components as:

$$[\sigma_{ij}] = \begin{bmatrix} \sigma_{11} & \sigma_{21} & \sigma_{31} \\ \sigma_{12} & \sigma_{22} & \sigma_{32} \\ \sigma_{13} & \sigma_{23} & \sigma_{33} \end{bmatrix} = \begin{bmatrix} \sigma_x & \tau_{yx} & \tau_{zx} \\ \tau_{xy} & \sigma_y & \tau_{zy} \\ \tau_{xz} & \tau_{yz} & \sigma_z \end{bmatrix} \quad \text{(B.1)}$$

The invariants

The stress may also be specified by the three principal components: the three tensor invariants (Hosford and Caddell 1983, 28-35). The principal stresses $(\sigma_1, \sigma_2, \sigma_3)$ are the roots of the cubic equation:

$$\sigma^3 - J_1\sigma^2 - J_2\sigma - J_3 = 0 \quad \text{(B.2)}$$

where J_1, J_2 and J_3 are the three invariants of the stress tensor $[\sigma_{ij}]$ and they are independent of the direction of the axes chosen. They are defined by the relations:

$$\left.\begin{aligned} J_1 &= \sigma_x + \sigma_y + \sigma_z = \sigma_1 + \sigma_2 + \sigma_3 \\ J_2 &= -(\sigma_x\sigma_y + \sigma_y\sigma_z + \sigma_z\sigma_x) + \tau_{xy}^2 + \tau_{yz}^2 + \tau_{zx}^2 = -(\sigma_1\sigma_2 + \sigma_2\sigma_3 + \sigma_3\sigma_1) \\ J_3 &= \sigma_x\sigma_y\sigma_z + 2\tau_{xy}\tau_{yz}\tau_{zx} - \sigma_x\tau_{yz}^2 - \sigma_y\tau_{zx}^2 - \sigma_z\tau_{xy}^2 = \sigma_1\sigma_2\sigma_3 \end{aligned}\right\} \quad \text{(B.3)}$$

For isotropic materials, such as aluminium alloys, plastic yielding can depend only on the magnitude of the three principal stresses $(\sigma_1, \sigma_2, \sigma_3)$ and not on their directions. Thus any yield criterion can be expressed as follows:

$$f(J_1, J_2, J_3) = C \text{ (constant)} \quad \text{(B.4)}$$

The first invariant ($J_1/3$) represents the hydrostatic pressure. Although this pressure may increase ductility it does not contribute to deformation.

Tresca yield criterion

The criterion postulates that yielding will occur when the largest shear stress reaches a critical value. Therefore:

$$\sigma_1 - \sigma_3 = C \text{ (constant)} \tag{B.5}$$

with $\sigma_1 \geq \sigma_2 \geq \sigma_3$. The constant may be determined from simple states such as uniaxial tension ($\sigma_1 = Y = \text{yeild strength}, \sigma_2 = \sigma_3 = 0$) and pure shear ($\sigma_1 = k = \text{shear yield strength}, \sigma_2 = 0, \sigma_3 = -\sigma_1$). Therefore the Tresca criterion becomes:

$$\sigma_1 - \sigma_3 = Y = 2k \tag{B.6}$$

Von Mises criterion

The criterion postulates that yielding will occur when some value of the root-mean shear stress reaches a constant such as:

$$(\sigma_1 - \sigma_2)^2 + (\sigma_2 - \sigma_3)^2 (\sigma_3 - \sigma_1)^2 = C \text{ (constant)} \tag{B.7}$$

The constant may be determined from simple states as described above. Therefore the criterion can be written as:

$$(\sigma_1 - \sigma_2)^2 + (\sigma_2 - \sigma_3)^2 (\sigma_3 - \sigma_1)^2 = 2Y^2 = 6k^2 \tag{B.8}$$

Appendix C

Experimental data for AA2014 and AA7075

	AA2014 (Veirod 1983)				AA7075 (Sheppard and Jackson 1997)		
	Strain rate (s^{-1})	Temperature (K)	Experimental flow stress (MPa)		Strain rate (s^{-1})	Temperature (K)	Experimental flow stress (MPa)
1	0.032	573.15	50.23		0.008	533.15	106.71
2	0.032	623.15	32.69		0.008	573.15	72.68
3	0.032	663.15	23.37		0.008	613.15	53.48
4	0.032	703.15	17.06		0.008	653.15	56.22
5	0.032	748.15	12.34		0.008	693.15	32.62
6	0.305	664.15	38.05		0.08	533.15	144.02
7	0.305	704.15	28.67		0.08	573.15	103.41
8	0.31	749.15	21.26		0.08	613.15	75.43
9	2.507	576.15	93.13		0.08	653.15	56.22
10	2.633	630.15	69.46		0.08	693.15	49.09
11	2.669	668.15	55.83		0.8	533.15	175.85
12	2.687	706.15	44.64		0.8	573.15	130.85
13	2.76	750.15	34.64		0.8	613.15	103.41
14	8.567	670.15	66.65		0.8	653.15	80.91
15	8.567	709.15	54.28		0.8	693.15	67.74
16	8.567	751.15	43.41		8	533.15	191.77
17	28.443	585.15	115.23		8	573.15	154.45
18	28.443	633.15	93.45		8	613.15	127.56
19	28.443	633.15	93.45		8	653.15	104.51
20	28.768	584.15	115.85		8	693.15	93.54
21	29.129	673.15	78.27		80	533.15	203.29
22	29.472	709.15	66.4		80	573.15	182.44
23	29.472	753.15	54		80	613.15	156.65
24	-	-	-		80	653.15	139.09
25	-	-	-		80	693.15	124.82

Table C1 Experimental data for AA2014 and AA7075

Appendix D

Derivation of the flow stresses

Norton-Hoff power law

$$\sigma_{N-H}^{power} = K_0 e^{\beta/T}\left(\sqrt{3}\right)^{1+m}\dot{\bar{\varepsilon}}^{m} \tag{D.1}$$

$$\frac{\partial\sigma_{N-H}^{power}}{\partial\dot{\bar{\varepsilon}}} = mK_0 e^{\beta/T}\left(\sqrt{3}\right)^{1+m}\dot{\bar{\varepsilon}}^{m-1} \tag{D.2}$$

$$\Rightarrow \frac{\partial\sigma_{N-H}^{power}}{\partial\dot{\bar{\varepsilon}}} = m\frac{\sigma_{N-H}^{power}}{\dot{\bar{\varepsilon}}} \tag{D.3}$$

Hansel-Spittel law

$$\sigma_{H-S} = Ae^{m_1 T}\dot{\bar{\varepsilon}}^{m_3} \tag{D.4}$$

$$\frac{\partial\sigma_{H-S}}{\partial\dot{\bar{\varepsilon}}} = m_3 Ae^{m_1 T}\dot{\bar{\varepsilon}}^{m_3-1} \tag{D.5}$$

$$\Rightarrow \frac{\partial\sigma_{H-S}}{\partial\dot{\bar{\varepsilon}}} = m_3\frac{\sigma_{H-S}}{\dot{\bar{\varepsilon}}} \tag{D.6}$$

Zener-Hollomon flow stress

$$Z = \dot{\bar{\varepsilon}}e^{\Delta H/GT} = A\left(\sinh\alpha\sigma_{Z-H}\right)^{n} \tag{D.7}$$

$$\begin{cases} \dfrac{\partial Z}{\partial\dot{\bar{\varepsilon}}} = e^{\Delta H/GT} \\ \dfrac{\partial Z}{\partial\sigma_{Z-H}} = \alpha nA\left(\sinh\alpha\sigma_{Z-H}\right)^{n-1}\left(\cosh\alpha\sigma_{Z-H}\right) \end{cases} \tag{D.8}$$

$$\Rightarrow \frac{\partial\sigma_{Z-H}}{\partial\dot{\bar{\varepsilon}}} = \frac{\partial\sigma_{Z-H}}{\partial Z}\cdot\frac{\partial Z}{\partial\dot{\bar{\varepsilon}}} = \left[\alpha nA\left(\sinh\alpha\sigma_{Z-H}\right)^{n-1}\left(\cosh\alpha\sigma_{Z-H}\right)\right]^{-1}e^{\Delta H/GT} \tag{D.9}$$

$$\Rightarrow \frac{\partial\sigma_{Z-H}}{\partial\dot{\bar{\varepsilon}}} = \frac{\left(\tanh\alpha\sigma_{Z-H}\right)}{\alpha n\dot{\bar{\varepsilon}}} \tag{D.10}$$

Appendix E

Data file for Conform extrusion in 3D

```
!!!!!!!!!!!!!!!!!!!!!!!!!!!!!!!!!!!!!!!!!!!!!!!!!!!!!!!
! File Type:    FORGE3 V7.0 Data File                  !
! Creator:      GLPre Version 2, 3, 0, 26-Release      !
! Author:       Xavier Velay                           !
! Creation Date:        -                              !
! GLPre active language:English                        !
! System language:  English (United Kingdom)           !
! Data File Name:   no_flash.ref                       !
! Data File Location:D:\F3\Conform3Dghost.tsv\No_Flash\!
!!!!!!!!!!!!!!!!!!!!!!!!!!!!!!!!!!!!!!!!!!!!!!!!!!!!!!!

! ================================= OBJECTS Block
.OBJETS
     ProjectName = Conform3Dghost
     SimulationName = No_Flash
     Fout = no_flash.out
     Fres = results\no_flash.res
     Faux = results\no_flash.vtf
     NBSD = 1
     objet 1, NAME=feedstock
     objet 1, FMAY=feedstock.may
     objet 1, NomGen=results\feedstock_
     objet 1, rheol=1
     outil 1, NAME=shoe
     outil 2, NAME=die23
     outil 3, NAME=abutment
     outil 4, NAME=ram
     outil 5, NAME=ghost_die
.FIN OBJETS
!=================================

!================================= APPROXIMATION Block
.APPROXIMATION
     Periode_Meca = 1
.FIN APPROXIMATION
!=================================

!================================= UNITS Block
.UNITES
     MM-MPA-MM.KG.S
.FIN UNITES
!=================================
```

```
!============================== RHEOLOGY Block
.RHEOLOGIE
!!!!!!!!!!!!!!!!!!!!!
MATERIAU 1      ! (object feedstock)
!!!!!!!!!!!!!!!!!!!!!
      EVP
      LOIV SIG0
      ZENER-H
      PAR DH = 141550.d0
      PAR R = 8.314d0
      PAR alpha = 0.04d0
      PAR n = 5.385d0
      PAR A = 5910522063.02d0
      FIN LOI

      !Thermal coefficients
      mvolumique = 2.800000e-06 !Density
      cmassique = 1.230000e+09 !Specific Heat
      conductmat = 2.500000e+05 !Conductivity
      epsilon = 5.000000e-02 !Emissivity
!-------------------------------
OUTIL1          !shoe
      !Friction between deformable object and rigid die
      Tresca          ! Friction Law
      mbarre = 9.000000e-01

      !Thermal Exchange between part and rigid die
      ! Unit = si
      alphat      = 10.000000e+03    ! Transfert
coefficient
      Effus = 9.590E+03   ! tool effusivity

      Temp = 478.000000
FIN OUTIL
!-------------------------------

!-------------------------------
OUTIL2          !die23

      Tresca          ! Friction Law
      mbarre = 4.000000e-01

      !Thermal Exchange between part and rigid die
      ! Unit = si
      alphat      = 10.000000e+03    ! Transfert
coefficient
      Effus = 9.590E+03   ! tool effusivity

      Temp = 478.000000
FIN OUTIL
!-------------------------------
```

```
!--------------------------------
OUTIL3          !abutment
     !Friction between deformable object and rigid die
     Tresca          ! Friction Law
     mbarre = 9.000000e-01

     !Thermal Exchange between part and rigid die
     ! Unit = si
     alphat      = 10.000000e+03    ! Transfert
coefficient
     Effus = 9.590E+03    ! tool effusivity

     Temp = 478.000000
FIN OUTIL
!--------------------------------

!--------------------------------
OUTIL4          !ram
     !Friction between deformable object and rigid die
     Tresca          ! Friction Law
     mbarre = 9.000000e-01

     !Thermal Exchange between part and rigid die
     ! Unit = si
     alphat      = 10.000000e+03    ! Transfert
coefficient
     Effus = 9.590E+03    ! tool effusivity

     Temp = 478.000000
FIN OUTIL
!--------------------------------

!--------------------------------
OUTIL5          !ghost_die
     !Friction between deformable object and rigid die -
sliding
     Tresca          ! Friction Law
     mbarre = 0.0

     !Thermal Exchange between part and rigid die -
adiabatic
     ! Unit = si
     alphat      = 0.000000e+03     ! Transfert
coefficient
     Effus = 9.590E+03    ! tool effusivity

     Temp = 50.000000
FIN OUTIL
!--------------------------------
```

```
     !Thermal Exchange between deformable object and air
     AlphaText = 1.000000e+001          ! Global
Transfert Coeff.
     TempExt = 50.000000           ! Ambient Temperature

     ! Initial temperature has been set in mesh file:
already exists in mesh file
!!!!!!!!!!!!!!!!!!!!!
FIN MATERIAU
!!!!!!!!!!!!!!!!!!!!!
.FIN RHEOLOGIE
!====================================

!==================================== TOLERCONV Block
.TOLERCONV
.FIN TOLERCONV
!====================================

!==================================== INCREMENT Block
.INCREMENT
     Deformation= 1.000000e-002
.FIN INCREMENT
!====================================

!==================================== EXECUTION Block
.EXECUTION
     Inertia
     dhSto = 2.000000e+000
     Calcul Outillage
     NO Folds_Detection
.FIN EXECUTION
!====================================

!==================================== THERMAL Block
.THERMIQUE
.FIN THERMIQUE
!====================================

!==================================== MESH BOXES Block
.BOITE
OBJET1
   BOX 1
     Type=10          ! BOX
     Lagrangian
     Die= 1           !shoe
     Size= 2
     !Param Info: NbPar, Xmin, Ymin, Zmin, Length, Width,
Height
     Parameters:, 6, 0, 0, 0, 50, 27, 14
     Matrix:, 1, 0, 0, -2,
           0, 1, 0, -2,
```

```
            0, 0, 1, -12,
            0, 0, 0, 1
    END BOX
    BOX 2
      Type=20          ! CYLINDER
      Lagrangian
      Die= 1           !shoe
      Size= 0.4
      !Param Info: NbPar, Xcenter, Ycenter, Zcenter, Rext,
Rint, H
      Parameters:, 6, 0, 0, 0, 8, 0, 11
      Matrix:, 5.96046e-008, 0, 1, 19,
            0, 1, 0, 10,
            -1, 0, 5.96046e-008, 0,
            0, 0, 0, 1
    END BOX
FIN OBJET
.FIN BOITE
!================================

!================================ REMESHING Block
.MAUTO
OBJET1
     periode = 10
     lbase = 5
FIN OBJET
.FIN MAUTO
!================================

!================================ KINEMATICS Block
.CINEMAT_OUT
    Outil4        ! ram
      maitre
      Axe = 2
    Fin Outil
.FIN CINEMAT_OUT

.PILOT
NbPass= 1
    Pass1
    Fin Pass
.FIN PILOT
!================================
```

Appendix F

Properties, constants and parameters of some aluminium alloys for thermo-mechanical calculations

Properties	Value
Density ($kg.m^{-3}$)	*2700*
Density ($kg.m^{-3}$) AA6063[&]	*2810*
Poisson's ratio	*0.3*
Poisson's ratio AA6063[$]	*0.35*

Table F.1 Density and Poisson's ration from Macey and Salim (1988), Gasiorczyk and Richert (2000)[&], and Lof and Huétink (2000)[$]

Properties	Value
Heat transfer coefficient billet/tooling ($W.m^2.K^{-1}$)	*10000*
Heat transfer coefficient billet/air ($W.m^2.K^{-1}$)	*10*

Table F.2 Heat transfer coefficients from Dashwood *et al* (1996) and Gasiorczyk and Richert (2000)

Temperature (°C)	0	20	100	300	500	658
Temperature (K)	273	293	373	573	773	931
Specific heat (heat capacity) ($J.kg^{-1}.K^{-1}$)	-	*900*	*935*	*1020*	*1110*	*1130*
Specific heat (heat capacity) ($J.kg^{-1}.K^{-1}$) ($285T^{0.205}$)*	*900*	*913*	*960*	*1048*	*1114*	*1157*
Thermal conductivity ($W.m^{-1}.K^{-1}$)	-	*210*	*218*	*222*	*230*	*230*
Thermal conductivity ($W.m^{-1}.K^{-1}$) ($665T^{-0.17}$)*	*256*	*253*	*243*	*226*	*215*	*208*
Thermal expansion coefficient (10^{-6})	*23.4*	-	*23.4*	-	*27.0*	-
Thermal expansion coefficient (10^{-6}) ($1.02T^{0.142}$)*	*22.6*	*22.9*	*23.6*	*25.1*	*26.2*	*26.9*

Table F.3 Specific heat, thermal conductivity and thermal expansion coefficient from Mollerbernd *et al* (1996) and Macey and Salim (1988)*

Temperature (°C)	-29	24	100	204	450*	500[$]	600
Temperature (K)	244	297	373	477	723	773	873
Modulus of elasticity ($10^9.N.m\text{-}^2$)	*71.4*	*70.0*	*68.6*	*63.0*	*49.0*	*40.0*	*41.7*

Table F.4 Modulus of elasticity from Mollerbernd *et al* (1996), Macey and Salim (1988)*, and Lof and Huétink (2000)[$]

Constant	Value
a	0.171
b	1.86
c	0
d	1
i	38.7
j	6.9

Table F.5 Constant parameters for strain rate calculation with AA2014 (Peng *et Al* 2004)

parameters	value
C'/M_{GB}	$5x10^{9}$
C_d	$2.6x10^{-6}$
ε_δ	$7x10^{-10}Z$
D_0	$50\ \mu m$
G	$2.05x10^{10}$MPa
b	$2.86x10^{-10}$m
ρ_0	$10^{11}\ m^{-2}$
δ_0	10^{-6}m
θ_0	0°
ε_θ	$5x10^{-10}\ Z^{1/4}$
$1/R_g$	$5x10^{-4}\ m^{-1}$
C_1	$3x10^{7}\ m^{-1}$
C_2	$2.09x10^{12}\ Pa^{-1}s^{-1}$
D	2.347

Table F.6 Constants and parameters for the microstructural models (Duan and Sheppard 2003)

Appendix G

Supportive calculations for the temperature evolution of the feedstock in the groove

Calculation of the temperature of the surrounding air

Figure G.1 shows a schematic diagram of the groove.

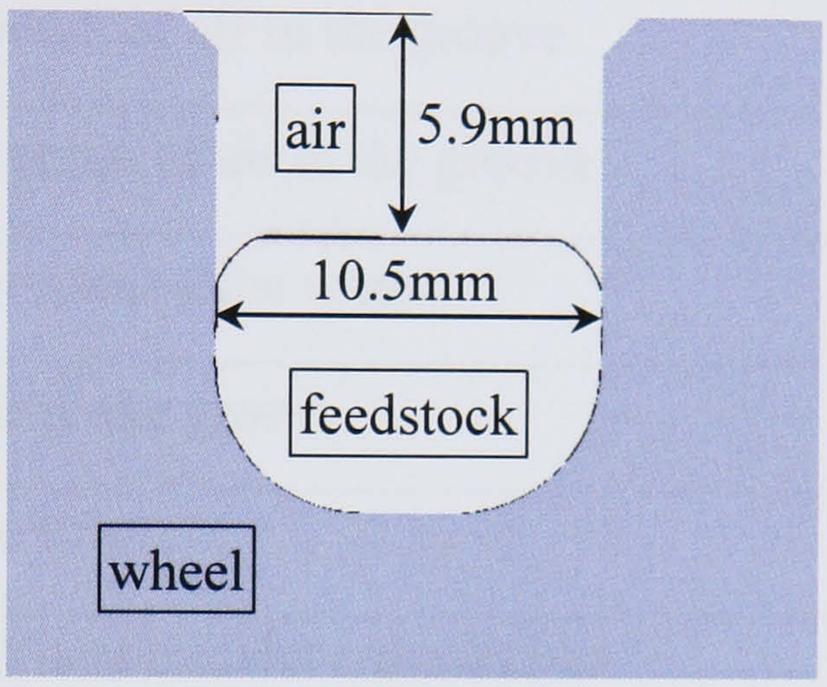

Figure G.1 Schematic diagram of the groove

It is assumed that the quantity of heat gained during a time t by the volume of air is equal to the heat transfer to the air by conduction during that time. Therefore the following equation, based on heat transfer theories, can be written:

$$C_{p(air)}\rho_{air}V_{air}(T_{fA}-T_{iA}) = tk_{air}A\frac{(T_{iW}-T_{fA})}{d} \qquad \text{(G.1)}$$

The parameters are listed in Table G.1.

Equation (G.1) can be re-formulated as follows:

$$T_{fA} = \frac{tk_{air}AT_{iW} + C_{p(air)}\rho_{air}V_{air}dT_{iA}}{tk_{air}A + C_{p(air)}\rho_{air}V_{air}d} \qquad \text{(G.2)}$$

By inputting the values from Table G.1 into the equation (G.2) the temperature of the air in the groove can be calculated as approximately 110°C.

Symbols	Description	Value
A	area of contact between the groove and air	$678.5\text{x}10^{-6}\text{m}^2$
$C_{p(air)}$	specific heat of air at 50°C with constant pressure	$1005\text{J.kg}^{-1}\text{.K}^{-1}$
d	half of the groove width	$5.25\text{x}10^{-3}\text{m}$
k_{air}	thermal conductivity of air at 50°C	$27.1\text{x}10^{-3}\text{W.m}^{-1}\text{K}^{-1}$
t	time	0.38s
T_{fA}	final temperature of air in the groove	to be calculated
T_{iA}	initial temperature of air in the groove	20°C
T_{iW}	initial temperature of the wheel	384°C
V_{air}	volume of air in the groove	$3.56\text{x}10^{-6}\text{m}^3$
ρ_{air}	air density at 50°C	1.127kg/m^3

Table G.1 Parameter for heat transfer calculations

Geometrical calculations of the coining process

Figure G.2 shows a schematic diagram of the coining process. The grey area represents the feedstock and the curved section a portion of the coining wheel. r_c is the radius of the coining roll, α is the angle of contact between the coining roll and the feedstock, and h is the height of the sector formed by the angle '$2\times\alpha$'.

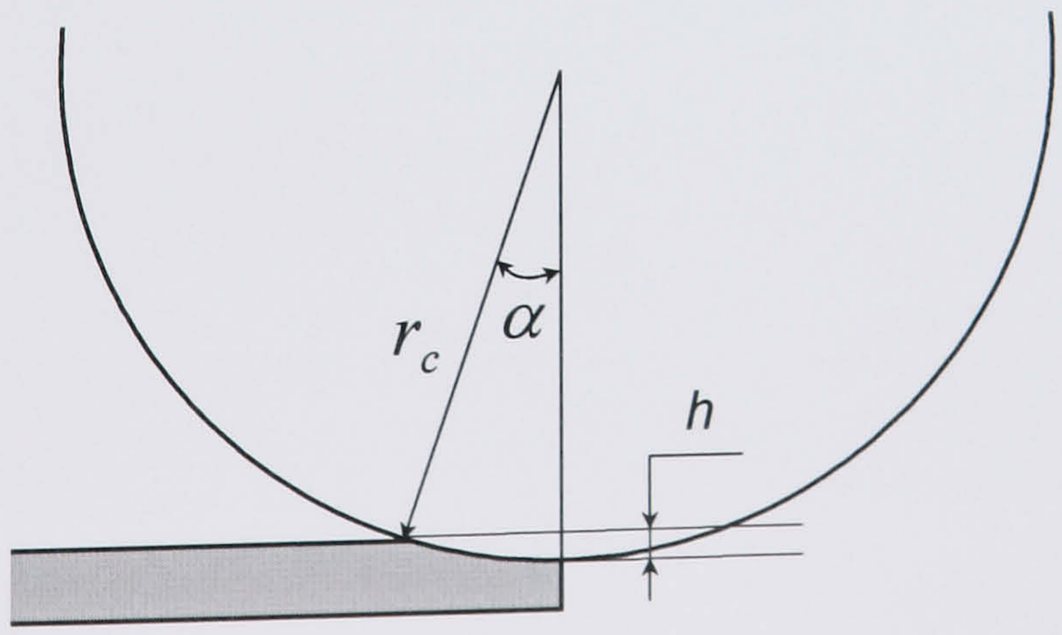

Figure G.2 Schematic diagram of the coining process

The following equation defines the height, h:

$$h = 2r_c(1 - COS\alpha) \tag{G.3}$$

therefore

$$\alpha = ACOS\left(1 - \frac{h}{2r_c}\right) \tag{G.4}$$

With $h = 2.1\text{mm}$ and $r_c = 66\text{mm}$, $\underline{\alpha = 10.23°}$.

References

ABTAHI, S., WELO, T. AND STOREN, S., 1996. Interface mechanism on the bearing surface in extrusion. In: *6th International aluminium extrusion technology seminar*, 14-17 May 1996 Chicago. Washington: Aluminium association and aluminium extruder councils, 2, 125-131.

ALTAN, T., THOMAS, W., VAZQUEZ, V. AND KOC, M., 1999. Simulation of metal forming processes - applications and future trends. In: M. GEIGER, ed. *6th International Conference on technology of plasticity*, 19-24 September 1999 Nuremberg. Berlin: Springer, 1, 23-40.

AZARKHIN, A. AND RICHMOND, O., 1992. Limits to adhesive friction. In: J.-L. CHENOT, R. D. WOOD AND O. C. ZIENKIEWICZ, eds. *Numerical methods in industrial forming processes Numiform 92*, Rotterdam: Balkema, 143-148.

BARRON, B. AND LARRICK, T., 2004. Thermal management practices for aluminium extrusion. In: *8th International aluminum extrusion technology seminar*, 18-21 May 2004 Orlando. Illinois: Extrusion technology for aluminum profiles foundation, 1, 209-215.

BAY, N., WANHEIM, T., RAVN, B. G. AND ARENTOFT, M., 1999. Examples on European industrial research on bulk metal forming. In: M. GEIGER, ed. *6th International Conference on technology of plasticity,* 19-24 September 1999 Nuremberg. Berlin: Springer, 1, 49-68.

BEHRENS, A. AND SCHAFSTALL, H., 1999. FE-process-simulation of cold forging processes with adaptive friction factors. In: M. GEIGER, ed. *6th International Conference on technology of plasticity*, 19-24 September 1999 Nuremberg. Berlin: Springer, 1, 323-328.

BEREZHNOY, V. L., HAHN, K. H. AND CHANG, J. Y., 1999. Extrusion defects: conditions of formation and methods of prevention. *Light metal age*, April 1999, 66-74.

BHATTACHARYYA, A., EL-DANAF, E., KALIDINDI, S. R. AND DOHERTY, R. D., 2001. Evolution of grain-scale microstructure during large strain simple compression of polycrystalline aluminum with quasi-columnar grains: OIM measurements and numerical simulations. *International journal of plasticity*, 17, 861-883.

BIRKENSTOCK, A., LINDNER, K-H. AND SUCKE, N-W., 2004. Manufacturing process of curved extrusions for aluminum. In: *8th International aluminum extrusion technology seminar*, 18-21 May 2004 Orlando. Illinois: Extrusion technology for aluminum profiles foundation, 2, 427-436.

BOCHMANN, E. AND DOEGE, E., 1992. Friction as a critical phenomenon in the simulation of metal forming. In: J.-L. CHENOT, R. D. WOOD AND O. C. ZIENKIEWICZ, eds. *Numerical methods in industrial forming processes Numiform 92*. Rotterdam: Balkema, 415-419.

BOURQUI, B., KRAHENBUHL, Y. AND FIETIER, N., 2004. Integration of 3-D finite element flow modeling in extrusion tool conception and fabrication . In: *8th International aluminum extrusion technology seminar*, 18-21 May 2004 Orlando. Illinois: Extrusion technology for aluminum profiles foundation, 2, 241-246.

BRIDGEWATER, M. AND MADDOCK, B., 1996. New developments in conform technology for continuous extrusion. In: *6th International aluminium extrusion technology seminar*, 14-17 May 1996 Chicago. Washington: Aluminium association and aluminium extruder councils, 2, 413-419.

BUNTORO, B. AND MULLER, K.B., 2004. Production of high-curved extruded profiles directly during the extrusion process. In: *8th International aluminum extrusion technology seminar*, 18-21 May 2004 Orlando. Illinois: Extrusion technology for aluminum profiles foundation, 2, 437-445.

CALISKANOGLU, D., AL BAOUNI, M., VOLLES, R., LEISTEN, B., LEITNER, H., EBNER, R. AND KOPP, R., 2002. Influence of the heat-transfer-coefficient on the temperature stress of hot forming tools. In: *Friction and wear in metal forming*, 18-20 June 2002 Valenciennes. Valenciennes: Euromech 435, 201-208.

CARR, N., AHMAD, H. Y. AND CLODE, M. P., 1996. Simulation and analysis of deformation in conform extrusion. In: *6th International aluminium extrusion technology seminar*, 14-17 May 1996 Chicago. Washington: Aluminium association and aluminium extruder councils, 2, 441-448.

CASTLE, A. F., 1992. Temperature control in aluminium extrusion. In: *5th International aluminium extrusion technology seminar*, May 1992 Chicago. Washington: Aluminium association and aluminium extruder councils, 1, 181-184.

CASTLE, A. F., 2000. The metallurgy of the extrusion die. In: *7th International aluminium extrusion technology seminar*, 16-19 May 2000 Chicago. Washington: Aluminium association and aluminium extruder councils, 2, 265-271.

CASTLE, A.F. AND SHEPPARD, T., 1976. Pressure required to initiate extrusion in some Al-alloys. *Metals Technology*, 2, 465-475.

CASTLE, A.F., 1976. *Continuum and structural aspects of aluminium extrusion.* Thesis (PhD). University of London. 202-207.

CERETTI, E., GIARDINI, C., MACCARINI, G. AND BUGINI, A., 1999. Process optimization and defects analysis in reverse extrusion through FEM simulations and experimental tests. In: M. GEIGER, ed. *6th International Conference on technology of plasticity*, 19-24 September 1999 Nuremberg. Berlin: Springer, 3, 1819-1824.

CHANDA, T., ZHOU, J. AND DUSZCZYK, J., 2001. Application of three-dimensional numerical simulation to analysis of development of deformation zone at beginning of aluminium extrusion process. *Materials science and technology*, 17, 70-74.

CHENOT, J.-L., COUPEZ, T., FOURMENT, L., DUCLOUX, R. AND WEY, E., 1999. Practical simulation of forging sequence of complex 3-D parts in industry. In: M. GEIGER, ed. *6th International Conference on technology of plasticity*, 19-24 September 1999 Nuremberg. Berlin: Springer, 3, 1597-1612.

CHENOT, J.L., FOURMENT, L., COUPEZ, T., DUCLOUX, R. AND WEY, E., 1998. *Forge 3 - a general tool for practical optimization of forging sequence of complex three-dimensional parts in industry*. London, UK: IMechE (C546/033/98)

CHO, J. R. AND JEONG, H. S., 2000. Parametric investigation on the surface defect occurrence in CONFORM process by the finite element method. *Journal of materials processing technology*, 104, 236-243.

CLIFT, S. E., HARTLEY, P., STURGESS, C. E. N. AND ROWE, G. W., 1990. Fracture prediction in plastic deformation processes. *International journal of mechanical sciences*, 32 (1), 1-7.

CLODE, M. P., 1992a. Material flow and microstructural development during extrusion of AA6063. In: *5th International aluminium extrusion technology seminar*, May 1992 Chicago. Washington: Aluminium association and aluminium extruder councils, 2, 79-99.

CLODE, M. P., 1992b. The development of microstructure and the consolidation of RSP aluminium alloys in conform extrusion. In: *5th International aluminium extrusion technology seminar*, May 1992 Chicago. Washington: Aluminium association and aluminium extruder councils, 1, 427-438.

COCKROFT, M. G. AND LATHAM, D. J., 1968. Ductility and the workability of metals. *Journal of the institute of metals*, 96, 33-39.

COUPEZ, T., 1994. A mesh improvement method for 3D automatic remeshing. In: N.P. WEATHERHILL et Al, ed. *Numerical grid generation in computational fluid dynamics and related fields*. Melksham: Cromwell Press, 615-626.

COUPEZ, T., MARIE, S. AND DUCLOUX, R., 1996. Parallel 3D simulation of forming processes including parallel remeshing and reloading. *Numerical methods in engineering*. Published 1996 by John Wiley & Sons Ltd. in Numer. Meth. in Eng. , Désidéri and al., eds. , ECCOMAS, Wiley and Sons, 1996, pp. 738-743.

CRAMLET, A., HENZ, B., PEARSON, B. AND COVEY, S., 2000. Smart quenching. In: *7th International aluminium extrusion technology seminar*, 16-19 May 2000 Chicago. Washington: Aluminium association and aluminium extruder councils, 1, 89-97.

DAIL, G.J., 2004. The analysis of a fatigue failure of a large indirect aluminum extrusion press container mantle. In: *8th International aluminum extrusion technology seminar*, 18-21 May 2004 Orlando. Illinois: Extrusion technology for aluminum profiles foundation, 1, 295-302.

DASHWOOD, R. J., MCSHANE, H. B. AND JACKSON, A., 1996. Computer prediction of extrusion limit diagrams. In: *6th International aluminium extrusion technology seminar*, 14-17 May 1996 Chicago. Washington: Aluminium association and aluminium extruder councils, 1, 331-339.

DAWSON, J. R., 1996. Development of conform technology for the manufacture of multi-port tube. In: *6th International aluminium extrusion technology seminar*, 14-17 May 1996 Chicago. Washington: Aluminium association and aluminium extruder councils, 2, 435-439.

DESPOY, J. J., KELLY, R. M. AND MC KAY, J. D., 1988. The advantages of aluminium extrusions compared with some competitive materials and methods of forming. In: *4th International aluminium extrusion technology seminar*, 11-14 April 1988 Chicago. Washington: Aluminium association and aluminium extruders council, 1, 445-450.

DION, G. W., 1988. The contribution of the die to surface quality. In: *4th International aluminium extrusion technology seminar*, 11-14 April 1988 Chicago. Washington: Aluminium association and aluminium extruder councils, 1, 13-16.

DOMANTI, A. D. J., HORROBIN, D. J. AND BRIDGEWATER, J., 2002. An investigation of fracture criteria for predicting surface fracture in paste extrusion. *International journal of mechanical sciences*, 44, 1381-1410.

DUAN, X, VELAY, X. AND SHEPPARD, T., 2004b. Application of finite element method in the hot extrusion of aluminium alloys. *Material science and engineering*, A369, 66-75.

DUAN, X, VELAY, X. AND SHEPPARD, T., 2004c. Prediction and control of subgrain size in the hot extrusion of aluminium alloys. In: S. GHOSH, J.M. CASTRO AND J.K. LEE eds. *Numiform 2004 Materials processing and design: modeling, simulation and applications*, 13-17 June 2004 Ohio. New York, American Institute of Physics, 428-433.

DUAN, X. AND SHEPPARD, T., 2002a. Influence of forming parameters on static recrystallization behaviour during hot rolling aluminium alloy 5083. *Modelling and simulation in materials science and engineering*, 10, 363-380.

DUAN, X. AND SHEPPARD, T., 2002b. Influence of forming parameters on the final subgrain size during hot rolling of alluminium alloys. *Journal of materials processing technology*, 130-131, 245-249.

DUAN, X. AND SHEPPARD, T., 2003. Simulation and control of microstructure evolution during hot extrusion of hard aluminium alloys. *Materials science and engineering A*, 351, 282-292.

DUAN, X., SHEPPARD, T. AND VELAY, X., 2004a. Prediction of flow stress and recrystallization by the finite element method during the hot extrusion of aluminum alloys. In: *8th International aluminum extrusion technology seminar*, 18-21 May 2004 Orlando. Illinois: Extrusion technology for aluminum profiles foundation, 1, 149-158.

DUPLANCIC, I., MIOC, M. AND BRACIC, Z., 2000. Case studies on control of metal flow in pre-chamber dies. In: *7th International aluminium extrusion technology seminar*, 16-19 May 2000 Chicago. Washington: Aluminium association and aluminium extruder councils, 2, 177-186.

ETHERINGTON, C. AND SLATER, H. K., 1984. The extrusion of aluminium and its alloys by the CONFORM process. In: *3rd International aluminium extrusion technology seminar*, 24-26 April 1984 Atlanta. Washington: Aluminium association and aluminium extruder councils, 2, 31-38.

ETHERINGTON, C., 1977a. The UKAEA Conform method of continuous extrusion forming - Part 1. *Wire Industry*, 2, 85-89.

ETHERINGTON, C., 1977b. The UKAEA Conform method of continuous extrusion forming - Part 2. *Wire Industry*, 3, 161-163.

FALK, B., ENGEL, U. AND GEIGER, M., 1998. Estimation of tool life in bulk metal forming based on different failure concepts. *Journal of materials processing technology*, 80-81, 602-607.

FINKELNBURG, W. D. AND SCHARF, G., 1992. Some investigations on the metal flow during extrusion of Al Alloys. In: *5th International aluminium extrusion technology seminar*, May 1992 Chicago. Washington: Aluminium association and aluminium extruder councils, 1, 475-484.

FLITTA, I. AND SHEPPARD, T., 2000. Material flow and prediction of extrusion pressure when extruding through bridge dies using FEM. In: *7th International aluminium extrusion technology seminar*, 16-19 May 2000 Chicago. Washington: Aluminium association and aluminium extruder councils, 1, 141-147.

FLITTA, I. AND SHEPPARD, T., 2003. Nature of friction in extrusion process and its effect on material flow. *Materials science and technology*, 19, 837-846.

FURU, T., PEDERSEN, K., WELO, T. AND ABTAHI, S., 1996. Microstructurally based modelling applied to cold extrusion of aluminum. In: *6th International aluminium extrusion technology seminar*, 14-17 May 1996 Chicago. Washington: Aluminium association and aluminium extruder councils, 1, 341-347.

GRASMO, G., HOLTHE, K., STOREN, S., VALBERG, H., FLATVAL, R., HANSSEN, L., LEFSTAD, M., LOHNE, O., WELO, T., ORSUND, R. AND HERBERG, J., 1992. Modelling of two-dimensional extrusion. In: *5th International aluminium extrusion technology seminar*, May 1992 Chicago. Washington: Aluminium association and aluminium extruder councils, 2, 367-376.
GREEN, D., 1972. Continuous extrusion-forming of wire sections. *Journal of the institute of metals*, 100, 295-300.

GROENBAEK, J., BIRKER, T. AND PEDERSEN, T. O., 1999. Optimisation of life performance and net-shape capability of cold-forging tools through minimisation of micro-plastic phenomena. In: M. GEIGER, ed. *6th International Conference on technology of plasticity*, 19-24 September 1999 Nuremberg. Berlin: Springer, 1,243-252.

HAEPP, H.-J. AND ROLL, K., 1999. Future perspectives and limits for the mathematical modelling of metal forming processes in automotive industry. In: M. GEIGER, ed. *6th International Conference on technology of plasticity*, 19-24 September 1999 Nuremberg. Berlin: Springer, 1, 481-488.

HALVORSEN, F. AND AUKRUST, T., 2004. Studies of the effects of flow imbalance on shape variations in aluminum extrusion by use of Lagrangian FEM software. In: *8th International aluminum extrusion technology seminar*, 18-21 May 2004 Orlando. Illinois: Extrusion technology for aluminum profiles foundation, 1, 243-251.

HARRIS, C., LI, Q. AND JOLLY, M.R., 2004. Prediction of extruded microstructures using experimental and numerical modelling techniques. In: *8th International aluminum extrusion technology seminar*, 18-21 May 2004 Orlando. Illinois: Extrusion technology for aluminum profiles foundation, 1, 159-167.

HAYAKAWA, K., NAKAMURA, T. AND TANAKA, S., 1999. Damage and fracture analysis of extrusion dies by local approach with continuum damage mechanics. In: M. GEIGER, ed. *6th International Conference on technology of plasticity*, 19-24 September 1999 Nuremberg. Berlin: Springer, 1, 259-264.

HERTZBERG, R.W., 1996. *Deformation and fracture mechanics of engineering materials*. New York: John Wiley & Sons.

HOSFORD, W.F. AND CADDELL, R.M., 1983. *Metal forming mechanics and metallurgy*. New Jersey, Prentice-Hall International.

HOU, J., BENGTSSON, B. AND LINDQVIST, H., 2000. FE-analysis of inward flow of surface materials at the back end of billet during Al-extrusion. In: *7th International aluminium extrusion technology seminar*, 16-19 May 2000 Chicago. Washington: Aluminium association and aluminium extruder councils, 1, 149-158.

HU, Z. M., PORNBENJAPAKKUL, V. AND DEAN, T. A., 1999. Tool/workpiece interface interaction and its influence on metal forming processes. In: M. GEIGER, ed. *6th International Conference on technology of plasticity*, 19-24 September 1999 Nuremberg. Berlin: Springer, 1, 317-322.

HUETINK, J. AND VAN DER HELM, P. N., 1992. On Euler-Lagrange finite element formulation in forming and fluid problems. In: J.-L. CHENOT, R. D. WOOD AND O. C. ZIENKIEWICZ, eds. *Numerical methods in industrial forming processes Numiform 92*. Rotterdam: Balkema, 45-54.

JACKSON, A. AND SHEPPARD, T., 1996. Structural modifications occurring during homogenization of some 7xxx alloys. In: *6th International aluminium extrusion technology seminar*, 14-17 May 1996 Chicago. Washington: Aluminium association and aluminium extruder councils, 1, 541-550.

JARRETT, M. AND PARSON, N. C., 1995. *Extrusion method*. UK patent GB2285941.

JIA, Z., GUNASEKERA, J. S. AND MALAS, J. C., 1996. Application of upper bound element technique (UBET) for aluminum extrusion. In: *6th International aluminium extrusion technology seminar*, 14-17 May 1996 Chicago. Washington: Aluminium association and aluminium extruder councils, 2, 247-252.

JOWETT, C., JOHANNES, V., LANGILLE, A. I., FRASER, W. AND YOSHIMURA, H., 2000b. The causes of variation in extruded section weight. In: *7th International aluminium extrusion technology seminar*, 16-19 May 2000 Chicago. Washington: Aluminium association and aluminium extruder councils, 1, 1-15.

JOWETT, C., PARSON, N., AND FRASER, W., 2000a. Simulation of billet surface into the extruded product. In: *7th International aluminium extrusion technology seminar*, 16-19 May 2000 Chicago. Washington: Aluminium association and aluminium extruder councils, 1, 27-42.

JOWETT, C.W., HAY, G. AND PARSON, N., 2004. Upset. .In: *8th International aluminum extrusion technology seminar*, 18-21 May 2004 Orlando. Illinois: Extrusion technology for aluminum profiles foundation, 1, 23-37.

KHAWAJA, K. A., SMITH, M. J., MADDOCK, B., SENEVIRATNE, L. D., LAKMAL, D. AND CLODE, M. P., 2000. Extrusion zone gap measurement and control of the conform process. In: *7th International aluminium extrusion technology seminar*, 16-19 May 2000 Chicago. Washington: Aluminium association and aluminium extruder councils, 1, 495-501.

KIM, Y. H., CHO, J. R., KIM, K. S., JEONG, H. S. AND YOON, S. S., 2000. A study of the application of upper bound method to the CONFORM process. *Journal of materials processing technology*, 97, 153-157.

KLEINER, M., SCHOMAECKER, M., SCHIKORRA, M. AND KLAUS, A., 2004. Manufacture of continuously reinforced profiles using standard 6060 billets. In: *8th International aluminum extrusion*

technology seminar, 18-21 May 2004 Orlando. Illinois: Extrusion technology for aluminum profiles foundation, 2, 461-468.

KO, D. C., KIM, B. M. AND CHOI, J. C., 1996. Prediction of surface fracture initiation in the axisymmetric extrusion and simple upsetting of an aluminium alloy. *Journal of materials processing technology*, 62 (1-3), 166-174.

KOBAYASHI, S., OH, S. AND ALTA, T., 1989. *Metal forming and the finite element method.* New York: Oxford University press.

KOCANDA, A., 1999. On performance and strength of metal forming tools subjected to local plastic strains under loading. In: M. GEIGER, ed. *6th International Conference on technology of plasticity*, 19-24 September 1999 Nuremberg. Berlin: Springer, 1, 281-290.

KONIG, M. AND MUSCHALIK, U., 2004. Special purpose extrusion press for the production of curved profiles. In: *8th International aluminum extrusion technology seminar*, 18-21 May 2004 Orlando. Illinois: Extrusion technology for aluminum profiles foundation, 1, 339-344.

KUSIAK, J., LIBURA, W., PIETRZYK, M. AND MISIOLEK, W. Z., 1996. Application of the finite-element technique to the simulation of the aluminium extrusion process. In: *6th International aluminium extrusion technology seminar*, 14-17 May 1996 Chicago. Washington: Aluminium association and aluminium extruder councils, 1, 361-367.

LANGERWEGER, J. AND MADDOCK, B., 1988. Recent developments in conform and castex continuous extrusion technology. In: *4th International aluminium extrusion technology seminar*, 11-14 April 1988 Chicago. Washington: Aluminium association and aluminium extruder councils, 1, 533-538.

LEA, G. AND JOWETT, C., 2004. The effect of die type and die design on heat generation and productivity when extruding AlMgSi alloys. In: *8th International aluminum extrusion technology seminar*, 18-21 May 2004 Orlando. Illinois: Extrusion technology for aluminum profiles foundation, 2, 251-260.

LEFSTAD, M., 1988. Die temperatures in aluminium extrusions. In: *4th International aluminium extrusion technology seminar*, 11-14 April 1988 Chicago. Washington: Aluminium association and aluminium extruder councils, 1, 297-301.

LI, Q., SMITH, C. J., HARRIS, C. AND JOLLY, M. R., 2003a. Finite element investigations upon the influence of pocket die designs on metal flow in aluminium extrusion part 1. Effect of pocket angle and volume on metal flow. *Journal of materials processing technology*, 135, 189-196.

LI, Q., SMITH, C. J., HARRIS, C. AND JOLLY, M. R., 2003b. Finite element modelling investigations upon the influence of pocket die designs on metal flow in aluminium extrusion part 2. Effect of pocket geometry configurations on metal flow. *Journal of materials processing technology*, 135, 197-203.

LIBURA, W., RICHERT, J., PACANOWSKI, J. AND SENDERSKI, J., 2000. Temperature-speed parameters in extrusion of thin-walled sections from aluminium alloys. In: *7th International aluminium extrusion technology seminar*, 16-19 May 2000 Chicago. Washington: Aluminium association and aluminium extruder councils, 1, 277-280.

LIN, Y.T. AND WANG, J.P., 1992. A coupled analysis of visioplasticity in plane extrusion with the flow-function elemental technique. *Journal of materials processing technology*, 35, 151-163.

LINDVIKSMOEN, P. AND RYSTAD, S., 1996. Simulation of tube extrusion in a two-dimensional, axisymmetric model. In: *6th International aluminium extrusion technology seminar*, 14-17 May 1996 Chicago. Washington: Aluminium association and aluminium extruder councils, 1, 369-373.

LISCOMB, R., 2004. Die design - the next generation. In: *8th International aluminum extrusion technology seminar*, 18-21 May 2004 Orlando. Illinois: Extrusion technology for aluminum profiles foundation, 2, 247-250.

LOF, J., HUETINK, J. AND NILSEN, K. E., 2000a. FEM simulations of the material flow in the bearing area of the aluminum extrusion process. In: *7th International aluminium extrusion technology seminar*, 16-19 May 2000 Chicago. Washington: Aluminium association and aluminium extruder councils, 2, 211-222.

LOF, J., KLASEBOER, G., HUETINK, J. AND KOENIS, P. T. G., 2000b. FEM simulations of aluminum extrusion using an elasto-viscoplastic material model. In: *7th International aluminium extrusion technology seminar*, 16-19 May 2000 Chicago. Washington: Aluminium association and aluminium extruder councils, 2, 157-168.

MADDOCK, B., 2000. The structure and development of a computer model to simulate the conform process. In: *7th International aluminium extrusion technology seminar*, 16-19 May 2000 Chicago. Washington: Aluminium association and aluminium extruder councils, 1, 519-526.

MAIER, J., 2004. CVD coating technology for increased lifetime of aluminum extrusion dies. In: *8th International aluminum extrusion technology seminar*, 18-21 May 2004 Orlando. Illinois: Extrusion technology for aluminum profiles foundation, 2, 351-356.

MANNINEN, T., RAMSAY, P. AND KORHONEN, A.S., 2002. Three-Dimensional Numerical Modeling of Continuous Extrusion. In : N. KIUCHI, H. NISHIMURA AND J. YANAGIMOTO eds. *7th International Conference on Technology of Plasticity*. 27 October - 1 November 2002 Yokohama. Japan: Japan Society for Technology of Plasticity, 439-444.

MARTHINSEN, K. AND NES, E., 2001. Modelling strain hardening and steady state deformation of Al-Mg alloys. *Materials science and technology*, 17, 376-388.

MASON, W. J., 1988. Die correction, weld plate and pocket dies. In: *4th International aluminium extrusion technology seminar*, 11-14 April 1988 Chicago. Washington: Aluminium association and aluminium extruder councils, 1, 21-23.

MC CAFFREY, T. J., 1988. A new hot work die steel for aluminium extrusion tooling. In: *4th International aluminium extrusion technology seminar*, 11-14 April 1988 Chicago. Washington: Aluminium association and aluminium extruder councils, 1, 127-130.

MOE, P.T., LEFSTAD, M., FLATVAL, R. AND STOREN, S., 2003. Measurement of temperature and die face pressure during hot extrusion of aluminium. *International journal of forming processes*, 6 (3), 241-270.

MOLYNEUX, R. H., 1988. Present capability and future potential of the CONFORM/CONKLAD universal machine. In: *4th International aluminium extrusion technology seminar*, 11-14 April 1988 Chicago. Washington: Aluminium association and aluminium extruder councils, 1, 553-561.

MOOI, H. G., DEN BAKKER, A. J., NILSEN, K. E. AND HUETINK, J., 1996. Simulation of aluminium extrusion based on a finite element method (FEM). In: *6th International aluminium extrusion technology seminar*, 14-17 May 1996 Chicago. Washington: Aluminium association and aluminium extruder councils, 2, 67-73.

MOOI, H.,1996. *Finite element simulations of aluminium extrusion.* Thesis (PhD). University of Twente. 7-8.

NES, E., VATNE, H.E., DAALAND, O., FURU, T., ORSUND, R. AND MARTHINSEN, K., 1994. *Physical modelling of microstructural evolution during thermomechanical processing of aluminium alloys*. Trondheim, Norway: SINTEF (STF24 S94003).

PARKINSON, R. D., 1988. The technical development of a new extrusion company solely using conform machines. In: *4th International aluminium extrusion technology seminar*, 11-14 April 1988 Chicago. Washington: Aluminium association and aluminium extruders council, 1, 545-552.

PARSON, N. C., HANKIN, J. D. AND BRYANT, A. J., 1992. The metallurgical background to problems occurring during the extrusion of 6XXX alloys. In: *5th International aluminium extrusion technology seminar*, May 1992 Chicago. Washington: Aluminium association and aluminium extruder councils, 1, 13-23.

PARSON, N. C., JOWETT, C. W., FRASER, W. C. AND PELOW, C. V., 1996. Surface defects on 6XXX alloy extrusions. In: *6th International aluminium extrusion technology seminar*, 14-17 May 1996 Chicago. Washington: Aluminium association and aluminium extruder councils, 1, 57-67.

PARSON, N., BARKER, S., SHALANSKI, A. AND JOWETT, C., 2004. Control of grain structure in AI-Mg-Si extrusions. In: *8th International aluminum extrusion technology seminar*, 18-21 May 2004 Orlando. Illinois: Extrusion technology for aluminum profiles foundation, 1, 11-22.

PAUSKAR, P. AND SHIVPURI, R., 1999. An integrated approach to modeling metal flow and microstructural evolution in hot rolling. In: *M. GEIGER, ed. 6th International Conference on technology of plasticity*, 19-24 September 1999 Nuremberg. Berlin: Springer, 3, 1967-1973.

PENG, Z. AND SHEPPARD, T., 2004. Prediction of static recrystallization during shaped extrusion. In: *8th International aluminum extrusion technology seminar*, 18-21 May 2004 Orlando. Illinois: Extrusion technology for aluminum profiles foundation, 1, 79-91.

PENG, Z., SHEPPARD, T. AND VELAY, X., 2004. A discussion on the scaling effect on numerical simulation of the extrusion process. *Material science and technology*, 20, 1335-1339.

PHAM, V. H., 1992. Heat transfer model for temperature profile of extruded sections at the extrusion press exit. In: *5th International aluminium extrusion technology seminar*, May 1992 Chicago. Washington: Aluminium association and aluminium extruder councils, 1, 341-352.

PYE, D., 1996. A review of surface modification techniques for pre-heat- treated H.13 extrusion dies and emerging technologies. In: *6th International aluminium extrusion technology seminar*, 14-17 May 1996 Chicago. Washington: Aluminium association and aluminium extruder councils, 2, 197-200.

RAGGENBASS, A. AND REISSNER, J., 2000. Computer-based design of extrusion tools. In: *7th International aluminium extrusion technology seminar*, 16-19 May 2000 Chicago. Washington: Aluminium association and aluminium extruder councils, 2, 187-194.

RICHARDS, P. J. AND BHATTACHARYYA, D., 1996. Numerical modeling of metal extrusion using phoenics with viscosity varying in the deformation zone. In: *6th International aluminium extrusion technology seminar*, 14-17 May 1996 Chicago. Washington: Aluminium association and aluminium extruder councils, 2, 359-366.

ROYSET, J., BJORNBAKK, E. B., NYBORG, T., REISO, O., SAETER, J. A.,TUNDAL, U., DONS, A. L. AND HAGELIEN, 2004. Almech - a computer program for alloy selection and extrusion process improvement. In: *8th International aluminum extrusion technology seminar*, 18-21 May 2004 Orlando. Illinois: Extrusion technology for aluminum profiles foundation, 2, 81-91.

RUTTIMANN, B.G., 2004. The effects of globalization on the aluminum extrusion industry. In: *8th International aluminum extrusion technology seminar*, 18-21 May 2004 Orlando. Illinois: Extrusion technology for aluminum profiles foundation, 1, 463-478.

SAHA, P. K., 1996. Influence of plastic strain and strain rate on temperature rise in aluminium extrusion. In: *6th International aluminium extrusion technology seminar*, 14-17 May 1996 Chicago. Washington: Aluminium association and aluminium extruder councils, 1, 355-360.

SAHA, P. K., 2000. *Aluminium extrusion technology*. Materials park, Ohio: ASM International.

SAHA, P.K., 2004. Use of tribology to improve performance and quality in aluminum extrusion. In: *8th International aluminum extrusion technology seminar*, 18-21 May 2004 Orlando. Illinois: Extrusion technology for aluminum profiles foundation, 2, 277-287.

SAITO, Y., UTSUNOMIYA, H. AND SUZUKI, H., 1999. Proposal of novel continuous high straining process-development of conshearing process. In: M. GEIGER, ed. *6th International Conference on technology of plasticity*, 19-24 September 1999 Nuremberg. Berlin: Springer, 3, 2459-2464.

SANDBERG, O., 1988. A new hot-work steel for improved tool performance in aluminium extrusion. In: *4th International aluminium extrusion technology seminar*, 11-14 April 1988 Chicago. Washington: Aluminium association and aluminium extruder councils, 1, 121-126.

SANO, H., ISHIKAWA, T. AND YOSHIDA, Y., 2004. Study on metal flow in extruded billet. In: *8th International aluminum extrusion technology seminar*, 18-21 May 2004 Orlando. Illinois: Extrusion technology for aluminum profiles foundation, 1, 47-53.

SARRAZIN, E., CESCUTTI, J. P., ALEXANDRE, J. AND MAGNIN, B., 2000. 3-D modeling strength of an industrial porthole die. In: *7th International aluminium extrusion technology seminar*, 16-19 May 2000 Chicago. Washington: Aluminium association and aluminium extruder councils, 2, 229-238.

SCHEY, J.A., 1983, *Tribology in metalworking: friction, lubrification and wear*. Ohio: ASM International.

SELLARS, C.M. AND ZHU, Q., 2000. Microstructural modelling of aluminium alloys during thermomechanical processing. *Material science and engineering*, A280, 1-7.

SHCHERBA, V. N., OVECHKIN, V. V., ALFEROV, V. N. AND SPICHAK, M. G, 2000. Extrusion of high-performance shapes out of hard deformable aluminium alloys by friction-assisted extrusion method. In: *7th International aluminium extrusion technology seminar*, 16-19 May 2000 Chicago. Washington: Aluminium association and aluminium extruder councils, 1, 343-356.

SHEPPARD, T. AND CLODE, M. P., 1988. The origin of surface defects during extrusion of AA6063 alloy. In: *4th International aluminium extrusion technology seminar*, 11-14 April 1988 Chicago. Washington: Aluminium association and aluminium extruder councils, 2, 329-341.

SHEPPARD, T. AND DUAN, X., 2002. Modelling of static recrystallization by combining FEM with empirical models. *Journal of materials processing technology*, 130-131, 250-253.

SHEPPARD, T. AND JACKSON, A., 1997. Constitutive equations for use in prediction of flow stress during extrusion of aluminium alloys. *Materials science and technology*, 13, 203-209.

SHEPPARD, T. AND WRIGHT, D.S., 1979. Determination of the constitutive equation for aluminium alloys at elevated temperatures. *Metals Technology*, 6, 215-223.

SHEPPARD, T., 1993. The extrusion of AA2024 alloy. *Material science technology*, 9, 430-440.

SHEPPARD, T., 1996. Development of structure, recrystallization kinetics and prediction of recrystallized layer thickness in some Al-alloys. In: *6th International aluminium extrusion technology seminar*, 14-17 May 1996 Chicago. Washington: Aluminium association and aluminium extruder councils, 1, 163-170.

SHEPPARD, T., 1999a. *Extrusion of aluminium alloys*. Dordrecht, The Netherlands: Kluwer Academic Publishers.

SHEPPARD, T., 1999b. Temperature changes occurring during extrusion of metals: comparisons of bulk, numerical, and integral profile predictions with experimental data. *Material science and technology*, 15, 459-463.

SHEPPARD, T., 2000. On the relationship between extrusion conditions, mechanical properties, and surface acceptability in some hard aluminium alloys. In: *7th International aluminium extrusion technology seminar*, 16-19 May 2000 Chicago. Washington: Aluminium association and aluminium extruder councils, 1, 307-321.

SHEPPARD, T., DUAN, X. AND VELAY, X., 2004. Consideration of surface formation and cracking and control by isothermal extrusion; simulation of these factors by the finite element method. In: *8th International aluminum extrusion technology seminar*, 18-21 May 2004 Orlando. Illinois: Extrusion technology for aluminum profiles foundation, 2, 209-220.

SHEPPARD, T., TUTCHER, M.G. AND FLOWER, H.M., 1979. Development of recovered dislocation substructure during plastic flow. *Metal Science*, 473-481.

SHI, H., MCLAREN, A. J., SELLARS, C. M., SHAHANI, R., AND BOLINGBROKE, R., 1997. Constitutive equations for high temperature flow stress of aluminium alloys. *Materials science and technology*, 13, 210-216.

SINHA, U. AND CHIA, E. H., 1988. Metallurgical considerations for quality improvements of CONFORM aluminium products. In: *4th International aluminium extrusion technology seminar*, 11-14 April 1988 Chicago. Washington: Aluminium association and aluminium extruder councils, 2, 539-544.

SLATER, H. K. AND COON, P. M., 1988. Aluminium extrusion by CONFORM - an update on development experience at the Springfields laboratories of the UK atomic energy authority. In: *4th International aluminium extrusion technology seminar*, 11-14 April 1988 Chicago. Washington: Aluminium association and aluminium extruder councils, 2, 525-532.

SMELSER, R. E. AND THOMPSON, E. G., 1992. Observations on steady-state extrusion modeling. In: J.-L. CHENOT, R. D. WOOD AND O. C. ZIENKIEWICZ, eds. *Numerical methods in industrial forming processes Numiform 92*. Rotterdam: Balkema, 657-661.

SOBIS, T., ENGEL, U. AND GEIGER, M., 1992. Transfer of contact conditions for failure analysis of metal forming tools. In: J.-L. CHENOT, R. D. WOOD AND O. C. ZIENKIEWICZ, eds. *Numerical methods in industrial forming processes Numiform 92*. Rotterdam: Balkema, 663-668.

STOREN, S., 1993. The theory of extrusion-advances and challenges. *International journal of mechanical sciences*, 35, 12, 1007-1020.

SUBRAMANIYAN, J., 1989. *Extrusion of 2024 aluminium alloy sections*. Thesis (PhD). University of London. 220-231.

SWEET, E.D., CARAHER, S.K., DANILOVA, N.V. AND ZHANG, X., 2004. Effects of extrusion parameters on coarse grain surface layer in 6xxx series extrusions. In: *8th International aluminum extrusion technology seminar*, 18-21 May 2004 Orlando. Illinois: Extrusion technology for aluminum profiles foundation, 1, 115-126.

TASHIRO, Y., YAMASAKI, H. AND OHNEDA, N., 1992. Extrusion conditions and metal flow to minimise both distortion and variance of cross sectional shape. In: *5th International aluminium extrusion technology seminar*, May 1992 Chicago. Washington: Aluminium association and aluminium extruder councils, 1, 191-205.

THACKRAY, R., DASHWOOD, R. AND MCSHANE, H., 2000. Simulation of the effect of tooling and billet condition on bulk and surface metal flow during extrusion. In: *7th International aluminium extrusion technology seminar*, 16-19 May 2000 Chicago. Washington: Aluminium association and aluminium extruder councils, 1, 213-223.

THEDJA, W. W., MULLER, K. B. AND RUPPIN, D., 1992. Tribomechanical process on the die land area during extrusion of AA6063 alloy. In: *5th International aluminium extrusion technology seminar*, May 1992 Chicago. Washington: Aluminium association and aluminium extruder councils, 1, 467-474.

THOMAS, W. M., 2000. Friction technology for the aluminum industries. In: *7th International aluminium extrusion technology seminar*, 16-19 May 2000 Chicago. Washington: Aluminium association and aluminium extruder councils, 2, 473-483.

TISZA, M., 1999. Integration of numerical modelling and knowledge based systems in metal forming. In: M. GEIGER, ed. *6th International Conference on technology of plasticity*, 19-24 September 1999 Nuremberg. Berlin: Springer, 1, 117-128.

TOMIMATU, S., FUKUOKA, S., OZAKI, M. AND HOSHINO, M., 1999. Thermal management in conform extrusion of multi-void tubes. *Advanced technology of plasticity*, 3, 1867-1870.

TONG, L., HORA, P. AND REISSNER, J., 1992. Application of the arbitrary Lagrangian-Eulerian method in the FE-simulation of 3D-bulk forming processes. In: J.-L. CHENOT, R. D. WOOD AND O. C. ZIENKIEWICZ, eds. *Numerical methods in industrial forming processes Numiform 92*. Rotterdam: Balkema, 669-674.

TRANSVALOR, 2004a. *Forge 2 reference guide*. Sophia Antipolis: Transvalor.

TRANSVALOR, 2004b. *Forge 3 reference guide*. Sophia Antipolis: Transvalor.

TUTCHER, M. G., 1979. *Deformation processing applied to the Al-Mg alloy system*. Thesis (PhD). University of London.
TVERGAARD, V., 1981. *International journal of fracture*, 18, 237-252.

VALBERG, H. AND MALVIK, T., 1996. Metal flow in die channels of extrusion investigated by an experimental grid pattern technique. In: *6th International aluminium extrusion technology seminar*, 14-17 May 1996 Chicago. Washington: Aluminium association and aluminium extruder councils, 2, 17-28.

VALBERG, H. AND POHL, C., 2002. Boundary conditions and metal flow in forward extrusion of aluminium alloys. In: *Friction and wear in metal forming*, 18-20 June 2002 Valenciennes. Valenciennes: Euromech 435, 33-45.

VALBERG, H., 1988. Physical simulation of metal extrusion by means of modern materials. In: *4th International aluminium extrusion technology seminar*, 11-14 April 1988 Chicago. Washington: Aluminium association and aluminium extruder councils, 1, 321-327.

VALBERG, H., 1996. A modified classification system for metal flow adapted to unlubricated hot extrusion of aluminum and aluminum alloys. In: *6th International aluminium extrusion technology seminar*, 14-17 May 1996 Chicago. Washington: Aluminium association and aluminium extruder councils, 2, 95-100.

VAN DE LANGKRUIS, J., BERGWERF, R., VAN DER ZWAAG, S. AND KOOL, W. H., 2000. Linking plane strain compression tests on AA6063 to laboratory scale extrusion via constitutive equations. *Materials science forum,* 331-337, 565-570.

VAN GEERTRUYDEN, W.H., MISIOLEK, W.Z. AND WANG, P.T., 2004. Analysis of peripheral coarse grain recrystallization in 6xxx aluminum alloy extrusion. In: *8th International aluminum extrusion technology seminar*, 18-21 May 2004 Orlando. Illinois: Extrusion technology for aluminum profiles foundation, 1, 107-113.

VAN RENS, B. J. E., BREKELMANS, W. A. M. AND BAAIJENS, F. P. T, 2000. Numerical simulation of the extrusion of complex (hollow) profiles. In: *7th International aluminium extrusion technology seminar*, 16-19 May 2000 Chicago. Washington: Aluminium association and aluminium extruder councils, 1, 99-107.

VATNE, H.E., PEROCHEAU, F., EKSTROM, H.-E., POIZAT, L., NORD-VARHAUG, K., MARTHINSEN, K., LINDH, E. HAGSTROM, J. AND FURU, T., 2000. Industrial verification of

microstructural models for thermomechanical processing by application to hot rolling of AA3104. *Material science forum*, vols 331-337, 551-556.

VEIROD, R.P., 1983. *Effect of copper additions on deformation processing of aluminium alloys*. Thesis (PhD). University of London. 196-198.

VELAY, X. AND SHEPPARD, T., 2000a. Plane strain and three-dimensional coupled thermomechanical simulation of the Conform process. In: *7th International aluminium extrusion technology seminar*, 16-19 May 2000 Chicago. Washington: Aluminium association and aluminium extruder councils, 1, 505-517.

VELAY, X. AND SHEPPARD, T., 2000b. Axisymmetric modeling of aluminum extrusion using an expansion chamber. In: *7th International aluminium extrusion technology seminar*, 16-19 May 2000 Chicago. Washington: Aluminium association and aluminium extruder councils, 1, 533-540.

VELAY, X., DUAN, X. AND SHEPPARD, T., 2003. Prediction of material flow pattern in the hot extrusion of aluminium alloys by the finite element method. *Material science forum*, vols 426-432, 3807-3812.

VELAY, X., SHEPPARD, T. AND DUAN, X., 2004. Prediction of material flow pattern in the hot extrusion of aluminum alloys by the finite element method. In: *8th International aluminum extrusion technology seminar*, 18-21 May 2004 Orlando. Illinois: Extrusion technology for aluminum profiles foundation, 2, 179-184.

WAGONER, R.H. AND CHENOT, J.L.,1997. *Fundamentals of metal forming*. New York: John Wiley & Sons, 317-318.

WANG, P.T., VAN GEERTRUYDEN, W.H. AND MISIOLEK, W.Z., 2004. Thermomechanical modeling of coarse grain formation of AI-Mg-Si alloy during extrusion. In: *8th International aluminum extrusion technology seminar*, 18-21 May 2004 Orlando. Illinois: Extrusion technology for aluminum profiles foundation, 1, 137-148.

WEATHERILL, N.P. AND HASSAN, O., 1994. Efficient three-dimensional Delaunay triangulation with automatic point creation and imposed boundary constraints. *International journal of numerical methods in engineering*, 37, 2005-2039.

WHITE, A., 1987. *Conform and conventional extrusion of cast and powder aluminium alloys*. Thesis (PhD). University of London.

WRIGHT, R. N., LEA, G. G. AND KRAFT, F. F., 1996. Constitutive equations and flow stress characterization concepts for aluminum extrusion. In: *6th International aluminium extrusion technology seminar*, 14-17 May 1996 Chicago. Washington: Aluminium association and aluminium extruder councils, 1, 259-263.

YANG, D. Y. AND LEE, Y. K., 1999. Automatic mesh generation and remeshing for finite element analyses of 3D bulk forming processes. In: M. GEIGER, ed. *6th International Conference on technology of plasticity*, 19-24 September 1999 Nuremberg. Berlin: Springer, 1, 521-532.

ZASADZINSKI, J. AND MISIOLEK, W., 1988. Estimating optimal speed/temperature parameters to maximise hot extrusion exit speed. In: *4th International aluminium extrusion technology seminar*, 11-14 April 1988 Chicago. Washington: Aluminium association and aluminium extruder councils, 1, 241-246.

ZASADZINSKI, J., LIBURA, W., MISIOLEK, W.Z., 2000. Minimal attainable wall thickness in aluminum extruded sections. In: *7th International aluminium extrusion technology seminar*, 16-19 May 2000 Chicago. Washington: Aluminium association and aluminium extruder councils, 1, 365-370.

ZHANG, X. AND HEATHCOCK, J., 2000. Modeling of metal flow for bearing design. In: *7th International aluminium extrusion technology seminar*, 16-19 May 2000 Chicago. Washington: Aluminium association and aluminium extruder councils, 2, 169-176.

Published Refereed Papers

Materials Science Forum Vols. 426-432 (2003) pp. 3807-3812
online at http://www.scientific.net

Prediction of Material Flow Pattern in the Hot Extrusion of Aluminium Alloys by the Finite Element Method

X. Velay, X. Duan and T. Sheppard

School of Design Engineering & Computing, Bournemouth University, 12 Christchurch Road, Bournemouth BH1 3NA, United Kingdom

Keywords: Extrusion, Aluminium, Finite Element Method, Material Flow, Friction

Abstract. Understanding the material flow pattern in the hot extrusion of aluminium alloys is useful for a better control of the process. The material flow pattern is greatly affected by the friction between the tool and billet interface. In this communication, an inverse analysis method is firstly adopted to match the calculated extrusion force with the measured force by treating the friction law and the friction coefficient as free parameters. Three widely accepted friction laws are investigated: Tresca friction, Coulomb friction and viscoplastic friction. The use of Tresca friction is shown to yield more accurate results and explanations than the other models. The influence of the constitutive laws on the material flow pattern is emphasized. It is found that the use of the elasto-plastic model gives a much better prediction than the use of the visco-plastic model. It is also found that the quasi-static deformation is not fully established until a short time after the peak load has occurred.

Introduction

In the numerical analysis of metal forming processes, the selection of the friction law and the determination of the friction coefficient has a great effect on the computed results, such as the material flow pattern, the computed load, the microstructural evolution and the product surface quality [1-2]. In spite of its complicated mechanics, the friction condition is always simplified by a simple friction law, and a constant friction coefficient in the finite element analysis. Various experimental methods have been proposed to determine the friction coefficient (factor) [3-5]. The present paper focuses on the determination of the most suitable friction law and friction coefficient for the hot extrusion of aluminium alloys. Aluminium hot extrusion processes have the following characteristics: non-full film lubrication, use of a flat faced die, a very high pressure and a substantial temperature rise from the beginning to end. These features indicate that the friction coefficient cannot be simply determined from the usual ring test.

Previous simulation work has shown that the peak load in the hot extrusion of aluminium alloys is reached before the die land region is fully filled [6]. The dead-metal-zone (DMZ) is also established at this stage [7]. The results of these analyses do not agree with the experimental observations by Tutcher and Sheppard [8,9]. Tutcher observed that (a) a considerable length of the material had been extruded before the peak load was attained and (b) the DMZ was only beginning to be identified when the peak load was reached. This indicates the necessity to re-simulate the extrusion process with greater attention to these areas.

In this work, an inverse analysis method is adopted to match the calculated extrusion force with the measured force by treating the friction law and the friction coefficient as free parameters. Three

widely accepted friction laws are investigated: Tresca friction, Coulomb friction and viscoplastic friction. The influence of the selected constitutive laws on the material flow pattern is then discussed. The material pattern in each stage of the load displacement curve is finally examined and compared with the experimental observations [9].

Finite element code and the experimental work

The commercial finite element code, FORGE2®, was used. This program is developed by TRANSVALOR S. A. It is a thermal-mechanical coupled program with automatic remeshing capacity. The heat dissipation due to plastic deformation and friction work was considered in all analyses.

The initial billet length is 95mm with a diameter of Ø73mm. The container diameter is Ø75mm. A flat-faced die with a land length of 5mm is used. The extrusion ratio is 40:1. AA2024 is used for the evaluation of friction law and friction coefficient (or factor). The flow stress data of this alloy is taken from the material database of FORGE2® and expressed in the form of Hensel & Spittle equation. The experimental results are taken from Subramaniyan's PhD thesis [10]. The initial billet temperature is 663K. The container temperature is 50K lower than the initial billet temperature. The die and ram temperatures are 100K lower than the initial billet temperature. A constant ram speed of 5mm/s is used throughout the whole extrusion process. The measured peak load is 3.94MN. AA5456 is used for the study of the material's flow pattern (results are shown in Fig. 5). The initial billet temperature is 723K. The die and ram temperature is 573K. The ram speed is 5mm/s.

Results analysis and discussion

Friction law. The extrusion load is affected by the alloy composition, the length and temperature of the billet, the tools (i.e. ram, container and die) temperature, friction and the type of extrusion (direct, indirect or hydrostatic extrusion). Among these factors, the friction coefficient is the most difficult parameter to be accurately defined. Three types of friction law are commonly used in the simulation of metal forming.

The Tresca friction law is written in the following form:

$$\tau = m\sigma_0 / \sqrt{3} . \tag{1}$$

Where σ_0 represents the yield stress, m is the friction coefficient, $0 \le m \le 1$ and $m=1$ correspond to the sticking condition.

The viscoplastic friction law is written in the following form:

$$\tau = \alpha K \Delta V^{p-1} . \tag{2}$$

Where α ($0 \le \alpha \le 1$) is a viscoplastic friction coefficient, which is a function of the normal interface stress. K is the material consistency and p is the sensitivity parameter to the sliding velocity.

The Coulomb friction law used in FORGE2® can be written as:

$$\begin{aligned} &\tau = \mu\sigma_n && \text{when } \mu\sigma_n < \sigma_0 / \sqrt{3} \\ &\tau = m\sigma_0 && \text{when } \mu\sigma_n > \sigma_0 / \sqrt{3} . \end{aligned} \tag{3}$$

With this relationship, the frictional shear stress is equal to the normal stress multiplied by the friction coefficient μ, or to a fraction of the maximum shear stress sustainable by the material.

Determination of the friction coefficient. For the extrusion process introduced above, the friction coefficients are derived by comparing the computed peak load with the measured value. With the exception of the friction law, each computational parameter, including the mesh, material properties etc., are held constant. The derived friction coefficients were $\mu = 0.1$, $m = 0.9$ and $\alpha = 0.5$ for the Coulomb friction law, Tresca friction law and viscoplastic friction law respectively. It is clear that the friction coefficient changes when the same extrusion condition is put under different friction laws. A lower value of friction coefficient is obtained for the Coulomb law than the other two friction laws. It can be attributed to the fact that a higher normal stress acts on the tool/billet interface (see Fig.1 for the distribution of normal stress on the inner container surface). Surprisingly, the normal stress is more than 10 times that of the frictional shear stress. In other words, the normal stress is roughly equivalent to 10 times the current flow stress (see Eq.1). According to Eq.3, it is understood that μ must be less than 0.1. In aluminium extrusion, it is very unusual to attempt full lubrication, especially for those aerospace products which require very high surface quality and mechanical properties. Sticking friction is always assumed at the billet/container interface. However, for such a sticking condition, the derived friction coefficient for the Coulomb friction law is less than 0.1. This does not fit with normal understanding.

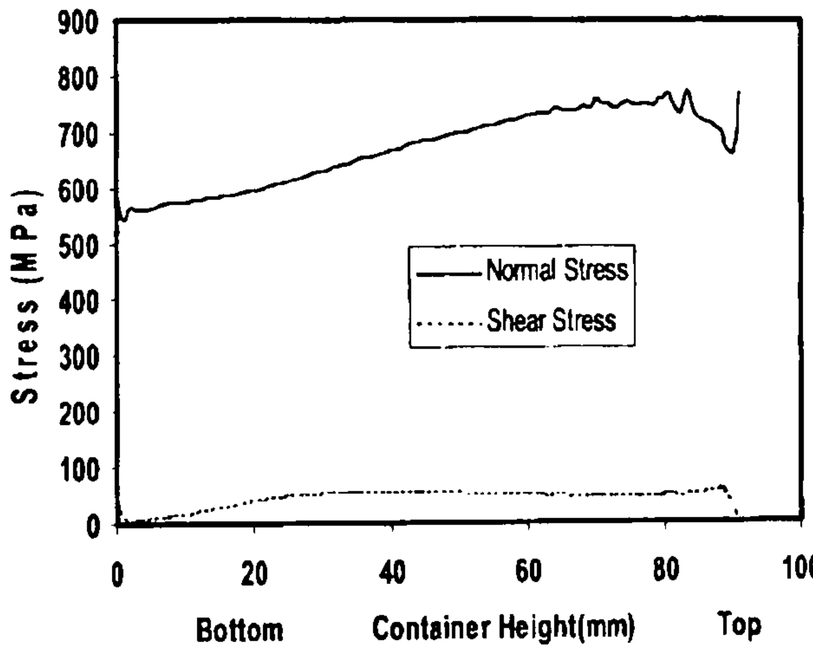

Figure 1 Distribution of stress on the container surface

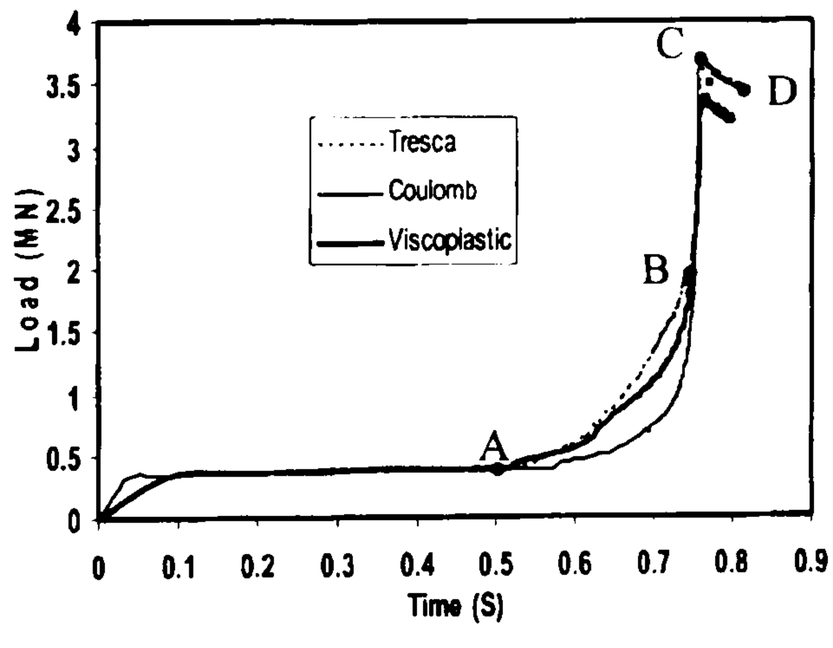

Figure 2 Influence of the friction law on the extrusion load

The computed extrusion load as the material traverses the die orifice is shown in Fig. 2. As expected, the extrusion load increases gradually in the process of upsetting. Once the container is filled the load starts to rise rapidly and reaches the peak value. However the gap is not filled completely as there is still a small amount of space at the right lower billet / container junction. At this point, the extrusion load decreases slowly with increasing displacement of the ram. This is due to the fact that the billet length within the container is getting shorter, as does the contact length. Another important factor is the rise in temperature due to plastic deformation and the friction work. From Fig. 2, it can be seen that Coulomb friction law and Tresca friction law predict nearly the same peak load. The viscoplastic friction law presents the lowest peak load of 3.3MN. For Tresca and Coulomb friction laws, the calculated peak load is 3.7MN. The relative error compared with the

measured peak load 3.94 MN is 6.3%. The error for the viscoplastic friction law is 15.5%. The curves of all three friction laws show nearly identical shapes, predicting the same time to reach the peak load. The difference between the Coulomb friction and Tresca friction curves lies in the early stages of extrusion. At that period the normal stress is not high and therefore the frictional stress is low. Once the frictional stress is greater than the shear yield stress ($\sigma_0/\sqrt{3}$), Coulomb friction uses the same expression as the Tresca friction (seeEq.1 and 3). Therefore, it can be seen that the two friction laws give the same prediction. In general, it can be concluded that the Tresca friction law is the most suitable one for the simulation of hot extrusion using FORGE2®.

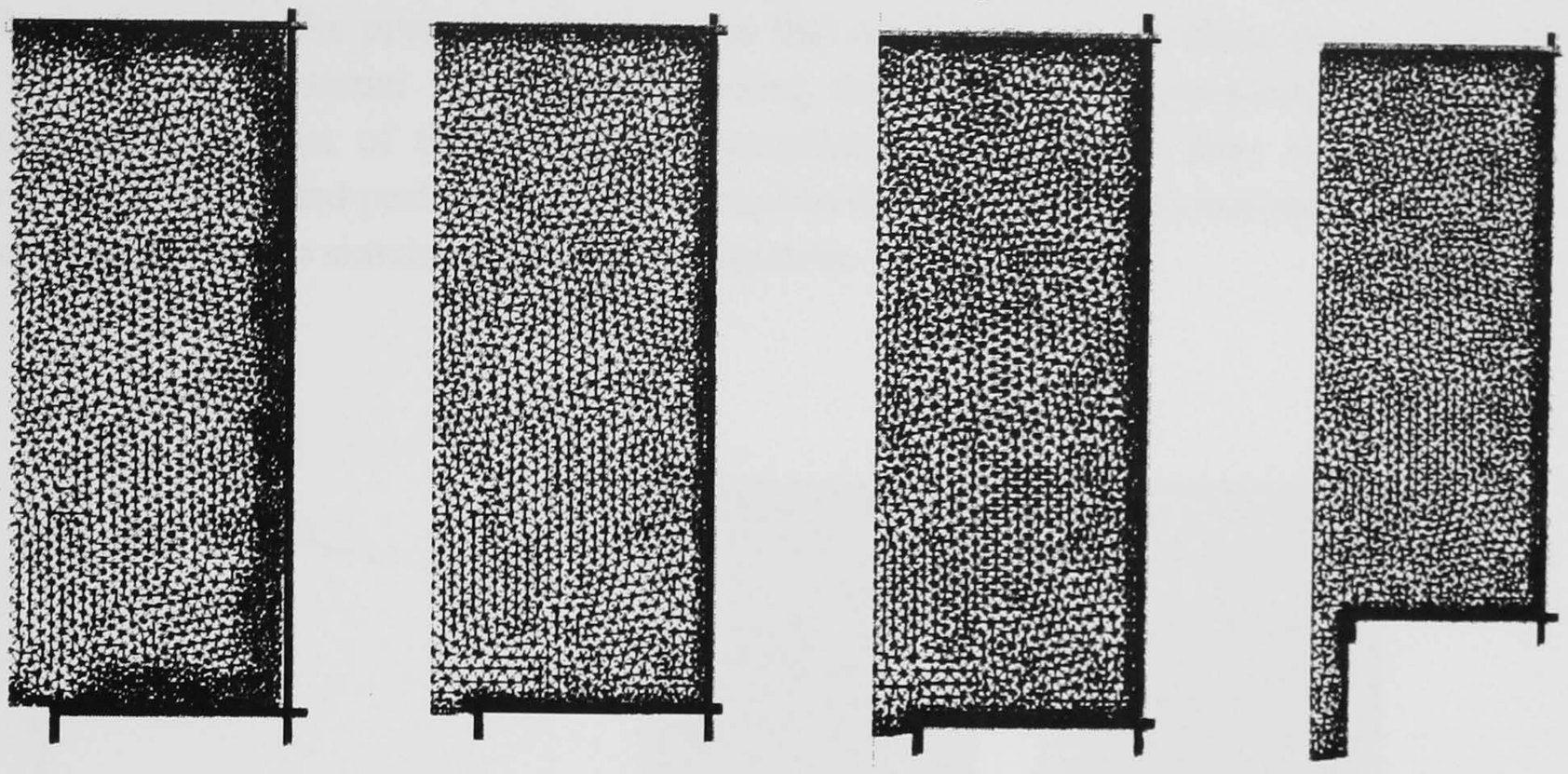

(a) Point A (b) Point B (c) Point C (d) Point D

Figure 3 The relationship between material flow and the extrusion/time curve

Material flow. The load/stroke curve has been discussed in the literature by both experimental observation [8,9] and finite element analysis [6,7]. Fig. 3 shows the flow of a viscoplastic material (ignoring the effects of elasticity) at different stages of the extrusion (i.e. point A, B, C & D in Fig.2). Point A represents the moment when the billet just starts to contact the container (see Fig.3a) and point B represents the moment when the billet/container gap is nearly filled (see Fig.3b). The peak load is attained when the material traverses the die orifice but is still within the die land (see Fig.3c). Fig.3d corresponds to point D. Konopleva and McQueen [6] gave the same description of the relationship between the load and the material flow in their simulation by the use of DEFORM®, another commercial FEM code.

However, the above prediction does not agree with the experimental observation [8,9]. Sheppard and Tutcher's measurement of the load/stroke is replicated in Fig.4. From this figure, we can clearly see that the extrudate has already formed before the peak load is attained. Therefore, we can conclude that the load/stroke curve predicted by the viscoplastic flow rule does not reflect reality. The reason may be attributed to the early softening phenomenon of the deformed material. When the elasto-plastic type of analysis was adopted for the same extrusion process, the computed flow pattern expressed by the deformation of the grids (see Fig.5) fits very well with Sheppard and Tutcher's experimental observation. It should be noted that the three-node triangle element is used in all of the simulations in the present paper. The square shaped grids presented in Fig.5 are not

elements. The corresponding locations of the four points in the load displacement curve are the same as presented in Fig. 3.

The length of the extrudate outside of the die land in Fig.5C is 13mm. With an extrusion ratio of 40:1, this corresponds to a ram displacement of approximately 0.33mm. In other words, the current contact length between the tool and the billet is 0.33mm less than the maximum contact length. The peak load is not attained when the contact length is at its maximum. This delay effect may be attributed to the strain hardening influence. Although it is always argued that the material flow behaviour of aluminium alloys under hot working conditions can be well represented by the viscoplastic flow rule, the present study indicates that we should use the elasto-plastic flow rule when we study the material flow. The computing time using the elasto-plastic flow rule is approximately twice that of the use of the viscoplastic flow rule and there is no noticeable difference in the computed peak load. This may explain the reason why the viscoplastic flow rule is commonly applied in the simulation of bulk deformation.

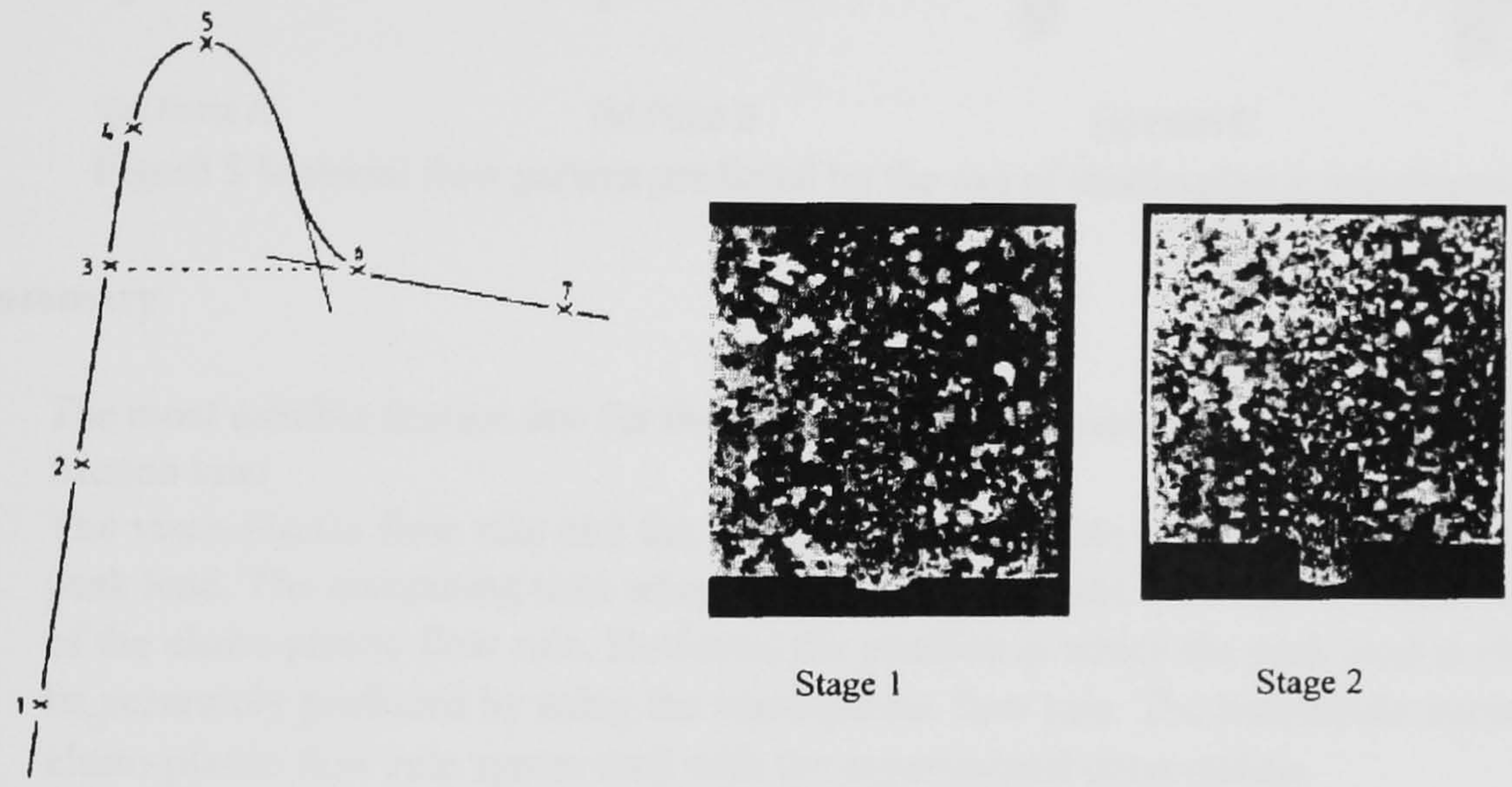

Figure 4 Material flow pattern and the load displacement curve [9]

The macrostructure changes in Fig. 4 show that at stage 6 the quasi-static deformation zone is about to be established and the DMZ is also identifiable. By stage 7, both the quasi-static deformation zone and the DMZ are fully established. Two intensive shear zones can also be clearly recognised.

From the deformation of the grids presented in Fig. 5c and Fig. 5d, it can be seen that the use of the elasto-plastic flow rule shows an excellent agreement with the experimental observations.

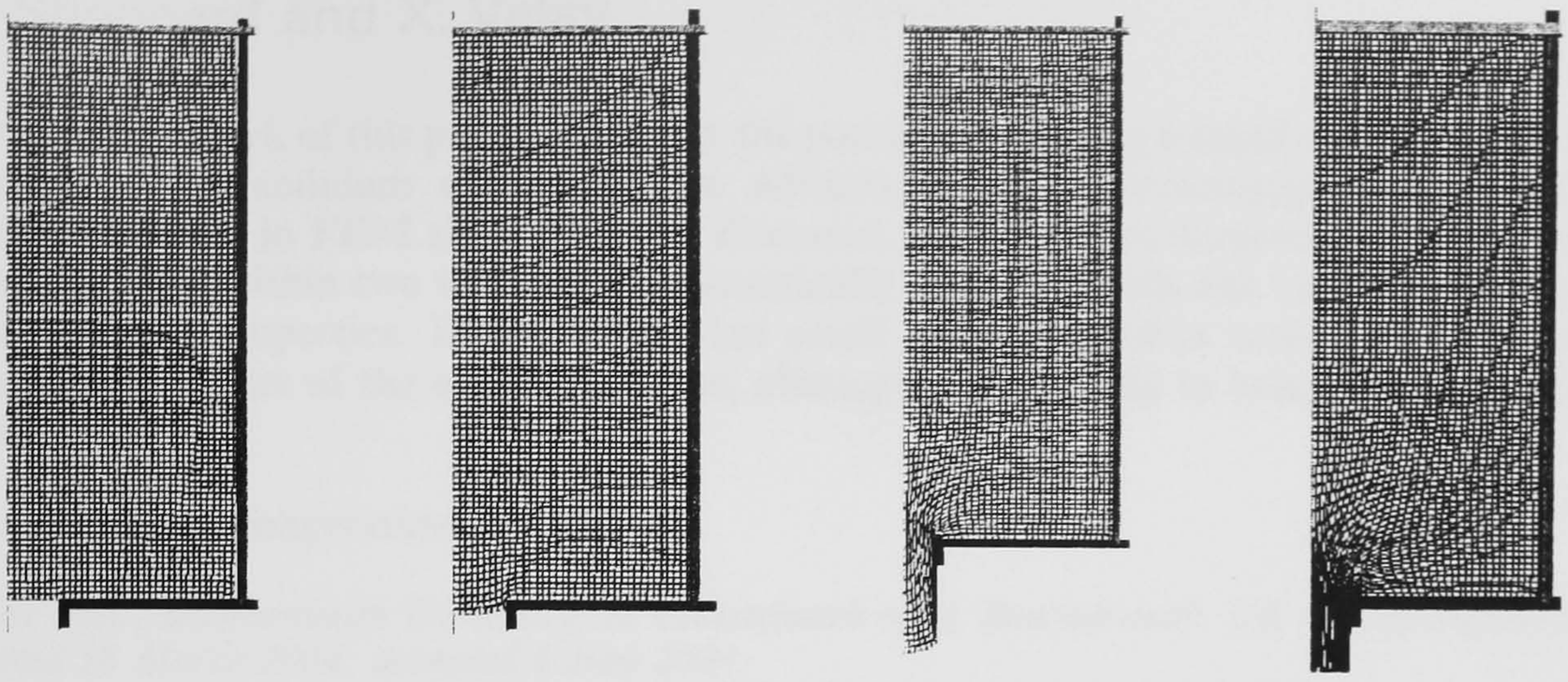

(a) Point A (b) Point B (c) Point C (d) Point D

Figure 5 Material flow pattern predicted by the use of elastic-plastic constitutive law

Summary

1 The most suitable friction law for the analysis of the aluminium extrusion process is the Tresca friction law.

2 The visco-plastic flow rule and the elasto-plastic flow rule produce nearly the same extrusion peak load. The computing time when using the visco-plastic flow rule is much shorter than that of the elasto-plastic flow rule. However, the position at which the peak load is obtained cannot be accurately predicted by using the visco-plastic flow rule. The load/stroke curve given by the elasto-plastic flow rule agrees well with the experimental observations.

3 The deformation zone is not fully established until a short time after the peak load has occurred.

References

1. X. Duan and T. Sheppard: Modell. Simul. Mat. Sci. Eng. 9 (2001), p.525-538
2. X. Duan and T. Sheppard: Factors influencing the surface quality in hot extrusion of aluminium alloy 2014. Modell. Simul. Mat. Sci. Eng. (Accepted).
3. S. J. Paterson: *PhD thesis* (University of London, 1981).
4. Xincai Tan: Tribology International 35 (2002), p.385-393
5. F. Wang and J. G. Lenard: J. Eng. Mater. Technol. 114 (1992), p.13-18
6. E.V. Konopleva and H.J. McQueen: Extrusion modeling of a 356 alloy and composite. In: Light Metals 1999, M.Bouchard and A. Faucher (eds). Met. Soc. 1999.
7. I. Flitta and T. Sheppard. Materials Science and Technology. (Accepted)
8. T. Sheppard: *Extrusion of Aluminium Alloys* (Kluwer Academic Publishers, Dordrecht, 1999.)
9. T. Sheppard and M. G. Tutche: Metals Science 14(12) (1980) 579-589
10. J. Subramaniyan: *PhD thesis* (University of London, 1989.)

A discussion of the scaling effect in numerical simulation of the extrusion process

Z. Peng, T. Sheppard and X. Velay

The main objective of the work of this paper is to study the possibility of using a small scale geometrical model in the numerical simulation of aluminium extrusion. The advantages and shortcomings of the application of the geometrically similar model in FEM simulation are discussed. Thermal–mechanical and metallurgical combined simulations are performed within two tests using geometrically similar models and assessment is made in terms of mechanical and material properties. It was found that small scale simulation could not reproduce most of the important forming parameters of the original process, although it could help to bring about significant savings in computation time.

MST/6169

Keywords: Extrusion, FEM, Temperature, Simulation

The authors are at DEC, Bournemouth University, 12 Christchurch road, Bournemouth, UK (tsheppar@bournemouth.ac.uk).
Manuscript received 18 March 2004; accepted 4 June 2004.

Introduction

Currently, computer modelling and simulation of the material forming process has been developed to the point that it may be used to solve industrial problems. It is often treated as a universal tool in all problems of metal forming processes. Taking a general view of the present state of the art in terms of numerical modelling, it appears that the finite element method is most suited to the three dimensional analysis of material forming processes. In fact, the finite element method can take into account practical nonlinearity in the geometry and material properties, besides producing accurate predictions of stress, strain, strain rate and temperature throughout the deforming billet. However, in some cases, this stage is extremely time consuming and there are limitations, which could cause fault in the design process. Physical simulation, in which a scaled down process is adopted, would result in the time spent in design to be significantly reduced. It is therefore of great interest to investigate if a small scale model can be adopted in numerical simulations. The relevant question that is frequently being asked concerns the accuracy between simplified modelling and simulation.[1] When some simplification (for example, a smaller scale but geometrically similar process) is adopted, will the simulation still be of sufficient accuracy? Can the simplified simulation reproduce most of the important forming parameters of the real process?

It should also be borne in mind that at the present time, the trend of numerical simulation is not only coupled thermally and mechanically, but also combined structurally or metallurgically. By empirical and physical means, a modest degree of prediction of microstructure can now be achieved. Excellent reviews on modelling of static recrystallisation (SRX) have been given by Gottstein *et al.*[2] and by Shercliff and Lovatt.[3] Recently, the inverse method combined with FEM has been adopted to integrate those values of parameters reported in the literature. The FEM is run iteratively until the appropriate value is found to match the experimental measurement. Duan and Sheppard[4] have used the inverse method to give the parameters for alloy 2014.

In the present paper, the possibility of the application of a small scaled model into numerical simulation of extrusion is discussed. It was found that although the small scale model is effective in saving computing time, there are some serious deviations in the simulation results. This indicates that this method is not suitable for the simulation of aluminium extrusion.

FEM setup

The composition of the material used in this study is shown in Table 1 and the main simulation tooling is shown in Table 2. Two simulations of rod extrusion were performed and the billet size in run 2 was 2·5 times smaller than that in run 1, in terms of diameter and length. In these two simulations, the extrusion ratio was 20, the ram speed was 12·4 mm s^{-1}, the initial temperature of the billet was 350°C and the container temperature was 50°C lower than the billet.

The FEM program, FORGE2 is used in the present study. It is a process simulation tool based on the FEM. The hyperbolic sine function was integrated into the FEM to describe the material behaviour. The constitutive equation can then be written as

$$\bar{\sigma} = \frac{1}{\alpha} \ln \left[\left(\frac{Z}{A} \right)^{\frac{1}{n}} + \left[\left(\frac{Z}{A} \right)^{\frac{2}{n}} + 1 \right]^{\frac{1}{2}} \right] \quad \ldots\ldots\ldots (1)$$

where α, A, n are temperature independent constants. $\bar{\sigma}$ is the flow stress. Z is the Zener–Hollomon parameter and it is written as

$$Z = \dot{\varepsilon} \exp(\Delta H / GT) \quad \ldots\ldots\ldots\ldots (2)$$

where $\dot{\bar{\varepsilon}}$ is the mean equivalent strain rate, ΔH is the

Table 1 Chemical composition of 2014 (balance Al)

Mg	Si	Ti	Cr	Mn	Fe	Cu	Zn
0·20–0·8	0·50–1·2	0·15	0·10	0·40–1·2	0·7	3·9–5·0	0·25

Table 2 Tooling of FEM model (as shown in Fig. 1)

Run	Billet length, mm	Billet diameter, mm
1	95	75
2	38	30

DOI 10.1179/026708304225022142

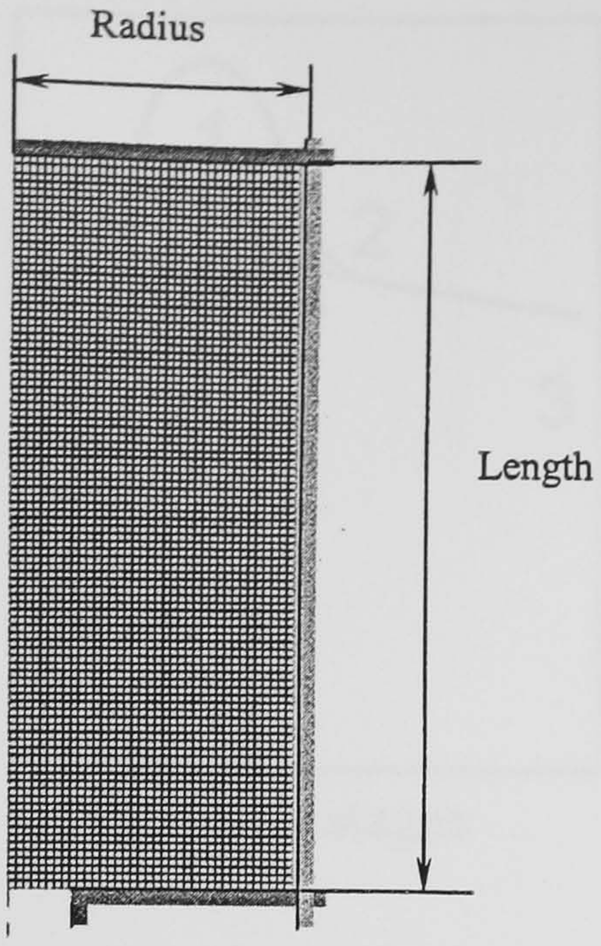

1 Reference grid pattern (undeformed)

activation energy, T is the temperature and G is the universal gas constant. For aluminium alloy AA 2014[5]

$$\Delta H = 144408 \text{ KJ mol}^{-1},\ \alpha = 0.0152 \text{ m}^2 \text{ MN}^{-1},\ n = 5{\cdot}27,$$
$$\ln A = 24{\cdot}41.$$

The Tresca friction law is adopted in the numerical model in this study. This is written in the following form

$$\tau = -m \frac{\bar{\sigma}}{\sqrt{3}} \quad \ldots \quad (3)$$

where τ is the friction shear stress, $\bar{\sigma}$ represents the flow stress, m is the friction coefficient, which is in effect a percentage of that which would represent sticking conditions. In this study, because the extrusion temperature is not high, $m = 0{\cdot}85$ was adopted.[6]

Discussion

In the following sections, the thermal–mechanical and the structural combined simulation results of the two runs are compared. The discussion concerning the computation time and material flow pattern were presented first.

MATERIAL FLOW PATTERN

Previous studies have confirmed that FEM simulation is effective in predicting the material flow pattern. Arentoft *et al.*[7] have studied the material flow in axi-symmetric extrusion with physical and two dimensional FEM simulation. Some studies in multi-hole die extrusion by three dimensional FEM simulation have also been published by the present authors.[8] In this study, a reference grid pattern was adopted to study the material flow pattern, as shown in Fig. 1. The simulation results of run 1 and run 2 are shown in Figs. 2 and 3 respectively.

As can be seen from Figs. 2 and 3, although the billet sizes are different in these two runs, the simulation results of the material flow pattern are similar. The different deformation areas can be shown clearly in both of these two runs and the predictions correspond well with the experimental results,[9] which are shown in Fig. 4. The complete computation time of the first run is about 25 h while in run 2, the total time is not more than 15 h. It is evident therefore that the computation time can be significantly saved (40%) with a small scale simulation and the simulation result is still approximate compared with

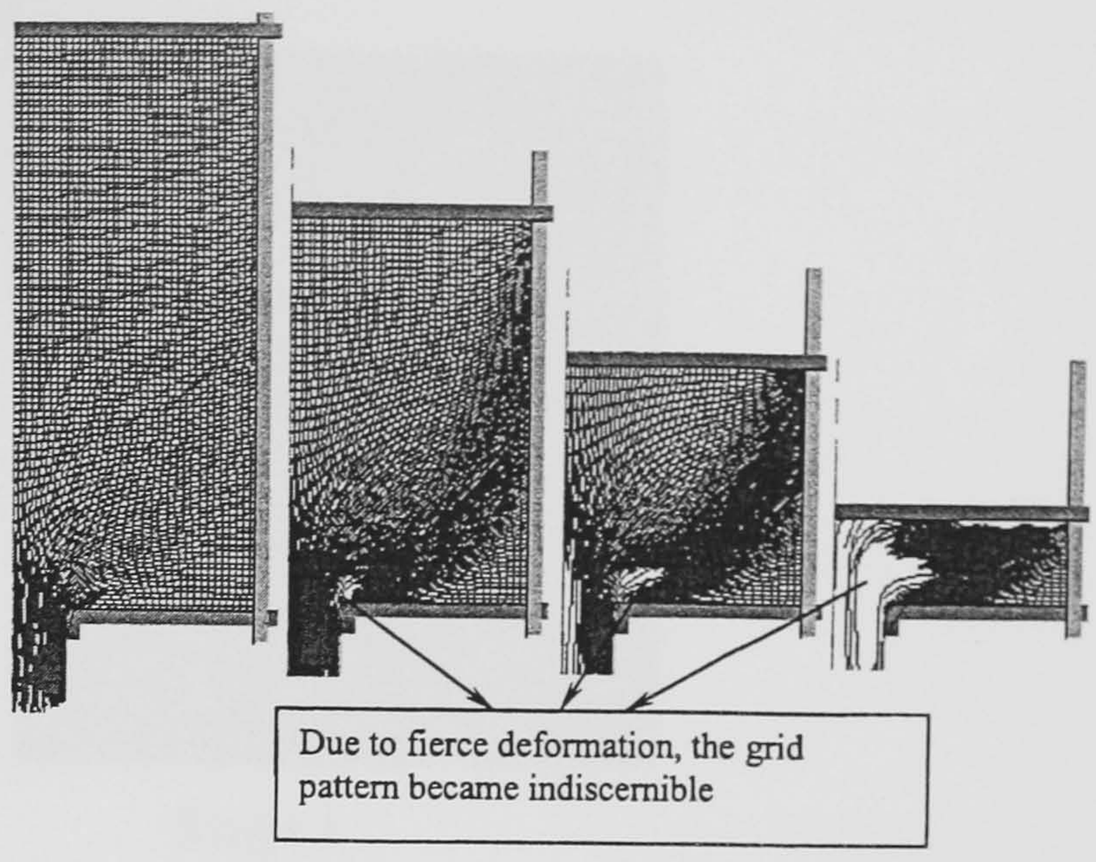

2 Simulation result using the full size billet

the material flow pattern of the original process. In fact, it is worth noting that small scale simulation has been used in the field of physical simulation, in which soft materials were adopted in experiments and the cost of design was then significantly saved.[2] However, the majority of the cases reported in the literature show that the usage of physical modelling is limited to qualitative analyses of the material flow.

It has been pointed out by Arentoft[7] that the basic problem lies in the transferral of the model experiment results to reality. In the case of extrusion, in which temperature rise is significant and strain rate is quite high, more important factors in addition to the material flow need to be considered, for example, the structure evolution. To ensure accurate results and interpretation, the model and the real process must be similar. For metalworking processes the following important similarity conditions must be created:[10,11] geometrical, plastic, frictional, thermal, elastic and dynamic. The fulfilment of all of these conditions is practically impossible. In most cases, the first four conditions are the most important, although they are also perhaps the hardest to fulfil. Therefore, it is essential to determine and select which material properties and process parameters are the most relevant for the purpose of the experiment.

During the process of extrusion, the press load, temperature rise, surface quality and extrudate mechanical properties are the most important factors to be considered. If any simulation is applied in extrusion, it has to be effective in predicting all of the above factors. In the following sections of this study, the analysis results of these forming parameters in the small scale simulation are discussed.

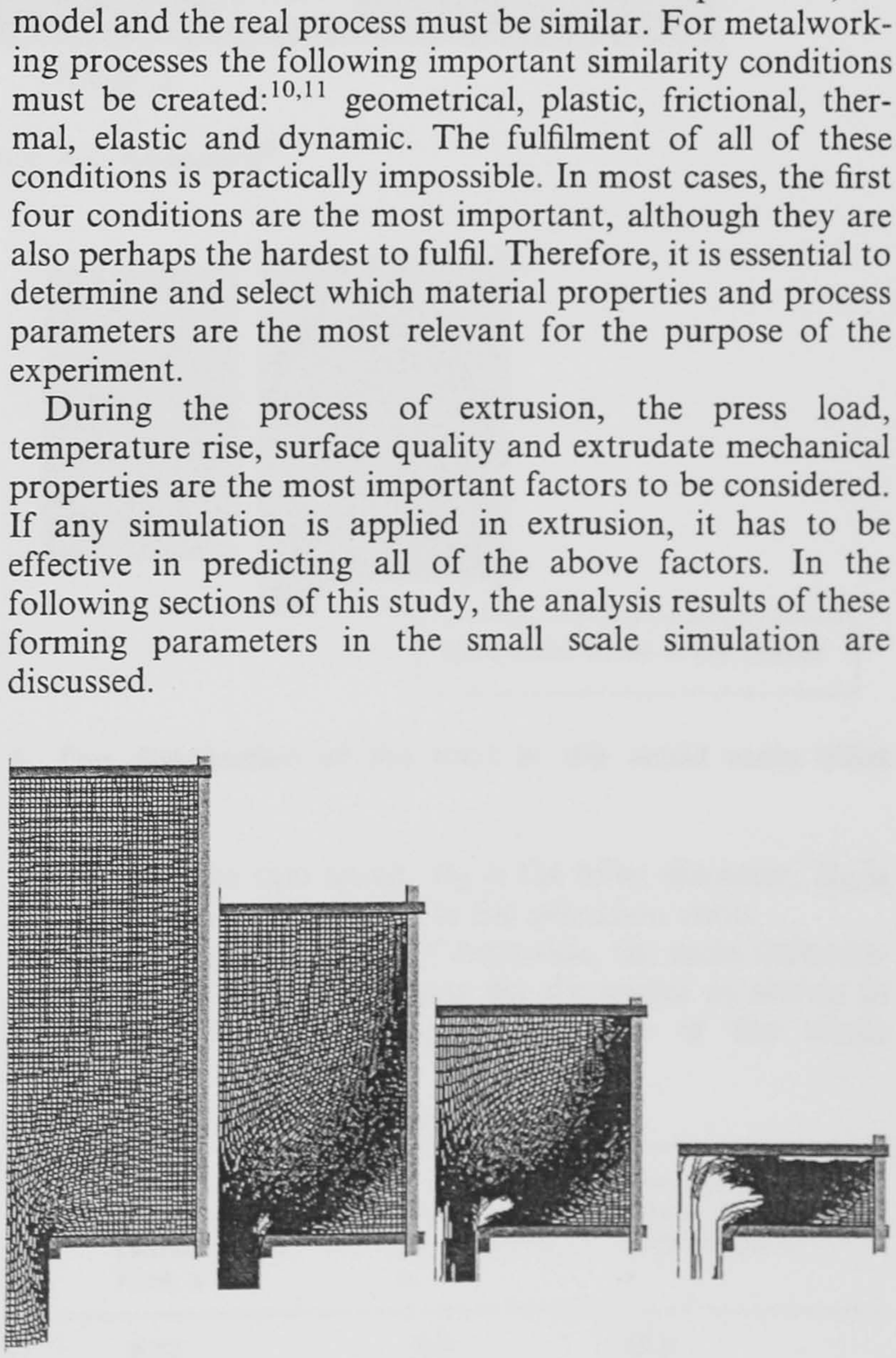

3 Simulation result using the small scale billet

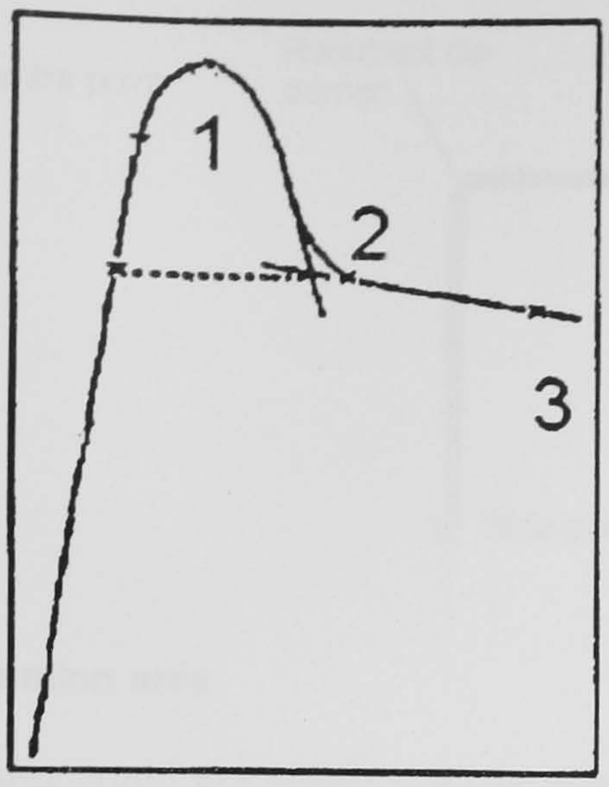

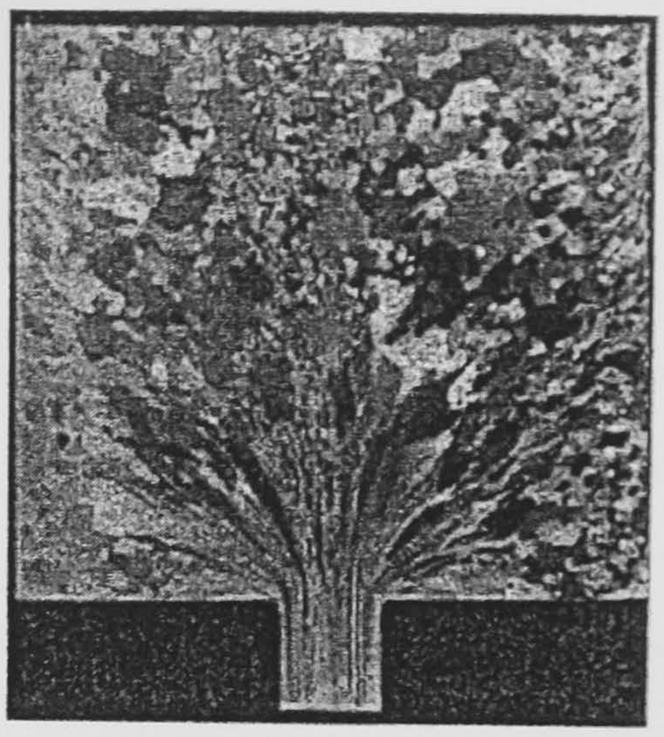

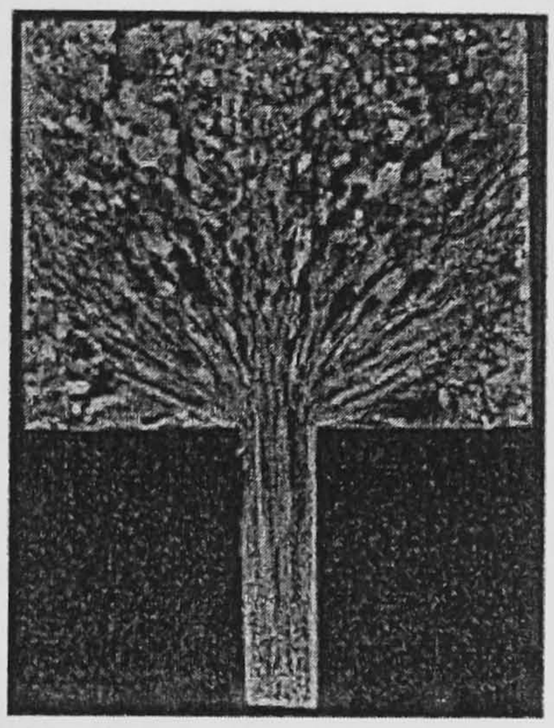

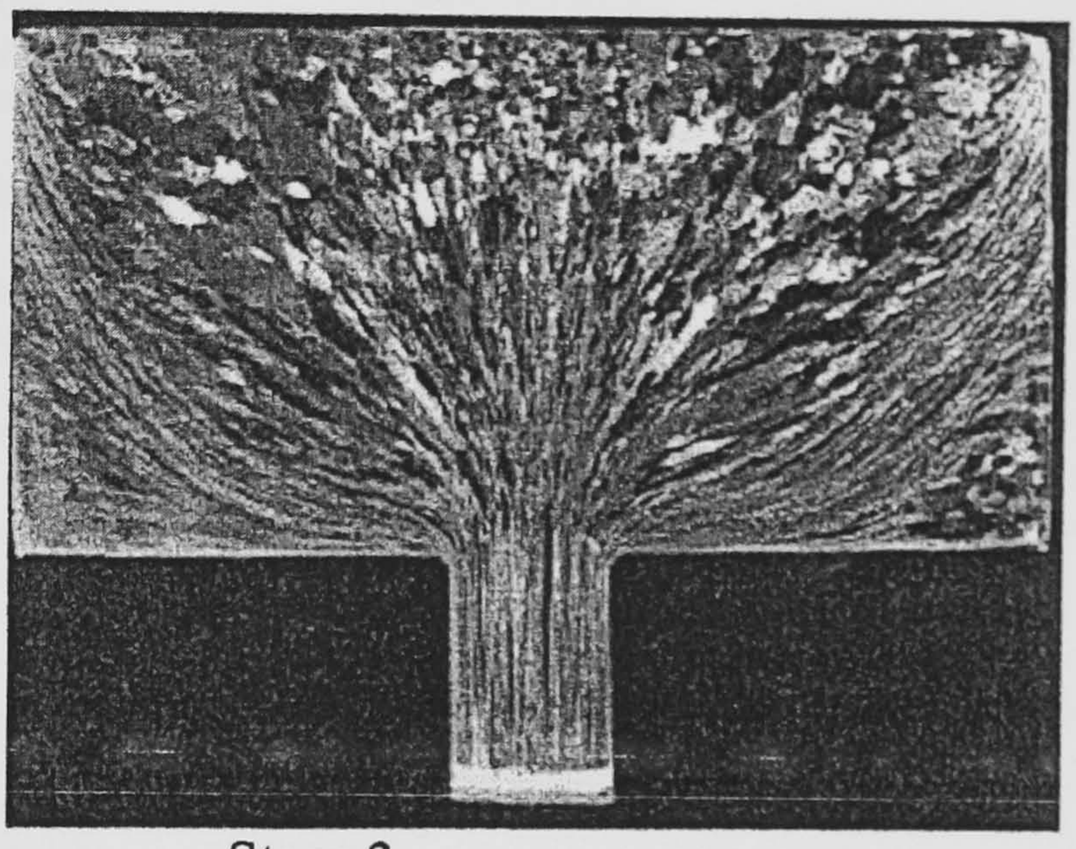

4 Experimental result of the material flow pattern after Tutcher and Sheppard[9]

MECHANICAL AND STRUCTURAL SIMULATION RESULTS

Firstly, the simulated instantaneous strain rate distributions ($\ln(\dot{\varepsilon})$) in these two runs are compared as shown in Figs. 5 and 6.

The average strain rates of the whole deformation area calculated by the FEM program and given by the upper bound method[12] according to equation (4) are shown in Table 3.

$$\bar{\dot{\varepsilon}} = \frac{6V_B D_B^2 (0{\cdot}171 + 1{\cdot}86 \ln R) \tan (38{\cdot}7 + 6{\cdot}9 \ln R)}{D_B^3 - D_E^3} \quad (4)$$

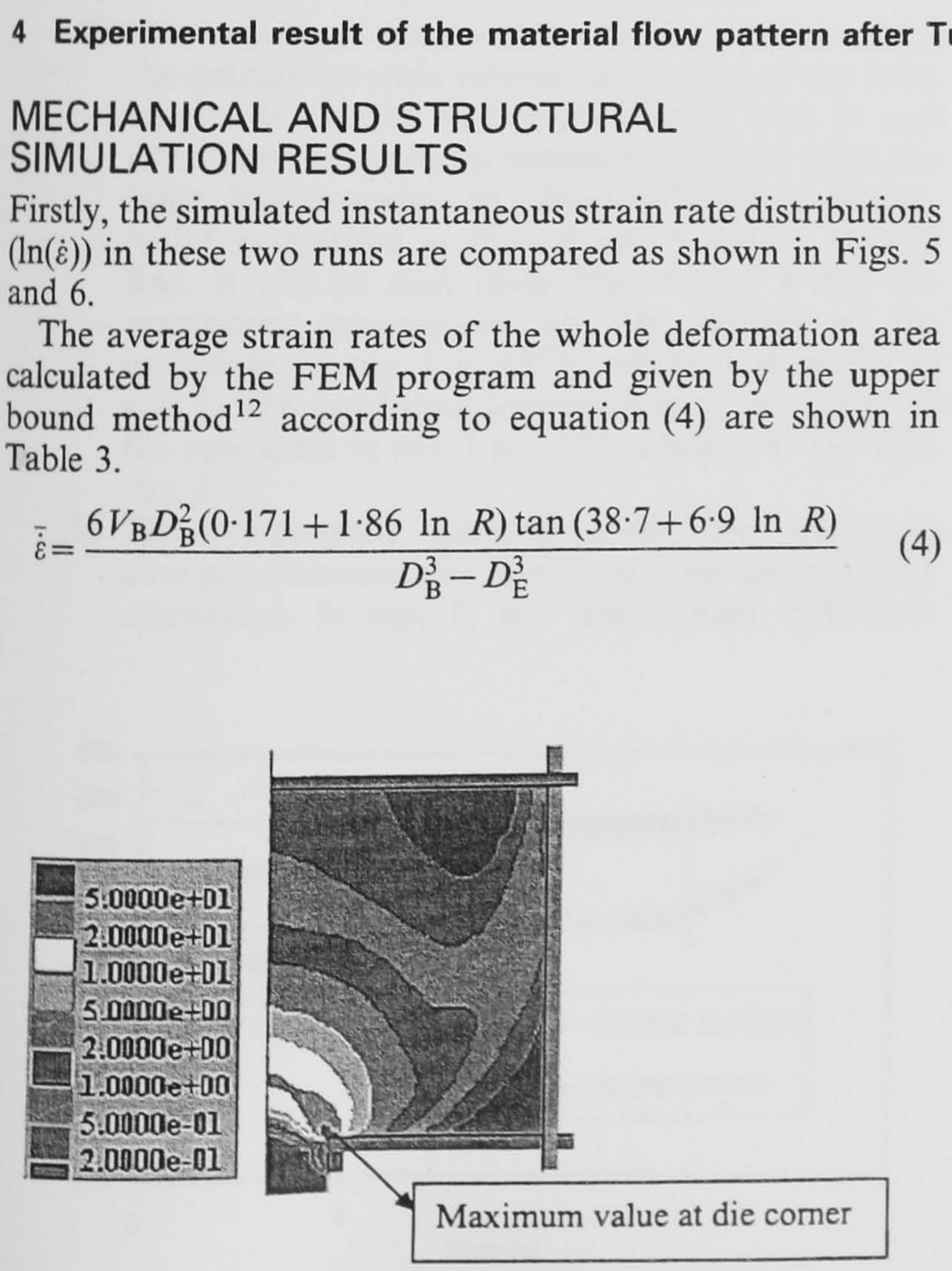

5 The distribution of the $\ln(\dot{\varepsilon})$ in the billet with full size (run 1)

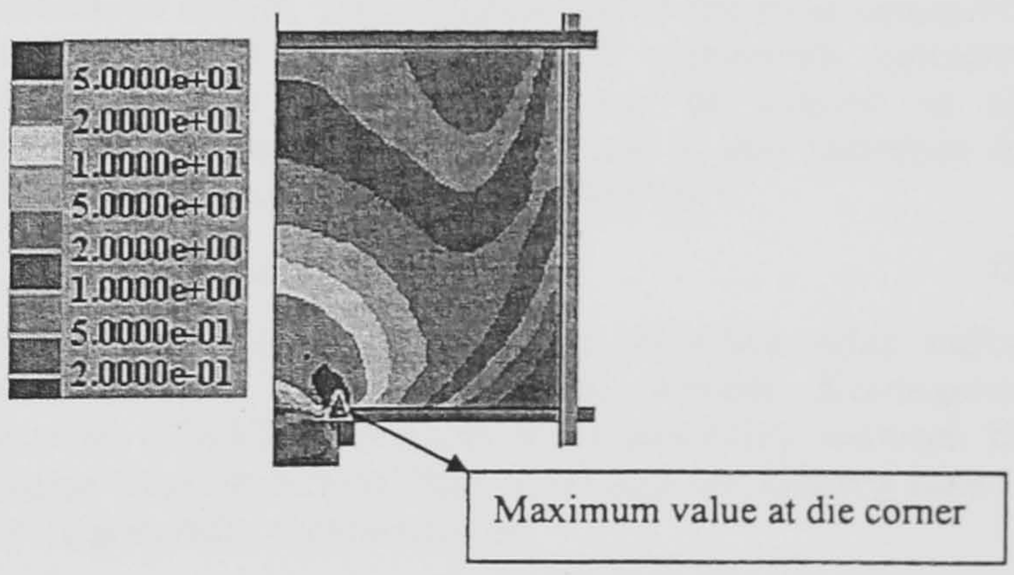

6 The distribution of the $\ln(\dot{\varepsilon})$ in the small scale billet (run 2)

where V_B is the ram speed, D_B is the billet diameter, D_E is the extrude diameter and R is the extrusion ratio.

However, in the process of extrusion, the main deformation occurred at the area near the die orifice as shown in Figs. 5 and 6. The average strain rate of the whole

Table 3 Average strain rate of extrusion

Run	$\bar{\dot{\varepsilon}}$ of the whole deformation area calculated by FEM, s^{-1}	$\bar{\dot{\varepsilon}}$ given by equation (4), s^{-1}	Average strain rate in the area with $\ln(\dot{\varepsilon}) > 1$, s^{-1}
1	6.57	5.6	28.3
2	15.1	14.4	31.7

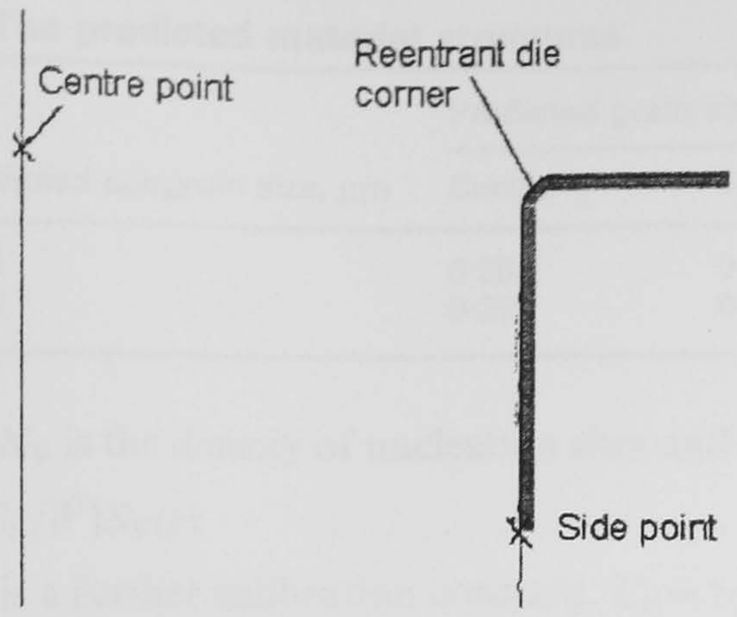

7 **The deformation area**

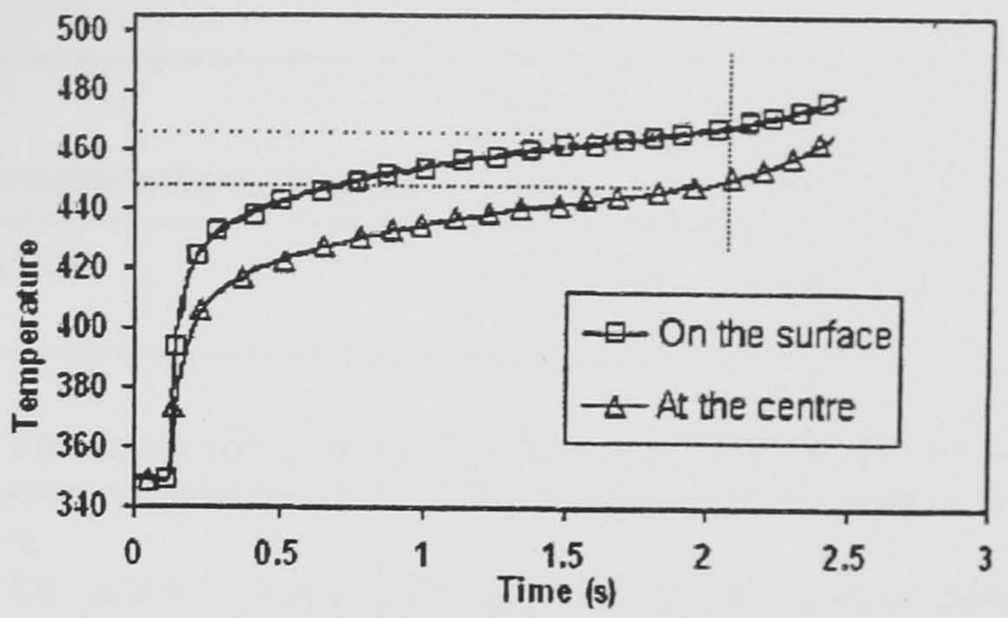

9 **Temperature rise at the small scale billet (run 2, temperature in °C)**

deformation area could not reflect the true condition of the process, so the average strain rate of the area with $\ln(\dot{\varepsilon}) > 1$ was calculated and the results are also shown in Table 3.

It can be seen from Figs 5 and 6, and Table 3 that the strain rate, either in the terms of 'average' or 'instant', is much higher in the small scale simulation than that predicted in run 1. So, it could be said that the small scale simulation could not reflect the original deformation properly in the terms of stain rate.

The temperature rise during extrusion was also studied. In extrusion, the temperature distribution in the billet is a critical process variable, affecting extrusion pressure, speed, surface finish and mechanical properties. Extrusion exit temperature also determines the surface finish and shape dimensions. The temperature rise is actually more significant than most of the other metal forming process. The simulation results of the exit temperatures of runs 1 and 2 are shown in Figs. 8 and 9 respectively. The side temperature and the centre temperature are extracted from the side point and the centre point, which are shown in Fig. 7.

The main difference concerning the temperature rise in these two runs can be concluded in two points.

(i) *The maximum temperature*. In the present study, the extrusions were carried to the end of the billet length. It should be borne in mind that in real situations, extrusion is normally stopped when the billet has extruded to about 90% of its length, which is marked in Figs. 8 and 9 with a vertical line. It can be seen from Figs. 8 and 9 that the maximum temperature on the surface of the extrudate in run 1 is 475°C while it is 466°C in run 2. The maximum temperature in the centre of the extrudate in run 1 is 432°C while it is 447°C in run 2

(ii) *The temperature gradient along the transverse direction (between the surface and the centre of the extrudate)*. In run 1, the temperature difference between the surface and the centre is maintained at 43°C while it is only 19°C in run 2. This is obviously a large difference.

As can be seen from the discussion above, although the geometrical conditions are similar in these two runs, there is no similar or proportional result concerning the exit temperature. The small scale simulation failed to predict the correct temperature distribution, especially in the die orifice area. It is well known that the exit temperature depends on the initial billet temperature, the magnitude of the work carried out during extrusion, and how this is divided between the work needed to overcome friction and the heat losses to the tooling.[13] The geometrically similar conditions cannot guarantee that the simulation result will be correct.

Because the material structure (subgrain size and recrystallised grain size) is closely related to the strain rate and the temperature, the small scale simulation will also give incorrect predictions.

SIMULATION RESULTS OF THE STRUCTURAL DEVELOPMENT

First, the models for the structural simulation are introduced below. The subgrain size is the most commonly used parameter in the study of aluminium extrudate structures. The subgrain size can be related to the temperature compensated strain rate Z and therefore the process condition for alloy AA 2014 by[12]

$$d^{-1} = 0{\cdot}096 \ln Z - 1{\cdot}747 \quad . \quad . \quad . \quad . \quad . \quad . \quad . \quad . \quad . \quad (5)$$

During aluminium extrusion, the extrudate often suffers recrystallisation. The Johnson–Mehl–Avrami–Kolmogorov equation (JMAK)[14] predicts the relationship between the volume fraction recrystallised (Xv) and the holding time (t) and is generally represented as

$$Xv = 1 - \exp\left\{-0{\cdot}693\left(\frac{t}{t_{50}}\right)^{k}\right\} \quad . \quad . \quad . \quad . \quad . \quad . \quad . \quad . \quad (6)$$

where t is annealing time, k is the Avrami exponent with a commonly reported value of 2, t_{50} is the time to 50% recrystallisation. Previous studies[14] have shown that the physical models describe the experimental results well for uniform processing conditions. More recent studies[15,16] have confirmed that the physical model will give better computed results than the empirical model in the simulation of aluminium extrusion. In this study, the physical model is adopted.

In equation (7), t_{50} is calculated based on the stored energy P_D and the density of recrystallisation nuclei N_V.[15]

$$t_{50} = \frac{C}{M_{GB} P_D}\left(\frac{1}{N_V}\right)^{1/3} \quad . \quad . \quad . \quad . \quad . \quad . \quad . \quad . \quad . \quad (7)$$

where C is a calibration constant. M_{GB} is the boundary

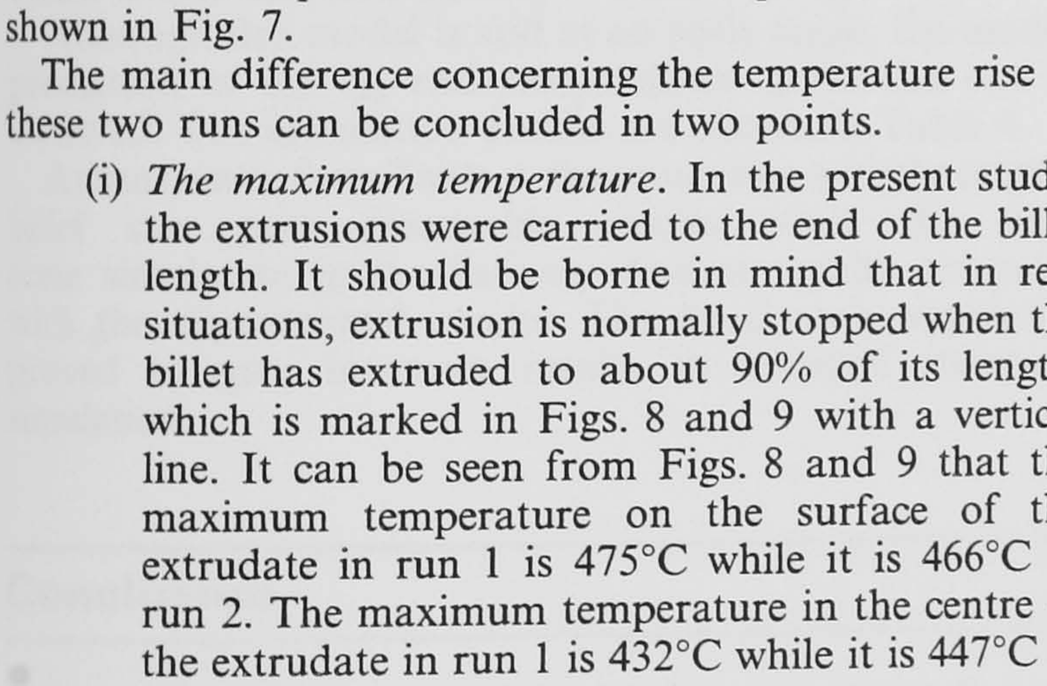

8 **Temperature rise at the full size billet (run 1, temperature in °C)**

Table 4 The predicted material structures

Run	Predicted subgrain size, μm	Predicted grain size, mm		Experimental subgrain size, μm	Experimental grain size, mm	
		Centre	Edge		Centre	Edge
1	1·75	0·294	0·273	1·43±0·25	0·321±0·04	0·266±0·04
2	2·26	0·250	0·232			

mobility. N_V is the density of nucleation sites and defined as

$$N_V=(C_d/\delta^2)S_V(\varepsilon) \quad . \quad . \quad . \quad . \quad . \quad . \quad . \quad . \quad . \quad . \quad (8)$$

where C_d is a further calibration constant, $C_d=1{\cdot}48\times10^{-4}$. δ is the subgrain size, S_V is the grain boundary area per unit volume

$$S_V(\varepsilon)=(2/d_0)[\exp(\varepsilon)+\exp(-\varepsilon)+1] \quad . \quad . \quad . \quad . \quad . \quad (9)$$

d_0 is the grain size after homogenisation. The stored energy P_D is approximated by

$$P_D=0{\cdot}5G\left(\frac{bC_\delta}{\delta}\right)^2+0{\cdot}05G\frac{b}{\delta} \quad . \quad . \quad . \quad . \quad . \quad . \quad . \quad (10)$$

where C_δ is a constant of typical value of the order 5, G is the shear modulus, b is the Burgers vector, d_0 is the initial grain size.

Selecting $C_\delta=5$ then the second terms will totally dominate as long as $\delta>0{\cdot}4$ μm. $G=2{\cdot}05\times10^{10}$ Pa, $b=2{\cdot}86\times10^{-10}$ m.[16] In Furu's study,[17] $C/(M_{GB}P_D)=1{\cdot}2\times10^5$ when the strain and strain rate are at high values.

For site saturated nucleation, the recrystallised grain size d_{rex} is simply calculated from nucleation density as

$$d_{rex}=DN_V^{-1/3} \quad . \quad . \quad . \quad . \quad . \quad . \quad . \quad . \quad . \quad . \quad . \quad . \quad (11)$$

where D is a constant (2·347).[18]

Although this model is still at an early stage, the modest prediction of the t_{50} and recrystallised grain size can be achieved. The calculation results are shown in Table 4.

As can be seen from Table 4, the simulation with the original billet size gave reasonable results while the small scale simulation gave relatively deviant results compared with the experimental results. The small scale simulation proved to give incorrect results in material structural simulation.

Conclusion

It has been confirmed in this study that a small scale simulation is capable of providing limited qualitative information of the extrusion process, for example, the material flow pattern.

The small scale simulation fails to accurately predict the correct temperature distribution, especially in the die orifice area.

The small scale simulation proved to give incorrect results in material structure (i.e. subgrain sizes and recrystallised grain size).

References

1. B. P. P. A. GOUVEIA, J. M. C. RODRIGUES, P. A. F. MARTINS and N. BAY: *J. Mater. Process. Technol.*, 2001, **112**, 244–251.
2. H. ARETZ, R. LUCE, M. WOLSKE, R. KOPP, M. GOERDELER, V. MARX, G. POMANA and G. GOTTSTEIN: *Modell. Simulat. Mater. Sci. Eng.*, 2000, **8**, 881–891.
3. T. FURU, H. R. SHERCLIFF, G. J. BAXTER and C. M. SELLARS: *Acta Materialia*, 1999, **47**, 2377–2389.
4. X. DUAN and T. SHEPPARD: *Modell. Simulat. Mater. Sci. Eng.*, 2002, **10**, 363–380.
5. T. SHEPPARD and A. JACKSON: *Mater. Sci. Technol.*, 1997, **13** 203–209.
6. I. FLITTA and T. SHEPPARD: *Mater. Sci. Technol.*, 2003, **19**, 837–846.
7. M. ARENTOFT, Z. GRONOSTAJSKI, A. NIECHAJOWICZ and T. WANHEIM: *J. Mater. Process. Technol.*, 2000, **106**, 2.
8. Z. PENG and T. SHEPPARD: *Mater. Sci. Eng. A*, 2004, **367**, 329–342.
9. M. G. TUTCHER and T. SHEPPARD: *Metals Technol.*, 1980, **7**, 488–493.
10. T. WANHEIM: 4th Conf. on 'Mechanical design and production', Cairo, Egypt, December 1988, Cairo University.
11. H. FERGUSON: *Adv. Mater. Process.*, 1993, **4**, 33–36.
12. T. SHEPPARD: Extrusion of aluminium alloys, 142; 1999, Dordrecht, Kluwer.
13. T. SHEPPARD: *Mater. Sci. Technol.*, 1999, **15**, 459–463.
14. T. FURU, H. R. SHERCLIFF, C. M. SELLARS and M. F. ASHBY: *Mater. Sci. Forum*, 1996, **217–222**, Vol. 1, 453–458.
15. E. NES, H. E. VATNE, O. DAALAND, T. FURU, R. ORSUND and K. MARTHINSEN: 4th Int. Conf. on 'Aluminium alloys: their physical and mechanical properties' (ICAA4), Atlanta, GA, USA, September 1994, Vol. 3, 18–49; 1994, Atlanta, GA, Georgia Institute of Technology.
16. X. DUAN and T. SHEPPARD: *Computat. Mater. Sci.*, 2003, **27**, 250–258.
17. T. FURU, H. R. SHERCLIFF, G. J. BAXTER and C. M. SELLARS: *Acta Materialia*, 1999, **47**, 2377–2389.
18. C. M. SELLARS and Q. ZHU: Mater. Sci. Eng. A: *Struct. Mater.: Propert., Microstruct. Process.*, 2000, **280**, 1–7.

ELSEVIER

Materials Science and Engineering A369 (2004) 66–75

MATERIALS SCIENCE & ENGINEERING A

www.elsevier.com/locate/msea

Application of finite element method in the hot extrusion of aluminium alloys

Xinjian Duan [a,*], X. Velay [b], T. Sheppard [b]

[a] *Department of Materials Science and Engineering, McMaster University, 1280 Main Street West, Hamilton, Ont., Canada L8S 4L7*
[b] *School of Design, Engineering & Computing, Bournemouth University, 12 Christchurch Road, Bournemouth, BH1 3NA UK*

Received 20 January 2003; received in revised form 7 October 2003

Abstract

The major objective of the present paper is to explore the complicated interactions between die design, forming parameters (i.e. ram speed, container temperature, billet temperature and extrusion ratio) and the product qualities (extrudate shape, surface condition and microstructure) by the use of finite element modelling (FEM). The various models (such as recrystallisation, damage criteria, etc.) have been integrated into the commercial codes, FORGE2® and FORGE3®, through user routines. The physical recrystallisation model proposed by Sellars and Zhu [Mater. Sci. Eng. A280 (2000) 1] and Vatne et al. [Acta Mater. 44 (1996) 4463] have been compared. The predicted distributions of the volume fraction recrystallised were also compared with the experimental results from the literature. The influences of forming parameters on the occurrence of surface cracks were studied by the combination of the Taguchi method with the FEM. It was found that the choked die could significantly reduce the possibility of producing surface cracks. Through simulating a shape extrusion process using two different die structures, it was found that the use of an expansion chamber can significantly reduce the degree of non-uniformity in terms of the extruded product shape and properties. The character of the complex material flow is also identifiable, which is very useful to help improve die design.

Keywords: Aluminium alloys; Ram speed; Die design; Recrystallisation; Surface damage

1. Introduction

For the aluminium extrusion industry, the most challenging and demanding work is to explore how to reduce or even eliminate die correction. If this is negated, the productivity and cost would be improved and the product will be more competitive with alternative engineering materials. This requires close co-operation between die designer, die manufacturer and the extrusion plant. The application of the finite element method in the extrusion industry acts as a bridge between die designer and plant, and also reduces the extent of dependence on the die manufacturer. A large amount of work in the modelling and simulation of aluminium extrusion processes by the use of FEM has been reported in the last few decades. The applications involve nearly every aspect of the extrusion process: predicting load [1], temperature [2], material flow pattern [3], surface formation [4], surface cracks [5], microstructure [6,7] and isothemal extrusion control [8]. The present paper does not attempt to review the previous work. The major objective concentrates on emphasising the complicated relationship between die design, forming parameter control and the product quality. Depending on the billet temperature, aluminium extrusion process is classified into cold extrusion (room temperature) and high temperature (temperature $> 250\,^{\circ}C$). The present study only concerns the problems occurring in hot extrusion, such as recrystallisation control, prevention of surface cracks and control of material flow.

The present paper is organised in such a structure so that the experimental details are first introduced in Section 2. In Section 3, the prediction of static recrystallisation (SRX) for T-shape extrusion is carried out by employing two metallurgical models: the model created by Sellars and Zhu [9] and the model created by Vatne et al. [10]. In Section 4, the prediction of surface cracks is based on the Cockroft and Latham criterion. The influence of forming parameters on the initiation of surface cracks is studied by the combination of Taguchi method with FEM. In Section 5, a thin

* Corresponding author. Tel.: +1-905-525-9140x24485; fax: +1-905-528-9295.
E-mail address: duanxj@mcmaster.ca (X. Duan).

0921-5093/$ – see front matter © 2003 Published by Elsevier B.V.
doi:10.1016/j.msea.2003.10.275

Table 1
Chemical composition of alloys (wt.%)

Alloys	Cu	Mn	Mg	Fe	Si	Zn	Ti	Cr	Al
AA2014	4.4	0.78	0.47	0.2	0.78	0.02	0.013	–	Balance
AA2024	4.66	1.35	0.069	0.19	0.08	0.02	0.01	–	Balance
AA6063	0.024	0.02	0.45	0.19	0.48	<0.01	0.014	–	Balance

semi-closed section extrusion process is used as an example to demonstrate the influence of die structure on the extruded product quality. Conclusions are finally given in Section 6.

2. Experimental

Three aluminium alloys AA2024, AA2014 and AA6063 are studied in Sections 3–5, respectively. The alloys were supplied by Alcan International Lt., Banbury, UK. The alloy compositions are given in Table 1. For hot extrusion of AA2024, the experimental data were taken from Subramaniyan's experiments [12]. For hot extrusion of AA2014, the experimental data were taken from Vierod's experiments [11].

All materials were homogenised in an air-circulating furnace for 24 h at 500 °C followed by furnace cooling to room temperature. All billets were subsequently scalped and extruded from a 75 mm diameter container using flat faced dies having a die land length of 5 mm. The billet length is 95 mm. The ram speed and the billet temperature were varied in the range of 3–13 mm/s and 300–500 °C, respectively. All extrudates were press quenched. The as-extruded samples were mounted, polished, and anodised using 5 vol.% HBF4 aqueous solutions at 20 V for a minimum of 2 min, and the volume fraction recrystallised was established using an Omnicon image analyser.

Both shape extrusion and rod extrusion processes were simulated by using the commercial finite element codes FORGE3® and FORGE2®, respectively. These two programs are both implicit and fully thermal-mechanically coupled and with automatic meshing and remeshing capabilities. Material flow is based on Lagrangian descriptions. For hot extrusion, strains are large and the elastic deformation may be ignored, the most economical constitutive laws are purely viscoplastic approximations. More details can be found in the literature [13,14].

3. Prediction of static recrystallisation

The mixed physical recrystallisation models were integrated into the two-dimensional commercial codes: FORGE2® to predict the static recrystallisation phenomenon in hot rolling [15] and hot rod extrusion [16]. The mixed models are due to Sellars and Zhu [9] and Vatne et al. [10] and Furu et al. [17]. The reader is referred to the above literature for a detailed description of the models. The focus of this section is to further refine some individual models to make them suitable for the extrusion of complicated three-dimensional sections.

Considering the real situation in which the accuracy of the measurement of dislocation density is problematic and is coupled with quite large assumptions in the models created by Sellars and Zhu [9], several simplifications have been made on the calculation of dislocation density in the present paper. Sellars and Zhu maintain that the total dislocation density is made up of the random dislocation density ρ_r and the geometrical necessary dislocation density ρ_g. However, there is a slight problem in their model on the calculation of ρ_g because they assumed a constant local lattice curvature and the value of this curvature is very difficult to determine. It was also recognised that $\rho_g = \rho_r$ under the constant strain rate condition [9], the calculation of ρ_g was hence neglected because the strain rate in extrusion remains almost constant after the initial extrusion stage (the peak load phase has been passed).

For the calculation of subgrain size, the following empirical equation was proposed for AA2024 [12] and is used in this simulation:

$$d^{-1} = -0.5778 + 0.0378 \ln Z, \tag{1}$$

where Z is Zener–Hollomon parameter, which is defined by

$$Z = \dot{\bar{\varepsilon}} \exp\left(\frac{Q_{\text{def}}}{RT}\right). \tag{2}$$

It should be noted that $\dot{\bar{\varepsilon}}$ in Eq. (2) is a mean strain rate, Q_{def} is the activation energy for deformation, R is the universal gas constant and T is the deformation temperature in Kelvin. The application of this type of equation into the calculation of subgrain size has been reported in the literature [18]. The reason for not using Sellars and Zhu's model is due to the difficulty in the determination of the initial subgrain size and it was found that the selection of the initial subgrain size has a significant influence on the predicted results [19]. It was also found that Eq. (1) can give a good prediction of subgrain size in three-dimensional rolling [20].

For the calculation of misorientation, the following approximate equation can be drawn based on the figures present in Nes's work [21]:

$$\theta = 3\bar{\varepsilon} \quad \text{when } \bar{\varepsilon} \le 1 \quad \text{or} \quad \theta = 3 \quad \text{when } \bar{\varepsilon} > 1, \tag{3}$$

where θ is the misorientation across subgrain boundaries and $\bar{\varepsilon}$ is the total equivalent plastic strain. All other formulae (i.e. calculating the stored energy, the density of nucleation sites, etc.) are kept the same as in [15].

In this part, a T-shape three-dimensional extrusion process was simulated by FORGE3®. The geometrical dimensions are presented in Fig. 1. Taking advantage of the geometrical symmetry, only half of the model was simulated and the setting of finite element mesh is shown in Fig. 2. To save time and ensure a high accuracy in the simulation, four remeshing boxes were added. The minimum element size is 0.18 mm

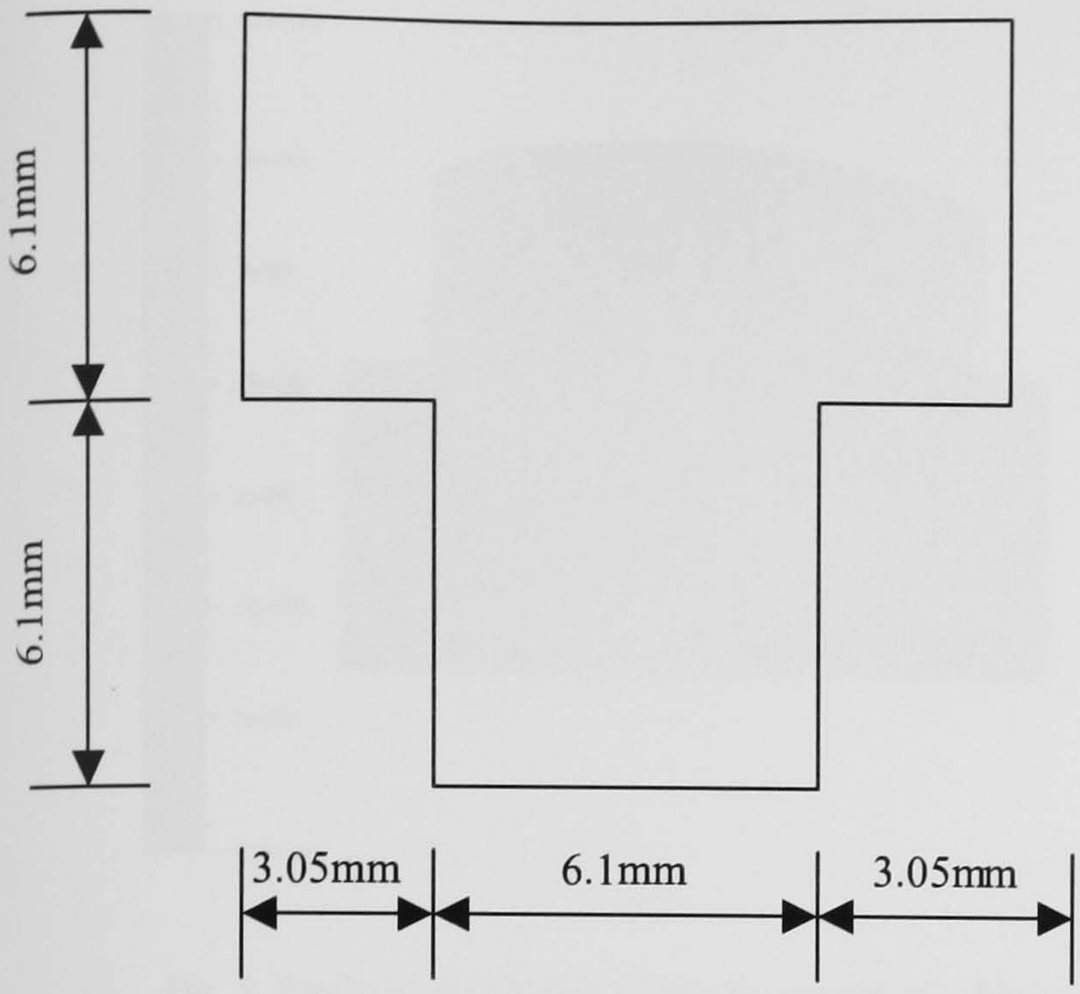

Fig. 1. Schematic drawing of the T-shaped die.

and the maximum element size is 10 mm. More than 30,000 4-node tetrahedron elements were used in the simulation. The Tresca friction law was used. The extrusion temperature is 340 °C. The constant extrusion speed is 7 mm/s and the extrusion ratio is 40:1.

The predicted distributions of the fraction recrystallised (X_V) and equivalent strain are shown in Fig. 4. X_V was calculated by the use of Johnson–Mehl [22]–Avrami [23]–Kolmogorov [24] equation. The description of this equation can be found in the literature [15]. According to Subramaniyan's measurements under such extrusion conditions, the fraction recrystallised after solution treatment at 500 °C for 30 min is 74.89% and the thickness of recrystallised layer is 1.7 mm [12], see Fig. 3. The results in Fig. 4a agree well with Subramaniyan's measurement. There is a thin recrystallised layer near the extrudate edge neighbouring the die and the maximum X_V appears at the die corner. It is also interesting to note that the maximum equivalent strain also appears at the same location (see Fig. 4b). That is not occasional. The reason is attributed to

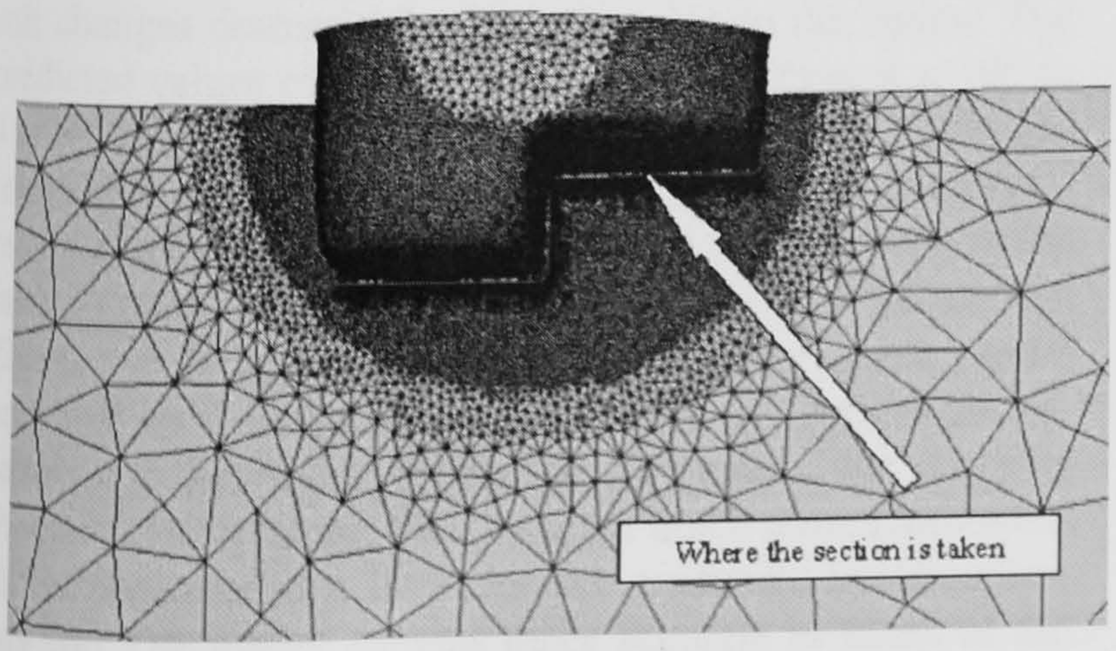

Fig. 2. Finite element model for T-shape extrusion. Extrusion ratio 40:1, extrusion temperature 340 °C and constant extrusion speed of 7 mm/s.

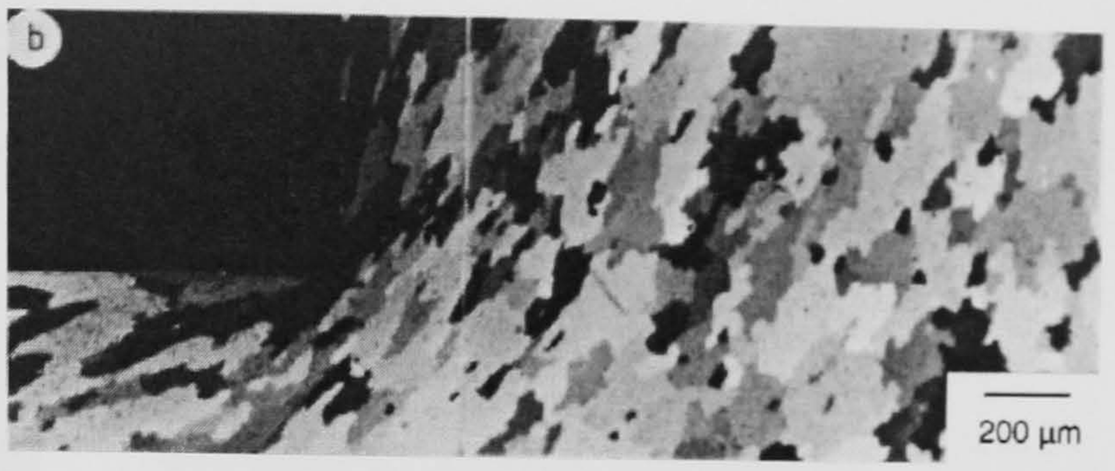

Fig. 3. The microstructure after solution treated for 30 min at 500 °C [12]. The greatest recrystallisation occurs at the die corner.

the assumption that nucleation sites only appear at grain boundaries. The density of nucleation sites is calculated by:

$$N_V = \left(\frac{C_d}{\delta^2}\right) S_v(\varepsilon), \tag{4}$$

where C_d is a constant, δ is subgrain size and S_v is the grain boundary area per unit volume

$$S_v(\varepsilon) = \left(\frac{2}{d_0}\right)[\exp(\varepsilon) + \exp(-\varepsilon) + 1], \tag{5}$$

where d_0 is the initial grain size, which is assumed to be 100 μm. This value is also based on Subramaniyan's

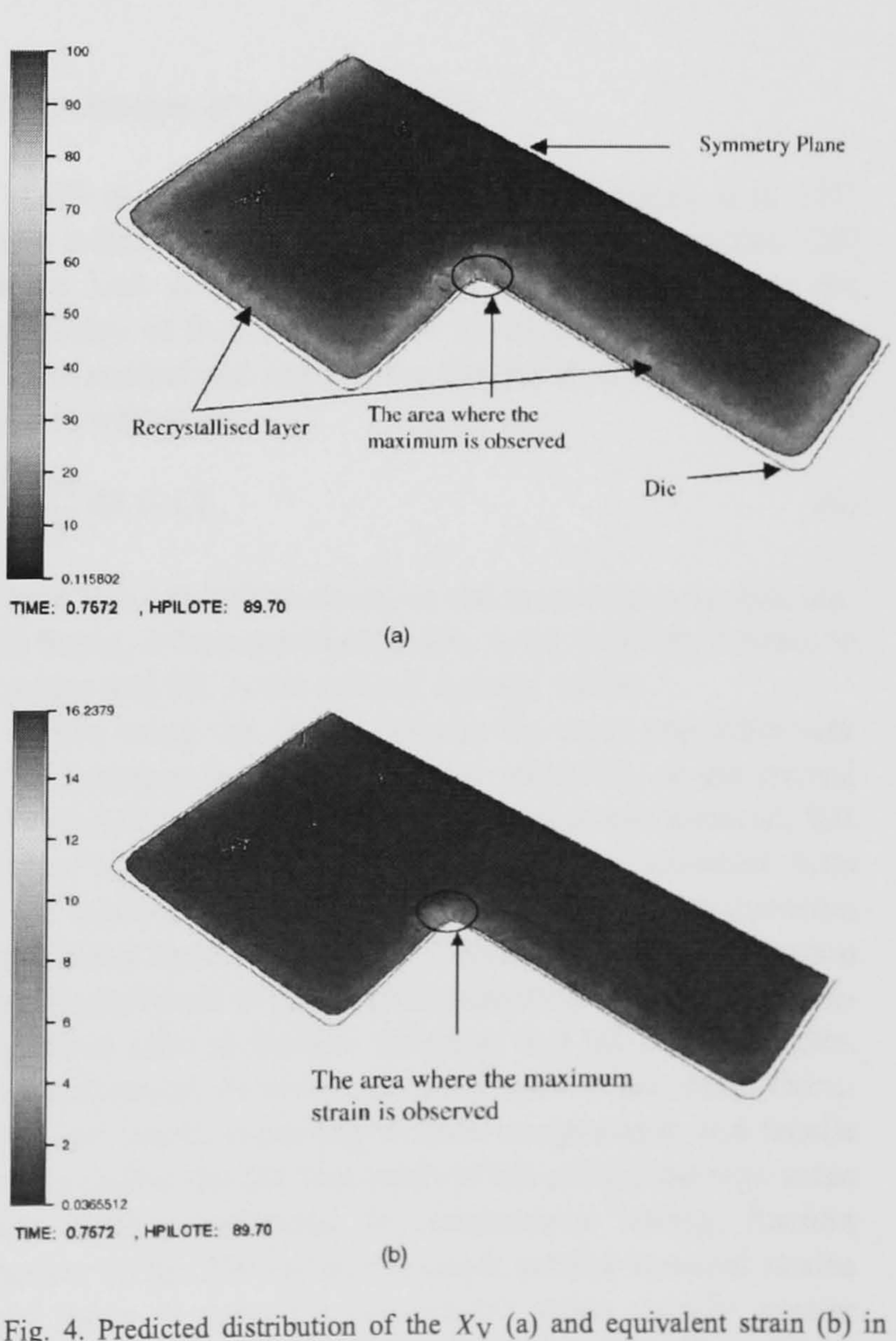

Fig. 4. Predicted distribution of the X_V (a) and equivalent strain (b) in the cross-section using the model proposed by Sellars and Zhu [9]. The location of the cross-section is shown in Fig. 2.

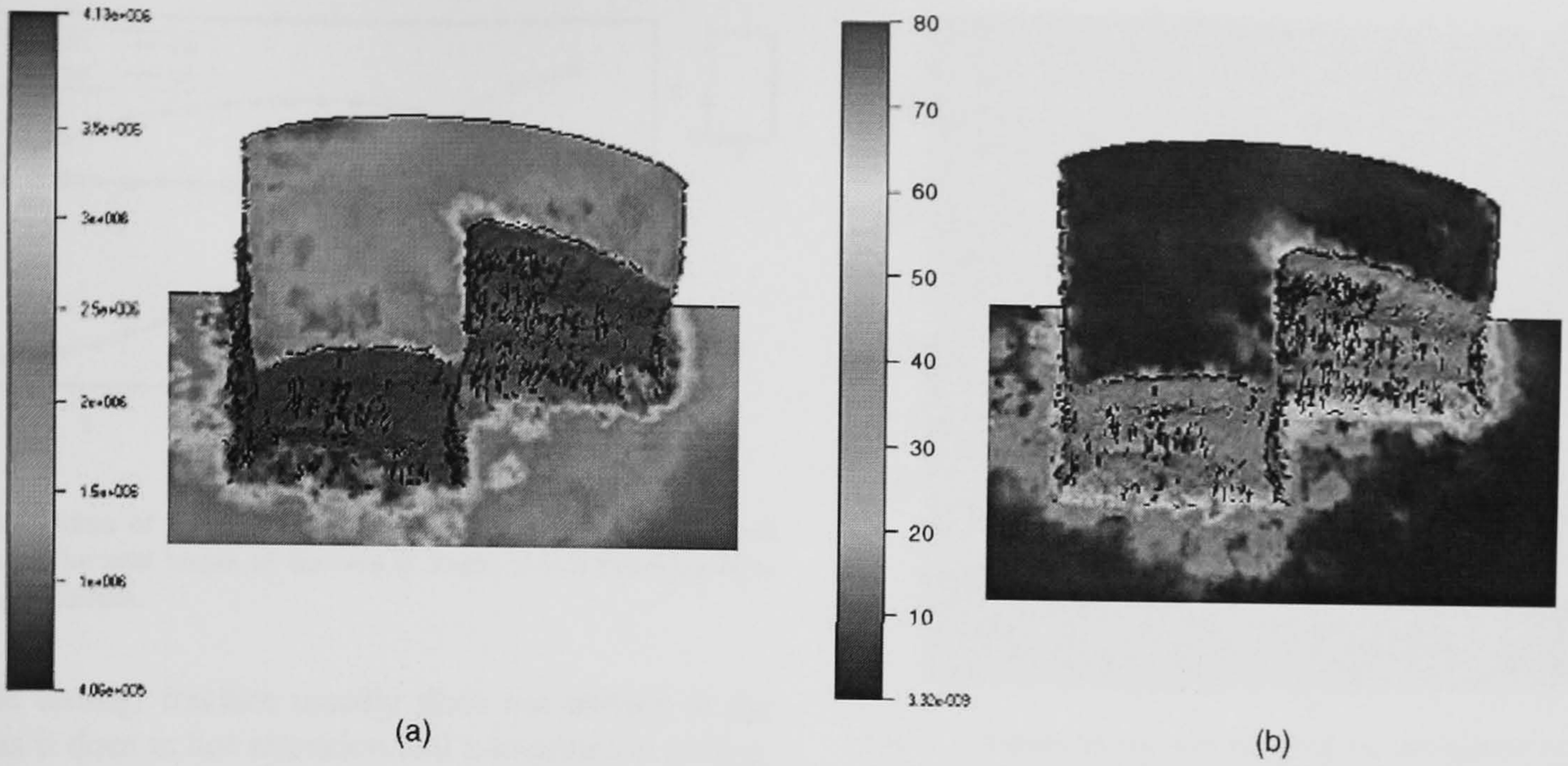

(a) (b)

Fig. 5. Predicted distribution of the P_D (a) and X_V (b) in the cross-section using the model proposed by Vatne et al. [10].

measurements [12]. Since $S_v(\varepsilon)$ is an exponential function of strain, the influence of strain change on the N_V is very strong. Therefore, we can roughly determine the possible region where maximum recrystallisation would occur just from looking at the computed distribution of strain.

There is another way to predict the static recrystallisation. This is by using the model proposed by Vatne et al. [10]. The most important feature of this model is the calculation of the density of the recrystallisation nuclei for different orientations: the particle stimulated nucleation (PSN), nucleation from cube bands and grain boundary areas (GB). It should be noted that this model was proposed for the modelling of aluminium alloys (AA3004 and the commercial purity aluminium) during the multi-pass hot rolling process. Compared with the hot rolling of aluminium alloys, there are few cube bands within the billet during the hot extrusion of the aluminium alloy 2024. Therefore, the contribution of the nucleation from cube bands can be ignored in the present study. For brevity, the formulae are not introduced.

The calculated distribution of the stored energy P_D and the X_V within the extrudate section are shown in Fig. 5. In a thin layer near the extrudate edges, the predicted result changes dramatically from the edge to the centre. The predicted values of the stored energy vary from 4×10^6 to 4×10^5 J (Fig. 5a). The predicted distribution of X_V agrees reasonably well with measurements (Fig. 5b). The maximum value of the fraction recrystallised occurs at almost the same location as that predicted by the use of the Sellars and Zhu model. Compared with the application of the model proposed by Sellars and Zhu, the values of many of the parameters in the model proposed by Vatne et al. can easily be found in the literature. This makes it much more convenient for the programming. However, the prediction by using Sellars and Zhu model appears more accurate in terms of the distribution of the calculated X_V. The unreported values of M_0 (a constant) and U_{GB} (the activation energy for grain boundary migration) in the work by Vatne et al. [10] were found to be 200 and 200 kJ/mol in the presented study. Other parameters remain the same as those that Vatne et al. adopted.

4. Prediction of surface cracks

Clift et al. [25], Ko et al. [26] and Domanti et al. [27] have indicated that the Cockcroft and Latham criterion [28] is the best amongst the various existing criteria for the prediction of fracture initiation for extrusion.

The normalised form of the Cockcroft and Latham criterion is written as:

$$\int_0^{\bar{\varepsilon}_f} \frac{\sigma_I}{\bar{\sigma}} \, d\bar{\varepsilon} = CL, \tag{6}$$

where $\bar{\sigma}$ is equivalent stress, σ_I the maximum principal tensile stress, $\bar{\varepsilon}$ the equivalent strain, $\bar{\varepsilon}_f$ the equivalent strain to fracture and CL is the critical damage value.

When using the above criteria, the most important task is to ascertain the critical damage value CL or the critical effective plastic strain, $\bar{\varepsilon}_f^p$. For a homogeneous material, this critical value can be considered as a material constant. Kim et al. reported that the value obtained from compression testing and tensile testing is different [29]. The explanation can be attributed to the different deformation history, different stress state at fracture locations and the fracture mode. The differences between surface cracks in hot direct extrusion and cracks occurring in both compression and tensile testing makes the determination of the critical damage value even more complicated. In compression testing, fracture appears on the free surface at much smaller nominal strains than those in extrusion (equivalent strain usually greater than 3 on the contact surface). Therefore, the effect of friction on the fracture initiation and propagation is ignored.

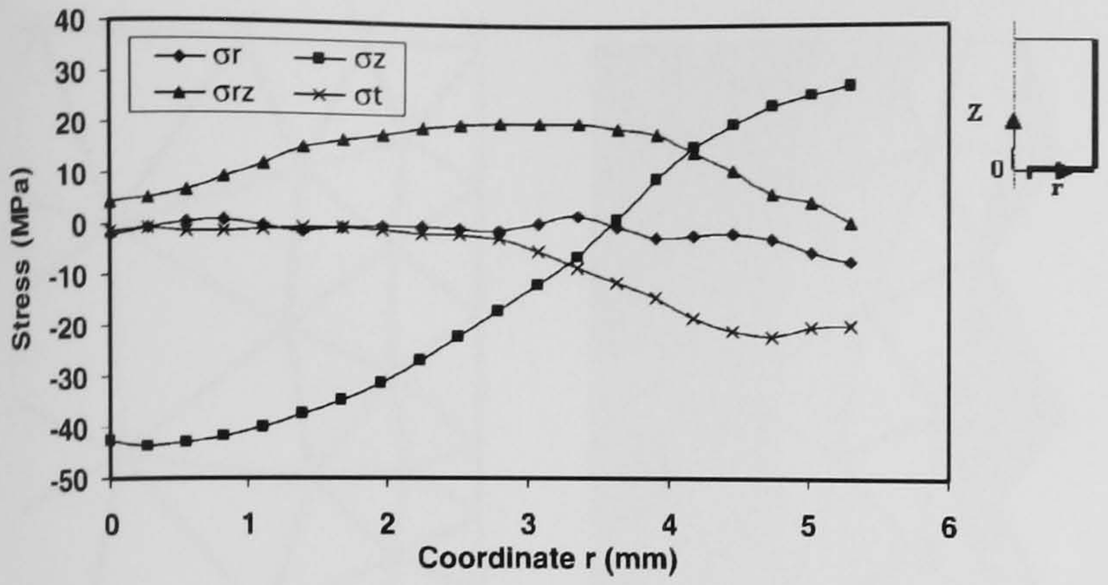

Fig. 6. Distribution of the stress components in the cross-section when $Z = -4$ mm. The total length of die land is 5 mm. $Z = 0$ corresponds to the die upper surface.

In tensile testing, fracture usually does not initiate at the surface as it does in hot extrusion and compression testing, and the stress and strain states at the crack initiation site are different. Furthermore, fracture initiates at much smaller nominal strains than those observed during extrusion.

In this section, aluminium alloy 2014 was studied. The experimental data were taken from Vierod's work [11]. The ram speed is 2.9 mm/s and the temperatures of the billet, container and die are 475, 425 and 375 °C, respectively. The billet and die are the same as described in Section 2. Axisymmetrical modelling (two-dimensional) was used in the simulation.

The computed distribution of the stress components in the extrudate cross-section ($Z = -4$ mm) are shown in Fig. 6, where σ_t is the hoop stress and σ_{rz} is the shear stress. Obviously, σ_z, the longitudinal stress, can be assumed to be the maximum principal stress, whilst σ_r, the radial stress, is considered as the minimum principal stress. For σ_z, it is negative (compressive) for $r \leq 3.4$ mm, which corresponds approximately to 2/3 of the extrudate cross-section, and is tensile at the surface. This suggests that crack will never occur at the centre (three-dimensional compressive stress state) and would possibly appear at the surface for this kind of die design. The longitudinal tensile stress is the major factor causing surface cracks. This has never been stated in previous workers' experimental studies since it would seem impossible to measure the instantaneous stress distribution in the extrudate within the die land area.

The process of crack evolution can be visualised by the use of element deletion techniques. It should be noted the term "crack" here is different from its meaning in fracture mechanics, which implies a sharp-tip. Since the Cockcroft and Latham criterion was proposed for the prediction of crack initiation, the process of crack growth cannot be accurately predicted by the use of this criterion. Also, the surface cracks observed in the hot extrusion of AA2014 are usually caused by the distribution, size and morphology of the second phase particles. Without considering these metallurgical factors, the calculated crack propagation by the use of the Cockcroft and Latham criterion can only be represented as an approximation.

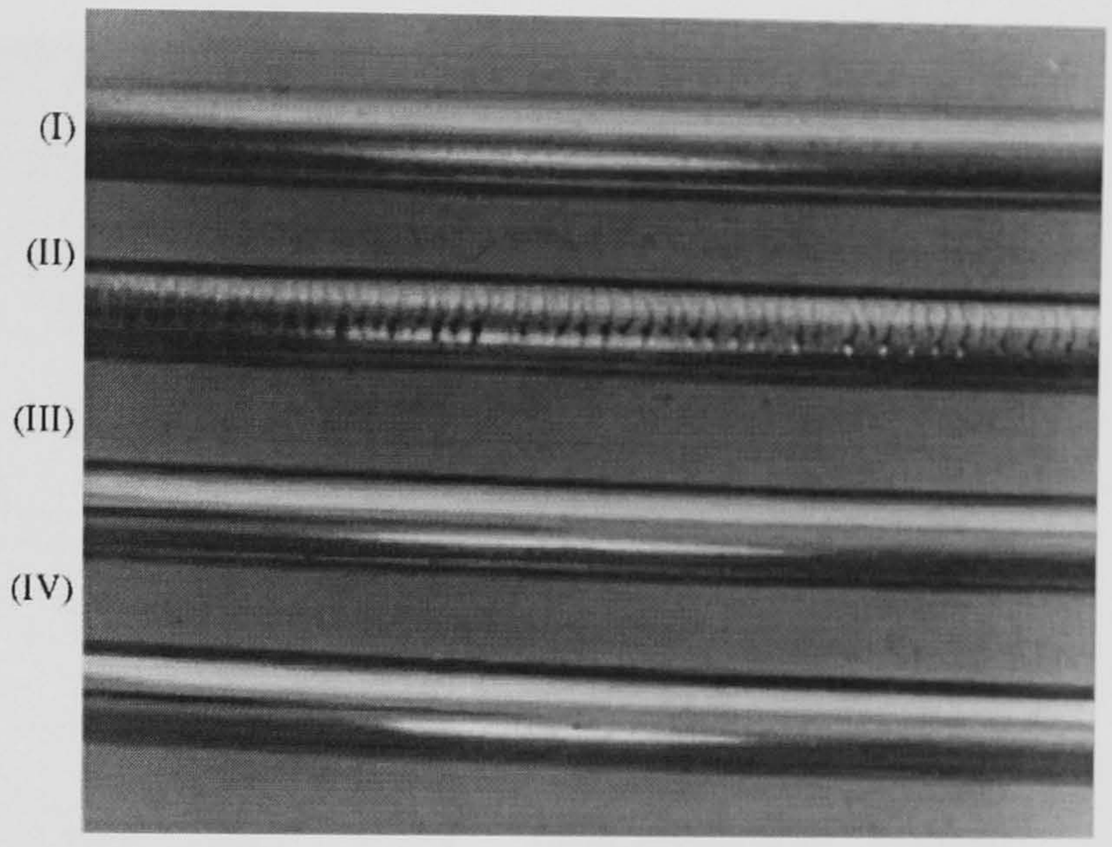

Fig. 7. Influence of the ram speed on the occurrence of surface crack. Extrusion ratio is 50:1. The extrusion temperature is 400 °C. (I) 6.4 mm/s; (II) 7.5 mm/s; (III) 6.2 mm/s; (IV) 5.9 mm/s [30].

Deleting element requires the determination of the critical damage values CL. To accurately determine this value, the calculated shape and depth of crack should correspond well with the experimental measurement. To determine this critical fracture value with confidence, a series of analyses were conducted. Fig. 7 shows the experimental observation conducted by Paterson [30] under different extrusion conditions. Fig. 8 shows the corresponding CL value in the cross-section that is 0.5 mm down to the die exit ($Z = -0.5$ mm). From Fig. 7, it can be seen that no surface crack can be observed. But there are obvious surface cracks when $V = 7.5$ mm/s. According to this information, it can be ascertained that the critical CL value should be greater than the computed maximum CL value which is produced by $V = 6.4$ mm/s. In other words, the critical value should be greater than 0.25, see Fig. 8. Fig. 9 shows the evolution of surface cracks. Clearly, the predicted shape is comparable with the measurement presented in Fig. 10. It should be emphasised again that results in Fig. 9 can only be treated as a qualitative prediction.The influences of the forming parameters

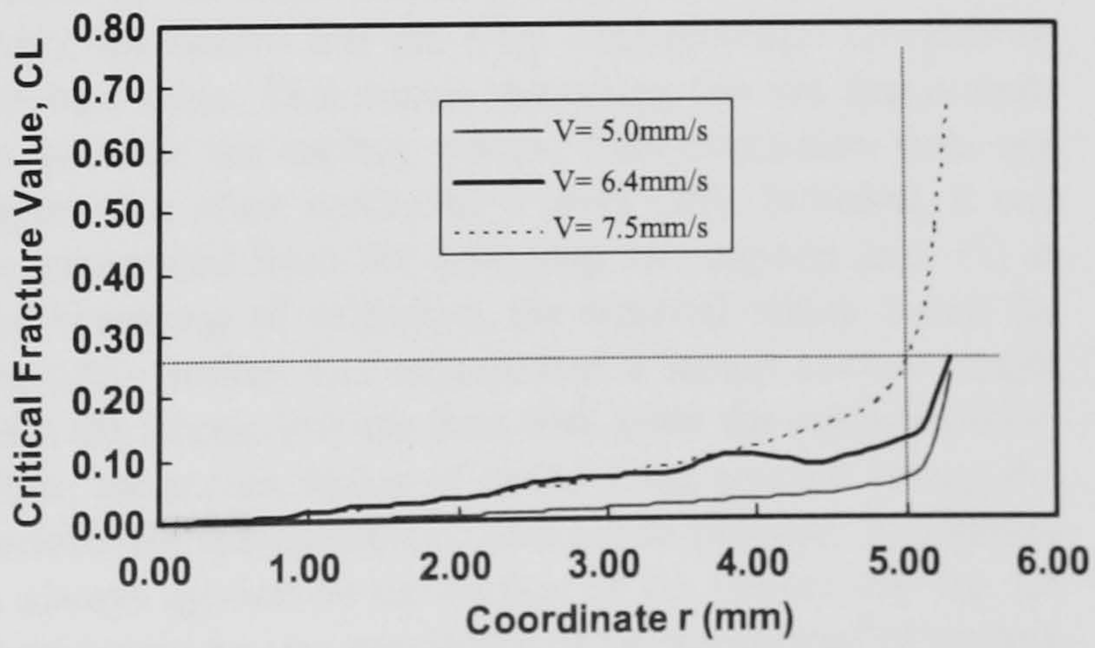

Fig. 8. The influence of the friction factor on the critical fracture value CL.

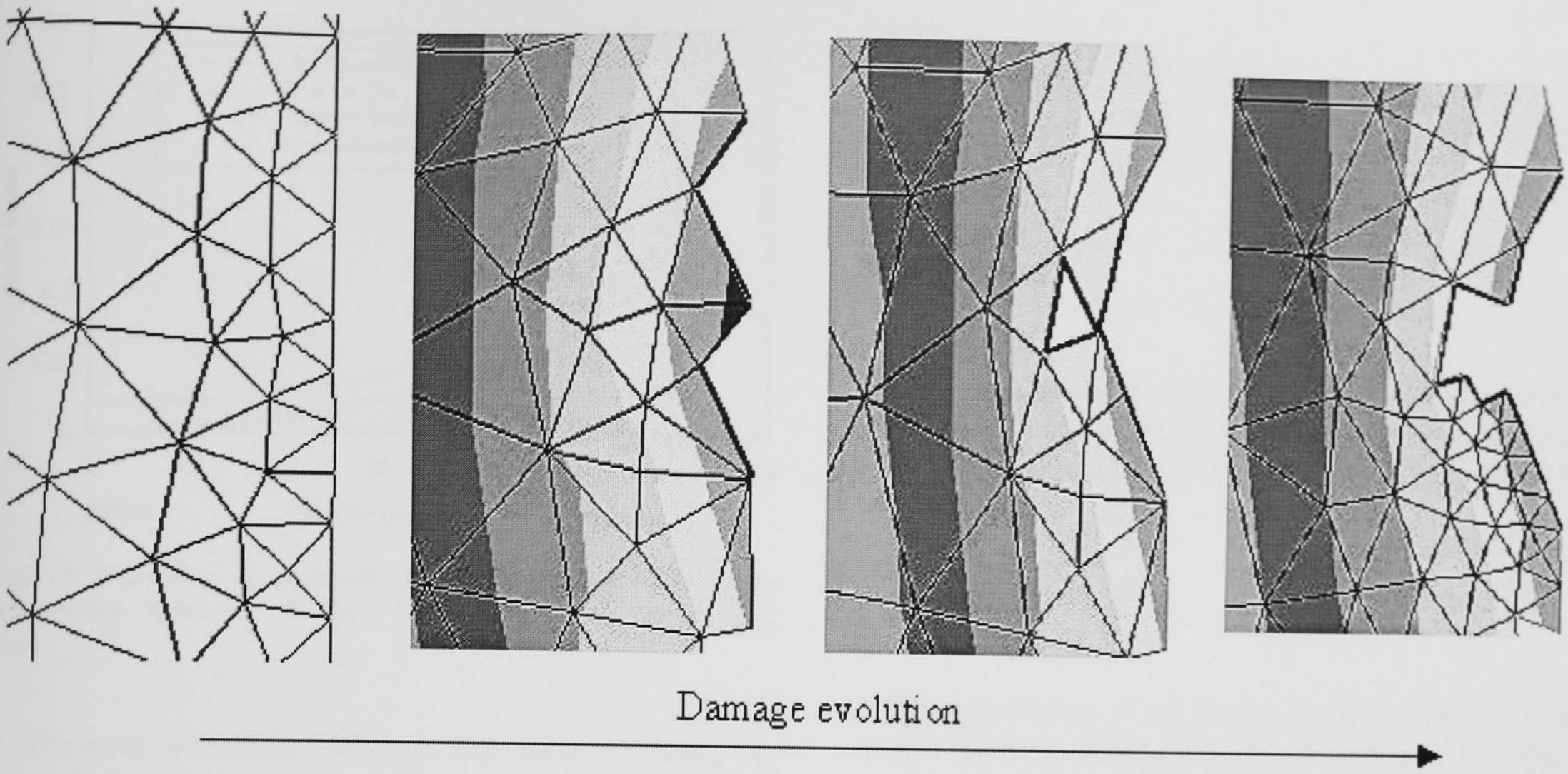

Fig. 9. Evolution of surface crack. Only the meshes near the surface are presented.

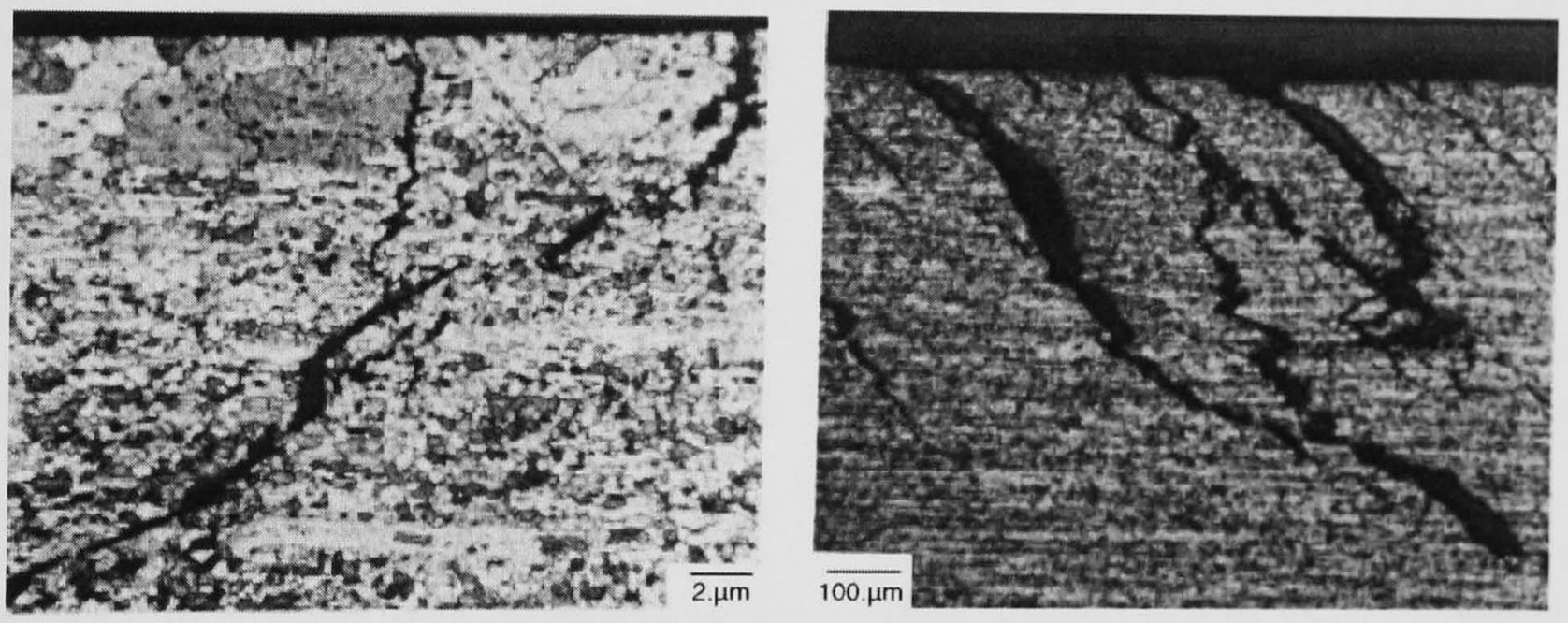

(a) Extrusion Ratio of 30:1 (b) Extrusion Ratio of 20:1

Fig. 10. The observed surface crack by Vierod [11] and Paterson [30] for AA2014.

and the die configuration were studied by combining the Taguchi method [31] with the finite element method. This methodology has been illustrated in several papers [32,33]. The detailed procedures are not repeated here.

Four kinds of die configurations were studied. The die configurations are shown in Fig. 11. The friction condition (friction factor of 0.6) is assumed to be the same for all die surfaces and all dies have the same length of 5 mm. The angle θ in Fig. 11b and c is 10°. The predicted distribution of the calculated Cockcroft and Latham fracture values in the cross-section are shown in Fig. 12. Surprisingly, the stream line die (Fig. 12c) produces the greatest fracture value. This means that using this die shape tends to generate the surface cracks. This conclusion does not agree with other researcher's work [27]. However, it can be interpreted from the following two aspects that: (1) at the beginning of extrusion, the material which forms the extrudate surface has experienced a longer contact length with the stream line die than with other die configurations. Thus, the accumulation of strain is the greatest among the various die configurations; and (2) in practice, lubrication is always applied on the surface of the stream line die. So there would be less possibility of the occurrence of surface cracks. However, in practice it is not possible to preserve a lubricated film throughout the extrusion process.

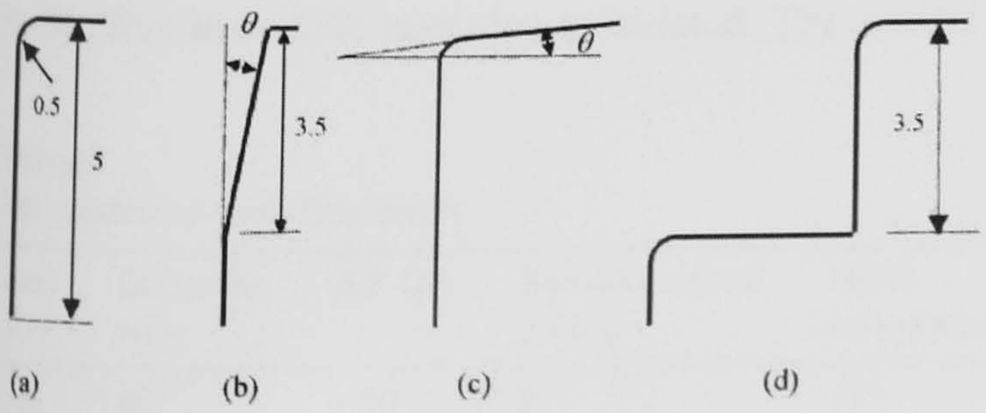

Fig. 11. Schematic drawing of the various die configurations: (a) flat-faced; (b) choked; (c) stream line; (d) prechambered.

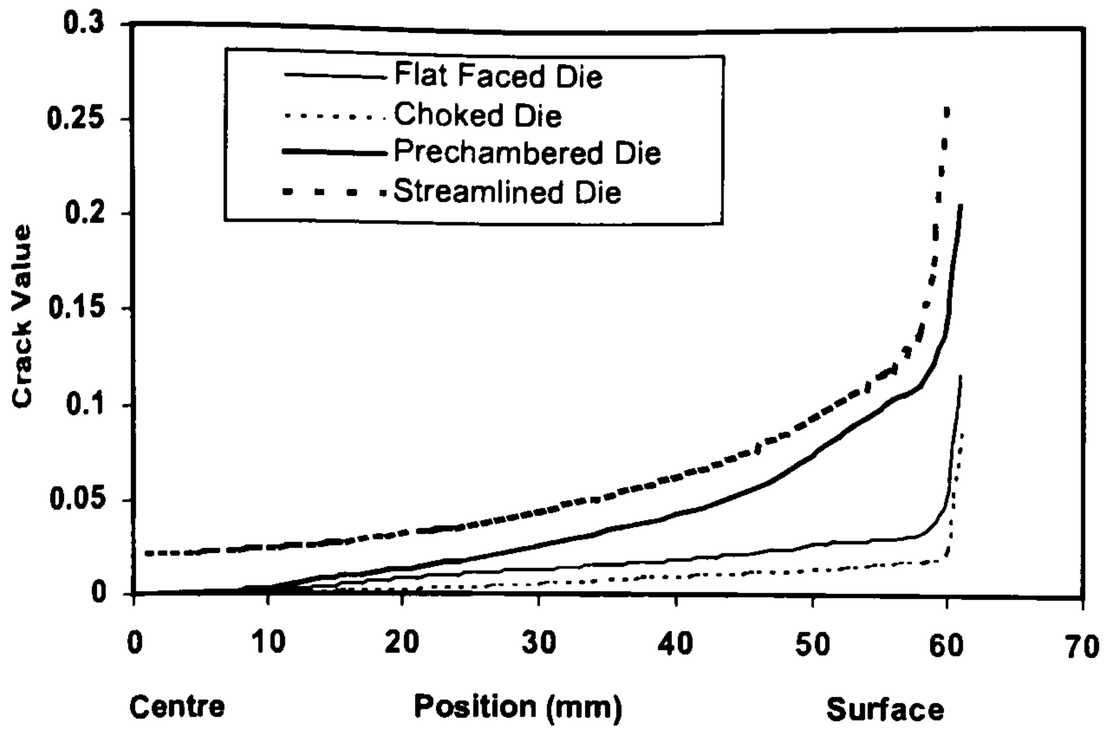

Fig. 12. Distribution of Cockcroft and Latham fracture value in the cross-section within the die land (1 mm higher than the die land end).

The most interesting finding in Fig. 10 is that using the choked die has the least possibility of producing surface cracks. The previous work also found that the choked die produces a propensity to prevent recrystallisation. Recrystallisation is very undesirable for the products used in the aerospace industry. Hence, the choked die can be recommended to replace the flat-faced die. The key parameters of the design of the choked die are the angle θ and the depth of the choke. Jarrett and Parson gave some clues in their patent [34]. Further work clearly needs to be performed to clarify this point bearing in mind that most dies in use for the production of hard alloys are presently produced with a small choke.

Four forming parameters were selected to study their influences on the formation of surface cracks. These parameters include: extrusion ratio, the temperature difference between the tool and the billet (ΔT), the extrusion speed and the billet temperature. Each parameter has three values, also called three levels. These values are shown in Table 2. The designed orthogonal table $L9(3^4)$ was used. $L9(3^4)$ indicates that there are four parameters, each parameter has three levels and a total of nine test runs need to be conducted. The computed contribution of each forming parameter to the fracture value is shown in Table 3.

It can be seen that the extrusion ratio is the dominating variable in the control of surface cracks, followed by the ram speed, the billet temperature, and the billet/tool temperature difference. The average effect of each parameter level on the fracture value was also calculated. The results show

Table 2
Test parameters and their levels

Level	Extrusion ratio	ΔT (K)	Extrusion speed (mm/s)	Billet temperature (K)
1	10	−50	3	573
2	30	0	6	633
3	50	50	9	693

Table 3
Analysis of variance of surface crack

	Surface crack (%)
Extrusion ratio	45
ΔT	8.65
Extrusion speed	23.2
Billet temperature	23.15

that the fracture value decreases with increasing extrusion ratio, and with decreasing the temperature difference between the billet and tools, the extrusion speed and the billet temperature.

5. Die design

The importance of die design on the control of product quality has been discussed in many literature [35]. The major objective of this section is to illustrate how the FEM can be used to improve the die design. A thin wide semi-closed section was selected as an example to emphasise the importance of using an expansion chamber and to characterise the complex material flow within the die chamber. Due to commercial sensitivity, both the geometrical dimensions and the extrusion conditions can not be listed. The material is AA6063.

The die set-ups are shown in Fig. 13. Only a half model is shown by taking advantage of the geometrical symmetry. All tools were assumed to be rigid in the simulation.

The simulated material flow patterns within and outside of the expansion chamber are shown in Fig. 14a–d in the sequence of the extrusion process. Fig. 14a shows that part of the material proceeding to the bottom surface of the expansion chamber. The outline of the extrudate appears near the symmetry plane where the material flow is faster than elsewhere. At this stage, there is little material flowing laterally to fill the chamber. Fig. 14b indicates that materials start to fill the chamber. At the same time, some material traverses through the die mouth to form the final shape. In Fig. 14c, only a small volume has not been fully filled. The expansion chamber has been completely filled and the height of the shape is nearly uniform in Fig. 14d. It should be pointed out that the same die land length is used for different parts of the die. It is generally accepted that the length of the die land plays an important role in the control of material flow. Any slight changes in the length of die land would produce an obvious difference in the extruded product shape. To simulate such an important aspect would require a very small time step and very fine element size (less than 0.1 mm) to simulate the resultant effects of friction at the tool/billet surface. Considering the regular requirements of remeshing to overcome the mesh distortion and to ensure the computation continuation, a significant amount of computing resource would be required even a simple shape extrusion process (like T shape). Although the com-

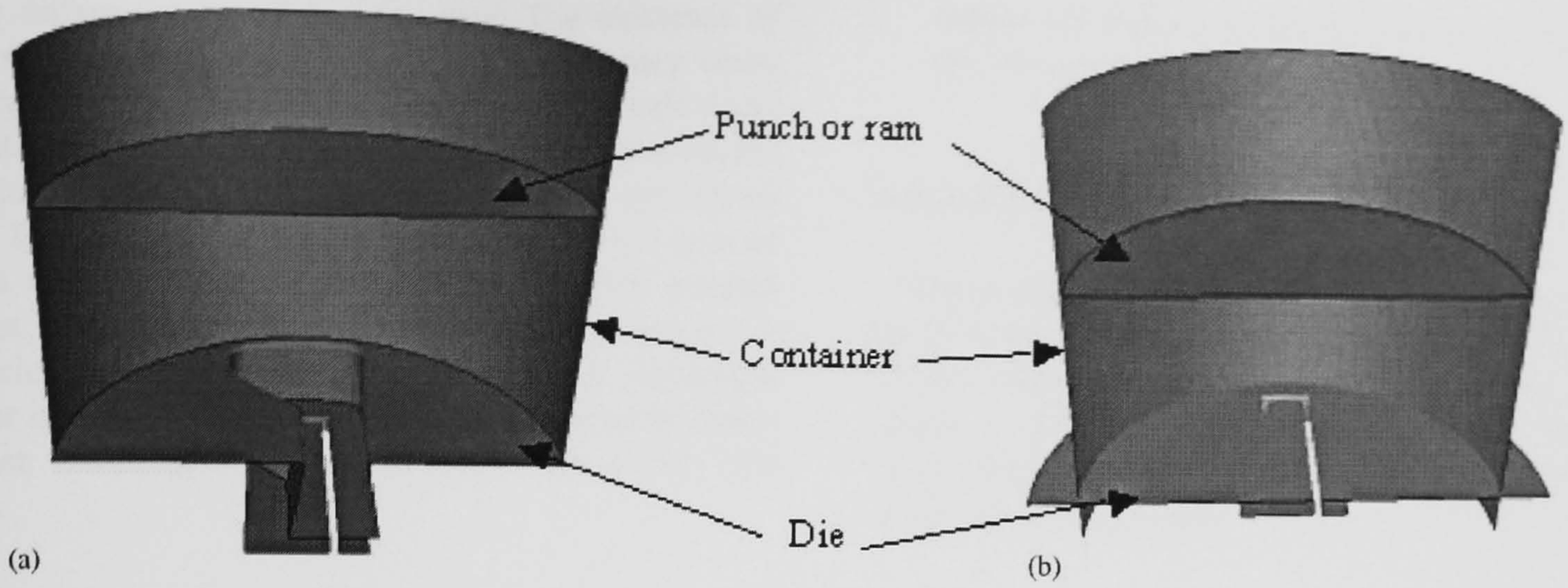

Fig. 13. Die set-up (a) with expansion chamber; (b) without expansion chamber.

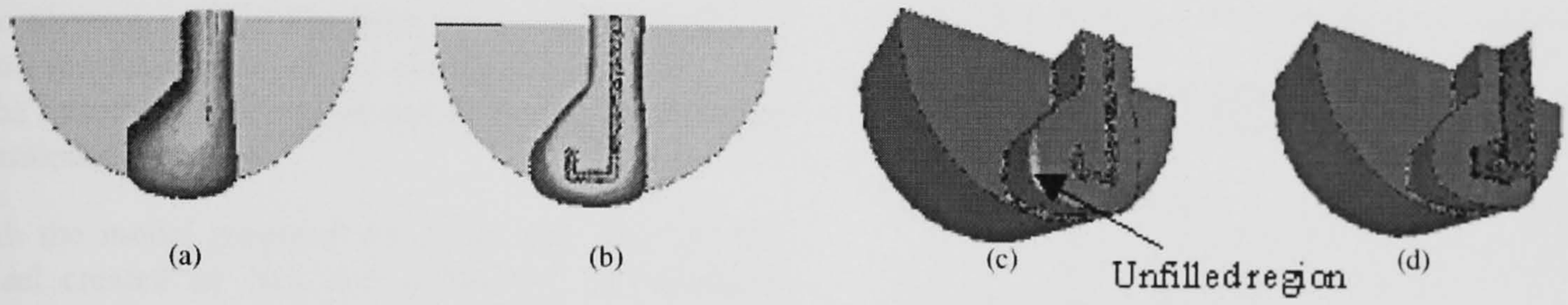

Fig. 14. Materials flow within and outside of the expansion chamber.

puting hardware and software have made great progresses in the last decades, the present authors still believe that it is not the time to study this subject by the use of Lagrangian based formulation unless a mainframe is adopted. The use of Eulerian based FEM formulation may solve this problem. However, the whole process of material flow cannot be visualised because the Eulerian FEM is based on a steady state assumption.

Fig. 15 shows the predicted product shape when the die without an expansion chamber was used. Unlike the previous case, the whole section of the shape appears at the same time. However, the height of the extrudate

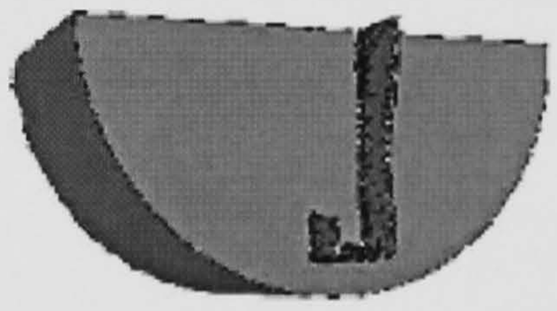

Fig. 15. Material flow without the use of expansion chamber.

is not uniform. The material near the die gravity centre flows faster than elsewhere, producing the longest height at this location. The non-uniform material flow is undesirable because internal tensile stress would be generated to

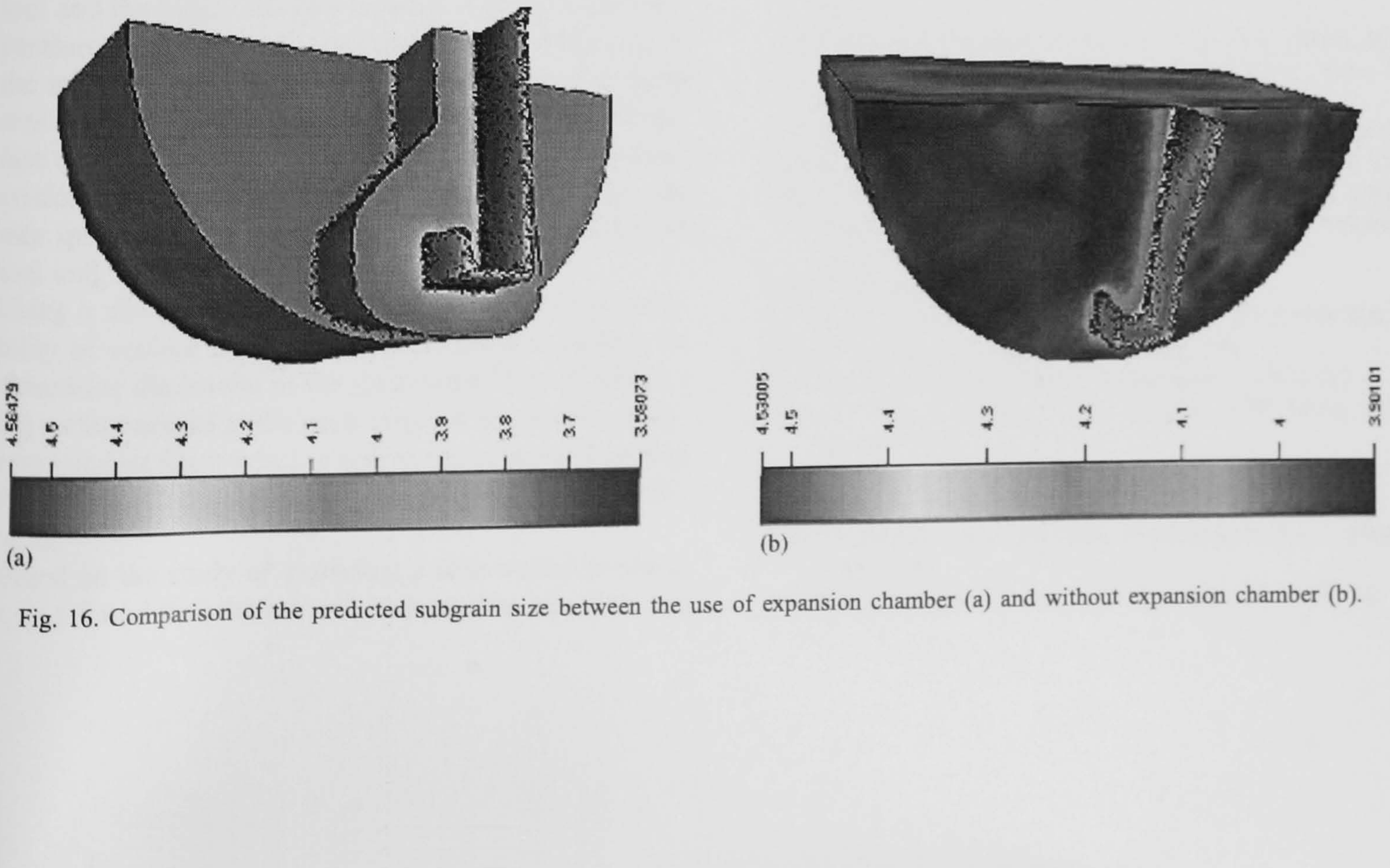

Fig. 16. Comparison of the predicted subgrain size between the use of expansion chamber (a) and without expansion chamber (b).

balance different parts of the extrudate. The existence of tensile stress tends to reduce the ductility and may cause microcracks within the deformed material. The calculated distribution of subgrain size by the method introduced in Section 3 for the use of two die structures are shown in Fig. 16. Using the die with chamber produces a more uniform distribution of subgrain in the extruded product than that without a chamber. From this observation it can be concluded that the use of a die with an expansion chamber is superior to the die without an expansion chamber when extruding a complex product with a very thin section.

6. Conclusions

Finite element method has been successfully applied to study the various aspects of the aluminium extrusion process. The following conclusions can be drawn based on the aforementioned analyses:

(1) Both the model proposed by Sellar and Zhu and the model created by Nes and co-workers are available for the prediction of static recrystallisation. It is easier to perform the model created by Nes et al. in the numerical analysis. This is attributed to the fact that the values of the parameters in their model can easily be found in the literature and there are no such problems as non-convergence caused by the inappropriate input of some parameter values. But the model proposed by Sellars and Zhu presents more accurate prediction.
(2) The maximum fraction recrystallised occurs at the die corners and the width of this recrystallised layer from the extrudate edge is non-uniform. The predicted results fit reasonably well with the experimental measurement.
(3) Among the forming parameters investigated (such as extrusion ratio, the temperature difference between the tool and the billet, the ram velocity and the billet temperature), extrusion ratio has the strongest influence on the initiation of surface cracks. The greater the extrusion ratio, the less possibility of the occurrence of surface cracks. The possibility of the occurrence of surface cracks increases with increasing billet temperature, the ram speed and the temperature difference between the tool and the billet.
(4) Using a choked die can significantly reduce the possibility of surface cracks. If no lubrication is added, the streamline die results in the great possibility of producing surface cracks in the early stage of the extrusion process because the contact length is the maximum among the various die configurations investigated in the present paper.
(5) Based on the study of extruding a thin-walled product, it was found that the use of an expansion chamber can reduce the degree of non-uniformity in terms of shape and the properties.

Acknowledgements

The authors recognise the excellent experimental work by Dr. R.P. Vierod, Dr. J. Subramaniyan, Dr. A.F. Castle and Dr. S.J. Paterson and express their appreciation for allowing its use in this paper. The authors also thank Bournemouth University for the support of each of the authors and supply of the computing power.

References

[1] X. Velay, X. Duan, T. Sheppard, Mater. Sci. Forum 426–432 (2003) 3807.
[2] J. Zhou, L. Li, J. Duszczyk, J. Mater. Process. Tech. 134 (2003) 383.
[3] Q. Li, C.J. Smith, C. Harris, M.R. Jolly, J. Mater. Process. Tech. 135 (2003) 189.
[4] T. Sheppard, X. Duan, in: Z. Jin (Ed.), Hot Deformation of Aluminum Alloys III, Times of Acadiana Pr, Inc., 2003, p. 289.
[5] J. Lof, Y. Blokhuis, J. Mater. Process. Tech. 122 (2002) 344.
[6] K. Marthinsen, B. Holmedal, S. Abtahi, S. Chen, E. Nes, Mater. Sci. Forum 426–432 (2003) 3777.
[7] R.J. Dashwood, H.B. McShane, A. Jackson, in: Proceedings of the 6th International Seminar on Aluminum Extrusion Technology, vol. 1, Chicago, IL, USA, May 1996, Aluminum Extruders Council, 1996, pp. 331–339.
[8] L. Li, J. Zhou, J. Duszczyk, Modell. Simul. Mater. Sci. Eng. 11 (2003) 401.
[9] C.M. Sellars, Q. Zhu, Mater. Sci. Eng. A280 (2000) 1.
[10] H.E. Vatne, T. Furu, R. Ørsund, E. Nes, Acta Mater. 44 (1996) 4463.
[11] R.P. Vierod, Ph.D. Thesis, University of London, 1983.
[12] J. Subramaniyan, Ph.D. Thesis, University of London, London, 1989.
[13] J.-L. Chenot, L. Fourment, E. Wey, in: Proceedings of the 16th International Forging Congress, Pékin, China, September 1999.
[14] J.L. Chenot, L. Fourment, T. Coupez, R. Ducloux, E. Wey, in: Proceedings of the International Conference on Forging and Related Technology (ICFT'98), Birmingham, 27–28 April 1998, Professional Engineering Publishing, Suffork, UK, 1998, pp. 113–122.
[15] X. Duan, T. Sheppard, Modell. Simul. Mat. Sci. Eng. 10 (2002) 363.
[16] X. Duan, T. Sheppard, Mater. Sci. Eng. A351 (2003) 282.
[17] F. Furu, H.R. Shercliff, C.M. Sellars, M.F. Ashby, Mater. Sci. Forum 217–222 (1996) 453.
[18] X. Duan, T. Sheppard, J. Mater. Process. Tech. 125–126 (2002) 181.
[19] X. Duan, T. Sheppard, Comput. Mater. Sci. 27 (2003) 250.
[20] X. Duan, T. Sheppard, in: R. Goncalves, R. Roy, A. Steiger-Garcao (Eds.), Advances in Concurrent Engineering, A.A. Balkema Publishers, 2002, pp. 227–234.
[21] E. Nes, Progr. Mater. Sci. 41 (1998) 129.
[22] W.A. Johnson, R.F. Mehl, Trans. AIME 135 (1939) 416.
[23] M. Avrami, J. Chem. Phys. 7 (1939) 1103.
[24] A.N. Kolmogorov, USSR Ser. Metemat 1 (1937) 355.
[25] S.E. Clift, P. Hartley, C.E.N. Sturgess, G.W. Rowe, Int. J. Mech. Sci. 32 (1990) 1.
[26] D.C. Ko, B.M. Kim, J.C. Choi, J. Mater. Process. Tech. 62 (1996) 166.
[27] T.J. Domanti, D.J. Horrobin, J. Bridgwater, Int. J. Mech. Sci. 44 (2002) 1381.
[28] M.G. Cockroft, D.J. Latham, J. Inst. Met. 96 (1968) 33.

[29] H. Kim, M. Yamanaka, T. Altan, Transactions of NAMRI/SME, vol. XXIII, 1995, 63 pp.
[30] S.J. Paterson, Ph.D. Thesis, University of London, London, 1981.
[31] G. Taguchi, Taguchi Methods—Research and Development, ASI Press, Michigan, USA, 1992.
[32] T. Sheppard, X. Duan, Modell. Simul. Mat. Sci. Eng. 10 (2002) 597.
[33] X. Duan, T. Sheppard, J. Mater. Process. Tech. 130–131C (2002) 1060.
[34] M. Jarrett, N.C. Parson, Extrusion Method, UK Patent GB2285941 (1995).
[35] P.K. Saha, Aluminum Extrusion Technology, ASM International, 2000.